University of Antwerp

sck cen

Faculty of Medicine and Health Sciences
Physiopharmacology lab, GENCOR Research Unit

Epigenetic Biomarkers Of Radiation-Induced Cardiovascular Disease And Secondary Cancers

PhD thesis submitted for the degree of Doctor of Medical Sciences at the University of Antwerp to be defended by Magy Sallam

Supervisors:
Prof. Dr. Pieter-Jan Guns
Dr. Benotmane Rafi
Dr. Raghda Ramadan
Dr. An Aerts (Mentor)

Antwerp, 2023

Doctoral Jury members:
Prof. Dr. Wim Vanden Berghe
Prof. Dr. Emeline Van Craenenbroeck
Prof. Dr. Pierre Sonveaux
Prof. Dr. Ans Baeyens
Prof. Dr. Pieter-Jan Guns
Dr. Benotmane Rafi
Dr. Raghda Ramadan

Table of Contents

Acknowledgements

PhDs are known to be long and winding roads where, based on personal experience, there are many opportunities to lose your way. Therefore, I'd like to thank all the individuals who guided me through this wild road to where I am today.

I spent all of my four PhD years at SCK CEN where my promoters tried to help me on the difficult journey of the two connected yet independent research ideas my project involved. Therefore, I'd like to personally thank my mentor, Dr. An Aerts, my promoter, Dr. Rafi Benotmane, and the Radiobiology (RDB) department head, Prof. Dr. Sarah Baatout, who were there with me from the start and supported me in my journey. Midway through the project, I was saddened by the step-down of An Aerts as a promoter. However, I was lucky enough to then be assigned Dr. Raghda Ramadan, who served both as promoter and ever supportive friend in times of need, which were many. So, thank you Dr. Raghda for all the laughs, tears and everything in between. I would also like to thank Dr Mohamed Mysara, the unofficial Godfather of my PhD. Being both a friend and a mentor was probably not easy and yet he excelled at both.

I would also like to thank Prof. Dr. Pieter-Jan Guns whom I was fortunate enough to have as my UAntwerpen promoter. Despite the physical distance, Prof. Pieter-Jan was a constant supportive presence in my PhD path. Whether it was pushing me that extra bit or offering support whenever/wherever it was needed, his contribution to my PhD as well as my personal progress was indispensable.

I would also like to thank the members of the internal doctoral committee, Prof. Dr. Wim Vanden Berghe and Prof. Dr. Emeline Van Craenenbroeck, for their contributions to the improvement of my PhD project during my midterm presentation as well as their valuable comments on my final thesis. I would also like to thank the members of my external doctoral committee, Prof. Dr. Pierre Sonveaux and Prof. Dr. Ans Baeyens, for their time and effort in the improvement of my PhD thesis.

To my RDB colleagues of lab technicians and fellow PhD students, I am truly thankful. Whether it was by helping with lab work or making me laugh on a difficult day, I will remain forever grateful.

On a personal note, I'd like to thank my family without whom I wouldn't be standing (or even sitting) here today. I'd like to thank my mom who has tolerated my complete absence for the past three years and yet her first questions to me are always about how I'm doing. I'd like to thank my sister, Maha, who is one of my best friends and giver of the warmest hugs in the world. I love you both to the moon and back.

I'd also like to thank my best friend and partner in crime, Pol. Four years ago, I arrived to Mol not knowing anyone, lonely and scared. Then there was Pol and all of a sudden it wasn't so lonely anymore. I couldn't have done it without you, Dobby.

Finally, I'd like to thank my daughter, Lana. Even though she didn't really do anything to help with my PhD, she is the light of my life and is a part of everything I'll ever do whether I mean to or not. I love you, Klein Aapje.

List of abbreviations

5-mC	5-methyl cytosine
8-OHdG	8-oxo-20-deoxyguanosine
AGO	Argonaute
AID	Activation-induced cytidine deaminase
ALARA	As low as reasonably achievable
APOBEC	Apolipoprotein B mRNA editing enzyme, catalytic polypeptide-like
ATM	Ataxia telangiectasia mutated
BER/NER	Base/nucleotide excision repair
CAC	Coronary artery calcium
CeRNA	Competitive endogenous RNA
cfDNA	Circulating cell-free DNA
CGI	CpG islands
circRNAs	Circular RNAs
CMRI	Cardiac magnetic resonance imaging
CT	Computed tomography
CVD	Cardiovascular disease
DAMP	Damage associated molecular pattern
DDR	DNA damage response
DMP	Differentially methylated position
DMR	Differentially methylated region
DNMT	DNA methyltransferase
EGFR	Epidermal growth factor receptor
EM radiation	Electromagnetic radiation
eRNAs	Enhancer RNAs
FA	Fanconi anemia
FI	Fractionated irradiation
GLS	Global longitudinal strain
HR	Homologous recombination
HZE	High (H) atomic number (Z) and energy (E)

IL	Interleukin
INF-γ	Interferon-gamma
IR	Ionizing radiation
JAK/STAT	Janus kinase/signal transducers and activators of transcription,
LET	Linear energy transfer
LINE-1	Long interspersed element-1
LncRNA	Long noncoding RNA
LVEF	Left ventricular ejection fraction
LXRα	Liver X receptor α
MBP	Methyl-CpG-binding protein
MCP-1	Monocyte chemoattractant protein-1
MC-seq	Methylation capture sequencing
MeV	Million electron volts
MHD	Mean heart dose
MHD	Mean heart dose
MiRNA	MicroRNA
mTOR	Mechanistic target of rapamycin
NcRNA	Noncoding RNA
NF1	Neurofibromatosis type 1
NF-κB	Nuclear factor kappa b
NHEJ	Non-homologous end joining
NMD	Nonsense mediated decay
NO	Nitric oxide
OD	Optical density
OGG1	8-oxoguanine DNA glycosylase
PANTHER	Protein analysis through evolutionary relationships
PATs	Promoter-associated transcripts
PCG	Protein coding gene
PCI	Phenol/chloroform/isoamyl alcohol mixture
PDGFRA	Platelet-derived growth factor receptor
PI3K	Phosphoinositide 3 kinase
PIP3	Phosphatidylinositol (3,4,5)-trisphosphate

piRNAs	Piwi-interacting RNA
PPARγ	Peroxisome proliferator-activated receptor γ1
PRC2	Polycomb repressive complex 2
Pre-miRNA	Precursor microRNA
Pri-miRNA	Primary microRNA
PTCs)	Premature termination codons
qRT-PCR	Quantitative Real Time PCR
REM	Random effect model
RICVD	Radiation-induced cardiovascular disease
RIEE	Radiation-induced epigenetic effects
RIGs	Radiation-induced glioblastomas
RISC	RNA-induced silencing complex
RNAi	RNA interference
ROS/RNS	Reactive oxygen/nitrogen species
rRNA	Ribosomal RNA
RT	Radiotherapy
SAM	S-adenyl methionine
siRNAs	Small interfering RNAs
SMRT	Single-molecule real-time sequencing
sncRNAs	Small ncRNAs
snoRNAs	Small nucleolar RNAs
snRNAs	Small nuclear RNAs
SSB/DSB	Single/double strand break
TE	Transposable element
TET	Ten-eleven-translocation
TF	Transcription factor
TNF-α	Tumor necrosis factor alpha
tRNA	Transfer RNAs
VCAM-1	Vascular cell adhesion molecule 1
VSMC	Vascular smooth muscle cell
vWF	Von Willebrand factor
WP	Work packages

Summary

Ionizing radiation (IR) is routinely used in diagnosis and therapy. However, incidental radiation exposure of out-of-target tissues and organs may lead to long-term radiation-induced adverse effects including radiation-induced cardiovascular disease (RICVD) and secondary cancers. Investigating the underlying biological mechanisms involved in RICVD and secondary cancers can contribute to the discovery of disease-specific biomarkers. These biomarkers can help identify at-risk patients before they develop pathological symptoms thereby tackling a primary clinical concern. Consequently, the aim of this PhD is to investigate epigenetic biomarkers for two IR delayed effects; RICVD and glioblastoma as a possible secondary cancer to IR.

RICVD is a delayed adverse effect of thoracic radiotherapy (RT) which occurs due to the incidental irradiation of the heart and large arteries. The underlying biological and molecular mechanisms of RICVD are not yet fully understood while presenting a pro-inflammatory environment and increased oxidative stress. DNA methylation is an epigenetic mechanism of gene expression regulation via the methylation of a cytosine in a CpG dinucleotide forming 5-methyl cytosine (5-mC). DNA methylation is altered in cardiovascular disease with evidence suggesting a pathophysiologic contribution. DNA methylation is also altered in response to IR exposure. However, the involvement of DNA methylation in RICVD pathogenesis is underexplored. Therefore, IR-induced DNA methylation alterations were investigated in whole-heart irradiated rats and breast cancer patients receiving RT.

Differentially methylated regions (DMRs) which are regions containing multiple differentially methylated positions (DMPs), differentially methylated CpG dinucleotides, were detected up to 7 months in rats receiving 27.6 Gy dose. Pathway analysis of DMRs revealed enrichment of cardiac-specific pathways such as Dilated cardiomyopathy at 1.5 and 7 months. Furthermore, E2F6 inversely correlated with decreased global longitudinal strain after 27.6 Gy. In breast cancer patients, E2F6 and SLMAP exhibited differential

expressions, mainly at higher mean heart doses (MHD) directly and 6 months after radiotherapy, respectively. Therefore, these results suggest a possible association of DNA methylation to RICVD pathophysiology which requires validations in future mechanistic studies.

Further, blood DNA methylation of breast cancer patients receiving adjuvant RT was assessed at different time points. DNA methylation alterations were detected in left sided patients 6 months after RT showing predominantly gene-specific hypermethylation. The expression of six DMRs and 2 DMPs was shown to be affected by either the breast cancer side (left/right) or MHD or both as in the case of ATP5G2. However, as most of these DMRs/DMPs are also dysregulated in breast cancer, future integration of cardiac function data (currently under analysis) is needed to identify clear functional associations.

On the other hand, Glioblastoma is a grade IV glioma of poor prognosis that can occur secondary to diagnostic or therapeutic radiation exposure. We performed a meta-analysis of publicly available glioblastoma tissue RNA-seq datasets to identify whole transcriptome changes, with special focus on non-coding RNA. Additionally, small RNA-seq was performed to identify differentially expressed microRNAs in glioblastoma tissues. 98 long noncoding RNAs (lncRNAs) as well as 360 mRNAs were found to be differentially expressed by meta-analysis. 5 differentially expressed microRNAs were also identified by small RNA-seq. Pathway analysis of differentially lncRNAs and mRNAs revealed an association with ferroptosis, a novel cell death pathway implicated in cancer development and therapeutic responses. Therefore, our results confirm the involvement of ferroptosis in glioblastoma pathophysiology while presenting a number of candidates for future research as biomarkers and/or therapeutic targets.

In conclusion, the current thesis identifies several candidate epigenetic biomarkers for both RICVD and glioblastoma. However, these candidates require validation by integration of DMR methylation/expression profiles with patient cardiac functional data for RICVD and investigation of meta-analysis miRNAs/lncRNAs in radiation-induced glioblastoma.

Dutch summary

Ioniserende straling (IR) wordt regelmatig gebruikt voor diagnose en therapeutische doeleinden. Incidentele blootstelling aan straling van weefsels en organen naast het bestraalde doel kan echter leiden tot langdurige door-straling-geïnduceerde bijwerkingen, waaronder door-straling-geïnduceerde hart- en vaatziekten (RICVD) en secundaire kankers. Onderzoek naar de onderliggende biologische mechanismen die betrokken zijn bij RICVD en secundaire kankers kan bijdragen aan de ontdekking van ziekte specifieke biomarkers. Deze biomarkers kunnen helpen bij het identificeren van risicopatiënten voordat ze pathologische symptomen ontwikkelen. Hiermee kan een primair klinisch probleem worden aangepakt. Het doel van dit doctoraatsonderzoek is dan ook om epigenetische biomarkers te onderzoeken op twee IR-verlate bijwerkingen; RICVD en glioblastoom als mogelijke secundaire kanker.

RICVD is een verlate bijwerking van thoracale radiotherapie (RT) dat optreedt als gevolg van de incidentele bestraling van het hart en de grote slagaders. De onderliggende biologische en moleculaire mechanismen van RICVD zijn nog niet volledig begrepen. Maar ze vormen een pro-inflammatoire omgeving met verhoogde oxidatieve stress. DNA-methylatie is een epigenetisch mechanisme dat gen expressie reguleert. Dit doet ze doormiddel van de methylatie van de cytosine in het CpG dinucleotide, waarbij 5-methyl cytosine (5-mC) wordt gevormd. In cardiovasulaire ziektebeelden is de DNA-methylatie vaak gewijzigd, wat kan wijzen op een mogelijke bijdrage tot de pathofysiologie. Ook als gevolg van IR-bloodstelling wordt ook de DNA-methylatie gewijzigd. Echter isde betrokkenheid van DNA-methylatie bij de pathogenese van RICVD onderbelicht. Daarom werden IR-geïnduceerde DNA-methylatieveranderingen onderzocht in ratten, waarbij het hele hart werd bestraald, en borstkankerpatiënten, die RT kregen.

Differentieel gemethyleerde regio's (DMRs), dit zijn regio's met meerdere differentieel gemethyleerde posities (DMPs), differentieel gemethyleerde CpG dinucleotides, werden tot 7 maanden na de bestraling gedetecteerd in de ratten, die een dosis van 27.6 Gy hadden

gekregen. DMR-pathwayanalyse toonde een verrijking aan van cardiaal specifieke pathways zoals gedilateerde cardiomyopathie 1,5 en 7 maanden na bestraling. Bovendien was er een negatieve correlatie tussen E2F6 en een verminderde global longitudinal strain (GLS) na bestraling met 27,6 Gy. Bij borstkankerpatiënten vertoonden E2F6 en SLMAP een veranderde expressie, voornamelijk bij hogere hartdoses (MHD>2,5Gy), direct na en 6 maanden na radiotherapie, respectievelijk. Deze resultaten suggereren daarom een mogelijke verband tussen DNA-methylatie en RICVD-pathofysiologie. Maar dit vereist nog verdere validatie in toekomstige studies.

Verder werd DNA-methylatie in bloed van borstkankerpatiënten, die adjuvante RT kregen, op verschillende tijdspunten beoordeeld. DNA-methylatieveranderingen werden gedetecteerd bij linkzijdig-bestraalde patiënten, 6 maanden na RT, met overwegend genspecifieke hypermethylatie. De expressie van zes DMR's en 2 DMP's bleek te worden beïnvloed door de borstkankerkant (links/rechts), MHD (gemiddelde hart dosis) of beide zoals in het geval van ATP5G2. Aangezien de meeste van deze DMR's/DMP's echter ook ontregeld zijn bij borstkanker, is hun integratie in de cardiale functionele data (momenteel onder analyse) in de toekomst nodig om duidelijke functionele associaties te identificeren.

Een tweede luik van de thesis bestudeerde epigenetische merkers in het kader van glioblastoom een graad IV glioom met slechte prognose, dat secundair kan optreden als gevolg van diagnostische of therapeutische stralingsblootstelling. We voerden een meta-analyse uit van openbaar beschikbare RNA-seq datasets van glioblastoom weefsel om zo de hele transcriptoomveranderingen te identificeren, met extra aandacht voor niet-coderend RNA. Bovendien werd er een RNA-seq uitgevoerd van "small-RNAs" (oftewel "small RNA-seq") om miRNA's, met veranderde expressie, in glioblastoomweefsels te identificeren. Uit de meta-analyse bleken 98 lange niet-coderende RNA's (lncRNA's) en 360 mRNA's een veranderde expressie te hebben. Ook werden 5 miRNA's met veranderde expressie geïdentificeerd in de "small-RNA" RNA-seq. Pathway-analyse van de geïdentificeerde lncRNA's en mRNA's onthulde een associatie met ferroptose, een nieuw celdoodmechanisme dat betrokken is bij de ontwikkeling van kanker en therapeutische

reacties. Hierbij bevestigen onze resultaten de betrokkenheid van ferroptose in de pathofysiologie van glioblastoom. Daarnaast hebben we ook een aantal andere mogelijke biomarkers en/of therapeutische merkers gevonden die interessant zijn voor toekomstig onderzoek.

Concluderend, in deze thesis werden een aantal mogelijke epigenetische biomerkers gevonden voor zowel RICVD als glioblastoma. Deze biomerkers vereiesen echter nog verdere validatie, bijvoorbeeld door DMR methylatie/expressie profielen te correleren met cardiaal functionele data van patiënten. Daarnaast heeft de meta-analyse van publiek beschikbare gliblastoom dataset een aantal miRNAs/lncRNAs geïntificeerd die het startpunt kunnen zijn van vervolgonderzoek rond stralingsgeïnduceerde glioblastoom.

Chapter 1   **Introduction**

Magy Sallam[1,2], Mohammed Abderrafi Benotmane[1], Sarah Baatout[1,3], Pieter-Jan Guns[2], An Aerts[1]

[1] Radiobiology Unit, Institute for Environment, Health and Safety, Belgian Nuclear Research Centre (SCK CEN), Mol, Belgium.
[2] Laboratory of Physiopharmacology, University of Antwerp, Wilrijk, Belgium.
[3] Department of Molecular Biotechnology, Ghent University, Ghent, Belgium.

This chapter is adapted from the following publication:

1.1 Ionizing radiation (IR)

Radiation is defined as the emission and propagation of energy through space or matter [1]. Ionizing radiation (IR) refers to radiation with sufficient energy to remove an electron from the atoms of the receiving matter [2]. There are two main sources of IR: natural and artificial. *Natural radiation* occurs spontaneously as a result of the sun's cosmic radiation and the decay of naturally occurring radioactive substances such as uranium and radium. *Artificial radiation* is manmade and results from the utilization of IR in medical exposures, household equipment (e.g. smoke detectors) as well as in the nuclear industry [3].

IR can be generally sub-classified into electromagnetic (EM) and particle radiation. In EM radiation, energy is propagated using photons which possess dual particle and wave properties. As such, the magnitude of emitted energy increases with increasing frequency and decreasing wavelength [1]. Examples of EM radiation in the direction of increasing frequency and energy include radio waves, microwaves, infrared, visible light, ultraviolet light, X-rays, and γ-rays (**Figure 1-1**). EM radiation at or below the ultraviolet spectrum is nonionizing while therapeutic radiation mostly has wavelengths of 10^{-11} to 10^{-13} m [1]. On the other hand, examples of particle radiation include electrons, protons, α-particles, β-particles and heavy charged ions [4]. These particles are released from radioactive nuclides attempting to stabilize by releasing energy in combinations of γ-rays and particle radiation [2].
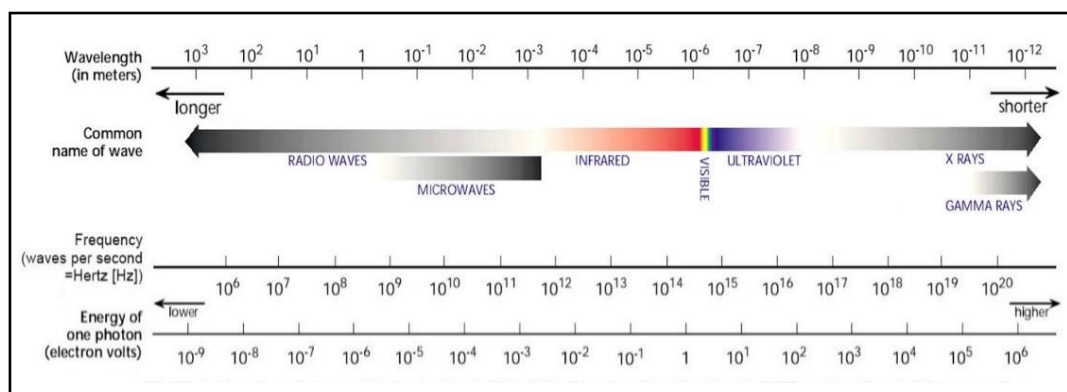
Figure 1-1 *Electromagnetic (EM) spectrum showing examples of EM radiation with EM waves having higher frequency (Hertz/Hz) and shorter wavelength (Meters/m) carrying the highest energy (electron volts/eVs, adapted from [5].*

1.1.1 IR uses in medicine

The diagnostic benefits of IR which rely on the distinct visualization of bone and soft tissue were introduced by Roentgen in the first radiograph of a hand [4]. This was followed by the discovery that X-rays could also kill living cells, and that the sensitivity for killing (radiosensitivity) varied from one cell type to another [6]. This radiosensitivity was shown by Bergonié and Tribondeau to be higher in immature cells and cells having high metabolism and proliferation such as cancer cells [7]. As such, IR was shown to be, and is still considered, a useful tool in cancer therapy with more than 50% of cancer patients receiving radiotherapy (RT) [8]. In modern radiation oncology, IR is administered by a device outside the body (external beam radiation therapy) or irradiation through radioactive material placement in the body near to cancer cells/tissue (brachytherapy) [9]. In addition, targeted molecular radiation therapy can be achieved using radiopharmaceuticals consisting of particle-emitting radionuclides chemically bound to a tissue specific vector molecules [10].

1.1.2 IR-induced tissue injury

The first recorded adverse effect of IR was experienced by Becquerel when he developed skin erythema and ulceration from a radium container left in his vest pocket [4]. Currently, adverse effects of IR are widely researched and can be classified according to the timeframe of their development to *early* or *late* effects. Early IR effects usually affect highly proliferative tissue such as bone marrow, epidermis or intenstinal tract muscosa and are observed during or shortly (up to 90 days) after irradiation. Early effects are predominantly caused by impairment of cell proliferation in these tissues causing progressive cell depletion. The presentation of these effects and their duration depends on the amount of radiation exposure [11,12]. However, these effects are normally completely repaired after medical IR doses. Late IR effects can occur in any tissue exposed to IR and represent a complex tissue reaction that is irreversible and progressive, with increasing severity occurring with longer follow-up times [12]. These effects, thus, significantly impact patients' lives, especially those whose life expectancy had been improved by IR [8].

As such, this PhD thesis is part of Horizon 2020 project MEDIRAD (http://www.medirad-project.eu/) which aims to better understand the health effects of IR exposure from diagnostic and therapeutic imaging and from off-target effects in RT [13]. This aim is achieved through the integration of six interdependent work packages (WPs), of which our present work is situated in 2 WPs. The first, WP4, focuses on breast cancer RT and secondary cardiovascular risks. The other, WP5, addresses the possible cancer risk following IR exposure in childhood and adolescence and studying the role of influencing factors such as age, genetic and epigenetic variants.

Our research on radiation-induced cardiotoxicity focuses on characterizing epigenetic alterations after IR in heart-irradiated rats and breast cancer patients receiving adjuvant RT. This research is planned to be integrated with classical cardiovascular biomarker measurements, noncoding microRNA profiling and cardiac function assessments performed by MEDIRAD partners. In this manner, WP4 aims to elucidate the mechanisms behind IR-induced cardiac effects and identify relevant associated biomarkers.

In WP5, the initial research plan was altered due to administrative delays, partly due to COVID-19, which hindered sample collection at MEDIRAD partners. Consequently, we opted to identify epigenetic players that are dysregulated in different transcriptomic datasets of glioblastoma tissues.

In the following paragraphs, we introduce IR's cellular and epigenetic effects in order to explore the epigenetic involvement in IR-induced adverse effects.

1.1.3 Cellular effects of IR

1.1.3.1 *How does IR interact with matter?*

IR can have different interactions with matter depending on its energy as follows:

Classic coherent scattering occurs when the incident photon is entirely absorbed by the atom with excitation and release of absorbed energy as a photon of equal energy scattered in a different direction, thereby resulting in a change in photon direction without change in its energy (**Figure 1-2A**). Classic scattering occurs primarily at energies below 10 keV and is therefore minor in medical diagnostic or therapeutic radiation.

Photoelectric interaction occurs when the incident photon strikes an electron in the inner shell leading to its ejection from the nucleus (**Figure 1-2B**). The electron is then referred to as a photoelectron which leaves behind a positively charged (excited) atom. Outer shell electrons then transition to fill the empty spots on the inner shells leading to the release of energy as X-rays. Photoelectric interaction depends on the energy of the incident photons occurring mainly at energies less than 100 keV and is the most common interaction in diagnostic radiation. The probability of photoelectric interaction also depends on the atomic number of the impacted tissues and thus varies from one tissue to another (e.g. soft tissues vs bone tissues).

Compton scattering occurs when the incident photon strikes an electron in the outer shell leading to its ejection using only a portion of its energy (**Figure 1-2C**). The remaining energy proceeds as a lower energy photon in a different direction than that of the parent photon. The ejected outer shell electron continues to travel until it combines with matter while the lower energy photon continues to interact with matter through further Compton or photoelectric interactions. Compton scattering predominantly occurs in the energy range of 0.1–10 MeV, is independent of the atomic number of impacted material and is the most common interaction in RT.

Pair production occurs when the incident photon interacts with the atom's electromagnetic field leading to its disappearance and the creation of two oppositely charged particles (a positron and a negatron) possessing equal energy which is equal to half the energy of the incident photon (**Figure 1-2D**). These particles proceed to ionize matter until the positron interacts with an electron destroying it and producing two photons of opposing directions. Pair production occurs only if the energy of the incident photon is ≥ 1.022 MeV which occurs in RT with high-energy photon beams. Pair production occurrence also increases with increasing atomic number of impacted matter.

Photodisintegration occurs when the incident photon interacts directly with the nucleus of the atom thereby exciting it with the release of a nuclear fragment (**Figure 1-2E**).

Photodisintegration requires very high energy photons to occur (10 MeVs) and is therefore not relevant to diagnostic or therapeutic radiation.
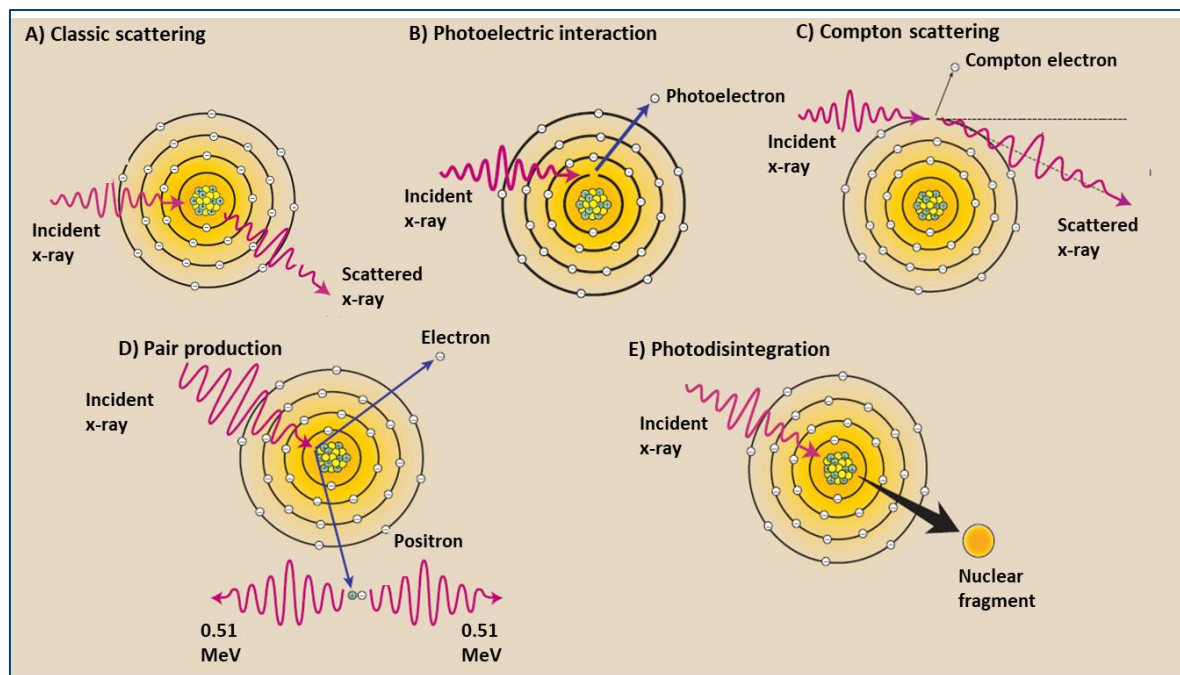
Figure 1-2 *IR's interaction with matter, adapted from [14].*

1.1.3.2 *Direct/indirect cellular effects of IR*

IR's interaction with cells affects them in two ways: *direct* and *indirect* effects. Direct effects of IR are caused by direct ionization and damage of cellular molecules, most importantly DNA. Indirect effects of IR are caused by radiolysis of the water molecules which compose 80% of the cell [7,15]. This results in the production of two ions (H^+ and OH^-) and two free radicals ($H^•$ and $OH^•$). The ions can either reform the water molecule or interact and damage cell macromolecules e.g. DNA thereby forming DNA radicals. These radicals can also undergo spontaneous repair by interacting with water molecules and thereby producing more reactive radicals. Most indirect IR effects are mediated by $OH^•$ and H_2O_2 which are often termed reactive oxygen species (ROS). Cellular damage may also occur as a result of other free radical species such as reactive nitrogen species (RNS) [16,17]

The attacks of these free radicals on DNA can result in single stranded or double stranded breaks in the DNA structure (SSBs and DSBs, respectively). SSBs, as the name suggests, are breaks in a single strand of DNA. These are normally easily repaired using the other DNA

strand as template. If repair is done inaccurately, mutations may occur which can affect gene transcription. On the other hand, DSBs involve breaks in both strands of DNA which result in the chromatin structure snapping open [4]. Consequently, DSBs are considered the most lethal of all free radical attacks whose improper repair can lead to chromosomal abnormalities which may induce cell death [2,12]. IR can also induce DNA inter-strand crosslinks, DNA base modifications such as oxidation, alkylation, deamination as well as loss of the nucleotide base producing apurinic or apyrmidinic sites; either of which capable of developing to SSBs and/or DSBs [2,18–20].

IR-induced damage can be modified by factors related to radiation itself or the target tissue. IR-related factors include the linear energy transfer (LET) of radiation, total radiation dose as well as the mode of administration (single dose or fractionated) of IR. The LET of IR is dependent on the energy transferred to the tissue by IR per unit tract length, which affects whether IR induces direct or indirect effects in the cells. Simply, more charged, slower moving protons (10 keV/μm) and α-particles (>100 keV/μm) have higher LET thereby causing direct cell damaging effects to tissues whereas lesser charged, faster moving X-rays and γ-rays ($\cong$1 keV/μm) induce cell damage in a mostly indirect manner [21,22]. Alternatively, fractionation is beneficial in reducing radiation damage especially to normal tissues as it allows for a better chance of cellular repair [11]. The primary tissue related factor affecting IR-induced damage is the radiosensitivity of irradiated cells. As stated by the law of Bergonié and Tribondeau, the degree of radiosensitivity of a biological tissue is dependent on its growth and metabolic rates as well as its degree of differentiation. Thus, lymphocytes, spermatogonia and intestinal crypt cells with their high replication rates are more sensitive to radiation than slow/non replicating neurons, muscle and parathyroid cells [7]. This also explains the rationale by which cancer cells with their uncontrolled growth are killed using IR [23]. Other tissue related factors include predisposing mutations or intrinsically radiosensitive genetic profiles, the repair capacity of irradiated cells, the stage of cell cycle -pre-mitosis G2 phase being the most sensitive- and degree of tissue oxygenation. The degree of tissue oxygenation is a representation of the so-called oxygen effect whereby oxygen availability affects cell damage [11]. Oxygen present in the

12

irradiated cells can combine with DNA radicals to form more damaging peroxy radicals ($RO_2 \cdot$) which are capable of causing more cellular damage [24]. Consequently, IR's cellular damage is enhanced by oxygen with improved cell killing which is especially relevant in cancer RT.

1.1.3.3 *Cellular repair in response to IR*

DNA damage induced by IR is sensed by the DNA damage response (DDR) (**Figure 1-3**) which causes temporary or permanent blocks in the cell cycle at cycle checkpoints, activates DNA repair pathways and, in case of irreparable damage, induces apoptosis of damaged cells [12,25,26]. Cells repair SSBs by base/nucleotide excision repair (BER/NER) where the damaged base/nucleotide is excised and the resulting gap is filled by repair replication using the complementary DNA strand as a template [27]. On the other hand, cells repair DSBs by either homologous recombination (HR) or non-homologous end joining (NHEJ). The choice of repair pathway for DSBs is related to the stage of the cell cycle (presence of sister chromatid as template) and the location of the DSBs [27,28]. For HR, physical contact with the undamaged chromatid (serving as a template) is necessary for repair. First, processing of the double-strand DNA ends into 3' DNA single-strand tails occurs. Then, HR initiates filling in the gaps using the undamaged sister chromatid as template. Alternatively,
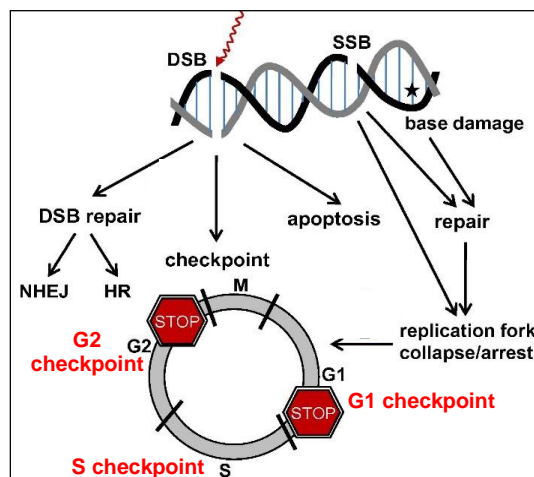
Figure 1-3 DNA damage response (DDR) following IR showing possible cell fates after base damage, single strand (SSBs) and double strand breaks (DSBs), adapted from [19].

NHEJ does not necessitate the presence of a sister chromatid, the damaged ends are only modified and ligated together regardless of homology. Consequently, NHEJ is error prone and can generate deletions or insertions thereby accounting for many of the pre-mutagenic lesions induced by IR [4,18].

1.1.4 Biological effects of IR

Biological effects of IR are usually classified as either *stochastic* or *deterministic*. Stochastic effects occur when cells survive IR-induced DNA damage but with mutation in their DNA [29]. Stochastic, in its definition, means random as in the manifestation and severity of the effect is independent of IR dose. However, the risk of stochastic effects seems to increase with increasing dose with no apparent threshold. Consequently, stochastic effects are regarded the primary health risk of radiation doses less than 100 mGy e.g. radiation-induced carcinogenesis and heritable effects which occur if the mutation occurs in a germ cell [30]. Deterministic effects are determined by IR dose which needs to be sufficiently high to cause cell killing. Thus, these effects only occur after a certain threshold dose is exceeded with effect severity being proportional to IR dose such as in radiation-induced cataracts [29,30]. Other factors influencing deterministic effects include volume of irradiated tissue, dose rate, type and quality of the radiation, concomitant physical trauma, presence of other disease conditions and individual susceptibility [31].

According to this, the conventional paradigm of radiobiology serves as a reference framework which states [32,33]:

- DNA damage in directly exposed cells is the main cause behind biological effects
- DNA damage occurs during, or very shortly after, irradiation of the nuclei in targeted cells
- The potential for biological consequences can be expressed within one or two cell generations
- At low doses, the biological effect is in direct proportion to the energy deposited in DNA.

14

Certain observations have challenged this conventional paradigm such as non-linear IR effects including bystander effects and genomic instability as well as radiation-induced epigenetic effects (RIEEs). Bystander effects are those observed in cells not directly traversed by radiation while genomic instability occurs in the genome of the progeny of irradiated or bystander cells [32]. On the other hand, RIEEs involve alterations in the epigenetic machinery of the cell and will be discussed in detail in the coming paragraphs.

1.2 Radiation as an epigenetic modifier

RIEEs were identified as early as the 1980s when ^{60}Co γ-radiation was shown to cause a dose-dependent decrease in DNA methylation levels (termed hypomethylation) in four cell lines [34]. In order to fully understand RIEEs, a brief introduction of epigenetics is provided in the following sections. Special focus is given to DNA methylation and noncoding RNA as they are the main investigational targets of the thesis.

1.2.1 Epigenetics explained

The term 'epigenetics' was first coined in 1942 by Conrad Waddington while examining cellular differentiation and its regulation by what he referred to as an 'epigenetic landscape'. Later, this definition was altered to *"The study of changes in gene function that are heritable and that do not entail change in DNA sequence"* [35,36]. Epigenetic alterations involve histone modifications, changes in DNA methylation, and the involvement of microRNAs (miRNAs).

1.2.1.1 *Histone modifications*

Genomic DNA is negatively charged at physiologic pH. In order to compact DNA into the limited nuclear space, DNA is wrapped around histone proteins by attraction to their positively charged amino acid residues (lysine and arginine). Thus, DNA is wrapped (in 147 nucleotides segments) around histone octamers (two copies of H2A, H2B, H3 and H4 histone proteins) forming nucleosomes which are connected together via linker DNA to form chromatin (**Figure 1-4**) [35].
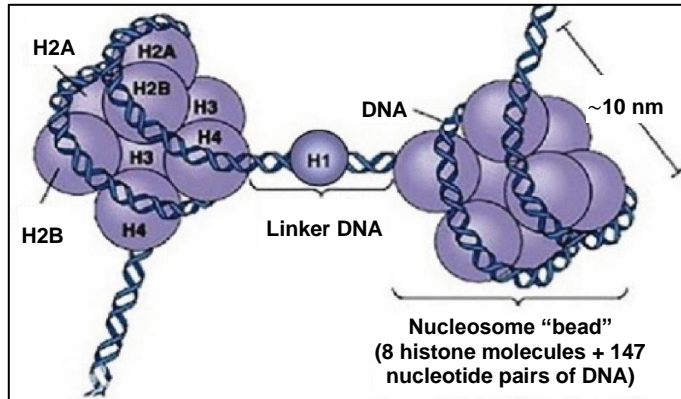
Figure 1-4 *Nucleosome structure consisting of a 147 nucleotide-long DNA sequence wrapped around a histone octamer core. Linker DNA connects adjacent nucleosomes, adapted from [37].*

Several histone post-translational modifications have been identified such as acetylation, methylation, phosphorylation, ubiquitinylation, sumoylation, ADP ribosylation, deamination, succinylation and butyrylation [38]. These modifications occur on the N-terminal tail of the histones which face outwards from the nucleosome and can influence how the nucleosome interacts [39]. For example, acetylation by histone acetyltranferases adds an acetyl group to the histone tail. As the acetyl group is positively charged, it disrupts the electrostatic interaction between histones and DNA. Consequently, histone acetylation has been associated with the open chromatin (euchromatin) structure while deacetylation by histone deacetylases is usually associated with the condensed chromatin (heterochromatin) structure [40]. Histone modifications have been linked to the pathophysiology of several diseases such as Huntington's disease, autoimmune diseases, diabetic kidney disease and cancer [41–44].

1.2.1.2 *DNA methylation*

DNA methylation involves the methylation of a cytosine base in a CpG dinucleotide leading to the formation of 5-methyl cytosine (5-mC). DNA methylation is essential for several genomic events such as silencing of transposable elements, genomic imprinting and X-chromosome inactivation [45].

The majority of CpG dinucleotides in the human genome are heavily methylated ($\cong$70%) while the rest are unmethylated and mainly part of so called CpG islands or CGIs. CGIs are defined as regions of DNA (>200 bps) that have a GC content higher than 50%, lack

methylation and consequently are not transcriptionally silenced [46]. This high content of CpGs in CGIs allows for DNA methylation-mediated regulation of gene expression. About 70% of gene promoters are associated with these CGIs and around 50% of these CGIs contain transcription start sites [47].

Non-promoter CGIs can be found in inter- and intragenic sequences and are likely to represent either alternative transcription start sites of protein coding genes or noncoding RNAs [48]. In fact, it was noticed that intragenic or gene body CGIs that are present in actively expressed genes show increased DNA methylation. This has been explained by multiple theories including gene body CGI's ability to block transcription at intragenic promoters, affect intragenic repetitive element activity and alter mRNA splicing by destabilizing nucleosomes at intron-exon junctions [49]. Other important methylation targets are CGI shores. These so-called CGI shores are regions having a lower CpG density than that of CGIs and can be found within $\cong$ 2kb of CGIs. Methylation of these CGI shores has also been linked to transcriptional silencing with special importance in tissue-specific differential methylation [50].

There are 3 main key players in the process of DNA methylation; methylation *writers*, *readers* and *editors*.

1.2.1.2.1 The writers

Historically, DNA methylation can be classified into two main types: *De novo methylation* which occurs mainly in the developing embryo and *maintenance methylation* which maintains the methylation patterns from the parent strand in the daughter strand during replication. Consequently, DNA methylation is an epigenetic pattern that is maintained in cellular progeny and is normally stable in non-dividing cells [51,52].

DNA methylation is carried out by the action of DNA methyltransferases or DNMTs causing transfer of a methyl group from S-adenyl methionine (SAM) to the 5th carbon of the pyrimidine ring of cytosine [53]. The DNMTs that methylate previously non-methylated cytosines thereby causing 'de novo' methylation (**Figure 1-5A**) are DNMT3-a & b whereas DNMT1 is the maintenance methyltransferase. Consequently, DNMT1 predominantly methylates hemi-methylated CpG dinucleotides and exhibits lower levels as cells reach

terminal differentiation [52,54,55]. To do this, DNMT1 is located at the replication fork and methylates newly synthesized DNA strands directly (**Figure 1-5B**) [52].

Another DNMT3 family member is the DNMT3 like (DNMT3l) which is incapable of individual methyltransferase activity but does increase the activity of DNMT3a and 3b by up to threefold [52].

Normally, the three major types of DNMTs (DNMT3a, DNMT3b and DNMT1) are active in the growing embryo with their levels decreasing after reaching cellular terminal differentiation. Their presence in the mature mammalian brain remains quite substantial which could indicate an importance for neuronal plasticity [54,56].

Non-CpG methylation can also occur on cytosines not followed by guanosine. This was found in pluripotent stem cells, oocytes, neurons, and glial cells and has been shown to be mediated by DNMT3a and b. Non-CpG methylation is nearly absent from adult somatic cells and accounts for only 0.02% of the overall 5-methylated cytosines (5-mCs) in somatic cells [57].
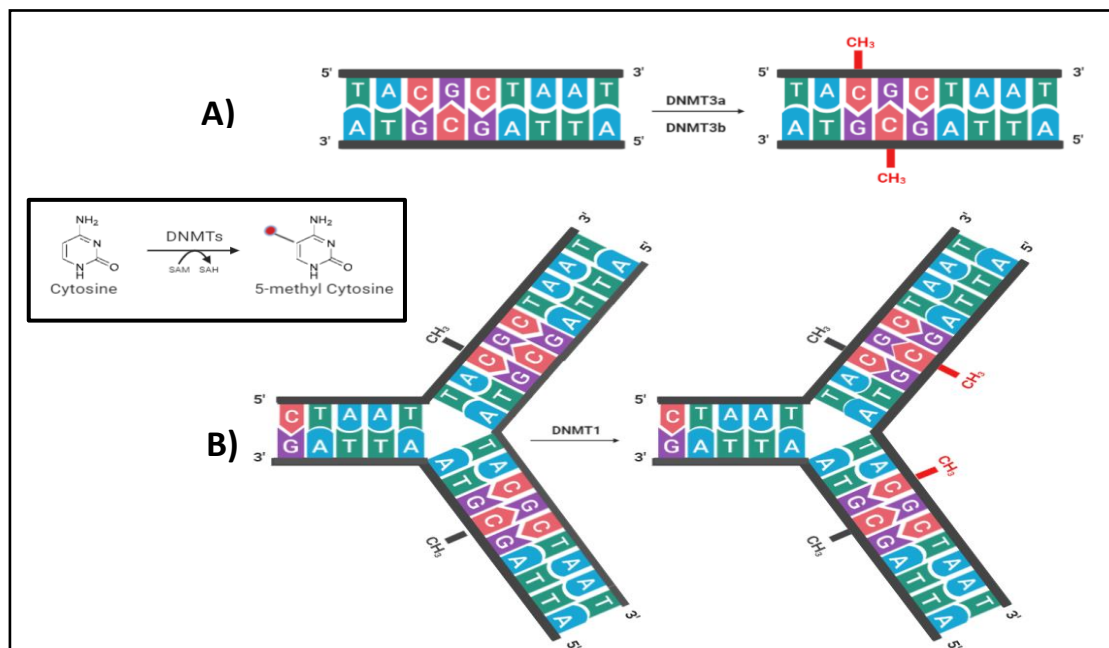
Figure 1-5 The writers of DNA methylation. DNMTs transfer a methyl group from SAM to the 5th carbon of cytosine. A) De novo methylation process mediated by DNMT3a and DNMT2b. B) Maintenance methylation process during DNA replication by DNMT1 present at the replication fork on hemimethylated DNA. DNMT: DNA methyltransferase, SAM: S- adenyl methionine, SAH: S-adenyl-L-homocysteine.

1.2.1.2.2 The readers

How does a cell interpret the methylation of promoter CpG islands as transcriptional repression?

Through DNA methylation-alterations in the binding affinity of transcription factors [58]. The hypothesized mechanisms for these alterations include either direct blockade of transcriptional activators from their DNA binding sites by the methylated DNA (steric hindrance) or methylated DNA recognition by methyl-CpG-binding proteins (MBPs). These MBPs then act as DNA methylation readers and recruit co-repressor molecules to silence transcription [55].

The reader proteins can 'read' the code –methylation- and convert it into functional silencing of the affected genes. Normally, this conversion includes an interaction with chromatin modifiers [58]. The MBP proteins are then able to convert DNA methylation to transcriptional repression by recruiting histone modifying and chromatin remodeling protein complexes. This interaction ultimately leads to the conversion of chromatin from the transcriptionally active and loosely packed euchromatin form to the transcriptionally repressed and tightly packed heterochromatin form (**Figure 1-6**).
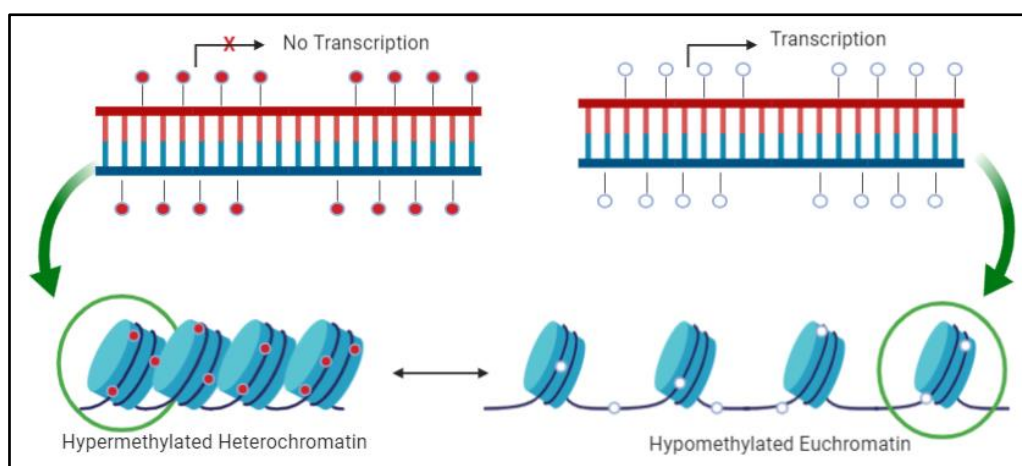
Figure 1-6 Schematic figure of DNA methylation effects on chromatin state. DNA methylation represses gene expression by steric hindrance of transcription activator binding and MBP recruitment. DNA methylation also induces histone modification from loosely packed euchromatin to tightly packed heterochromatin by MBP-induced recruitment of histone deacetylases as well as direct interaction between DNMTs and histone methylases. Abbreviations: MBP: Methyl-binding protein, DNMT: DNA methyltransferase.

1.2.1.2.3 The editors

DNA methylation is a reversible process and DNA can also be demethylated either passively or actively. Passive demethylation occurs by inhibition of -or reduction in- DNMT levels. This leads to a loss of 5-mC during successive rounds of replication in the absence of functional DNMTs to maintain methylation [59]. Active demethylation involves the modification of the methyl group of 5-mC by enzymatic action and subsequent restoration of the non-methylated cytosine by DNA repair. The enzyme families involved in methyl group modification are the ten-eleven translocation (TET) family and the activation-induced cytidine deaminase (AID) and apolipoprotein B mRNA editing enzyme, catalytic polypeptide-like (APOBEC) family. The TET enzyme family modifies methylated cytosines by hydroxylation and further oxidation, while the AID/APOBEC family deaminates 5-mC. Then, a family of BER glycosylases repairs the DNA by replacing the intermediates produced by the enzyme modification with cytosine [59,60].

One intermediate metabolite formed during active demethylation, 5-hydroxymC, has also been shown to be a stable regulator of gene expression most abundant in the central nervous system [61]. The presence of 5-hydroxymC at promoters, gene bodies and enhancers is associated with transcriptional activation [62]. 5-hydroxymC also shows a particular affinity to lineage-specific transcription factor binding sites thereby suggesting a connection to tissue-specific transcriptional differences [63]. Interestingly, alterations in DNA hydroxymethylation have been associated with cardiac hypertrophy in mice as well as coronary atherosclerosis in elderly coronary heart disease and carotid atherosclerosis patients [64–66]. In addition, several studies reported DNA hydroxymethylation alterations in response to radiation [67–70] which were also found to be dose-dependent [67]. As such, future research might reveal a contribution of DNA hydroxymethylation to early and late radiation-induced effects.

1.2.1.3 Noncoding RNA

Noncoding RNAs (ncRNA), as the name suggests, are RNA transcripts that are not translated into proteins. NcRNAs are classified according to their function into housekeeping and regulatory ncRNAs. Housekeeping ncRNAs are constitutively expressed RNA species that

are necessary for cell viability. Examples include ribosomal RNA (rRNA), transfer RNAs (tRNA), small nuclear RNAs (snRNAs), small nucleolar RNAs (snoRNAs) and telomerase RNAs [71]. Regulatory ncRNAs are divided into two categories according to their size: short or small ncRNA (18-200 nucleotides) and long ncRNA (>200 nucleotides). Small ncRNAs (sncRNAs) include small interfering RNAs (siRNAs), miRNAs and piwi-interacting RNA (piRNAs) [72,73]. Some ncRNAs possess variable length and thus belong to two classifications at the same time. Examples include promoter-associated transcripts (PATs), enhancer RNAs (eRNAs), and circular RNAs (circRNAs) [71].

1.2.1.3.1 Small ncRNAs (SncRNAs)

Both siRNAs and miRNAs are sncRNAs which play essential roles in the RNA interference (RNAi) pathway. RNA interference (RNAi) refers to sequence homology-dependent gene silencing mechanisms initiated by RNAse III endonuclease (Dicer)-mediated production of siRNAs and miRNAs (**Figure 1-7**) [74]. SiRNAs are 20-30 nucleotide long double-stranded RNA molecules produced by the action of Dicer on double stranded RNA structures. Dicer then assists in loading siRNAs onto an argonaute (AGO) protein (AGO2 in mammals) then the siRNA binds to a complementary mRNA which is cleaved by AGO2 [75]. On the other hand, miRNA biogenesis starts with primary miRNAs (pri-miRNAs) transcribed by RNA polymerase II. These pri-miRNAs carry stem loop structure(s) that are released to form precursor miRNAs (pre-miRNAs) by the action of the nuclear microprocessor complex composed of Drosha and DGCR8. These pre-miRNAs are then transported to the cytoplasm to be cleaved by Dicer into a miRNA duplex which binds to an AGO protein to form the core of miRNA-induced silencing complexes (miRISCs) which bind to partially or fully complimentary mRNA sequences [75,76]. Fully complimentary mRNAs are broken down by AGO2. However, when the mRNA targets are only partially complimentary to miRNAs, cleavage by AGO proteins is not possible. In these instances, AGO proteins recruit other proteins which then mediate silencing by a combination of translational repression, deadenylation, decapping and mRNA degradation [77].

MiRNAs are the most abundant sncRNAs. They also have the capacity to bind and silence hundreds of different mRNAs thereby regulating more than half of the protein coding genes

in humans [77,78]. As such, miRNAs have been considered a research hotspot in recent years.
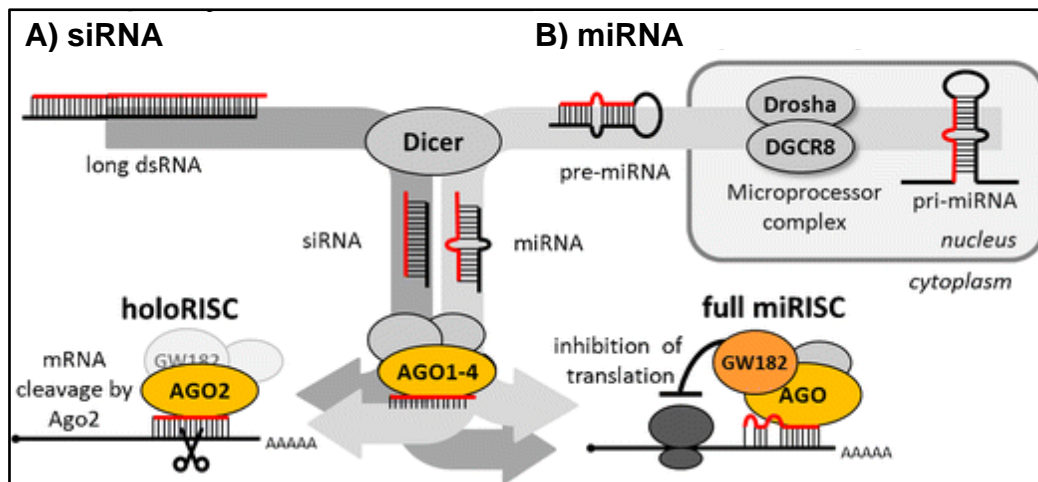
Figure 1-7 *Overview of siRNA (A) and miRNA (B) production as part of RNAi pathway. SiRNAs are produced by Dicer from long double stranded RNA while miRNAs are produced from pre-miRNA precursors. Both siRNAs and miRNAs exert their silencing effects by binding to Argonaute (AGO) proteins to form RNA-induced silencing complexes (RISCs) which mediate translational repression, adapted from [75].*

Alternatively, piRNAs are 24-32 nucleotides long and are enriched in the germline where they bind to PIWI proteins [79]. PiRNAs in most organisms originate from long single-stranded precursors transcribed from piRNA clusters. These precursors are then transported out of the nucleus, cleaved by Zucchini endonuclease (Zuc) to pre-piRNAs which are loaded onto PIWI proteins where they are trimmed and methylated at the 3' end to produce primary piRNAs. Through a so-called ping-pong cycle, secondary production of large amounts of piRNAs is mediated by AGO and AUB proteins [80]. Together with PIWI proteins, piRNAs function to silence transposable elements (TEs) in the germ line as TE can disrupt and alter the genome if their transposition is not controlled [81].

1.2.1.3.2 Long ncRNAs (LncRNAs)

Based on their location with respect to protein coding genes (PCGs), long ncRNAs (lncRNAs) can be divided into five classes: 1) Long intergenic ncRNAs: transcribed from both strands in intergenic regions; 2) Long intronic ncRNAs: transcribed from PCG introns; 3) Sense lncRNAs: transcribed from the sense strand and containing exons of PCGs; 4) Antisense lncRNAs: transcribed from the antisense strand and 5) Bidirectional lncRNAs which are localized proximally to a PCG on the opposite strand [71,82]. LncRNAs can also be classified

according to their regulatory effects on DNA sequences to cis-lncRNAs which regulate close by genes and trans-lncRNAs which regulate distant genes [83].

LncRNAs regulate gene expression at the transcription phase through a number of mechanisms. First, lncRNAs can function as chromatin regulators by recruiting chromatin-remodeling complexes such as polycomb repressive complex 2 (PRC2) which catalyzes histone H3 methylation at gene promoters leading to gene silencing (**Figure 1-8A**). In addition, some lncRNAs can bind to chromatin-activating complexes thereby inducing gene expression [84,85]. Second, lncRNAs can function as scaffolds coordinating the activity of repressive histone modifying complexes (**Figure 1-8B**) [86–88]. Third, lncRNAs can regulate gene transcription by modifying transcription factor activity or providing steric hindrance to transcription (**Figure 1-8C**) [89]. Finally, lncRNAs can limit the availability of regulatory factors, e.g. transcription factors (TFs), by acting as decoy binding sites thereby preventing the regulatory factors binding to their targets (**Figure 1-8D**) [90,91].
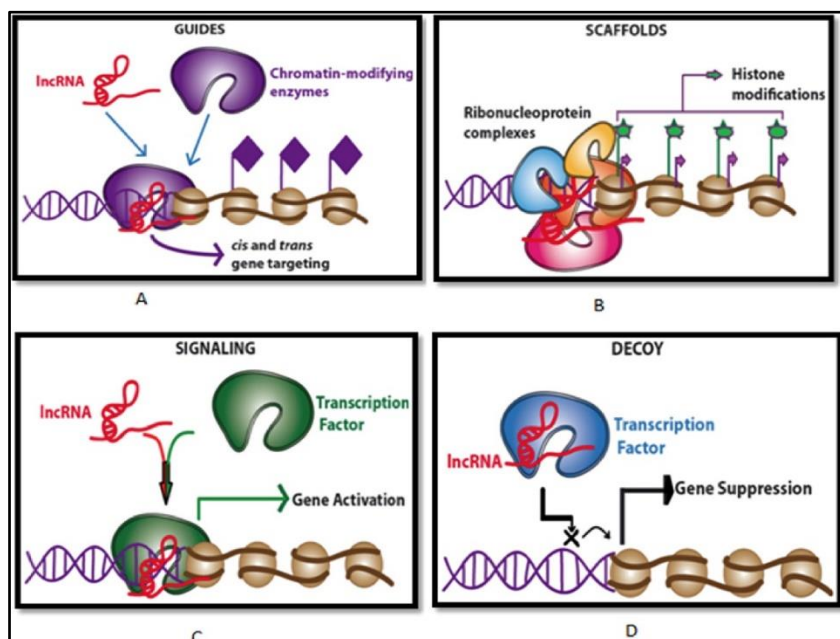
Figure 1-8 LncRNA-mediated transcriptional regulation of gene expression. A) LncRNAs can recruit chromatin-remodeling complexes thereby regulating the accessibility to certain gene. B) LncRNAs can act as scaffolds for coordinating the activity of repressive histone modifying complexes. C) LncRNAs can regulate transcription by transcription factor (TF) recruitment as well as blocking the binding of other TFs. D) LncRNAs can act as decoys which bind to TFs thereby preventing their interaction with their relevant targets [85].

LncRNAs can also regulate gene expression at a post transcriptional level. LncRNAs interact with splicing regulator proteins to regulate gene alternative splicing [92,93]. LncRNAs can also interact with miRNAs to activate or repress gene expression. This is achieved by lncRNAs serving as either biogenic miRNA precursors or miRNA-sponges/competitive endogenous RNAs (ceRNAs) which bind miRNAs and block their effects [94–97]. Finally, lncRNAs can directly interact with mRNAs to increase their stability or mediate their decay [98–101].

1.2.2 Radiation-induced adverse effects from an epigenetic viewpoint

Research has shown that IR can induce alterations in global and gene specific DNA methylation [32,34,102–106], histone modifications [107–112] as well as alterations in noncoding RNA levels especially miRNAs [113–118]. However, research regarding radiation-induced epigenetic modifications in the context of radiation-induced toxicities or secondary cancers is underexplored. Consequently, under the framework of MEDIRAD, our current research explores the epigenetic profile of **radiation-induced cardiotoxicity** after breast cancer RT and the ncRNA profile of glioblastoma as a possible **radiation-induced secondary cancer.**

1.2.2.1 *Radiation-induced cardiovascular disease*

Radiation-induced cardiovascular disease (RICVD) is one of the main long-term effects of breast cancer RT [119]. Breast cancer is the leading cause of global cancer incidence, with as many as 2.3 million new cases diagnosed in 2020. Given that breast cancer has a high survival rate (79%-93%), minimizing long-term adverse effects of cancer treatment is at the forefront of a clinician's concerns [120]. The standard radiation dose used for local and/or regional adjuvant irradiation in breast cancer is 50 Gy in 25 fractions of 2 Gy with a boost dose of 10–16 Gy in 2 Gy single doses [121]. A radiation boost is administered to deliver a radiation dose to the initial tumor site where 44-90% local recurrence occur in or near [122].

As a result of RT, incidental irradiation of important tissues in proximity to the affected breast, such as the heart, occurs [123]. Previously, the heart was considered insensitive to

radiation doses less than 30 Gy in accordance to the law of Bergonié and Tribondeau due to its non-dividing tissues [124,125]. In 2013, Darby et al. reported a linear relationship between the mean heart dose (MHD) and the rate of major coronary events in women receiving breast cancer RT with no safe dose threshold (7.4% increase in rate per Gy) (**Figure 1-9**) [126]. Due to the high survival rate of breast cancer, the late manifestations of RICVD are the primary cause of mortality in breast cancer survivors [127–129].

Risk factors for the development of RICVD strongly overlap with conventional CVD risk factors such as diabetes, hypertension, obesity, smoking, chronic obstructive pulmonary disease and hypercholesterolaemia. Additionally, therapy-dependent factors such as the cumulative dose from RT, chemotherapeutic administration (e.g. anthracyclins) and regular analgesic use represent additional risk factors [126,130]. Interestingly, a significantly higher rate of major coronary events was observed in irradiated left-sided breast cancer patients over their right-sided breast cancer counterparts [126]. This difference only seemed to increase with passing time since radiation and could be explained by the higher MHD of left sided breast cancer [123,126,131].
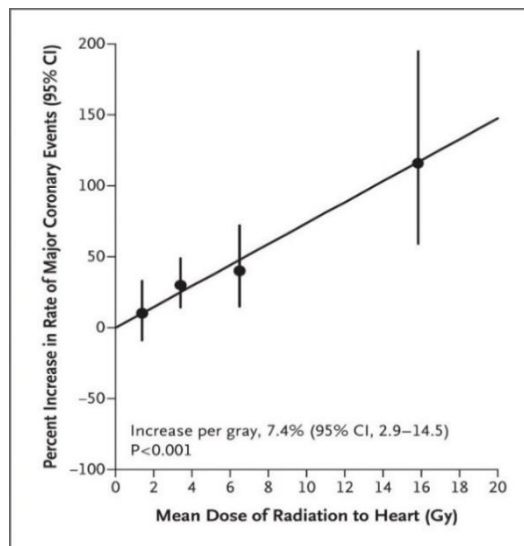
Figure 1-9 Rate of major coronary events according to mean heart dose (Gy), as compared with the estimated rate with no radiation exposure to the heart as shown in [126].

As there are currently no clinical means of reversing RICVD, guidelines recommend intensive screening and management of cardiovascular risk factors in patients [132]. This

initial screening includes risk factor identification, comprehensive clinical examinations and a baseline transthoracic echocardiography before RT, with yearly monitoring and clinical exams after RT [132]. Currently, no blood or imaging biomarkers have been implemented in practice for predicting RICVD risk or detecting subclinical disease [133]. Therefore, there is a growing interest in biomarkers for identifying and monitoring at-risk patients. Moreover, such biomarkers might also help validate the findings of preclinical trials showing the beneficial effects of statin, ACE inhibitor and aspirin administration in the setting of RICVD [134–136].

1.2.2.1.1 RICVD manifestation

RICVD can manifest in different ways: coronary heart disease, pericarditis, cardiomyopathy and valvular heart disease which share the element of fibrosis in both acute and chronic phases [137] (**Figure 1-10**). These manifestations can occur 5-30 years after RT completion with up to 88% of patients remaining asymptomatic [130].

Radiation-induced coronary heart disease presents as atherosclerosis with complex interplay of lipid accumulation, local inflammation, smooth muscle cell proliferation and formation of atherosclerotic plaques. Stable atherosclerotic plaques may narrow the lumen and hamper blood flow, while rupture of unstable plaques may cause a total occlusion of blood flow through thrombosis, leading to myocardial infarction. The risk of developing radiation-induced coronary heart disease is dose dependent, increases within the first 5 years after irradiation and continues for at least 20 years. Radiation-induced coronary heart disease is particularly important when considering RICVD as it can develop at doses well below than 10% of the tolerance dose of other cardiac tissues (e.g. 36-40 Gy MHD for the pericardium and 40 Gy for the myocardium) with the risk increasing with dose increase [126,138,139].

Radiation-induced pericardial disease describes a state of inflammation of the pericardium surrounding the heart. It can have either an acute or delayed onset with symptoms occurring immediately or months to years after RT. The tolerance dose of the human pericardium is estimated to be a MHD higher than 36 or 40 Gy or a dose of 50 Gy

administered to more than 30% of the heart [138]. Consequently, due to current radiation-sparing techniques, acute radiation-induced pericardial disease is extremely rare while chronic pericardial disease incidence dropped from 20 to 2.5% [138].

Radiation-induced valvular disease risk is dose dependent and has a relatively delayed onset, occurring in certain cases 20 years after RT. It leads to endocardial fibrosis which starts by thickening and calcification of the valvular endocardium [140,141]. Radiation-induced valvular disease was reported to occur in 81% of patients receiving more than 35 Gy to the heart [137].

Radiation-induced cardiomyopathy presents with myocardial fibrosis, systolic and diastolic dysfunction, conduction disturbances and autonomic dysfunction leading to impaired left ventricular ejection fraction (LVEF). Radiation-induced cardiomyopathy most commonly occurs secondary to preexisting valvular or pericardial disease [138]. While LVEF is insensitive to subclinical cardiomyopathy, asymptomatic myocardial perfusion defects have been detected as early as 6 months after breast cancer RT [142,143].
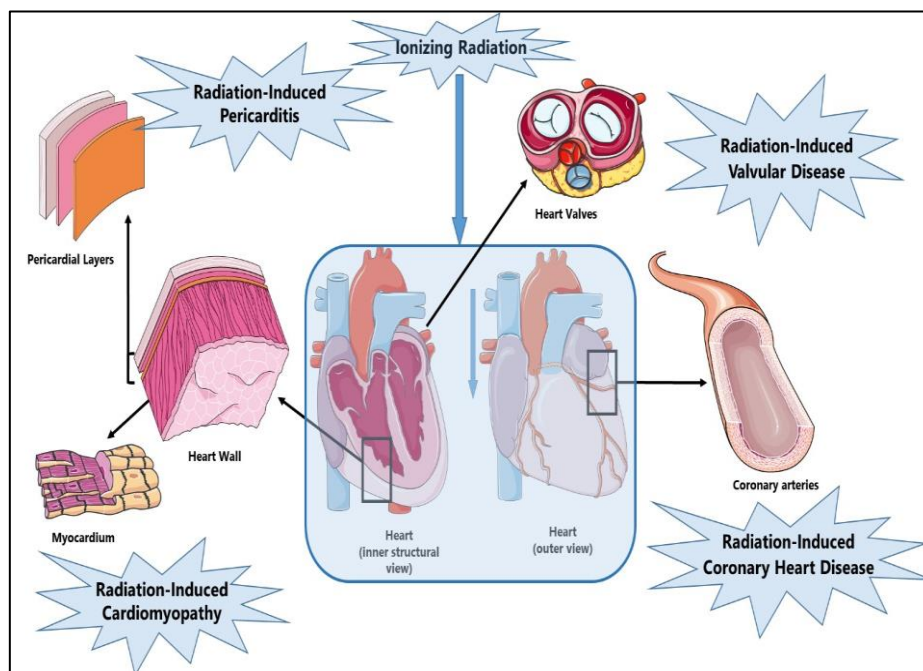
Figure 1-10 RICVD clinical presentation

1.2.2.1.2 RICVD pathophysiology

Several hypothesized mechanisms underlying RICVD have been described in literature [138,139,144–148], the first being *endothelial activation to a pro-inflammatory state* by nuclear factor kappa b (NF-κB). NF-κB is induced by ROS and DSBs produced by IR as well as by damage-associated molecular patterns (DAMPs) released from stressed or dying cells. NF-κB activation stimulates the expression of various pro-inflammatory cytokines (e.g. Interleukins 1 & 6 and tumor necrosis factor alpha (TNF-α)), chemokines (e.g. Monocyte chemoattractant protein-1 or MCP-1), cell adhesion molecules (e.g. Vascular cell adhesion molecule 1 or VCAM-1 and E-Selectin) and matrix metalloproteinases, leading to an activated pro-inflammatory endothelium. Another hypothesized mechanism is *vascular tone deterioration* due to ROS-induced decreased nitric oxide (NO) availability, decreased vasodilating prostacyclin and increased vasoconstrictive endothelin-1 and angiotensin-II levels. Another mechanism involves the formation of *a pro-coagulative and pro-thrombotic endothelial cell phenotype*. This leads to atherosclerotic plaque formation via stimulation of lipid aggregation and release of pro-fibrotic cytokines e.g. TGF-β. These plaques can then rupture resulting in thrombosis. Endothelial cell damage can also lead to the secretion of von Willebrand factor (vWF), platelet-activating factor and tissue factor while reducing thrombomodulin and prostacyclin production. Together, these factors lead to increased platelet aggregation and thrombus formation.

Cell death and premature endothelial senescence is also a suggested RICVD mechanism involving activation of Ataxia telangiectasia mutated (ATM)/p53/p21 and protein Kinase B/phosphatidylinositol 3-kinase/mechanistic target of rapamycin (Akt/PI3K/mTOR) pathways. In addition, accelerated telomere shortening results from oxidative stress and mitochondrial dysfunction which can accelerate endothelial senescence. Finally, *mitochondrial dysfunction* is another suggested RICVD mechanism occurring partly due to release of calcium from its endoplasmic reticulum stores leading to mitochondrial calcium overload, mitochondrial membrane swelling and release of apoptotic factors. In addition, mitochondrial DNA is especially sensitive to radiation-induced damage due to its limited repair capacity, lack of protective histones, high exon/intron ratio and its proximity to the

electron transport chain. Consequently, radiation can directly damage the mitochondria leading to increased mitochondrial membrane permeability, mitochondrial calcium overload and increased chronic mitochondrial ROS generation.

1.2.2.1.3 RICVD screening

Echocardiography is the conventional screening test for RICVD offering a low risk means of assessing diastolic and systolic function as well as valvular and pericardial disease. Other imaging modalities such as cardiac computed tomography (CT) and cardiac magnetic resonance imaging (CMRI) are sometimes used to confirm and evaluate the extent of RICVD [149].

Cardiotoxicity is conventionally diagnosed based on a decrease of 10% or more in LVEF, as determined by echocardiography, relative to normal levels [150,151]. However, LVEF is rather insensitive to early radiation-induced cardiotoxicity and thus other imaging measurements have been investigated [152]. Of which, a decrease of more than 10% in global longitudinal strain (GLS), was associated with subclinical left ventricular dysfunction early after breast RT which also correlated with radiation dosimetry [153,154]. In addition, cardiac CT-based coronary artery calcium (CAC), measuring calcification and atherosclerosis in the coronary arteries, was found to be an early predictor of acute cardiovascular events, both in the general population and in breast cancer patients after RT [155,156].

1.2.2.1.4 Does Radiation Impact DNA Methylation and How?

Radiation has been shown in previous studies to cause DNA methylation alterations [106,157–161]. However, the interplay between IR and DNA methylation is highly complex and may be tissue-dependent as well as model and strain-specific [162]. A summary of the literature ([34,104,157–160,163–173] addressing the effect of radiation on DNA methylation is provided in **Table 1-1**.

Research addressing radiation-induced DNA methylation alterations was found to involve different radiation types, doses and sampling times. Subsequently, the task of arriving to a simple conclusion regarding the exact effects of IR on DNA methylation becomes extremely

difficult. Some studies address the effects of IR exposure during spaceflight. Subsequently, those employ low doses of high LET protons and heavier high atomic number and energy (HZE) ions such as ^{56}Fe radiation [157,160,170] . On the other hand, studies that address the effects of the medical applications of radiation tend to use different types and doses of radiation to mimic the doses regularly received by patients. In addition, even among those studies, different doses, dose intensities and study durations are employed. This is because of the varying aims of these studies which range from the investigation of radiation-induced carcinogenesis, radiation-induced genomic instability and bystander effects [34,103,158,159,167,168,172,173] to cellular responses to radiation and radiosensitivity [104,163,164,171]. In addition, some studies addressed the difference between the effects of IR on somatic and germinal tissues [169].

DNA methylation can be investigated on either a global or a gene-specific scale. Global DNA methylation offers a representation of the total 5-mC content in the genome but lacks gene-specific information. On the other hand, gene-specific methylation focuses on the methylation alterations of specific genes. In **Figure 1-11**, we attempt to summarize the studies addressing the effect of radiation on DNA methylation from a global DNA methylation perspective. From **Figure 1-11,** IR generally causes a decrease in global methylation (hypomethylation) which frequently persists for several months. This suggests a link between DNA methylation alterations and IR-induced late effects observed years after RT [103,157,160,168]. Global hypomethylation is mainly measured by the methylation of DNA repetitive elements (REs) which account for about 50% of the human genome. Of which, Alu element and long interspersed element-1 (LINE-1) are the most abundant human RE sequences. Hypomethylation of these REs will therefore lead to their reactivation, retrotransposition and resultant genomic instability [174]. On the other hand, attempting a similar overview for gene-specific methylation is more difficult. Different studies reported different sets of methylated genes with no clear patterns. Of note, IR was reported to elicit both hyper- and hypo-methylation of individual genes. However, overall radiation-induced gene-specific hypermethylation occurred at a higher frequency than gene-specific hypomethylation.

Table 1-1 *Literature review of radiation-induced DNA methylation alterations*

Study	Sample	Radiation dose	Methylation Assay	Results
A) Animal studies				
Jangiam et al. [169]	8-10 weeks old male BALB/cJ mice	Irradiation doses: 0.05, 0.1, or 1.0 Gy of ^{137}Cs γ rays at a dose rate of 0.75 Gy/min Sampling time: 6 months	-ELISA for global DNA methylation	Non-significant hypermethylation for all used doses
Acharya et al. [170]	6 months old C57Bl 6/J male mice	Irradiation doses: 20 cGy of ^{28}Si particles at a dose rate of ~20cGy/min Sampling times: 2, 24 hours and 1 month	Immunofluorescence staining of 5-mC and 5-hydroxymC of hippocampal sections	Significant increase in 5-mC levels at all time points
Koturbash et al. [165]	Rat spleen tissue	Irradiation doses: 2 x 10 Gy of X-rays at a dose rate of 0.05 Gy/s Sampling times: 24 hrs and 7 months	-Cytosine extension assay -COBRA	Cytosine extension assay -Persistent DNA hypomethylation after 24 hrs and 7 months COBRA -Hypomethylation and activation of retrotransposable LINE-1 promoters after 7 months -DNMT1, DNMT3a, DNMT3b and MeCP2 downregulated at 24 hours
Loree et al. [167]	Long-Evans female rats	Irradiation doses: 5 Gy of X-rays Sampling times: 6 and 96 hrs	Cytosine Extension Assay	-Global DNA hypomethylation -Low levels of DNMT1, DNMT3- a&b and MeCP2

Study	Sample	Radiation dose	Methylation Assay	Results
Luzhna et al. [168]	Six-week-old intact female Long-Evans rats	Irradiation doses: 80kVp/0.1 Gy, 80kVp/1 Gy, 80kVp/2.5 Gy, 30kVp/0.1 Gy of X-rays Sampling times: 6, 96 hours, and 4, 12 and 24 weeks	COBRA	-Hypomethylation of LINE-1 was observed at the following time points: *80kVp/0.1 Gy*: 6 hrs; *80kVp/1 Gy*: 96 hrs; *80kVp/2.5 Gy:* 6 and 96 hrs, 24 weeks; *30kVp/0.1 Gy:* 96 hrs, 4 weeks -This short term hypomethylation was correlated with increased LINE-1 expression at 12 and 24 weeks after exposure to 80kVp/ 1 and 2.5 Gy and 30kVp/ 0.1 Gy
Miousse et al [158]	Eight-week-old male radioresistant C57BL/6J and radiosensitive CBA/J mice	Irradiation doses: 0.1 or 1 Gy of ^{137}Cs at a dose rate of 1.21 Gy/min Sampling times: 2 months	Methylation-sensitive McrBC-qPCR of LINE-1 5'-UTR	-Significant decreases in LINE-1 DNA methylation in bone marrow hematopoietic stem cells (HSCs) of CBA/J mice 2 months after irradiation with either 0.1 and 1 Gy.
Miousse et al. [157]	Six-month-old C57BL/6J male mice	Irradiation doses: 0.1, 0.2 or 0.4 Gy of ^{56}Fe ion Sampling times: 4 and 22 weeks	-Methylation-sensitive McrBC- qPCR of LINE-1 and SINE B1 -ELISA	McrBC- qPCR Both LINE-1 and SINE B1 were hypomethylated in bone marrow mononuclear cells (BM-MNCs) and hypermethylated in hematopoietic progenitor and stem cells (HPSCs) in a dose-dependent manner ELISA 4 weeks post-irradiation: Non-significant alterations in global DNA methylation were observed in both HPSCs and MNCs 22 weeks post-irradiation: significant loss of global DNA methylation in HPSCs after exposure to 0.4 Gy Significantly decreased expression of DNMT3A in HPSCs 4 weeks post-irradiation

Study	Sample	Radiation dose	Methylation Assay	Results
Pogribny et al. [159]	C57/BL6 mice	Irradiation doses: 0.5 Gy X-ray as single acute dose or in 10 daily fractions Sampling times: 4 hrs	Cytosine Extension Assay	-Fractionated radiation: global DNA hypomethylation and Low levels of DNMT1, DNMT3- a&b, MeCP2 and MBD2 -Acute radiation: low levels of DNMT3a and of DNMT3b in females only
Tawa et al. [161]	Adult C57BL/6NJc1 mice	Irradiation doses: 4-10 Gy whole body X-rays, dose rate unknown Sampling times: 8, 24, 48 and 72 hrs	HPLC	Global hypomethylation after 10 Gy X-rays in mice liver at 8 hours post irradiation and until 72 hours
Wang et al. [164]	BALB/c mice	Irradiation doses: 0.5 Gy X-rays acutely or in 0.05 Gy daily fractions for 10 days at a dose rate of 0.27 Gy/min Sampling times: 2 hours and 1 month	-HPLC -MeDIP-on-chip -MeDIP-qPCR -Methylation specific PCR on Rad23b and DNA-damage-inducible transcript 3 (Ddit3)	HPLC -Chronic exposure: Hypomethylation relative to acute exposure and control did not persist after 1 month after treatment MeDIP-on-chip Chronic exposure: hypermethylation relative to control and acute exposure of 811 regions including Rad23b, Tdg, Ccnd1, Ddit3, Llgl1, Rasl11a, Tbx2, Scl6a15 which were confirmed by MeDIP-qPCR -2 hours after chronic exposure: Decreased expression of DNMT1 relative to control and acute exposure in peripheral blood mononuclear cells (PBMC), kidney and liver tissues -1 month after chronic exposure: DNMT1 upregulation in liver tissue and upregulation 1 month after irradiation relative to control and acute exposure
B) Cell line studies				

Study	Sample	Radiation dose	Methylation Assay	Results
Kalinich et al. [34]	Chinese hamster ovary (CHO) clone K-1, Chinese hamster lung, HeLa clone S-3fibroblast (V79) clone A03, HeLa clone S-3	Irradiation doses: 0.5-10 Gy of ^{60}Co γ radiation at a dose rate of 1 Gy/min Sampling time: 24, 48, and 72 hrs	High performance liquid chromatography (HPLC)	-Global dose dependent hypomethylation except a 1-5 Gy plateau region at 24 hours for HeLa cells -Reduced total cellular DNMT activity (*de novo* and maintenance) over the 72 hour period
Kennedy et al. [160]	human bronchial epithelial cell line (HBEC3- KT)	Irradiation doses: -0, 0.1, 0.3 or 1.0 Gy ^{56}Fe ions at a dose rate of 0.1,0.3 and 1.0 Gy/min respectively -0.3, 1.0 Gy ^{28}Si ions at a dose rate of 0.28 and 0.63 Gy/min respectively. -1.0 Gy of X-rays at a dose rate of 1 Gy/min Sampling time: 48 hrs and weekly samples until 2.5 months	Infinium HumanMethylation450k BeadChip	-^{56}Fe ions: dose dependent average trend of hypermethylation across all time points - X-rays: dose dependent average trend of hypomethylation across all time points -For both, the changes persisted more than 50 days post-irradiation.
Antwih et al. [171]	MDA-MB-231 breast cancer cell line	Irradiation doses: 0, 2, or 6 Gy of X-ray at a rate of 0.86 Gy/min Sampling times: 1, 2, 4, 8, 24, 48, and 72 hrs	Infinium HumanMethylation450k BeadChip	For 2 Gy dose: Initial hypermethylation followed by hypomethylation from 4 hour time point onward. For 6 Gy dose: Short termed initial hypermethylation (< 1 hour) followed by transient hypomethylation at 8 hour time point and then hypermethylation from 24 hour time point onward, DNMT1 downregulation.

Study	Sample	Radiation dose	Methylation Assay	Results
				Differentially methylated genes (DMGs) for 2 Gy dose: DIP2B, DIP2C, ENOX1, HLA-DQA1, HLA-DRB1, MAML2, ZBTB20, ZIC1 DMGs for 6 Gy: ASPH, HLA-DRB6, IGF1R, ITPR2, KRAS, LMF1, MAD1L1, MBNL1, MCF2L, MEIS2, NCOA2, PCDHGA/B, PRH1, SRGAP1 Shared DMGs for 2 & 6 Gy: AGAP2, ARHGEF10, ATP11A, HDAC4, PRR4, PTPRD, TBCD
Aypar et al. [172]	GM10115 human-hamster hybrid cell line	Irradiation doses: -0.5, 1 and 2 Gys of X-rays at a dose rate of 2.4 Gy/min -0.1 and 1 Gy of Fe ions at a dose rate of 0.2 Gy/min Sampling time: 1 hr post irradiation	-Methylation Specific PCR (MSP) for specific loci (nuclear factor-kappa B (NF-κB), tumor suppressor in lung cancer 1 (TSLC1) and cadherin 1 (CDH1) -Combined bisulfite restriction assays (COBRA) for Long interspersed nucleotide element 1 (LINE-1) and Alu repeat elements methylation -Methylation-Sensitive Arbitrarily Primed PCR (MSAP-PCR) for global methylation analysis	Methylation Specific PCR: No significant change was detected COBRA: -For X-rays: hypomethylation of LINE-1 and Alu at 2 Gy and hypermethylation of LINE-1 at 0.5 Gy -For Fe ions: hypomethylation of LINE-1 and Alu at 1 Gy, MSAP-PCR: -For X-ray: hypermethylation at the internal cytosine at doses > 0.5 Gy -For Fe ions: Hypomethylation at the external cytosine at 1 Gy
Chaudhry and Omarrudin [104]	human lymphoblast cell lines TK6 (radiation sensitive)	Irradiation doses: 2 Gy of X-rays at a dose rate of 1.7 Gy/min	- Arbitrarily primed PCR (APPCR)	APPCR: Differential DNA methylation fingerprints were observed between TK6 and WTK1

Study	Sample	Radiation dose	Methylation Assay	Results
	and WTK1 (radiation resistant)	Sampling time: 0, 2, 4, 8, 12, and 24 hrs post irradiation	- enzyme-linked immunosorbent assay (ELISA) for global DNA methylation analysis	Global DNA methylation: For WTK1: DNA methylation levels continued to decrease until 8 hrs, followed by an increase until 12 hrs. Return to background levels of methylated DNA was observed at 24 hrs. For TK6: Initial decrease followed by a steady increase until 24 hrs DNMT1 expression was increased in TK6 and decreased in WTK1 at 8 hrs with a statistically significant difference in expression. Increased DNMT3 A and B as well as TET1 was observed in both TK6 and WTK1.
Goetz et al. [173]	RKO cells human colorectal carcinoma cell line, Primary, AG01522D human diploid skin fibroblasts, NC10 normal lymphocyte, SW48 colon carcinoma cells	Irradiation doses: Total dose of 0.1Gy or 1 Gy of: -X-rays at a dose rate of 2.4 Gy/min -Fe ions at dose rates of 1 Gy/min or 0.1 cGy/min -Protons at dose rates of 0.02 Gy min Sampling time: 2 hours after irradiation	- MSP of p16 and MGMT - LINE-1 and Alu COBRA - Methylation-Sensitive Arbitrary Priming (MSAP) PCR	Methylation specific PCR: -Hypermethylation of p16 promoter in both RKO and SW48 -Hypermethylation of MGMT promoter in SW48 -Surviving RKO and AG01522 populations after 16–20 doublings showed no significant changes in promoter methylation COBRA: - Surviving RKO and AG01522 populations after 16-20 doublings showed LINE-1 hypomethylation in both doses of protons and Fe ions - 1 Gy of X rays after 16–20 population doublings caused hypomethylation for RKO cells and hypermethylation for AG01522 cells

Study	Sample	Radiation dose	Methylation Assay	Results
				- Hypomethylation of Alu element after exposure of both cell lines to protons and Fe ions and after exposure of RKO cells to X-rays MSAP PCR: - Non significant DNA hypermethylation in RKO and AG01522a after proton and Fe ions irradiation - Hypomethylation after10 cGy and 1 Gy X-ray relative to corresponding proton and Fe ion doses in RKO and 3 out of 4 AG01522 cell groups
Kuhmann et al. [163]	MCF7 breast cancer cell line	Irradiation doses: 2 Gy/day for 1 and 2 weeks of Cs-137 at a dose rate of 0.5 Gy/min Sampling times: 2, 3, 14 and 24 days	-Methyl-CpG immunoprecipitation (MCIp) -CpG island microarray analysis	Methylation changes confirmed by quantitative MassARRAY analysis -Promoter hypermethylation of ADAMTS9 and FOXC1 after 10 and 20 Gy fractionated irradiation - Intragenic hypermethylation of TRAPPC9 after 10 Gy fractionated irradiation – Promoter hypomethylation of AMIGO3 after 20 Gy fractionated irradiation FOXC1 and TRAPPC9 hypomethylation was found after cell regrowth 14 days after irradiation Global methylation changes as represented by methylation levels of LINE-1 and other repetitive elements (Alu sequences, long terminal re-peats, satellite DNA) were not significant.
Kumar et al. [166]	Radioresistant MDA-MB-453 breast cancer cell line and	Irradiation doses: doses ranging from 1–8 Gy of ^{60}Co γ radiation at a dose rate of 1 Gy/min	-Reverse Phase HPLC(RP-HPLC)	-At 4 Gy, global demethylation in a time dependent manner - Increased p16^{INK4a} and ATM promoter activity in transfected SiHa and SaOS2 after 4 Gy irradiation

Study	Sample	Radiation dose	Methylation Assay	Results
	SiHa cervical cancer cell lines Radiosensitive SaOS2 osteosarcoma cell line and WM115 melanoma cell lines	Sampling times: Post-irradiation	-Transfection of luciferase reporter assay	

Within these literature studies, several possible mechanisms have been put forward. The first mechanism involves ROS produced by radiation-induced water radiolysis. These ROS can alter DNA methylation via several ways [175]. ROS may act directly on the DNA by oxidizing the guanine base in CGIs forming 8-oxo-20-deoxyguanosine (8-OHdG), which can be repaired by its removal by 8-oxoguanine DNA glycosylase (OGG1) followed by BER. If not repaired, 8-OHdG can prevent the methylation of the adjacent cytosine leading to subsequent hypomethylation. Alternatively, ROS may directly convert 5-mC to 5-hydroxymC by interaction of DNA with hydroxyl radicals. ROS may affect DNA methylation indirectly by altering the activity of methylation related enzymes [175]. However, ROS effects on DNMTs seem to be bidirectional.
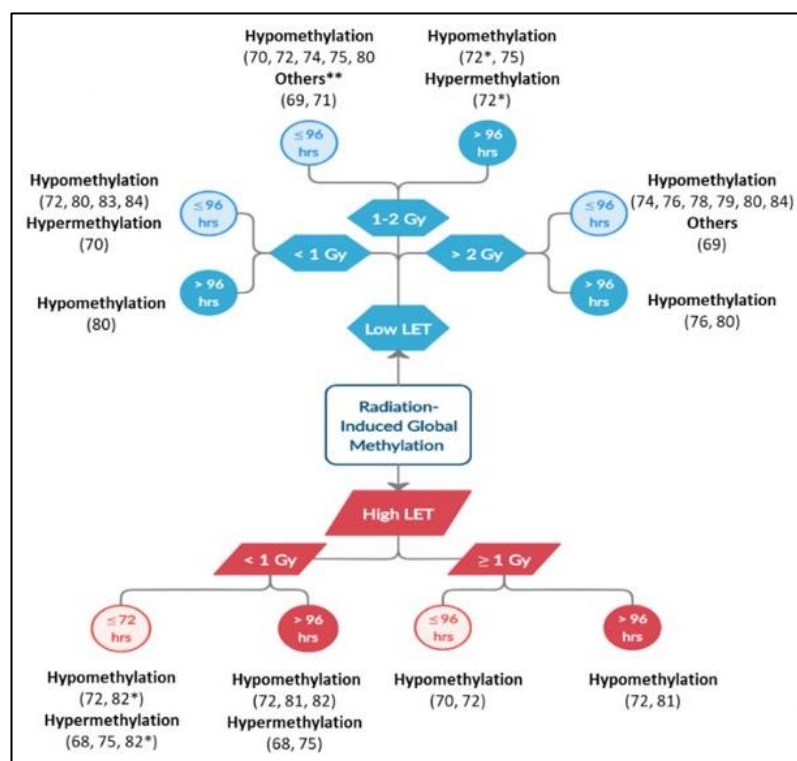
Figure 1-11 Overview of the shared outcomes of the different studies involving radiation-induced global methylation (* indicates different cell lines or sampled tissues and ** indicates alternating stages of methylation)

ROS can lead to hypermethylation by upregulating DNMTs or increasing their recruitment by H_2O_2. ROS can also lead to hypomethylation by reducing the availability of SAM which is an essential cofactor for DNMT activity. Finally, other studies have shown that ROS can lead

to DNA hypermethylation due to their nucleophilic action on the 5 position of cytosine molecule leading to its deprotonation and accelerating its reaction with SAM [176,177]. In summary, ROS can lead to hypomethylation by 8-OHdG formation, 5-mC hydroxylation or reducing SAM availability. On the other hand, ROS can also lead to hypermethylation by DNMT upregulation or increased recruitment as well as 5-mC deprotonation. Despite the counter intuitiveness of ROS having opposing effects on DNA methylation, this 'dual' effect may contribute to the observed similar opposing effects of radiation on DNA methylation.

Secondly, radiation can also cause DNA hypermethylation by activation of NF-κB [178–181]. NF-κB activation leads to alterations in DNA methylation through two different mechanisms. Firstly, the RelA/p65 subunit of NF-κB can directly recruit DNMT-1 to chromatin [182]. Secondly, NF-κB regulates DNA methylation indirectly by the production of Interleukin-6 (IL-6), which has been shown to also regulate DNMT1 expression leading to increased DNMT1 activity [183–185]. This increased availability/activity of DNMT1 subsequently leads to hypermethylation.

1.2.2.1.5 DNA Methylation and CVD; Possible Disease Collaborator?

A number of studies have linked DNA methylation alterations to CVD development [186–194]. The focus of these studies is mostly atherosclerosis as it is the underlying cause of most cardiovascular diseases (CVDs) [65,195,196]. The majority of studies report global DNA hypomethylation in atherosclerosis [197–202]. This state of hypomethylation was detectable in atherosclerosis prone murine aorta even before the development of atherosclerosis [203]. In addition, gene specific hypermethylation has also been observed in atherosclerosis [189,194,204]. Interestingly, focal gene-specific hypermethylation offers higher biological relevance than that of global hypomethylation [205].

We examined the literature concerning differentially methylated genes in CVD (summarized in **Table 1-2**). In most cases, differentially methylated genes are associated with key elements in CVD pathogenesis, such as lipid metabolism, inflammation, oxidative stress, atherosclerosis and endothelial cell dysfunction. This consequently points to a contribution of DNA methylation to CVD pathophysiology.

The association between altered DNA methylation and CVD is further proven in experimental models of atherosclerosis. Dunn et al. have shown DNMT inhibitor 5-Aza-2'-deoxycytidine (also known as decitabine) to be effective atheroma preventive measures in a ApoE$^{-/-}$ mouse model of atherosclerosis [206]. In addition, decitabine was shown to decrease atherosclerosis development in LDLr$^{-/-}$ mice through decreased macrophage inflammation and suppressed macrophage endoplasmic reticulum stress [207]. This could be explained by decreased methylation and subsequent increased expression of liver X receptor α (LXRα) and peroxisome proliferator-activated receptor γ1 (PPARγ). LXRα and PPARγ are atheroprotective as they regulate lipid metabolism and macrophage inflammation [208–210]. As a result, DNA methylation inhibitors have been suggested as candidates drugs for treating atherosclerosis [211–213].

Table 1-2 Gene specific methylation and cardiovascular disase. Abbreviations: ACS: acute coronary syndrome, CAD: coronary artery disease, FH: Familial Hypercholesterolemia, FHS: Framingham Heart Study, GOLDN: Genetics of Lipid Lowering Drugs and Diet Network, KAROLA: Langzeiterfolge der KARdiOLogischen Anschlussheilbehandlung, KORA: Cooperative health research in the Region of Augsburg, LBC: Lothian Birth Cohorts, PIVUS: Prospective Investigation of the Vasculature in Uppsala Seniors Study, PBMCs: peripheral blood mononuclear cells.

Gene	Cohort	Sample	Methylation assay	Results	Possible Connection to CVD	Refs
ABCA1 ATP-Binding Cassette A1	110 CAD patients, 110 ethnically matched controls	Cellular fraction from fasting blood samples	methylation specific PCR (MSP)	Hypermethylation	Reduction of cholesterol accumulation in macrophages which helps in preventing foam cell formation [214]	[215]
	heart surgery patients (38 CAD, 50 no CAD)	Buffy coat	Bisulfite pyrosequencing			[216]
	97 FH patients	Fasting leucocyte and whole blood	Bisulfite pyrosequencing			[217]
	150 atherosclerosis patients, 150 controls	Peripheral blood samples	Nested MSP			[186]
ABCG1 ATP-Binding Cassette G1	614 hypertensive African-Americans (51% Metabolic Syndrome)	Buffy coat	Infinium HumanMethylation450 K BeadChip	Hypermethylation	Reduction of cholesterol accumulation in macrophages which helps in preventing foam cell formation [187]	[218]
	1494 FHS participants + ≤812 PIVUS participants + n≤380 LBC 1921	FHS: Buffy coat PIVUS, LBCs: Whole blood	Infinium HumanMethylation450 k BeadChip			[219]

Gene	Cohort	Sample	Methylation assay	Results	Possible Connection to CVD	Refs
	+ n≤654 LBC 1936 + 991 GOLDN	GOLDN: CD4+ T cells				
	1776 KORA F4 participants, 60 of which previously hospitalized MI	Whole blood	Infinium HumanMethylation450 k BeadChip			[188]
	85 patients ≥ 50% coronary artery occlusion, 54 controls	Peripheral blood samples	MSP			[187]
ACAT1 Acyl-coenzyme A:cholesterol acyltransferase-1	150 atherosclerosis patients, 150 controls	Peripheral blood samples	Nested MSP	Hypomethylation	Cholesteryl ester formation in macrophages thereby linked to foam cell formation [220]	[186]
ALDH2 Aldehyde Dehydrogenase 2	Adult male Sprague-Dawley rats	Myocardial infarction border	Bisulfite PCR sequencing	Hypermethylation	-Protection against ischemia reperfusion injury [221,222] -Protection from endoplasmic reticulum stress and subsequent apoptosis [223]	[224]
ANGPTL2 Angiopoietin-like protein 2	122 CHD patients, 58 controls	Peripheral blood	Bisulfite pyrosequencing	Hypomethylation	Promotion of inflammatory cell recruitment and extracellular matrix remodeling [225,226]	[226]
	33 post-acute coronary syndrome (ACS) patients, 40 controls	Leucocytes from fasting blood samples	Infinium HumanMethylation450 k BeadChip	Hypomethylation		[227]

43

Gene	Cohort	Sample	Methylation assay	Results	Possible Connection to CVD	Refs
BRCA1 BReast CAncer gene 1	8 atherosclerosis patients and 8 controls with replication of data in atherosclerotic plaque material and post-hoc analysis in control males	Whole blood	Infinium HumanMethylation450k BeadChip	Hypermethylation	Involvement in DNA damage repair and lead to increased resistance to ROS induced endothelial cell damage [228]	[189]
CCDC62/ERAP75 Coiled-coil domain containing 62	128 postmortem specimens of the aortic intima from 64 deceased patients	aortic intima tissues	Infinium MethylationEPIC BeadChip	Hypomethylation	Unknown but might have an effect on the activation of ER-α [229]	[230]
CDKN2B/p15^{INK4b} Cyclin-dependent kinase inhibitor 2B	36 CHD patients, 36 controls	Peripheral blood samples	Bisulfite pyrosequencing	Hypermethylation	Part of a genomic locus that has been associated with susceptibility to coronary artery disease [231]	[232]
COMT Catechol-O-Methyltransferase	48 CHD patients, 48 controls	Peripheral blood samples	Bisulfite pyrosequencing	Hypermethylation	Polymorphisms causing lowered COMT activity have been linked to an increased risk of cardiovascular disease due to lowered rate of catecholamine inactivation [233]	[234]
CRISP2	8 atherosclerotic patients and 8 controls with	Whole blood	Infinium HumanMethylation450k BeadChip	Hypermethylation	Unknown	[189]

Gene	Cohort	Sample	Methylation assay	Results	Possible Connection to CVD	Refs
Cysteine-rich secretory protein 2	replication of data in atherosclerotic plaque material and post-hoc analysis in control males					
CXCL12 C-X-C motif chemokine 12	Reprocessing data from samples used in (85), validation in 303 CAD patients and 303 controls	PBMCs	Bisulfite Sequencing	Hypermethylation	Atheroprotective and reparative function by increasing plaque stability, endothelial progenitor cell and inflammatory cell recruitment and mobility [235–237]	[238]
DDAH2 Dimethylarginine dimethylaminohydrolase 2	25 CAD patients, 15 controls	endothelial progenitor cells differentiated from participant PBMCs	Nested MSP sequencing	Hypermethylation	Atheroprotective by inhibition of endothelial nitric oxide synthase (eNOS) inhibitor, asymmetric dimethylarginine (ADMA) [239,240]	[240]
ER-α Estrogen Receptor α	67 patients undergoing coronary artery bypass grafting (CABG), or directional coronary atherectomy (DCA)	Heart tissue	Southern blot after methylation sensitive restriction enzymes	Hypermethylation	Atheroprotective by eNOS activation, reduced endothelial cell apoptosis, regulation of serum lipid cholesterol concentrations and decrease of vascular smooth muscle cell growth and migration [241–243]	[244]

Gene	Cohort	Sample	Methylation assay	Results	Possible Connection to CVD	Refs
	ApoE/Lepr double knockout mice	vascular smooth muscle cells	Bisulfite sequencing PCR			[245]
	54 atherosclerosis patients, 28 controls	fasting blood samples	Nested MSP			[204]
F2RL3 F2R Like Thrombin Or Trypsin Receptor 3	KAROLA cohort [246], 1206 participants of inpatient cardiovascular rehabilitation programs	Whole blood	Sequenom matrix-assisted laser desorp-tion ionization time-of-flight mass spectrometry	Hypomethylation	Associated with platelet activation, intimal hyperplasia, and inflammation and F2RL3 methylation has been associated with smoking [247,248]	[247]
FHIT Fragile Histidine Triad Diadenosine Triphosphatase	128 postmortem specimens of the aortic intima from 64 deceased patients	aortic intima tissues	Infinium MethylationEPIC BeadChip	Hypomethylation	Unknown but FHIT loss has been associated with genomic instability [249]	[230]
FOXP3 forkhead box p3	188 acute coronary syndrome (ACS) patients, 68 controls	CD4$^+$CD25$^+$ T cells	MSP	Hypermethylation	Regulation of regulatory T cells (Tregs) which suppress T cell mediated immune responses contributing to atherosclerotic plaque development [250]	[251]
	89 patients with ACS, 35 controls	CD4$^+$CD25$^+$T cells	PCR pyrosequencing			[250]

Gene	Cohort	Sample	Methylation assay	Results	Possible Connection to CVD	Refs
GALNT2 GalNAc-T2	85 patients ≥ 50% coronary artery occlusion, 54 controls	Peripheral blood samples	MSP	Hypermethylation	Modulation of HDL and triglyceride levels [252,253]	[187]
GCK Glucokinase	36 CHD patients, 36 controls	Peripheral blood samples	Bisulfite pyrosequencing	Hypomethylation	Hypomethylated gene body leads to decreased GCK expression which has been identified as a candidate gene for type 2 diabetes mellitus [254,255]	[190]
	47 essential hypertension patients, 47 controls	Peripheral blood samples	Bisulfite pyrosequencing			[256]
GDF6 Growth Differentiation Factor 6	128 postmortem specimens of the aortic intima from 64 deceased patients	aortic intima tissues	Infinium MethylationEPIC BeadChip	Hypomethylation	Unknown GDF6 is involved in Klippel-Feil syndrome which has been associated in 4%–29% of the cases with cardiovascular abnormalities [257]	[230]
HOTAIR HOX Transcript Antisense RNA				Hypermethylation	Reduced expression has been associated with elevated expressions of calcification-related genes in aortic valves [258]	
HOXA6 Homeobox A6				Hypomethylation	-HOX genes are involved in the embryonic development of the cardiovascular system and also regulate the adult expression of growth factors associated with endothelial cell differentiation such as vascular endothelial growth factor (VEGF), fibroblast growth factor 2 (FGF2), platelet-derived growth factor (PDGF), and transforming growth factor β1 (TGF-β1) [259,260]	
HOXA9 Homeobox A9						
HOXA10 Homeobox A10						
HOXA10-AS Homeobox A10-antisense RNA						

Gene	Cohort	Sample	Methylation assay	Results	Possible Connection to CVD	Refs
HOXA-AS3 Homeobox A-antisense RNA 3	128 postmortem specimens of the aortic intima from 64 deceased patients			Hypermethylation		
HOXC4 Homeobox C4						
HOXC4/5 Homeobox C4/5						
HOXC11 Homeobox C11						
HOXC11-AS Homeobox C11-antisense RNA				Hypermethylation		
HOXC-AS2 Homeobox C-antisense RNA2				Hypomethylation		
IL-6 Interleukin-6	265 CAD patients, 205 controls	Whole blood	MSP	Hypomethylation	Acute production is cardioprotective while chronic production leads to chronic inflammation, hypertrophy and depressed cardiac function [261]	[191]
IL-12b Interleukin-12b	25 CAD patients, 25 controls	PBMCs	Methylation sensitive-high resolution melting (MS-HRM)	Hypomethylation	IL-12b is a common subunit of interleukin 12 and Interleukin 23. Increased levels IL-12 and IL-23 have been associated with a variety of cardiovascular abnormalities [262]	[192]
iNOS (NOS2) inducible nitric oxide synthase					Produced in response to pro-inflammatory signaling and contributes to nitrosative stress, myocardial ROS and dysfunction [263,264]	
JAK1 janus kinase 1					JAK1/2 are part of JAK-STAT signaling which can be induced by pro-inflammatory cytokines such as IL-6.	

Gene	Cohort	Sample	Methylation assay	Results	Possible Connection to CVD	Refs
JAK2 janus kinase 1					JAK-STAT signaling has been shown to be induced in response to biomechanical stress causing compensatory cardiac hypertrophy. Chronic stress due to hypertension or myocardial infarction leads to a transition from compensatory hypertrophy to heart failure in which JAK/STAT signaling is crucial [265].	
MHC2/ HLA class II Major histocompatibility complex 2/ human leukocyte antigen class II					-Expressed in endothelial and vascular smooth muscle cells within atherosclerotic plaques in vivo and some HLA alleles have been found to be associated with CHD in Chinese population [254,255]. -Can also contribute to the atherosclerotic process by aiding in dendritic cell presentation of peptide fragments of oxidized LDLs to helper T cells [266]. -There is a controversial relationship between certain HLA alleles and lipoprotein A which has been linked to the development of CHD [267,268].	
MYOM2 Myomesin 2	128 postmortem specimens of the aortic intima from 64 deceased patients	aortic intima tissues	Infinium MethylationEPIC BeadChip	Hypomethylation	-MYOM2 is normally expressed in adult cardiomyocytes where –with other myomesin proteins- its protein functions to cross-link the titin and myosin filaments of the M-band [269,270]. -A genetic variant of MYOM2 has been shown to increase the risk for major adverse cardiovascular events in patients with acute coronary syndromes (ACS) [271].	[230]
eNOS (NOS3) endothelial nitric oxide synthase	33 male CAD patients, 42 male controls	Whole blood	Bisulfite sequencing	Hypermethylation	NO produced by eNOS is a physiological vasodilator which also inhibits platelet aggregation and release	[193]

Gene	Cohort	Sample	Methylation assay	Results	Possible Connection to CVD	Refs
					of growth factors as well as controls the expression of genes involved in atherogenesis [272].	
NPC1 Niemann-Pick type C1 (NPC1)	50 CVD patients, 50 controls	Peripheral blood leukocytes	Nested MSP	Hypermethylation	Regulates cholesterol trafficking to maintain the balance between macrophage cholesterol import and export which is an important effector in atherogenesis [273].	[274]
PLA2G7 Platelet-activating factor acetylhydrolase	36 CHD patients and 36 controls	Peripheral blood samples	Bisulfite pyrosequencing	Hypermethylation	Hydrolyzes oxidized phospholipids produced during LDL oxidation to generate lysophosphatidylcholine and free oxidized fatty acids which have inflammatory effects and might therefore contribute to the atherogenic process [275,276].	[277]
RNase6 Ribonuclease A family member k6	128 postmortem specimens of the aortic intima from 64 deceased patients	aortic intima tissues	Infinium MethylationEPIC BeadChip	Hypomethylation	Unknown but RNase6 has been found to be expressed in neutrophils and monocytes as well as possess some anti-microbial properties which might indicate a function in immunity [278,279] .	[230]
SMAD7	45 atherosclerosis patients, 26 controls	Peripheral whole blood and paraffin-embedded arterial tissues	MSP	Hypermethylation	Decreased SMAD7 has been shown to activate NF-κB atherogenic pro-inflammatory signaling [280]	[194]
SMARCA4 SWI/SNF-Related Matrix-Associated Actin-Dependent	192 male myocardial infarction patients and 192 controls	Fasting blood samples	Infinium HumanMethylation450 k BeadChip	Hypomethylation	SMARCA4 codes for brahma-related gene 1 (BRG1) which is an ATP-dependent helicase that mediates chromatin remodeling. BRG1's expression in adult cardiomyocytes leads to a pathological shift from	[283]

Gene	Cohort	Sample	Methylation assay	Results	Possible Connection to CVD	Refs
Regulator Of Chromatin Subfamily A Member 4					adult to fetal myosin heavy chain isoforms leading to cardiac hypertrophy in heart failure [281,282].	
STAT1 Signal transducer and activator of transcription 1	25 CAD patients, 25 controls	PBMCs	MS-HRM	Hypomethylation	In addition to what was previously mentioned under JAK1/2, STAT1 has been associated with oxidative stress, cardiac cell death signaling and macrophage apoptosis promotion thereby contributing to atherogenesis and ischemic heart disease [284].	[192]
TBX20 T-Box 20	128 postmortem specimens of the aortic intima from 64 deceased patients	aortic intima tissues	Infinium MethylationEPIC BeadChip	Hypomethylation	-Essential for the normal development of many cardiac structures during embryogenesis [285]. -Gene body hypomethylation leading to reduced expression could lead to reduced endothelial cell tolerance to atherogenic oxidized-LDL-induced cell injury [286].	[230]
TIMP1 Tissue inhibitor of metalloproteinas es 1	150 atherosclerotic patients, 150 controls	Peripheral blood samples	Nested MSP	Hypermethylation	-Normally inhibits extracellular matrix degrading metalloproteinases (MMPs). Reduced TIMP1 expression leads to decreased MMP inhibition leading to atherogenesis and increased plaque rupture [287].	[186]
TNNT1 slow skeletal muscle troponin T	276 FH patients, 88 non-FH men with (n = 38) and without CAD (n = 50)	FH patients: Fasting whole blood Non-FH: buffy coat	Bisulfite sequencing	Hypermethylation in non-FH men with CAD	Unknown. However, TNNT1 DNA methylation status positively correlated with HDL- cholesterol levels which could affect atherosclerotic risk by altering lipid profiles [188,288].	[289]
TUBA4B Tubulin Alpha 4b	128 postmortem specimens of the	aortic intima tissues		Hypomethylation	Unknown	[230]

Gene	Cohort	Sample	Methylation assay	Results	Possible Connection to CVD	Refs
TUBA3A Tubulin alpha chain	aortic intima from 64 deceased patients		Infinium MethylationEPIC BeadChip			
WNT8B Wnt Family Member 8B					Unknown but could be linked to CVD through the wnt-frizzled cascade or another proatherogenic wnt-signaling [188,288].	
ZFHX3 Zinc Finger Homeobox 3	192 male myocardial infarction patients and 192 controls	Fasting blood samples	Infinium HumanMethylation450k BeadChip	Hypomethylation in regulatory noncoding region	-Down-regulation in atrial myocytes leads to increased sarcoplasmic reticulum calcium content and calcium leak which could lead to atrial fibrillation. -Some genetic variants of ZFHX3 have been associated with increased risk for atrial fibrillation and stroke [290–292].	[283]
ZNF609 Zinc Finger Protein 609	128 postmortem specimens of the aortic intima from 64 deceased patients	aortic intima tissues	Infinium MethylationEPIC BeadChip	Hypomethylation	-Circular ZNF609 is one of the top 10 most expressed circular RNAs in endothelial cells. -cZNF609 expression has been linked to vascular dysfunction and has been found to be down-regulated in CAD or hypertensive patients [293,294].	[230]

1.2.2.1.6 Functional analysis of differentially methylated genes in CVD

To validate the involvement of DNA methylation in CVD pathogenesis, we performed a functional analysis of genes reported in literature to be differentially methylated in CVD (**Table 1-3**). This was done by investigating these genes in the pathway analysis functionality of PANTHER (protein analysis through evolutionary relationships) classification system [295,296]. Our PANTHER analysis of differently methylated genes in **Table 1-3** reveals that these genes were connected to several pathophysiological mechanisms of CVD, such as inflammation, oxidative stress and endothelial activation. In addition, four pathways showed statistically significant pathway involvement, namely Janus kinase/signal transducers and activators of transcription (JAK/STAT) signaling pathway, interferon-gamma (INF-γ) signaling pathway, phosphoinositide 3 kinase (PI3K) pathway and interleukin signaling pathway. These pathways have been associated with cardiac myocyte response to injury and stress as well as cardiovascular inflammation [297–305]. Activation of JAK/STAT signaling contributes to atherosclerosis development by aiding immune cell recruitment and vascular smooth muscle proliferation, hypertrophy, and migration [306]. In addition, STAT1 synergizes with NF-κB in its inflammatory signaling [307]. Conversely, IFN-γ promotes endothelial cell adhesion, immune cell recruitment with a conflicting effect on foam cell formation [308–310]. PI3K catalyzes second messenger, phosphatidylinositol (3,4,5)-trisphosphate (PIP3), production. In the heart, four isoforms (PI3Kα, PI3Kβ, PI3Kδ, and PI3Kγ) are differentially expressed in different cell subsets (cardiomyocytes, fibroblasts, endothelial cells and vascular smooth muscle cells). Subsequently, they are associated with varying effects on myocardial contractility, physiological growth and pathobiological remodeling as well as smooth muscle cell and immune cell migration [311–313]. In addition, PI3Ks function as scaffolding proteins in cardiac excitation-contraction coupling and autophagy [312]. Finally, interleukins are a family of cytokines strongly associated with chronic inflammation and atherogenesis. Some interleukins can have proatherogenic effects while fewer interleukins can have atheroprotective effects [308,314–319]. These DNA methylation alterations in pathways associated with atherogenesis suggest a usefulness for DNA methylation-based CVD biomarkers. First, Istas et al. found that differentially methylated regions in BRCA1 and

CRISP2 genes were reproducibly differentially methylated in independent atherosclerotic human aorta tissue and human carotid plaque samples [189]. In addition, these methylation changes at BRCA1 and CRISP2 genes were consistently associated with subclinical atherosclerosis in an independent sample cohort of middle-aged men. This study provides a concrete example of how gene-specific methylation could be used to monitor the development of atherosclerosis, even before the condition is clinically diagnosable [189]. Second, p16^{INK4a} was found to be differentially methylated by IR while also influencing epicardial adipose tissue development and subsequent CVD risk [320]. Thus, examining gene-specific radiation-induced methylation alterations after radiation that are associated with CVD could offer an untapped source of functional biomarkers.

Table 1-3 *Functional analysis of CVD differentially methylated genes identified in literature*

PANTHER Pathways	No. of genes	raw P-value	False Discovery Rate (FDR)
JAK/STAT signaling pathway	3	0	0.001
Interferon-gamma signaling pathway	3	0.0001	0.0035
PI3 kinase pathway	3	0.0003	0.0112
Interleukin signaling pathway	3	0.0012	0.0393
PDGF signaling pathway	3	0.0048	0.13
Angiogenesis	3	0.0076	0.177
TGF-beta signaling pathway	2	0.0222	0.404
Inflammation mediated by chemokine and cytokine signaling pathway	3	0.0214	0.438
Androgen/estrogen/progesterone biosynthesis	1	0.0295	0.483
5-Hydroxytryptamine degradation	1	0.0494	0.736
Adrenaline and noradrenaline biosynthesis	1	0.0667	0.781
Axon guidance mediated by Slit/Robo	1	0.0624	0.787
CCKR signaling map	2	0.0606	0.828
Dopamine receptor mediated signaling pathway	1	0.125	1
p53 pathway	1	0.184	1
Wnt signaling pathway	2	0.166	1
VEGF signaling pathway	1	0.147	1
p53 pathway feedback loops 2	1	0.111	1
Ras Pathway	1	0.159	1
Oxidative stress response	1	0.121	1
Gonadotropin-releasing hormone receptor pathway	1	0.417	1

PANTHER Pathways	No. of genes	raw P-value	False Discovery Rate (FDR)
Endothelin signaling pathway	1	0.174	1
EGF receptor signaling pathway	1	0.271	1
Cadherin signaling pathway	1	0.31	1
Blood coagulation	1	0.103	1
Apoptosis signaling pathway	1	0.235	1
Alzheimer disease-presenilin pathway	1	0.25	1

1.2.2.2 *Radiation-induced secondary cancers*

The development of secondary cancers after primary cancer survival occurs in 17-19% of cancer patients. This is especially relevant in children as they have a longer lifespan which allows more time for the development of these secondary cancers [321]. Several factors contribute to the development of secondary cancers including patient lifestyle, genetic susceptibility and treatment modality choice (chemotherapy and/or RT). Consequently, it becomes difficult to assess the effect of RT alone on secondary cancer development [322]. Certain criteria need to be achieved in order for a cancer to be considered radiation induced. These criteria include that the patient should not have a secondary cancer-predisposing mutation and the secondary cancer should originate from the primary cancer's previous irradiation field while remaining histologically different from the primary cancer. In addition, The duration between irradiation and secondary cancer onset should be sufficiently long (longer than 5 years) to allow for the usual latency of onset [323].

1.2.2.2.1 How does IR induce secondary cancers?

Secondary cancer risk due to IR stems from the improper repair of IR-induced DSBs with development of cancer promoting mutations including deletions and chromosomal rearrangements leading to malignant cell transformation [322,324]. In addition, mitochondrial dysfunction occurring as a result of IR-induced free radicals (as discussed in RICVD) has been previously implicated in carcinogenesis [325,326]. One example of a particularly challenging radiation-induced secondary cancer is radiation-induced glioblastomas (RIGs) which is an aggressive grade IV glioma. RIG can occur years (median= 8.75 years [327]) after intracranial radiation exposure with either therapeutic or diagnostic intent [328]. Recently, a large multinational study (> 600,000 pediatric participants) reported an increase in the relative risk of gliomas with increasing cumulative brain CT dose

(1.11 excess relative risk per 100 mGy) [329]. As RIGs are not histologically nor genetically different from de novo glioblastomas, investigating the molecular characteristics of RIGs may provide novel targets for monitoring their development as well as their treatment or prevention [330,331].

1.2.2.2.2 MiRNAs and lncRNAs in cancer

MiRNAs were first shown to be dysregulated in human cancers by Calin et al. investigating tumor suppressors at chromosome 13q14 region in B-cell chronic lymphocytic leukemia cells [332]. Calin et al. showed that this region contains miR-15a and miR-16-1; two miRNAs that were either deleted or downregulated in the majority of chronic lymphocytic leukemia patients [332]. Further research revealed that deletion of these two miRNAs in mice recapitulated chronic lymphocytic leukemia-associated phenotypes, subsequently confirming the miRNAs' tumor-suppressive effects [333]. Since then, miRNAs dysregulation has been characterized in a number of cancers including breast cancer and gliomas [334–336] as well as radiation-induced cancers [337–339].

MiRNA dysregulation in cancer occurs by virtue of different mechanisms. First, cancer induction of miRNA gene amplification, deletion or translocation results in oncogenic miRNA overexpression or tumor-suppressive miRNA inhibition [340]. Also, miRNAs are often tightly regulated by transcription factors such as c-MYC and p53 whose dysregulation in cancer subsequently induces miRNA dysregulation [341,342]. Alterations in DNA methylation and histone modification can also cause altered miRNA expression [343,344]. Finally, mutations and/or aberrant expression of the components of the miRNA biogenesis machinery can also cause miRNA dysregulation [345,346].

Similarly, lncRNA dysregulation has also been implicated in all cancers [347,348]. This dysregulation is induced by similar mechanisms to those causing miRNA dysregulation, namely lncRNA amplification or deletion, dysregulation of relevant transcription factors or mutations in lncRNA gene sequence [349].

Examination of dysregulated miRNAs and lncRNAs in cancer has helped identify new disease mechanisms as well as provided candidate diagnostic/prognostic biomarkers for disease progression and treatment response [350–353].

Chapter 2   **Aims of the thesis**

The use of ionizing radiation (IR) in diagnosis and therapy is associated with an increased risk for developing delayed radiation-induced adverse effects. Identification of specific disease biomarkers can help provide mechanistic insight and/or allow the identification of patients at-risk leading to improved diagnosis, monitoring and intervention. Consequently, the current PhD research investigated epigenetic biomarkers for two IR delayed adverse effects: i) radiation-induced cardiovascular disease (RICVD) and ii) glioblastoma as a possible secondary cancer.

The pathophysiology of RICVD is not fully characterized with an underexplored contribution of DNA methylation. DNA methylation is an epigenetic mechanism with known associations to both cardiovascular disease and IR. We hypothesize that IR induces DNA methylation alterations, quantifiable in blood, that influence gene expression. Identifying differentially methylated genes in response to IR could help reveal new disease mechanisms. In addition, genes correlating with rat functional cardiac data could serve as novel candidate RICVD biomarkers. These biomarkers can then help identify at-risk patients which allows earlier intervention and better patient outcomes.

On the other hand, miRNAs and lncRNAs are often dysregulated in cancer tissues. Advancements in sequencing technology have allowed access to transcriptomic cancer datasets which can be integrated to identify common cancer-specific coding and noncoding players. Therefore, identification of differentially expressed miRNAs and lncRNAs in glioblastoma can provide more insight to glioblastoma pathophysiology. These miRNAs and lncRNAs could also provide potential biomarkers thereby allowing the diagnosis and monitoring of glioblastoma development as a secondary cancer after IR.

Thus, the aims of the current thesis are:

- Investigating radiation-induced DNA methylation alterations in a RICVD rat model while evaluating the expression of the top DMRs in breast cancer patients receiving adjuvant radiotherapy (**Chapter 3**).

- Investigating the DNA methylation profile of breast cancer patients receiving adjuvant radiotherapy (up to 24 months after radiotherapy) (**Chapter 4**).

- Identification of differentially expressed miRNAs and lncRNAs in glioblastoma tissues through in silico meta-analysis (**Chapter 5**).

Chapter 3 DNA methylation alterations in fractionally irradiated rats and breast cancer patients receiving radiotherapy

Magy Sallam[1,2], Mohamed Mysara[1,3], Mohammed Abderrafi Benotmane[1], Anne P. G Crijns[4], Daan Spoor[4], Filip Van Nieuwerburgh[5], Dieter Deforce[5], Sarah Baatout[1,6], Pieter-Jan Guns[2], An Aerts[1†] and Raghda Ramadan[1]

[1] Radiobiology Unit, Interdisciplinary Biosciences, Belgian Nuclear Research Centre, SCK CEN, Mol, Belgium;
[2] Laboratory of Physiopharmacology, University of Antwerp, Wilrijk, Belgium;
[3] Current affiliation: Bioinformatics Group, Center for Informatics Sciences (CIS), School of Information Technology and Computer Science (ICTS), Nile University, Giza, Egypt;
[4] Department of Radiation Oncology, University of Groningen, University Medical Center Groningen, Groningen, The Netherlands
[5] Laboratory of Pharmaceutical Biotechnology, Ghent University, 9000 Gent, Belgium.
[6] Department of Molecular Biotechnology, Ghent University, Ghent, Belgium;

3.1 Introduction

Thoracic radiotherapy has been shown to increase the risk of cardiac toxicity in cancer patients [126,137,146]. Despite the current radiation-sparing techniques, which limit cardiac exposure, radiation-induced cardiovascular disease (RICVD) is still a primary clinical concern that manifests mainly as coronary heart disease, remaining asymptomatic until 10 to 15 years after radiotherapy (RT) [354]. However, a 6% decrease in global longitudinal strain (GLS), an early sign of subclinical left ventricular dysfunction, has been reported in breast cancer patients as early as 6 months after radiotherapy [154,355]. Consequently, investigating early molecular changes in the cardiovascular system after radiotherapy could identify novel, unexamined players in RICVD pathology and/or potential biomarkers to identify patients at risk, thereby allowing earlier countermeasures.

DNA methylation is an epigenetic process essential for development and maintenance of cellular homeostasis, normally associated with transcriptional silencing when affecting gene promoters [356,357]. Alterations in DNA methylation have been reported in many diseases, including neurodegenerative diseases such as Parkinson's disease [358], diabetes mellitus [359] and cancer [360]. In addition, recent research indicates a connection between DNA methylation and cardiovascular disease risk [361,362] with methylation alterations preceding histologically evident atherosclerosis [203]. DNA methylation has been hypothesized to affect atherosclerosis pathogenesis by regulating oxidative stress, inflammation and vascular smooth muscle cell (VSMC) phenotype [363]. Interestingly, radiation has also been shown to affect DNA methylation. Both radiation-induced global hypomethylation, as well as gene-specific hypermethylation, have been reported [65,230,354]. However, the contribution of DNA methylation in X-irradiation-induced cardiac toxicity is underexplored. Consequently, the current study aims to investigate the effects of ionizing radiation on DNA methylation in the blood of irradiated rats and breast cancer patients to provide more clarity on the involvement of DNA methylation in RICVD.

The current study is part of the Horizon 2020 project MEDIRAD (http://www.medirad-project.eu) which addresses the implications of medical low dose radiation exposure [166]. Within MEDIRAD, the effect of radiation on cardiac dysfunction is investigated using preclinical and clinical experimental models [364,365]. In the current study, we assess the methylation profile of irradiated rats of the preclinical model, with special focus on cardiac-relevant differentially methylated regions (DMRs). We also investigate the expression profile of the cardiac-relevant rat-identified DMRs in 25 breast cancer patients from the MEDIRAD EARLY-HEART cohort. The latter cohort being a European multicenter study involving 250 breast cancer patients treated with adjuvant radiotherapy and followed up for 2 years after initial treatment [365].

3.2 Materials and Methods

3.2.1 Animals and irradiation

Adult female Wistar rats (12-14 weeks old) underwent whole heart X-irradiation of 0.04, 0.3 and 1.2 Gy for 23 consecutive days (weekend excluded), resulting in cumulative doses of 0.92, 6.9 or 27.6 Gy. Control rats were sham-irradiated (0.0 Gy) following the same procedure. This translational experimental model was performed at MEDIRAD consortium partner, Centro Cardiovascular da Universidade de Lisboa (CCUL) [364]. There, blood was collected at 1.5, 3, 7 and 12 months after irradiation. Blood samples were received on dry ice and stored at -80°C until further processing.

3.2.2 DNA extraction

DNA was extracted from 200 µL frozen blood pellets using QIAamp DNA mini kit (Qiagen, Germany) according to kit protocol. However, the extracted DNA concentration was found to be low (1-5 ng/µL; data not shown). To increase the efficiency of DNA extraction, phenol/chloroform/isoamyl alcohol mixture (25:24:1 PCI) was incorporated into the DNA extraction protocol. Briefly, after sample thawing, samples were incubated with proteinase K and buffer AL at 56°C for 10 minutes. 700 µL PCI was added per sample and mixed for 1.5 hours at 1400 rpm at room temperature (Eppendorf Thermomixer C, Eppendorf AG,

Germany). Next, samples were centrifuged for 5 minutes at 14000 x g. The upper aqueous layer containing the DNA was collected and 1 -1.5 mL 100% ethanol as well as 50 μL buffer AL were added to precipitate the DNA. Finally, this mixture was transferred to QIAamp DNA mini kit column in 700 μL aliquots. Extraction was continued using QIAamp DNA mini kit following manufacturer recommendations. DNA concentration and purity were determined by comparing the ratio of optical density (OD) at 260 and 280 nm.

3.2.3 Global DNA methylation using MethylFlash Global DNA Methylation

Absolute global 5-methyl cytosine (5-mC) levels were analyzed in extracted DNA using MethylFlash Global DNA Methylation (5-mC) ELISA Easy Kit (Epigentek Group Inc., USA) according to manufacturer protocol. The kit measures 5-mC content as a percentage of total cytosine content. 100 ng of purified DNA was added to the ELISA plate. The methylated fraction of DNA was detected using 5-mC specific antibodies and quantified colorimetrically by measuring OD at 450 nm. The positive control supplied with the kit was used to generate a standard curve. The slope of the standard curve was calculated and used to determine the concentration of 5-mC in the samples as follows: 5-mC% = [(Sample OD – Negative control OD)/(Slope * DNA quantity)]x100.

3.2.4 Gene-specific DNA methylation analysis using SureSelect Methyl-Seq

Gene-specific methylation analysis was performed with the Rat SureSelect Methyl-Seq platform (Agilent Technologies Inc., USA). SureSelect MethylSeq is a type of methylation capture sequencing (MC-seq) using biotinylated RNA baits to capture the genomic areas of interest for subsequent bisulfite sequencing. This method allows quantitative analysis of DNA methylation with single base resolution [366,367]. The rat SureSelect MethylSeq has been designed to target non-redundant promoters, CpG islands, island shores as well as previously identified GC-rich sequences [368]. Sixteen samples were selected to undergo SureSelect Methyl-Seq library preparation: sham-irradiated rats at 1.5 months (n=4), 27.6 Gy irradiated rats at 1.5 months (n=4), sham-irradiated rats at 7 months (n=4) and 27.6 Gy

irradiated rats at 7 months (n=4). Due to technical limitations which necessitated high DNA sample concentrations (3 µg) with limited available blood per rat, sample size per group was limited. Library preparation and sequencing were performed in collaboration with the Ghent University sequencing facility NXTGNT (Ghent, Belgium) and GENEWIZ global genomics service company (GENEWIZ Germany GmbH, Leipzig, Germany). Library preparation, probe-based target enrichment, bisulfite treatment, and library indexing PCR were performed according to SureSelect^{XT} Methyl-Seq Library Preparation kit (Agilent Technologies Inc., USA) protocol (Version E0, April 2018). The libraries were equimolarly pooled and sequenced together with a 20% PhiX control spike-in v3 (Illumina) on Illumina Hiseq 4000, generating approximately 1.2E+09 paired-end reads of 150 base pair length.

For the sequencing data analysis, similar methods were applied as was previously described [369]. Raw read quality control was assessed using FASTQC (version 11.9). This was followed by reads trimming using Trim Galore (version 0.6.4) with the paired-end mode using the default parameters. Reads quality post trimming was re-assessed as well (using FASTQC). Using Bismark (version 0.19.0), reads were mapped to *Rattus norvegicus* genome which utilizes bowtie 2 (version 2.3.3), with a maximum of 1 mismatch in the seed region. The *Rattus norvegicus* reference genome (Rnor6.0) was downloaded from ftp://ftp.hgsc.bcm.edu/Rnorvegicus/Rnor6.0/, and then indexed using Bismark with *bismark_genome_preparation* script. After mapping, these temporary changes were reverted. Subsequently, PCR duplications were removed using *deduplicate_bismark* script and a post-alignment quality control was performed using *flagstat* option of samtools (version 1.6) and *stats* option of BamUtil (version 1.0.14). The methylation level was assessed for each methylation context separately (for cytosines followed by guanines (CpGs), non-guanines and guanines (CHGs), two non-guanines (CHHs) or any other possibilities (CNs)). This was executed using *bismark_methylation_extractor* with the following flags: paired-end, no-overlap, and minimum coverage of at least 1 read, whilst the remaining parameters were set to the default settings.

For the rest of the analysis, only CpG methylations were included. For this, BSseq package (version 1.18.0) was used in Bioconductor. First, the data was smoothed using *BSmooth* function allowing 20 CpGs as a minimum within a window of 500 thereby smoothing the methylation levels across the CpGs within that window. This was used to establish thresholds for t-statistics (calculated using BSmooth.tstat function) across the groups using 1st and 99th quantile percentiles. Only CpGs with a minimum coverage of 10x within at least 3 samples were retained, and differentially methylation regions (DMRs) were identified using *dmrFinder* command. Each identified DMR was subjected to 1000 iterations of permutations (with randomization) that re-calculate the t-statistics for each permutation, and p-values were calculated and corrected using Benjamini-Hochberg false discovery rates (FDRs), for multiplicity problem. The p-values were calculated as the fraction of null areas (retrieved after each permutation) exceeding the observed area (before permutation). This was executed twice, performing pairwise comparison between sham-irradiated vs 27.6 Gy at 1.5 and 7 months, separately. After that, DMRs were annotated to the rat genome (assembly Rnor_6.0) using closest from bedtools.

3.2.5 Pathway analysis of rat differentially methylated regions (DMRs) by STRING-db

Pathway analysis of significant SureSelect MethylSeq DMRs (p-value< 0.05) at 1.5 and 7 months after 27.6 Gy or 0 Gy (sham) was performed using the STRING database (V.11.2). STRING is a database dedicated to organism-wide protein association networks by integrating known and predicted associations between proteins, including both physical interactions and functional associations [370]. The produced protein-protein interaction (PPI) network was then exported to Cytoscape 3.9.0 [371] where STRING enrichment was retrieved and enrichment maps were constructed using *EnrichmentMap* app in Cytoscape (V.3.3.3).

3.2.6 Investigation of expression alterations in DMRs using quantitative PCR

Validation of the rat DMRs was performed by quantitative Real Time PCR (qRT-PCR) in the blood of rats irradiated with 0, 0.92, 6.9 and 27.6 Gy FI at 1.5, 3, 7 and 12 months. Selection of the "top" target genes was performed by filtering the SureSelect MethylSeq output to show only DMRs with significant (p-value<0.05) methylation difference (>25%) to limit downstream analyses [372–374]. Afterwards, a literature search of the filtered DMRs was performed to focus on genes with documented association to cardiovascular disease. This led to 8 selected genes: SLMAP, LDLR, ITPR2, CDH18, CACNA1C, CELF4, E2F6 and PTPN2. Only SLMAP, LDLR, ITPR2, E2F6 and PTPN2 were detectable in rat blood.

RNA was extracted from frozen rat blood using NucleoSpin RNA Blood Mini kit (Macherey-Nagel GmbH & Co. KG, Germany) according to manufacturer instructions. Then, reverse transcription of extracted RNA was performed using GoScript Reverse Transcription Mix employing random primers (Promega Corporation, USA). Four genes were assayed as reference genes (POLR2A, TBP, ACTB and PHLPP1). Selection of the reference gene was performed using NormFinder [375] whereby PHLPP1 showed the highest stability and was selected for normalization. The expression levels of selected DMR transcripts were determined by qPCR using TaqMan Gene Expression Assays (Thermo Fisher Scientific, USA) (SLMAP: Rn01401804_m1; LDLR: Rn00598442_m1; ITPR2: Rn00579067_m1; E2F6: Rn01499181_m1; PTPN2: Rn00588846_m1; PHLPP1: Rn00572211_m1). qPCRs were performed using Fast Advanced Master Mix (Thermo Fisher Scientific, USA) on qTOWER^3 touch thermal cycler (Analytik Jena, Germany). Relative quantification was calculated using the equation $\log 2^{-\Delta\Delta CT}$, where $\Delta\Delta C_T = [C_T \text{ of target gene} - C_T \text{ of reference gene}]_{\text{irradiated group}} - [C_T \text{ of target gene} - C_T \text{ of reference gene}]_{\text{sham group}}$.

Significantly dysregulated proteins in cardiac tissues of rats receiving 27.6 Gy FI, supplied by MEDIRAD consortium partners [364], were queried in STRING-db (showing 50 interactors in 1st and 2nd shell) to reveal any relevant interactions with the rat DMGs.

3.2.7 Correlation of rat global DNA methylation and DMR expression with global longitudinal strain (GLS)

MEDIRAD consortium partner, CCUL, evaluated the cardiac function of the irradiated rats and reported a dose dependent reduction of GLS (>15%) [364]. 5-mC% levels and qPCR expression levels of rat DMGs were correlated with GLS in rats sacrificed at 12 months after irradiation.

3.2.8 Investigating gene expression of selected DMRs in breast cancer patients' blood

3.2.8.1 *Patient Selection*

Blood was collected from MEDIRAD EARLY HEART cohort of breast cancer patients treated with adjuvant radiotherapy (RT). This was performed at our consortium partner University Medical Center Groningen (UMCG), including a random selection of 25 breast cancer patients with right sided (n=9) and left sided breast cancer (n=16) [376]. The study was approved by the Ethics committee at UMCG (NL62360.042.17). Female unilateral breast cancer patients aged 40-75 years treated with primary breast conserving surgery and postoperative RT were recruited during their first visit with the radiation oncologist. All patients signed a written informed consent form. Patients with previous medical history of coronary artery disease and/or myocardial infarction and/or atrial fibrillation were excluded. The patients were classified as having left- or right sided breast cancer according to the anatomical position of the tumor.

3.2.8.2 *RT protocol*

The total dose for the breast was 40.05-43.6 Gy. This dose was delivered in 15-20 separate fractions with a volumetric modulated arc therapy/ fixed-field intensity-modulated RT (VMAT/IMRT) technique. Left-sided breast cancer patients were treated with deep inspiration breath hold using the active breathing control system in order to lower the cardiac dose as much as possible. The MHD of the included patients was provided by UMCG (**Supplementary table 1.1 in Supplementary materials for Chapter 3**)

3.2.8.3 *Blood collection and reverse transcription qPCR*

Blood was collected from the patients in EDTA vacutainers at 3 time points: at diagnosis (V0), directly after RT (V1) and 6 months after RT (V2). Blood samples were centrifuged at 1500 x g for 15 min to separate the plasma. Blood pellets were then stored at -80°C until further processing. RNA extraction, cDNA synthesis and gene expression analysis were performed using the same protocols detailed for the rat samples. TaqMan real-time PCR assays were used for qPCR quantification of SLMAP, LDLR, ITPR2, E2F6, PTPN2 expression relative to reference gene, TBP (SLMAP: Hs01058330_g1; LDLR: Hs00181192_m1; ITPR2: Hs00181916_m1; E2F6: Hs01034552_m1; PTPN2: Hs00959888_g1; TBP: Hs00427620_m1).

3.2.9 Statistical Analysis

Normality of all datasets was assessed by Shapiro-Wilk test. Analysis of global methylation was performed using a generalized linear model with least significant difference (LSD) correction for multiple comparisons. Analysis of normally distributed parametric rat qPCR data was performed using a general linear model with LSD correction for multiple comparisons. For non-parametric rat qPCR data, analysis was performed using a generalized linear model with LSD correction for multiple comparisons. Correlation with functional data was performed by calculating Pearson correlation coefficient. Statistical analysis of breast cancer patient qPCR data was performed using a generalized estimating equation to accommodate for the nonparametric characteristics of the data. All detailed statistical analyses were performed using SPSS version 28 (IBM Corp., NY, USA).

3.3 Results

3.3.1 Global hypomethylation observed at 12 months after whole heart rat irradiation

The percentage of 5-methyl cytosine (5-mC%) in rat blood DNA after the different irradiation doses at the four sampling time points is shown in **Figure 3-1**. The irradiated rats exhibited dose dependent reduction of global longitudinal strain (GLS) (>15%), as measured by echocardiography, at 12 and 18 months along with decreased cardiac apex

microvascular density after 27.6 Gy [364]. Significant hypomethylation was observed at 12 months after all irradiation doses relative to sham-irradiated rats. This is especially evident in rats irradiated with 0.92 and 6.9 Gy with significantly lower methylation levels observed at 7 and 12 months relative to 1.5 months. Global hypomethylation, as measured by 5-mC%, strongly correlated with the GLS of rats receiving 6.9 and 27.6 Gy at 12 months after fractionated irradiation (FI) (r=|0.998|, p-value<0.05 and r=|0.884|, p-value=0.12, respectively; 6.1).
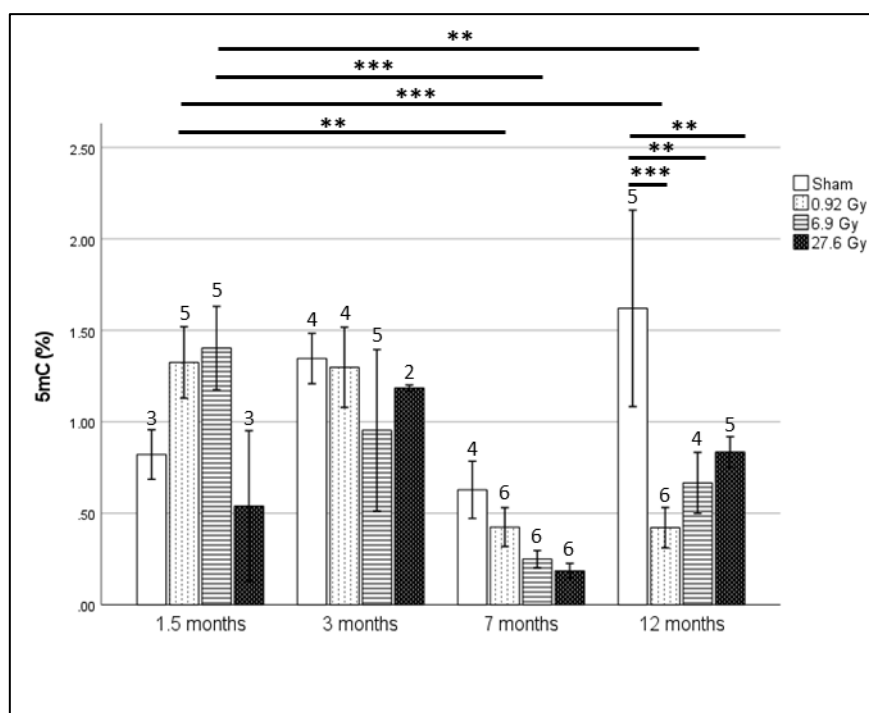
Figure 3-1 *Percentage of 5-mC (%) after fractionated irradiation of 0, 0.04, 0.3 and 1.2 Gy resulting in total irradiation dose of 0, 0.92, 6.9 and 27.6 Gy as measured by MethylFlash Global DNA Methylation (5-mC) ELISA Easy Kit at 1.5, 3, 7 and 12 months after irradiation. Plotted values represent group means ± standard error of mean (SEM) with the number of rats per group indicated per bar. Statistical analysis was performed using SPSS generalized linear model module and multiple comparison correction was performed using least significant difference (LSD) (**=p-value<0.01, ***<0.001).*

3.3.2 Gene-specific DNA methylation analysis and enriched pathways of rat DMRs

A total of 67098 and 684433 DMRs were identified across all chromosomes at 1.5 and 7 months after 27.6 Gy FI relative to sham-irradiated rats, respectively**.** After DMR filtering according to significance (p-value< 0.05), the number of DMRs dropped to 7344 and 8620

at 1.5 and 7 months, respectively. Of those, 3933 and 4710 DMRs were hypomethylated while 3411 and 3910 DMRs were hypermethylated at 1.5 and 7 months after irradiation, respectively (**Figure 3-2**).
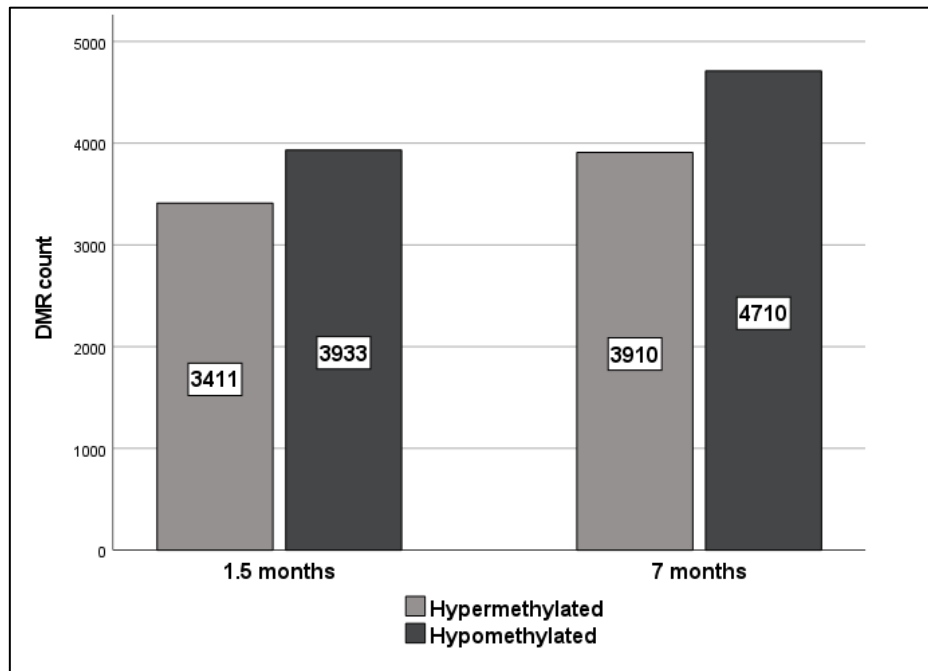
Figure 3-2 *Significant hyper- (pale grey) and hypo- (dark grey) methylated DMR counts (p-value<0.05) identified by SureSelect MethylSeq in rats receiving 27.6 Gy FI relative to sham-irradiated rats at 1.5 and 7 months after irradiation.*

Pathway analysis of significant DMRs (p-value<0.05) revealed the enrichment of several pathways, including the dilated cardiomyopathy pathway at both 1.5 and 7 months (**Figure 3-3**). Other cardiac relevant KEGG pathways were also enriched at 1.5 months (adrenergic signaling in cardiomyocytes, cardiac muscle contraction, hypertrophic cardiomyopathy, arrhythmogenic right ventricular cardiomyopathy, calcium signaling pathway and Hippo signaling pathway) as well as at 7 months (regulation of actin cytoskeleton and tight junction).

For downstream qPCR validation, cutoff criteria were applied yielding 10 and 24 DMRs at 1.5 and 7 months, respectively (**Supplementary table 1.2 and 1.3 in Supplementary materials for Chapter 3**). Next, the DMR list was further reduced by selection of DMRs

previously linked to cardiovascular function in literature. qPCR validation was performed for 8 DMRs (SLMAP, LDLR, ITPR2, CDH18, CACNA1C, CELF4, E2F6 and PTPN2). A brief description of these genes, their connection to cardiovascular function/disease and observed methylation status is provided in **Table 3-1.**

From STRING-db, multiple interactions were identified between dysregulated cardiac proteins and LDLR (calnexin), ITPR2 (Phopholipase C beta3), E2F family (RBBP7) and PTPN family (SLM2, Thioredoxin, Ubiquiting-protein ligase B, galectin1, hrRNP K, cysteine and glycin-rich protein 1). In addition, two of the significantly dysregulated cardiac proteins were shown to interact with CACNA1 family (Calsequestrin 2 and Myosin 4).
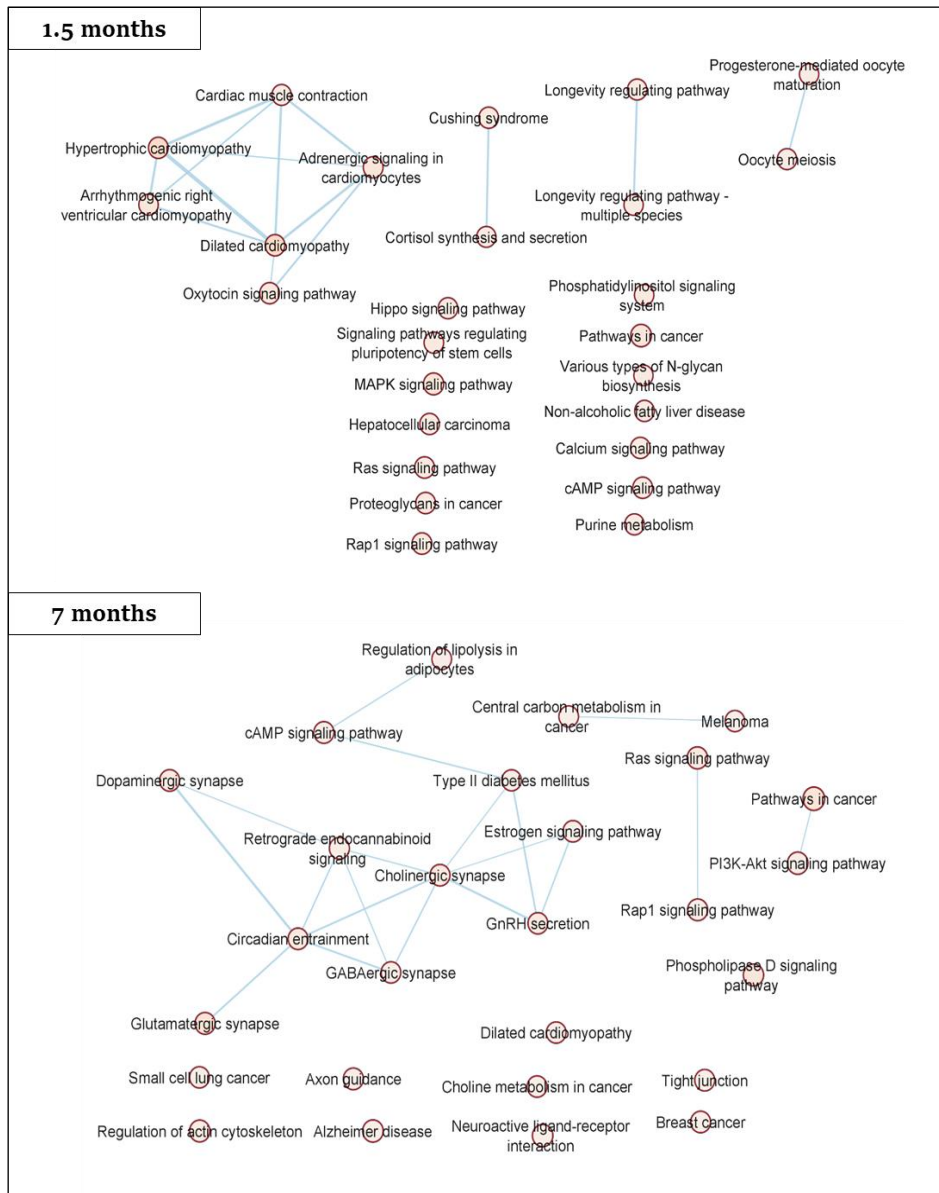
Figure 3-3 Pathway analysis of significant DMRs (p-value<0.05). Statistically significant KEGG pathways (p-value<0.05, Q-value<0.25) were visualized by STRING-db and Cytoscape, respectively.

Table 3-1 DMRs selected for downstream validation, their correlation to cardiovascular function/disease and their altered methylation status after 27.6 Gy FI.

Gene	Connection to cardiac function/disease	Methylation state after 27.6 Gy FI dose relative to sham irradiated rats (p-value<0.05)
SLMAP	SLMAP is a component of cardiac membranes involved in excitation-contraction (E-C) coupling and	Hypomethylated at 1.5 months after irradiation

Gene	Connection to cardiac function/disease	Methylation state after 27.6 Gy FI dose relative to sham irradiated rats (p-value<0.05)
(Sarcolemma Associated Protein)	its perturbation results in progressive deterioration of cardiac electrophysiology and function [377].	
	SLMAP also interacts with cardiac myosin suggesting a direct role in controlling cardiomyocyte contraction [378].	
LDLR (Low Density Lipoprotein Receptor)	Knockouts and/or mutations in LDLR lead to ineffective clearance of serum low density lipoprotein (LDL) cholesterol and contribute to premature atherosclerosis and cardiovascular disease [379].	Hypomethylated at 7 months after irradiation
ITPR2 (Inositol 1,4,5-Trisphosphate Receptor Type 2)	Certain polymorphs of ITPR2 have been associated with higher systolic blood pressure. ITPR2 is expressed widely in myocytes with altered expression in heart failure [380,381].	Hypomethylated at 7 months after irradiation
CDH18 (Cadherin 18)	A deletion involving CDH18 was reported to be found in a case of congenital heart disease [382].	Hypomethylated at 1.5 months after irradiation
	In a study involving copy-number variants and the risk of sporadic congenital heart disease, rare deletions in study participants with congenital heart disease were in found in a number of genes including CDH18 [383].	
CACNA1C (Calcium Voltage-Gated Channel Subunit Alpha1 C)	CACNA1C is a part of voltage-gated L-type calcium channel gene which plays an important role in cardiac electrical excitation [384].	Hypomethylated at 1.5 and 7 months after irradiation
CELF4 (CUGBP Elav-like family member 4)	A polymorphism of CELF4 has been reported to have a modifying effect on anthracycline-related cardiomyopathy [385].	Hypomethylated at 7 months after irradiation
E2F6 (E2F Transcription Factor 6)	E2F6 is a cell cycle regulator, abrogation of expression of E2F6 in neonatal cardiac myocytes leads to a significant decrease in myocyte viability suggesting a role in myocardial regeneration [386]. [386,387]	Hypomethylated at 1.5 months after irradiation
	Forced E2F6 expression activates gene expression in myocardium resulting in dilated cardiomyopathy [387].	
PTPN2	Decreased expression of PTPN2 through activation of miR-201 leads to attenuation of apoptosis and	Hypomethylated at 7 months after irradiation

Gene	Connection to cardiac function/disease	Methylation state after 27.6 Gy FI dose relative to sham irradiated rats (p-value<0.05)
(Protein Tyrosine Phosphatase Non-Receptor Type 2)	improvement of migration of cardiac stem cells exposed to hypoxia which would in turn increases their potential to repair the injured myocardium [388].	

3.3.3 Hypomethylation of SLMAP at 1.5 months translates into a dose-dependent increase in gene expression

Of the eight DMRs assessed by qPCR, only five genes were present in detectable quantities (SLMAP, LDLR, ITPR2, E2F6 and PTPN2) (from now on called differentially methylated genes (DMGs)). SLMAP expression was significantly increased after 1.5 months in all irradiated rats **Figure 3-4 A**). This increased expression follows the observed hypomethylation after 27.6 Gy FI. Significantly increased SLMAP expression continues to 3 and 12 months after 0.92 Gy FI. For the other genes, LDLR, ITPR2, E2F6 and PTPN2 (**Figure 3-4 B-E**), a number of gene expression alterations were detected, yet without consistent trends across radiation doses or follow-up time. Moreover, qPCR results did not reproduce the observed methylation pattern.

Correlation between DMG expression and rat GLS measurements identified a strong correlation between E2F6 expression and the GLS of rats receiving 27.6 Gy FI (r= |0.872|, p-value<0.05).
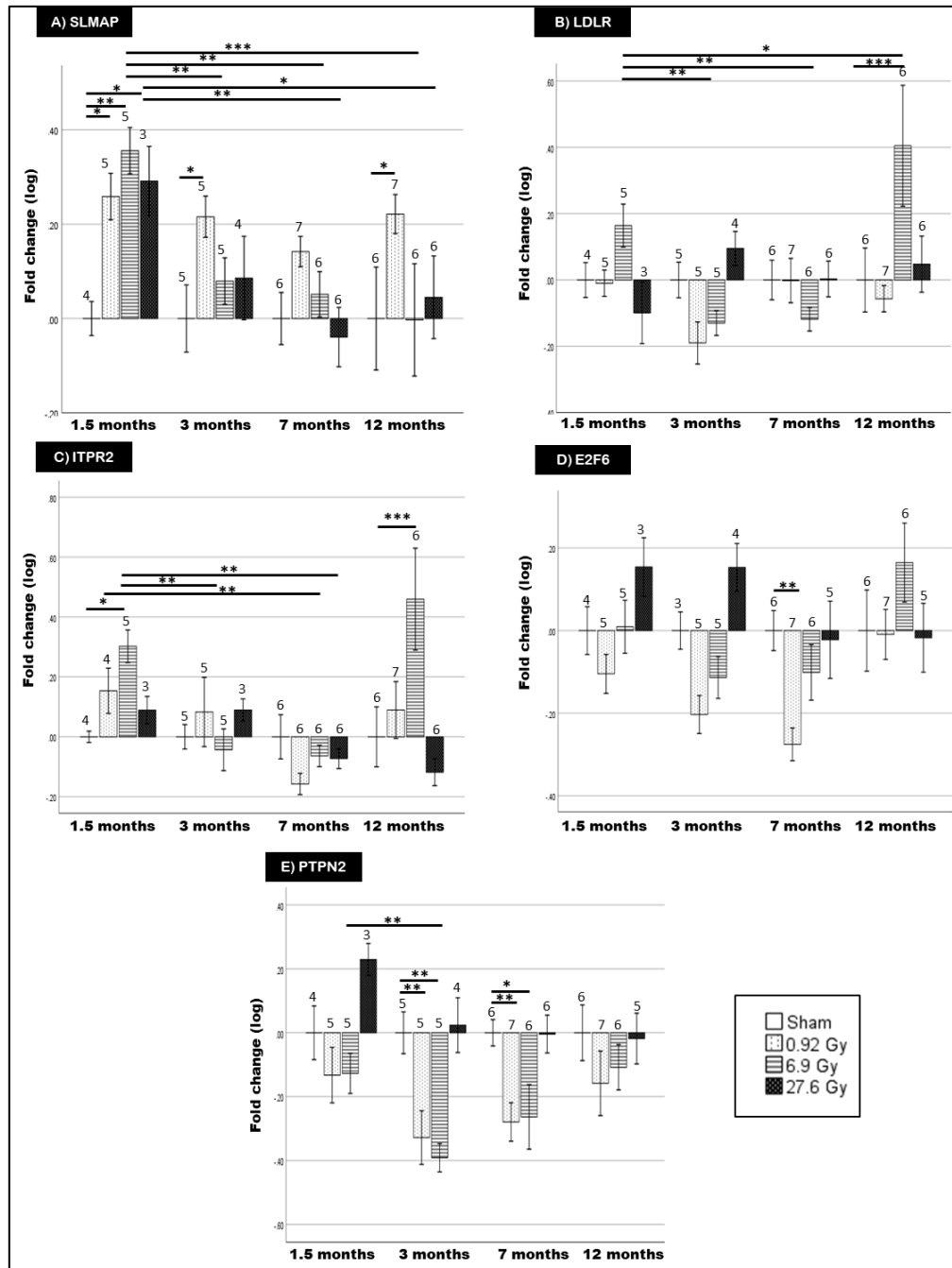
Figure 3-4 *mRNA expression levels of SLMAP (A), LDLR (B), ITPR2 (C), E2F6 (D) and PTPN2 (E) in the blood of rats receiving either sham irradiation (0 Gy) or fractionated irradiation of 0.92, 6.9 and 27.6 Gy and sampled after 1.5, 3, 7 and 12 months. Data is presented as log fold change normalized to PHLPP1 (*=p-value<0.05, **<0.01, ***<0.001). Number of rats per group is indicated atop their respective bars. Plotted values represent group means ± standard error of mean (SEM). Statistical analysis was performed by SPSS General linear model and generalized linear models for data following normal and non-normal distribution, respectively. Multiple comparison correction was performed using Fisher's LSD.*

3.3.4 Two of the selected rat DMGs show altered expression in breast cancer patient blood

Patients of the MEDIRAD cohort with significantly higher cardiac radiation exposure showed a GLS-based subclinical left ventricular dysfunction (GLS decrease >15%) 6 months after RT [376]. In the assayed breast cancer patient blood, SLMAP showed a trend of increased expression for left sided breast cancer patients at V1 relative to V0, which decreases significantly at V2 (**Figure 3-5A**). Both ITPR2 and E2F6 showed increased expression at V1 relative to V0. However, the increase for ITPR2 was only significant in right sided breast cancer patients, while for E2F6 it was in left sided breast cancer patients (**Figure 3-5 C and D**). Previously, we demonstrated that selective inhibition of Connexin-43 (CX43) hemichannels alleviated radiation-induced endothelial cell damage [389]. In addition, E2F6 was reported to affect the expression of CX43 gene (GJA1) in transgenic mice [387]. In our current experiments, we also found CX43 expression to be significantly increased at V1 in left sided breast cancer patient blood relative to V0 (**Figure 3-5F**).

In addition, patient stratification was performed according to whether the mean heart dose (MHD) was higher or lower than 2.5 Gy. The 2.5 Gy MHD threshold was selected according to the German Society for Radiation Oncology (DEGRO) recommendations to minimize radiation-induced cardiotoxicity [390]. After stratification of data, the changes in E2F6 and SLMAP were found to occur mainly at the higher radiation doses (>2.5 Gy). Correlation of MHD dose and gene expression indicated a medium correlation at V1 for ITPR2, E2F6 and CX43 (GJA1) (ITPR2: $r=|0.54|$, p-value= 0.032; E2F6: $r=|0.52|$, p-value= 0.037; GJA1: $r=|0.51|$, p-value= 0.043) and at V2 for SLMAP (Pearson correlation coefficient $r = |0.59|$, p-value = 0.017).
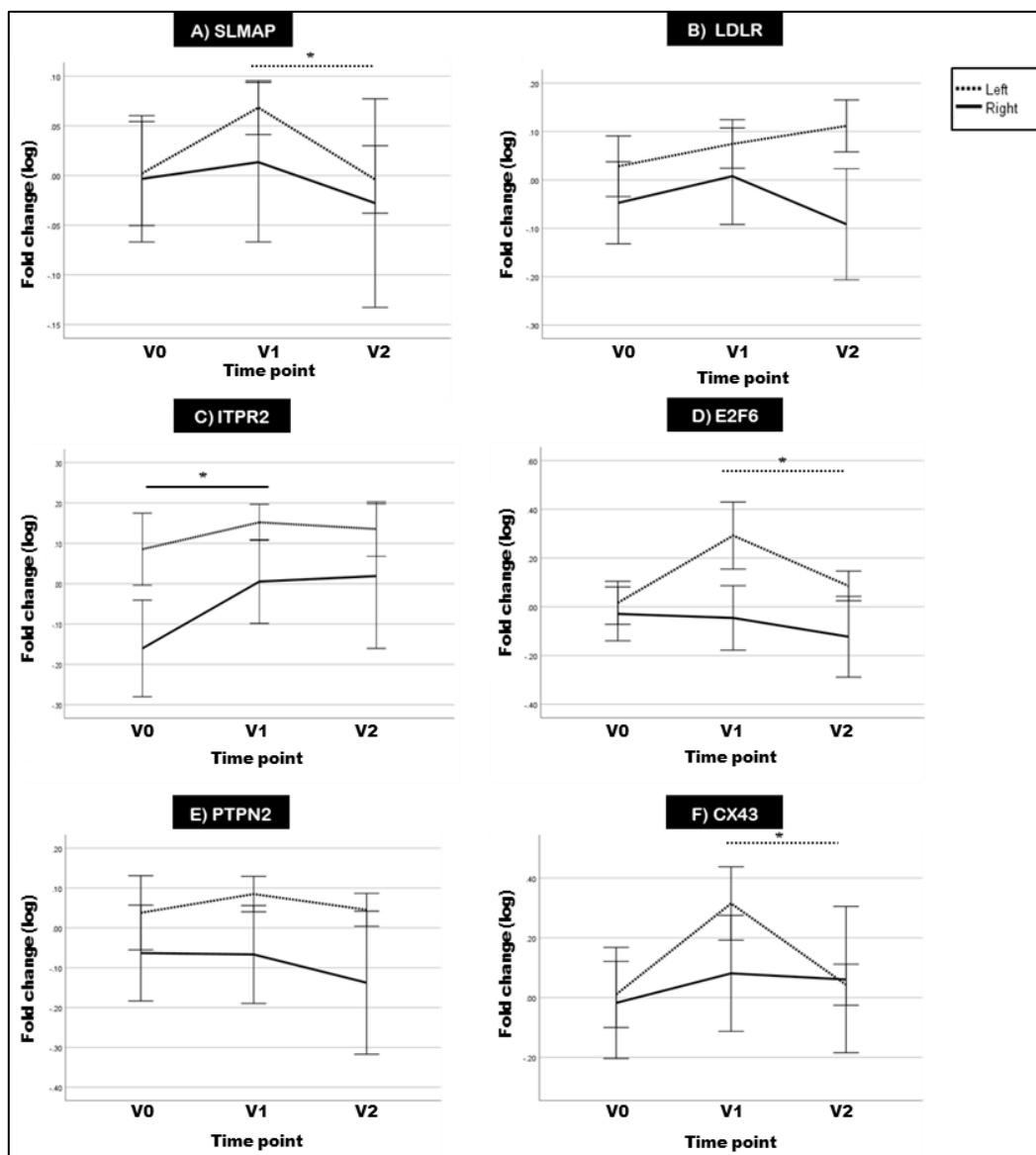
Figure 3-5 *Mean log fold change of SLMAP (A), LDLR (B), ITPR2 (C), E2F6 (D), PTPN (E) and CX43 (GJA1) (F) expression in the blood of right (n=9) and left sided (n=16) breast cancer patients sampled at diagnosis (V0), immediately after RT (V1) and 6 months after RT (V2). Data are presented as mean log fold changes in gene expression normalized to TBP ± SEM. Displayed significance values were calculated using observed log expression fold changes (*=p-value<0.05). Statistical analysis was performed using SPSS generalized estimating equations module and multiple comparison correction was performed using LSD.*

3.4 Discussion

In the current study, we evaluated the effects of local heart irradiation on global and gene-specific DNA methylation in an experimental RICVD rat model. The validity of this model was previously confirmed by Ribeiro et al. who reported significant myocardial dysfunction

76

(i.e. GLS decrease of >15%) at 12 and 18 months after 27.6 Gy FI [364]. Moreover, irradiated rats showed a decreased microvascular density (MVD) in apex of these rats' hearts which has been proposed as a predictor of early left ventricular remodeling [364]. Previous research investigating radiation-induced global methylation effects has reported variable effects of hyper- and hypo-methylation [167,171,391], as well as an occasional absence of methylation effects [163,169,392]. Our results showed global hypomethylation at 12 months for all doses while a hypomethylation trend was observed over time after 0.92 and 6.9 Gy FI. However, interpretation of our global methylation results is difficult due to the high inter-replicate variability and low sample numbers in certain groups. Nevertheless, a strong association between global methylation and GLS levels was observed at 12 months after the 2 higher doses (6.9 and 27.6 Gy). The global hypomethylation observed after 27.6 Gy follows previous reports linking global DNA methylation with cardiac dysfunction [337,393–395]. As for gene-specific methylation, higher numbers of hypomethylated DMRs were found at both 1.5 and 7 months after 27.6 Gy FI. Although there are limited studies addressing the effects of ionizing radiation on gene specific methylation, most of these studies declare a higher predilection to hypermethylation [354,396]. However, the direction of gene specific methylation appears to vary according to employed animal model/cell line and irradiation protocol [354].

Pathway analysis of significant DMRs revealed dilated cardiomyopathy as an enriched pathway in rat blood at both 1.5 and 7 months. Interestingly, Ribeiro et al. (MEDIRAD colleagues) performed a proteomic analysis on the rats' cardiac tissues and also identified dilated cardiomyopathy as a significantly dysregulated protein pathway [364]. Other overlapping pathways between the rat DMRs (current study) and proteomics dataset [364] include cardiac muscle contraction, hypertrophic cardiomyopathy, adrenergic signaling in cardiomyocytes and longevity regulating pathway (DMRs at 1.5 months), as well as gonadotropin releasing hormone (GnRH) secretion, dopaminergic synapse, tight junction and circadian entrainment (DMRs at 7 months). All of these pathways have been previously implicated in cardiovascular impairment [270,397–405]. Dysregulation of these pathways has been known to result from oxidative stress, a proven contributor in radiation-induced

cardiotoxicity [400,406–411]. Overall, pathway analyses of DMRs and proteomics datasets seem to support the occurrence of radiation-induced DNA methylation alterations in cardiac relevant genes which can affect functional protein levels.

Only SLMAP presented concurrent hypomethylation and overexpression at 1.5 months after 27.6 Gy FI. SLMAP represents a family of tail-anchored sarcolemmal membrane-associated proteins in the myocardium which regulates cardiac excitation-contraction [377,378,412]. Altered SLMAP methylation was previously documented in advanced atherosclerotic plaques of coronary heart disease patients [413]. SLMAP can also inhibit Hippo signaling; a DMR enriched pathway at 1.5 months previously associated with dilated cardiomyopathy and ischemic heart disease [414]. Specifically, Hippo pathway activation induces DNA damage-induced cardiomyocyte apoptosis after irradiation which is particularly relevant in the ensuing cardiac toxicity [415,416]. Consequently, the observed hypomethylation and overexpression may serve as a protective mechanism against radiation-induced cardiac effects by promoting cardiac regeneration and cardiomyocyte proliferation. However, as SLMAP overexpression gradually decreases at the later time points, these protective effects seem to be time-limited.

For the other DMGs (LDLR, ITPR2, E2F6 and PTPN2), there was poor correlation between methylation status and gene expression. This discordance could be due to the occurrence of the DMRs primarily in gene body locations (c.f. gene promoters). While the exact function of gene body DNA methylation is poorly understood, hypothesized functions include inhibition of alternative splicing [417] and prevention of transcription initiation at intergenic promoters [418]. Previous research has indicated a positive correlation between gene body methylation and gene expression [49,419]. However, other studies have also shown a negative relationship between gene body methylation and gene expression [420–425]. This could be due to gene body CpGs representing functional elements such as enhancers, alternative promoters, transcription factor binding sites, repetitive elements and enrichment of nucleosomes at intron-exon junctions [49,422]. Therefore, these observations suggest that DNA methylation's regulation of gene expression is bidirectional

with the location of CpG sites, disease context and relevant genes influencing the methylation effect [426].

Interestingly, Yao et al. previously reported the differential methylation of E2F, PTPN and CDH families in rat cardiac tissues after 6 months of acute 18 Gy of local heart irradiation [396]. As these rats also presented with RICVD, this suggests these gene families' responsiveness to radiation-induced methylation alterations. In addition, CACNA1C, a DMR exhibiting >25% differential methylation at 1.5 and 7 months, was also differentially methylated in RICVD rats after acute 18 Gy irradiation [396]. Despite not being detectable by qPCR in our samples, CACNA1C was identified in a number of our enriched DMR pathways concurrently dysregulated in the cardiac proteome including dilated cardiomyopathy and hypertrophic cardiomyopathy [364]. The reproducible enrichment of CACNA1C points to a role for CACNA1C in myocardial dysfunction with extrapolated relevance in RICVD [427,428]. Therefore, further investigations of CACNA1C's methylation status after FI and its involvement in RICVD are warranted. From predicted STRING protein-protein interactions (PPI), significantly dysregulated cardiac proteins in the irradiated rats [364] were shown to interact with LDLR, ITPR2, E2F, PTPN and CACNA1 families, as well as the methylation relevant DNMT3a [429,430]. This points to a multi-dimensional regulation of cardiac responses to ionizing radiation.

Finally, selected DMGs were explored in the blood of breast cancer patients treated with adjuvant RT. SLMAP expression tended to increase at V1 compared to V0 in left sided breast cancer patients. Statistical significance was not reached, possibly due to the limited sample numbers and high inter-individual variation of DNA methylation, especially in blood [431–434]. Interestingly, after an initial increase at V1, SLMAP expression decreased at 6 months after RT (V2) in irradiated left sided breast cancer patients while presenting a medium correlation with MHD at V2. A similar initial SLMAP upregulation, which gradually decreases over time, was also observed in the irradiated rats. As decreased expression of SLMAP was found in human dilated ventricles, the observed SLMAP downregulation over time could contribute to cardiac dysfunction [378,435]. Interestingly, decreased SLMAP protein levels

were also observed in cardiac tissues of Mayak workers diagnosed with ischemic heart diseases after occupational exposure to >500m Gy external gamma rays [436], which further supports the possible involvement of SLMAP in RICVD.

ITPR2 is the major cardiac isoform of a family of calcium channels whereby increased ITPR2 expression activates calcium dependent signaling and modulates excitation-contraction coupling in cardiomyocytes [381]. In addition, ITPR2 overexpression has been linked to many cardiac pathologies including cardiac arrhythmias, failure and hypertrophy [381,437–439]. In our study, hypermethylation was associated with an increased expression of ITPR2 for the 6.9 Gy FI dose at 1.5 and 12 months after irradiation in rats. In humans, right-sided breast cancer patients showed significantly higher ITPR2 expression at V1 relative to V0. Consequently, ITPR2 dysregulation seems to occur as a result of radiation in both rats and breast cancer patients.

E2F6 is a member of the E2F family that functions as a transcriptional repressor [440]. In-vivo, forced E2F6 overexpression was associated with cardiac remodeling and dilated cardiomyopathy [387,441]. In addition, pathway analysis of Mayak nuclear workers' cardiac tissue proteomes showed that E2F family was dysregulated in irradiated groups compared to controls [147]. Our findings show E2F6 hypomethylation at 1.5 months after 27.6 Gy FI in rats with variable expression and a seemingly dose differential effect whereby low doses induce E2F6 downregulation (c.f. 0.92 Gy), as shown in mouse embryos exposed to low dose X-rays [442]. In addition, the strong correlation between E2F6 and GLS alterations after 27.6 Gy FI suggests a possible contribution to the observed myocardial dysfunction. E2F6 also exhibits significantly higher expression at V1 relative to V0 in left sided patients. Stratification of patients, according to the received mean heart dose (MHD), showed E2F6 dysregulation at higher MHDs (>2.5 Gy) in left-sided breast cancer RT patients while maintaining a medium correlation to MHD. This further strengthens the potential involvement of E2F6 in developing radiation-induced cardiac effects. However, further investigations in larger cohorts could help characterize the functional impact.

Finally, Connexin-43 (CX43) is a transmembrane protein forming gap junctions and hemichannels which are involved in intercellular communication [443]. CX43 was reported to increase the formation of atherosclerotic lesions in vivo [444,445]. We previously reported that single and fractionated X-irradiation induced an acute and persistent increase in CX43 gene and protein levels in human endothelial cells while selective inhibition of CX43 hemichannels alleviated radiation-induced endothelial cell damage [389,446]. In the current study, CX43 expression was significantly increased at V1 in the blood of left sided breast cancer patients relative to V0, in a similar manner to E2F6. Therefore, further investigation into the relationship between E2F6 and CX43 in the scope of radiation-induced cardiovascular dysfunction is needed.

3.4.1 Study limitations

Despite having the advantages of offering long-term longitudinal follow-up of identified DMRs over time, our study has a number of limitations: 1) Our first sampling time point for the rats was 1.5 months after irradiation. Consequently, we are unable to comment on any methylation alterations occurring at earlier time points. 2) Methylation analysis was performed in peripheral blood which introduces the confounder of different methylation profiles due to differing blood cell fraction counts [447–449]. DNA in blood is a mixture of DNA from blood cells and circulating cell-free DNA released from dying cells [449–451]. Local heart irradiation, as in our experimental rat irradiation model, primarily affects the methylation of the heart, as well as circulating blood cells. However, considering the short lifespan of circulating blood cells, delayed methylation alterations are most likely not the result of irradiated blood cells [452]. In addition, peripheral blood/leucocyte fraction methylation patterns have been frequently employed in DNA methylation biomarker research for cardiovascular disease identifying associations near genes unrelated to immune function or inflammation [186,453,454]. This supports the usefulness of blood-based DNA methylation investigations despite confounders, especially when considering the convenience of blood as a sample source. 3) The number of available samples was limited for certain rat sampling time points/doses due to technical limitations. 4) The

primary validation in breast cancer patients treated with adjuvant RT involved a somewhat limited number of patients (right sided patients (n=9) and left sided patients (n=16)) which necessitates confirmation in bigger patient cohorts.

3.5 Conclusion

The involvement of DNA methylation alterations in RICVD pathogenesis is underexplored. In the current study, we attempted to identify DNA methylation alterations related to rat whole heart irradiation. The highest dose of radiation (27.6 Gy FI) resulted in blood DMRs associated with multiple cardiac relevant pathways including dilated cardiomyopathy and hypertrophic cardiomyopathy. This suggests the involvement of DNA methylation alterations in the onset of myocardial dysfunction. The expression of selected DMRs (significant differential methylation > 25% with cardiovascular relevance) was assayed and discordance between methylation-predicted expression and observed expression suggests that gene body DNA methylation regulates gene expression in a multi-factorial bidirectional manner. SLMAP, ITPR2, E2F6 and PTPN2 showed differential methylation and expression in irradiated rats, while E2F6 expression correlated with GLS measurements at 12 months after 27.6 Gy FI. Three of these rat DMGs (SLMAP, ITPR2 and E2F6) also exhibited altered expression in breast cancer patient blood, of which SLMAP and E2F6 overexpression occurs mainly at higher MHDs. While this study provides some preliminary insights into radiation-induced DNA methylation alterations and their possible contribution to RICVD, further mechanistic validation by gene knockout/overexpression experiments, as well as large scale clinical studies are needed to validate their connections to RICVD.

Chapter 4   **Characterization of DNA methylation profiles of breast cancer patients receiving adjuvant radiotherapy**

4.1 Introduction

Thoracic radiotherapy (RT), as in breast cancer treatment, leads to the inevitable irradiation of the heart and surrounding blood vessels with the subsequent development of radiation-induced cardiovascular disease (RICVD) [137,146,355,455,456]. RICVD manifests mainly as chronic coronary heart disease with symptoms manifesting 10 to 15 years after RT [354]. Due to the high survival rates of breast cancer patients (79%-93%), delayed therapy-induced toxicities are becoming a growing concern [120]. Consequently, finding circulating biomarkers of RICVD that allow early detection and intervention in at risk patients is a topic of ongoing research [457,458].

The current research serves as part of Work Package 4 (WP4) of the Horizon 2020 project MEDIRAD (http://www.medirad-project.eu). WP4 aims to establish predictive models for clinical support of secondary cardiac risks after breast cancer RT. To this end, results of pre-clinical and clinical investigations, covering both the functional and systemic effects of heart irradiation will be integrated in a single predictive framework. Consequently, the current study aims to profile early radiation-induced DNA methylation alterations that can, after integration, serve as candidate biomarkers of RICVD.

DNA methylation is an epigenetic regulator of gene expression which was proposed as a molecular pathophysiological mechanism. In cardiovascular disease, DNA methylation has been associated with inflammation and vascular smooth muscle cell (VSMC) phenotype regulation [356,361,362,453,459–461]. DNA methylation alterations in cardiovascular

disease present an array of hypo- and hyper-methylation with more focal hypermethylation [337,462,463]. On the other hand, DNA methylation is altered by IR leading to global hypomethylation and gene-specific hypermethylation [65,196,219,230,413].

In the current chapter, blood DNA methylation profiles of 16 breast cancer patients receiving adjuvant RT were characterized using Illumina EPIC methylation beadchip at 3 time points: at diagnosis (V0), immediately after RT (V1) and 6 months after RT (V2). The expression of a selected set of differentially methylated regions (DMRs) and differentially methylated positions (DMPs) was then quantified by qPCR in all samples, including those collected at 24 months after RT (V3) which were not yet available during DNA methylation analysis. These DMRs/DMPs were selected based on the degree of differential methylation in addition to an extensive literature search. Only genes with documented links to cardiovascular disease (CVD) were retained. In this manner, we aimed to provide DMRs/DMPs that could serve as candidate RICVD biomarkers after integration with functional cardiac data.

4.2 Materials and methods

4.2.1 MEDIRAD EARLY HEART breast cancer patient recruitment, cancer therapy and blood sample collection

4.2.1.1 Patient Recruitment

The patients in this chapter, as in **Chapter 3**, are from the MEDIRAD EARLY HEART cohort which is a European multicenter prospective cohort used to identify cardiac imaging and blood-based biomarkers of radiation-induced cardiotoxicity [365]. Female unilateral breast cancer patients aged 40-75 years treated with primary breast conserving surgery and postoperative RT using modern planning-CT based RT technologies were recruited by our MEDIRAD partners, University Medical Center Groningen (UMCG) and Technische Universität München (TUM), as part of the H2020 project MEDIRAD [41]. Patients with previous medical history of coronary artery disease and/or myocardial infarction and/or

atrial fibrillation were excluded from the study. Selected patients were offered participation in the study during their first visit with the radiation oncologist. Included patients were requested to sign a written informed consent form. Patient mean heart dose (MHD) was measured and provided by UMCG. Patients were classified as having left- or right sided breast cancer according to the anatomical position of the tumor.

4.2.1.2 *RT protocol*

The total RT dose was 40.05-43.6 Gy in 15-20 fractions, delivered with a volumetric modulated arc therapy (VMAT)/ intensity-modulated radiation therapy (IMRT) technique. Left-sided breast cancer patients were treated with deep inspiration breath hold (DIBH) using the active breathing control (ABC) system in order to lower the cardiac dose as much as possible. A more detailed recruitment and RT protocol is available here [376].

4.2.1.3 *Blood collection*

Blood was collected from patients at 4 time points: at diagnosis (V0), directly after RT (V1), 6 months after RT (V2) and 24 months after RT (V3). Blood samples were stored at UMCG/TUM at -80°C until they were finally shipped on dry ice and stored at -80°C at SCK CEN until further processing.

For our analyses, patients were included if a blood sample was collected at V0 and at least one other time point. Accordingly, 43 breast cancer patients including 15 right sided breast cancer ($n_{total=}$ $n_{UMCG}+n_{TUM}=12+3=15$) and 28 left sided breast cancer (($n_{total=}$ $n_{UMCG}+n_{TUM}=22+6=28$) were selected for further analyses.

4.2.2 Illumina EPIC beadchip methylation assay of breast cancer patient blood

Sixteen patients, for which V0, V1 and V2 blood samples were available, were selected for DNA methylation analysis using Illumina EPIC beadchip methylation assay (Illumina, USA). DNA was extracted from 200 μL frozen blood using QIAamp DNA mini kit (Qiagen, Germany) according to manufacturer's instructions, as previously described [354]. DNA concentration and purity were determined by comparing the ratio of optical density at 260

and 280 nm. Bisulfite conversion and EPIC array protocol were performed at The Human Genomics Facility (HuGe-F) (Erasmus MC, The Netherlands).

From the Illumina beadchip raw data analysis, two metrics were used to calculate the proportion of methylation at each CpG locus; a methylated intensity (denoted by M) and an unmethylated intensity (denoted by U). Methylation levels were reported as either beta values ($\beta=M/(M+U)$ $\beta=M/(M+U)$) or M-values ($Mvalue=log2(M/U)$ $Mvalue=log2(M/U)$).

For our analyses, the *minfi* framework was applied. Raw data was imported into R software using the *read.metharray.sheet* function. Quality control was then evaluated by calculating a detection p-value for every CpG in every sample. This was executed by comparing the total signal (M+U) for each probe to the background signal level, estimated from the negative control probes.

Data normalization was performed, to minimize unwanted variation within and between samples, using *preprocessQuantile* function that implements a stratified quantile normalization procedure [464]. Poor performing probes that failed in one or more samples, based on detection p-value, or those with single nucleotide polymorphisms (SNPs) at a CpG site were filtered out.

Following this, probe-wise differential methylation analysis was performed using *lmFit* function (limma package) on the M-values thereby obtaining moderated t-statistics and associated p-values for each CpG site. Finally, p-values were adjusted for multiple testing per gene using Benjamini-Hochberg false discovery rate (FDR).

4.2.3 Pathway analysis of DMRs identified in breast cancer patients

Pathway analysis of DMPs and DMRs (adjusted p value and FDR< 0.1, respectively) was performed using STRING v11.5 (Search Tool for the Retrieval of Interacting Genes/Proteins) online public database (https://string-db.org/) [370]. STRING employs the widely used

overrepresentation analysis approach for pathway analysis similar to that used in g:Profiler [370,465]

4.2.4 qPCR of selected DMRs and DMPs in breast cancer patient blood

A set of DMRs were selected for qPCR validation based on certain criteria, namely having≥ 10 CpGs, absolute maximum differential methylation ≥ 0.092, FDR<0.1 and having an association to CVD in literature. These DMRs and a random selection of the top identified DMPs (adjusted p<0.1) were thus quantified in available breast cancer patient blood samples (n=43). RNA was extracted from frozen blood using NucleoSpin RNA Blood Mini kit (Macherey-Nagel GmbH & Co. KG, Germany) according to manufacturer instructions. Then, reverse transcription of extracted RNA was performed using GoScript Reverse Transcription Mix with random primers (Promega Corporation, USA) according to manufacturer's instructions. The expression of selected DMR and DMP transcripts was determined by quantitative real Time PCR (qPCR) using Fast Advanced Master Mix and TaqMan Gene Expression Assays (Thermo Fisher Scientific, USA) according to manufacturer's recommendations on qTOWER³ touch thermal cycler (SPRED2: Hs00986219_m1; ADCY9: Hs00181599_m1; S100A9: Hs00610058_m1; FXYD1: Hs00245327_m1; CCRL2: Hs00243702_s1; LTBP1: Hs01558763_m1; SSH3: Hs00215309_m1; ATP5G2: Hs01086654_g1; RNH1: Hs00161407_m1; MAP4: Hs01104794_m1; BRCA2: Hs00609073_m1; STK38L: Hs00960027_m1; CTSZ: Hs00938366_m1; NDUFS2: Hs00190020_m1; AIP: Hs04935271_m1; STAT5A: Hs00234181_m1).

The ΔCt values for all genes were determined relative to the reference gene TBP (Hs00427620_m1; Thermo Fisher Scientific, USA). Selection of the reference gene was performed using NormFinder [375] whereby the gene with the highest stability was selected. Relative quantification was calculated using the equation: $\log2^{-\Delta\Delta CT}$, where $\Delta\Delta C_T =$ [C_T of target gene − C_T of reference gene]$_{irradiated\ group}$ − [C_T of target gene − C_T of reference gene]$_{sham\ group}$.

Statistical multiple comparison testing was performed according to the side on which the patient's breast cancer was located (left/right). After the receipt of patient MHD data, qPCR expression data was re-analyzed using a patient classification based on whether the patient's MHD was ≥2.5 Gy. This dose threshold was selected following the MHD recommendations of the German Society for Radiation Oncology (DEGRO) to minimize radiation-induced cardiotoxicity [390].

Correlation between DMR and DMP expression and the received MHD supplied by MEDIRAD partners was performed by calculating Pearson correlation coefficient (r).

4.2.5 Statistical Analysis

Normal distribution of data was assessed by the Shapiro-Wilk test. Statistical analysis of qPCR data was performed using a generalized estimating equation to accommodate for the nonparametric characteristics of data and for handling missing time points. All statistical analyses were performed using SPSS version 28 (IBM Corp., USA).

4.3 Results

4.3.1 Differentially methylated positions and regions were identified after RT in left sided breast cancer patients

8261 differentially methylated positions (DMPs) and 3026 differentially methylated regions (DMRs) were identified at V1 relative to V0 in left-sided breast cancer patients (adjusted p value and FDR< 0.1, respectively). DMPs were found across the genome in all autosomal chromosomes with 23% being located in CpG islands as well as island shores and shelves located up to 2Kb and 4Kb from the CpG island, respectively (**Figure 4-1A**) [466]. Our results also show a predilection to hyper- rather than hypo-methylation with 10546 hypermethylated vs 4361 hypomethylated DMPs (**Figure 4-1B**). Pathway analysis of DMPs (**Table 4-1**) and DMRs (**Table 4-2**) (p<0.1) revealed enrichment of a number of KEGG and Reactome pathways. Moreover, one enriched pathway showed cardiovascular specificity being Adrenergic signaling in cardiomyocytes. The genes responsible for pathway

enrichment are detailed in (**Supplementary tables 2.1 and 2.2 in Supplementary materials for Chapter 4**) .
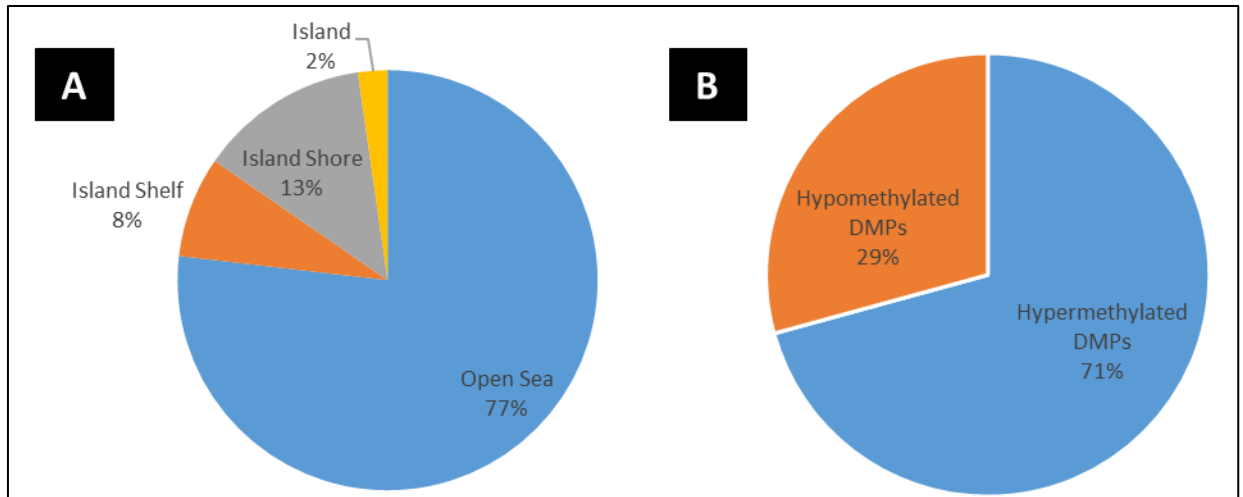
Figure 4-1 *A) Distribution of DMPs (p<0.1) according to their location relative to CpG islands, island shores (2 kb from island), island shelves (4 kb from island) and open sea. B) Distribution of DMPs (p<0.1) according to the direction of methylation alterations to hypo- and hypermethylated.*

DMRs were filtered according to previously detailed criteria and 9 DMRs were selected for downstream qPCR validation: SPRED2, RNH1, NDUFS2, ADCY9, S100A9, FXYD1, CTSZ, CCRL2 and STK38L. A brief description of these genes and their connection to cardiovascular function/disease is provided in **Table 4-3**.

Table 4-1 *Pathway analysis of breast cancer patient DMP, false discovery rate (FDR) <0.05.*

Category	Enriched pathway	Strength	FDR
KEGG	Chemokine signaling pathway	0.24	0.0183
KEGG	PI3K-Akt signaling pathway	0.18	0.0183
KEGG	Osteoclast differentiation	0.27	0.0183
KEGG	Th1 and Th2 cell differentiation	0.32	0.0183
KEGG	Th17 cell differentiation	0.33	0.0183
KEGG	T cell receptor signaling pathway	0.31	0.0183
KEGG	Insulin resistance	0.31	0.0183
KEGG	Yersinia infection	0.27	0.0183
KEGG	Human T-cell leukemia virus 1 infection	0.21	0.0183
KEGG	Pathways in cancer	0.14	0.0183
KEGG	TNF signaling pathway	0.26	0.0295
KEGG	Rap1 signaling pathway	0.19	0.0344
KEGG	Adrenergic signaling in cardiomyocytes	0.23	0.0344
KEGG	Regulation of actin cytoskeleton	0.19	0.0344
KEGG	Shigellosis	0.19	0.0344
KEGG	cAMP signaling pathway	0.19	0.0364
KEGG	Phospholipase D signaling pathway	0.22	0.0364
KEGG	AMPK signaling pathway	0.24	0.0364
KEGG	Platelet activation	0.23	0.0364
KEGG	Hematopoietic cell lineage	0.27	0.0364
KEGG	PD-L1 expression and PD-1 checkpoint pathway in cancer	0.27	0.0364
KEGG	Glycerolipid metabolism	0.31	0.0408
KEGG	cGMP-PKG signaling pathway	0.2	0.0408
KEGG	Sphingolipid signaling pathway	0.24	0.0408
KEGG	Focal adhesion	0.18	0.0408
KEGG	C-type lectin receptor signaling pathway	0.25	0.0408
KEGG	Viral protein interaction with cytokine and cytokine receptor	0.25	0.0438
KEGG	Hedgehog signaling pathway	0.34	0.0438
KEGG	Endocytosis	0.16	0.0458
KEGG	Viral carcinogenesis	0.18	0.0485
Reactome	Immune System	0.17	1.43E-14
Reactome	Innate Immune System	0.19	1.85E-09
Reactome	Neutrophil degranulation	0.26	3.61E-08
Reactome	Hemostasis	0.18	0.00018
Reactome	Cytokine Signaling in Immune system	0.17	0.0003
Reactome	Signaling by Interleukins	0.19	0.0035

Category	Enriched pathway	Strength	FDR
Reactome	Adaptive Immune System	0.14	0.0039
Reactome	Vesicle-mediated transport	0.14	0.0103
Reactome	Platelet activation, signaling and aggregation	0.22	0.0103
Reactome	Fcgamma receptor (FCGR) dependent phagocytosis	0.33	0.0352

Table 4-2 *Pathway analysis of breast cancer patient DMRs, false discovery rate (FDR) <0.05.*

Category	Enriched pathway	Strength	FDR
KEGG	Human T-cell leukemia virus 1 infection	0.39	0.032
KEGG	Adherens junction	0.53	0.0473
KEGG	Th1 and Th2 cell differentiation	0.49	0.0473
KEGG	T cell receptor signaling pathway	0.49	0.0473
KEGG	Parathyroid hormone synthesis, secretion and action	0.48	0.0473
KEGG	Transcriptional misregulation in cancer	0.38	0.0473
KEGG	Prostate cancer	0.48	0.0473
Reactome	Innate Immune System	0.37	3.65E-13
Reactome	Immune System	0.27	9.64E-12
Reactome	Neutrophil degranulation	0.45	2.15E-09
Reactome	Diseases of signal transduction by growth factor receptors and second messengers	0.38	0.00022
Reactome	Signal Transduction	0.14	0.0025
Reactome	Nef and signal transduction	1.19	0.0074
Reactome	Vesicle-mediated transport	0.26	0.0074
Reactome	Signaling by Receptor Tyrosine Kinases	0.29	0.0093
Reactome	Generation of second messenger molecules	0.81	0.0105
Reactome	Signaling by NOTCH	0.41	0.011
Reactome	Membrane Trafficking	0.25	0.0217
Reactome	Signaling by Interleukins	0.29	0.0217
Reactome	Disease	0.16	0.0311
Reactome	The role of Nef in HIV-1 replication and disease pathogenesis	0.77	0.0311
Reactome	DAP12 interactions	0.69	0.0311
Reactome	Notch-HLH transcription pathway	0.77	0.0311
Reactome	SUMOylation of intracellular receptors	0.76	0.0311
Reactome	RUNX3 regulates NOTCH signaling	0.95	0.0311
Reactome	Intracellular signaling by second messengers	0.33	0.0311
Reactome	FCGR3A-mediated IL10 synthesis	0.68	0.0322
Reactome	Hemostasis	0.22	0.0499
Reactome	Cytokine Signaling in Immune system	0.22	0.0499
Reactome	Signaling by SCF-KIT	0.64	0.0499

Category	Enriched pathway	Strength	FDR
Reactome	Pre-NOTCH Transcription and Translation	0.57	0.0499
Reactome	Signaling by NOTCH1	0.53	0.0499
Reactome	Phosphorylation of CD3 and TCR zeta chains	0.84	0.0499
Reactome	NOTCH3 Intracellular Domain Regulates Transcription	0.76	0.0499

Table 4-3 *Cardiovascular associations of selected DMRs as supplied by literature research.*

DMRs	Methylation status	Relation to cardiovascular disease	Refs
SPRED2 Sprouty Related EVH1 Domain Containing 2	Hypomethylation	Deficiency elicits cardiac arrhythmias and premature death in SPRED2$^{-/-}$ mice. Significantly differentially methylated in rheumatic heart disease patient blood .	[467,468]
RNH1 Ribonuclease/Angiogenin Inhibitor 1	Hypomethylation	Inhibits Rnase 1 which attenuates septic cardiomyopathy and cardiac apoptosis in a murine model of polymicrobial sepsis Protein expression differentially altered in acute myocardial infarction patients relative to control.	[469,470]
NDUFS2 NADH: Ubiquinone Oxidoreductase Core Subunit S2	Hypomethylation	Mutations were identified in patients with cardiomyopathy.	[471]
ADCY9 Adenylate Cyclase 9	Hypomethylation	Promotes atherosclerosis in mice Regulates endothelial signaling involved in atheroprotection. Inactivation protects against atherosclerosis in mice. The effects of dalcetrapib –an antiatherosclerotic agent- on atherosclerotic outcomes are determined by correlated polymorphisms in the ADCY9 gene.	[472–475]
S100A9 S100 Calcium Binding Protein A9 *a.k.a* MRP14	Hypomethylation	Plays an important role in the inflammatory and reparatory immune responses to myocardial infarction in mice Expression was found to increase before ST-segment elevation in myocardial infarction. Increasing plasma concentrations in healthy individuals predict the risk of future cardiovascular events.	[476–478]

DMRs	Methylation status	Relation to cardiovascular disease	Refs
		High levels in human atherosclerotic plaques correlate with the characteristics of rupture-prone lesions.	
FXYD1 FXYD Domain Containing Ion Transport Regulator 1	Hypomethylation	Knockout mice show increased cardiac mass, larger cardiac myocyte area, and higher ejection fraction. Expression levels drastically increase after myocardial infarction. Absence is associated with a female-specific pro-inflammatory and hypercholesterolemic environment.	[479–483]
CTSZ Cathepsin Z *a.k.a* Cathepsin X or P	Hypomethylation	Overexpression in T-lymphocytes leads to enhanced migration thereby aiding in the early inflammatory phase of atherosclerosis. Cathepsin X was found to co-localize with leucocyte LFA-1 which functions as an adhesion molecule to ICAM-1.	[484–486]
CCRL2 C-C Motif Chemokine Receptor Like 2	Hypomethylation	Increased expression promotes atherosclerotic plaque formation in ApoE deficient mice. Deletion attenuates atherosclerotic plaque development in ApoE deficient mice.	[487,488]
STK38L Serine/Threonine Kinase 38 Like *a.k.a.* NDR2	Hypomethylation	m^6A modification was associated with platelet activation and apoptotic pathways in rat left ventricle tissues. Differential expression was shown in endomyocardial biopsies of left ventricular failure. Identified as a potentially novel heart failure-associated gene through gene expression and network data integration.	[489–492]

In addition to these DMRs, a number of DMPs with literature-based cardiac relevance were also analyzed: SSH3, ATP5G2, MAP4, BRCA2, AIP and STAT5A. A description of these DMPs and their connection to cardiovascular disease/function is shown in **Table 4-4.**

Table 4-4 *Cardiovascular associations of selected DMPs as supplied by literature research.*

DMP	Relation to cardiovascular disease	Refs
SSH3 Slingshot Protein Phosphatase 3	Mediates cofilin activation and subsequent VSMC migration. while facilitating neointima formation following vascular injury in *vivo*.	[493,494]
ATP5G2 ATP synthase, H+-transporting, mitochondrial F0 complex, subunit C2	Expression was increased in mice after myocardial infarction and in coronary artery disease patients.	[495–497]
MAP4 Microtubule Associated Protein 4	Increased phosphorylation was linked to microtubule instability and mitochondrial dysfunction and subsequent cardiac pathology. Translocation of its phosphorylated form from cytosol to mitochondria in hypoxic neonatal cardiomyocytes leads to apoptosis induction.	[498–501]
BRCA2 BReast CAncer gene 2	Cardiac-specific disruption of BRCA2 was associated with higher anthracycline-induced cardiac toxicity risk. Deficiency exacerbates oxidized LDL-induced DNA damage and endothelial apoptosis.	[502–504]
AIP Aryl Hydrocarbon Receptor Interacting Protein *a.k.a* ARA9 or XAP2	Deletion leads to cardiac malformation and embryonic lethality in mice. Key driver in regulatory gene networks of coronary artery disease.	[505,506]
STAT5A Signal Transducer And Activator Of Transcription 5A	Member of the JAK-STAT pathway which has been implicated in post myocardial infarction remodeling. Required for ischemic preconditioning-mediated cardioprotection as knock-out mice were more susceptible to myocardial ischemia–reperfusion injury.	[305,507,508]

4.3.2 STK38L, SPRED2, LTBP1, CCRL2 and ATP5G2 show altered expression in breast cancer patients over time that is affected by breast cancer side

Upon stratifying breast cancer patients according to side (right/left), all genes except NDUFS2 and RNH1 showed significantly altered expression over time. Increased expression of STK38L, SPRED2, LTBP1 and CCRL2 as well as decreased expression of LTBP1 and ATP5G2 was shown to be affected by side ($p<0.05$) (**Figure 4-2**). Namely, SPRED2, LTBP1 and CCRL2 expression was increased while ATP5G2 expression was decreased in left sided breast

cancer patients. On the other hand, STK38L showed increased expression while LTBP1 showed decreased expression in right sided patients.

4.3.3 Sub-analyses to explore the effect of MHD on selected DMP/DMR expression

Stratifying patients according to mean heart dose (MHD) showed that patients exposed to MHDs higher than 2.5 Gy had significantly increased expression of STAT5A, ATP5G2, FXYD1 and RNH1. STAT5A, RNH1 and ATP5G2 showed increased expression in patients receiving MHD higher than 2.5 Gy while FXYD1 showed increased expression in all patients. More importantly, all four genes presented higher expression at V2 in patients receiving higher MHDs (**Figure 4-3**). However, this differential expression between the two patient groups normalizes at V3.

Correlation analysis revealed a positive correlation between MHD and CCRL2 expression (0.312, respectively, $p < 0.001$) (**Figure 4-4**).
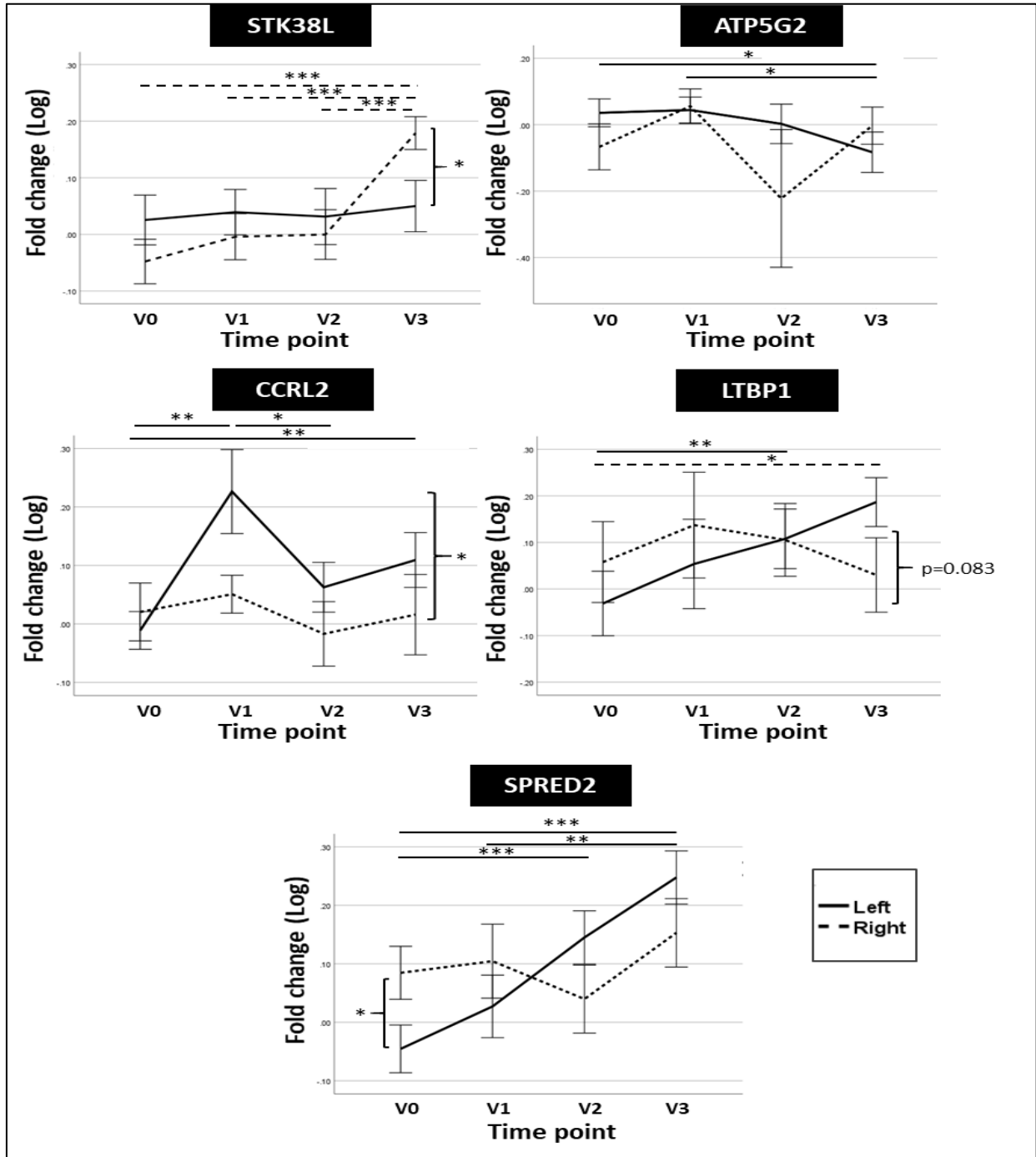
Figure 4-2 *Mean log fold expression change of STK38L, ATP5G2, CCRL2, LTBP1 and SPRED2 in the blood of right (n=15, dashed line) and left sided (n=28, continuous line) breast cancer patients sampled at diagnosis (V0), immediately after RT (V1), 6 months after RT (V2) and 24 months after RT (V3). Data is presented as mean log fold changes in gene expression normalized to TBP ± standard error of mean. Displayed significance values were calculated using observed log fold expression changes (*=p<0.05, **=p<0.01, ***=p<0.001). Statistical analysis was performed using SPSS generalized estimating equations module and multiple comparison correction was performed using least significant difference (LSD).*
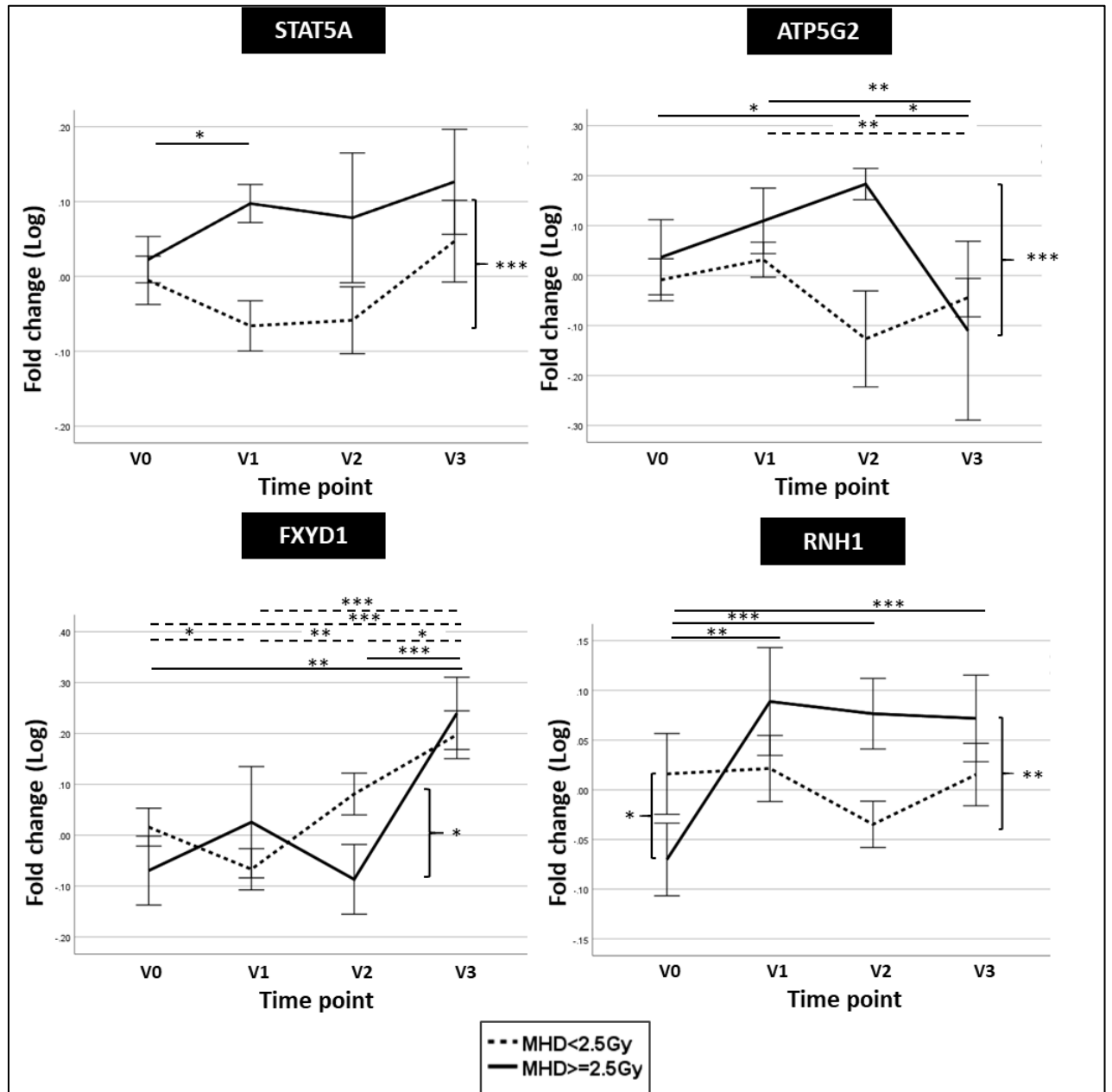
Figure 4-3 *Mean log fold expression change of STAT5A, ATP5G2, FXYD1 and RNH1 in breast cancer patients who received MHD < 2.5 Gy (n=35, dashed line) or ≥2.5 Gy (n=8, continuous line) sampled at diagnosis (V0), immediately after RT (V1), 6 months after RT (V2) 24 months after RT (V3). Data is presented as mean log fold changes in gene expression normalized to TBP ± standard error of mean. Displayed significance values were calculated using observed log fold expression changes (*=p<0.05, **=p<0.01, ***=p<0.001). Statistical analysis was performed using SPSS generalized estimating equations module and multiple comparison correction was performed using least significant difference (LSD).*
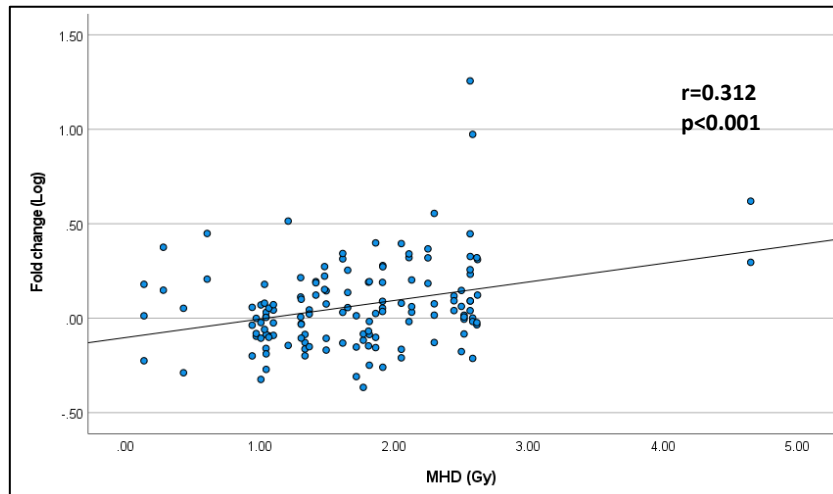
Figure 4-4 Scatter plot showing the correlation between CCRL2 log fold change and MHD (Gy) in breast cancer patients receiving RT.

4.4 Discussion

In the current chapter, we evaluated the effects of RT on blood methylation profiles of 16 breast cancer patients from the MEDIRAD EARLY HEART cohort. These methylation profiles are still to be integrated with circulating biomarker analyses and cardiac function data from MEDIRAD partners at a later stage. Patients of this cohort who received a MHD over 2.5Gy showed more than 15% reduction in GLS at 6 months after RT, which is considered a sign of subclinical left ventricular dysfunction [154,376]. The risk of left ventricular dysfunction in these patients was also found to increase with MHD (Odds ratio: 1.74) [376]. Currently, there are no available blood methylation biomarkers for cardiovascular disease. However, specific DNA methylation signatures were associated with the development of coronary heart disease [453,509]. As such, integrating our patient DNA methylation analyses with cardiac function data could help identify biomarkers for RICVD risk. As the cardiac function data for the patients in the current study is still under analysis by MEDIRAD partners, interpreting our results in a clinically relevant manner is difficult.

DNA methylation alterations were found directly after RT in samples of left sided breast cancer patients relative to levels at diagnosis. The occurrence of differential methylation

specifically in left sided patients may reflect the higher MHD (2.21 Gy in left vs 0.97 Gy in right sided patient) [376]. A higher predilection to hypermethylation was observed, as evidenced by the higher number of hypermethylated DMPs. This comes in agreement with reports of gene-specific hypermethylation being the major effect of radiation both in *vitro* and in *vivo* [105,164,510,511].

Expression of selected DMRs with hypomethylated promoters did not always correlate with increased expression, contrary to previous research [512,513]. One reason could be that the patients in the current study are patients undergoing breast surgery with subsequent cancer excision. As previously mentioned in **Chapter 3**, methylated DNA in the blood originates from both blood cells and circulating free DNA (cfDNA). Cancer patients usually have a high level of cfDNA in their blood due to cellular necrosis or apoptosis of rapidly dividing cancer cells [514], which further increases due to RT-induced cell death [515]. As all DMRs/DMPs showing differential expression also show changes in breast cancer [516–523], arriving to conclusions on the isolated effect of altered whole blood methylation after RT is complicated.

Despite the non-specificity of blood for cardiovascular disease investigations, Adrenergic signaling in cardiomyocytes was identified as an enriched KEGG pathway. This enrichment could offer a new therapeutic target for RICVD amelioration as activation of α-adrenergic signaling alleviated cardiomyocyte death after doxorubicin administration in mice [524]. The specificity of this pathway to cardiomyocytes shows that blood DNA methylation can identify heart specific enrichments. Interestingly, CACNA1C, a rat DMR identified in **Chapter 3** irradiated rats at 1.5 and 7 months, was one of the DMRs contributing to Adrenergic signaling in cardiomyocytes pathway enrichment. CACNA1C also contributed to the enrichment of two other pathways with cardiovascular relevance; cAMP signaling and cGMP-PKG signaling", which have been associated with cardiotoxicity resulting from doxorubicin and ionizing radiation (IR) [525,526]. Thus, CACNA1C provides an interesting target for future mechanistic RICVD research.

Other DMR/DMP enriched pathways that are linked to CVD include NOTCH signaling which contributes to radiation-induced fibrosis, DAP12 signaling and interactions for immune modulation as well as Nef signal transduction and Neutrophil degranulation [527–533]. However, these pathways, as well as cGMP-PKG signaling pathway, are also dysregulated in breast cancer [534–539]. Planned integrative analysis of DMR/DMP methylation and expression profiles with functional cardiac outcomes as well as other traditional and microRNA circulatory biomarkers measured at MEDIRAD partners could help remove the breast cancer confounder.

As biomarkers aim to identify patients at risk of developing RICVD, we identified DMPs/DMRs showing altered expression over time that is affected by breast cancer side (left/right). STK38L, ATP5G2, CCRL2, LTBP1 and SPRED2 showed different expression profiles in left and right sided patients over time. STK38L was recently identified as a core mediator of the Hippo pathway which mediates YAP inhibition thereby promoting endothelial activation and atherosclerosis in APOE$^{-/-}$ mice [540]. ATP5G2 encodes subunit c of ATP synthase enzyme which is inhibited by IR leading to the development of mitochondrial dysfunction, a hypothesized driver of RICVD [541,542]. CCRL2 encodes a chemokine receptor which regulates leukocyte migration thereby impacting inflammatory processes [543]. CCRL2 deletion attenuates atherosclerotic plaque development while inhibition of its ligand ameliorates atherosclerosis progression in ApoE$^{-/-}$ mice [487,488,544]. LTBP1 belongs to a family of latent transforming growth factor beta (TGF-β) binding proteins whose ligand, TGF-β, contributes to radiation-induced vascular injury and endothelial dysfunction [541,545,546]. SPRED2 inhibits pro-inflammatory matrix metalloproteinase release and aortic smooth muscle cell migration and is targeted by microRNA-210; a biomarker for atherosclerotic lipid accumulation, inflammation and plaque stability [467,520,547–549]. The literature report above suggests that CCRL2, SPRED2 and LTBP1 can influence endothelial activation, inflammation, mitochondrial dysfunction and lipid accumulation thereby possibly affecting the development of RICVD. Progressively decreasing ATP5G2 expression was observed until 24 months after RT in left

sided breast cancer patients which could impact mitochondrial integrity leading to radiation-induced mitochondrial dysfunction. On the other hand, increased STK38L expression was only observed at 24 months after RT in right sided patients which could serve an atheroprotective Hippo activating effect that extends to 24 months after RT. Only CCRL2 showed a positive correlation to patient MHD (0.312, p<0.001) which suggests a possible dose response effect.

A sub-analysis used to assess the effect of MHDs exceeding the 2.5 Gy threshold also showed significantly higher expression of ATP5G2 as well as FXYD1, RNH1 and STAT5A 6 months after RT. FXYD1, or Phospholemman maintains cardiac contractility while protecting against vascular dysfunction with knockout mice showing increased oxidative stress and a heightened blood pressure response [550,551]. RNH1 inhibits angiogenein, a ribonuclease recently found to protect against atherosclerosis by decreasing endoplasmic reticulum stress [552,553]. Finally, STAT5A was found to be enriched in atheroprone areas of porcine arteries [554]. Administration of STAT5A-inhibitor decreased inflammation and attenuated atherosclerosis in ApoE$^-$/$^-$ mice receiving a high fat diet [555]. Thus, dysregulation of these four genes can impact inflammation and oxidative stress with subsequent effects on atherogenesis which can compound coronary heart disase risk. However, further mechanistic research is needed to investigate whether this dose-differential expression is clinically significant in the context of RICVD.

In an effort to corroborate the effects of IR on DMP/DMR differential expression, we examined the profiles of irradiated cardiac proteomes in literature. NDUF, ATP5 and S100A families were frequently dysregulated in irradiated cardiac proteomes till up to 7 months after irradiation [436,556–566] with specific dysregulation of NDUFS2 [436,558,559,563] and S100A9 [436,562]. MAP4, RNH1, CTSZ, STK38L and FXYD1 were also dysregulated in the cardiac tissue of personnel of Mayak's plutonium enrichment plant who were occupationally exposed to >500 mGy [436]. MAP4 and CTSZ were also dysregulated after 20 weeks of 16 Gy local heart irradiation in mice [558]. The dysregulation of these genes in

irradiated cardiac proteomes suggests their specific involvement in the response of cardiomyocyte to IR.

While the selected DMPs/DMRs show statistically significant alterations in gene expression after IR, determining the biological relevance of these alterations requires integration of patients' methylomes, transcriptomes and cardiac function data. This integration would help eliminate the confounding influence of breast cancer and identify RICVD-specific biomarkers for better risk prediction.

4.5 Conclusion

RICVD is a major concern after thoracic RT, especially in breast cancer with its high patient survival rate. We investigated the DNA methylation profile of sixteen breast cancer patients receiving adjuvant RT and assayed the expression of selected DMRs/DMPs. The specific enrichment of the Adrenergic signaling in cardiomyocytes pathway in patient blood suggests that blood can provide relevant cardiovascular information despite its lack of specificity. Nonetheless, the dysregulation of selected DMRs/DMPs in breast cancer presents a strong confounder to the interpretation of our results. Altered expression of selected DMRs/DMPs could influence atherosclerotic development by impacting endothelial activation, oxidative stress, mitochondrial dysfunction and inflammation. While promising, our data requires future validation. In addition, integration of the DNA methylation data in a large predictive model encompassing the circulatory biomarkers e.g. C protein, pro-BNP, troponin I and T as well as cardiac function data e.g. cardiac magnetic resonance imaging (MRI) will provide further insight.

Chapter 5 **Meta-analysis of RNA-seq datasets identifies novel players in glioblastoma**

Magy Sallam[1,2], Mohamed Mysara[1,3], Sarah Baatout[1,4], Pieter-Jan Guns[2], Raghda Ramadan[1], Mohammed Abderrafi Benotmane[1]*

[1] Radiobiology Unit, Interdisciplinary Biosciences, Belgian Nuclear Research Centre, SCK CEN, Mol, Belgium.
[2] Laboratory of Physiopharmacology, University of Antwerp, Wilrijk, Belgium.
[3] Current affiliation: Bioinformatics Group, Center for Informatics Technology and Computer Science (ITCS), Nile University, Giza, Egypt.
[4] Department of Molecular Biotechnology, Ghent University, Ghent, Belgium.

This chapter is adapted from the following publication:

5.1 Introduction

Glioblastoma is the most common primary brain cancer of glial origin [567,568]. While considered the most aggressive grade of gliomas (grade IV), the etiology of glioblastoma remains largely unclear [569]. Conventional treatment modalities for newly diagnosed glioblastoma patients include surgery with adjunctive radiotherapy and chemotherapy (e.g. temozolomide) [570]. Despite these modalities, the median patient survival for glioblastoma is less than 14 months [571]. Unfortunately, glioblastoma tumors exhibit substantial genetic, epigenetic and transcriptional heterogeneity which adds to the challenge of early diagnosis and therapy development [572]. Recently, non-coding RNAs such as long non-coding RNAs (lncRNAs) and microRNAs (miRNAs) have been associated with different aspects of glioblastoma pathogenesis such as tumorigenesis, proliferation, invasiveness, drug resistance and survival [573,574]. LncRNAs are non-coding RNA transcripts of sizes larger than 200 nucleotides [575]. They regulate gene expression by acting as transcription factor and chromatin modifier guides, molecular scaffolds for enzymatic complexes, and decoy inhibitors of RNA-binding proteins, transcription factors and miRNAs [576,577]. On the other hand, miRNAs are a species of short non-coding RNAs (18–25 nucleotides) which regulate gene expression by binding to mRNAs untranslated regions and mediating mRNA decay [578]. Consequently, examination of the interaction between these non-coding RNAs and coding mRNAs could reveal novel disease pathways.

Transcriptome research using RNA-seq is regularly used to investigate novel coding and noncoding disease biomarkers, leading to the creation of public databases containing published omics data [579–581]. As such, meta-analyses aim to combine this raw data from multiple studies to improve power, accuracy and reproducibility of individual studies [582]. In the current study, we performed a meta-analysis of glioblastoma RNA-seq datasets with differentially expressed protein coding genes (PCGs) and long non-coding RNAs (lncRNAs), while investigating differentially expressed microRNAs (miRNAs) in glioblastoma tissue samples and normal tissue controls by small RNA-seq. We also identified the overlap between meta-analysis identified PCG/lncRNAs with those identified in The Cancer

Genome Atlas Glioblastoma (TCGA-GBM) cohort. Thus, we conducted a transcriptomic examination of de novo/non-recurrent glioblastoma with the aim of identifying novel involvements/pathways. A schematic overview of the methodology employed in our study is shown in **Figure 5-1**.

5.2 Materials and Methods

5.2.1 RNA-seq and small RNA-seq study selection for meta-analysis

We searched glioblastoma-related RNA-seq datasets in GEO DataSet [583] using the following search terms: ("Glioblastoma"[Mesh] OR ("glioblastoma"[MeSH Terms] OR Glioblastoma[All Fields])). The search was performed on 01/02/2020. Filters were applied to only show studies containing expression profiling by high throughput sequencing or non-coding RNA profiling by high throughput sequencing. Thus, we selected the suitable datasets using the following criteria: 1) the study was performed in humans; 2) the study in the dataset was designed using the case-control method; 3) the study presented at least two samples per condition (case and control); 4) the assayed samples were sampled from de novo or non-recurrent glioblastoma tumor tissues; 5) the study participants/samples had not received any treatments (radio/chemotherapy); 6) the dataset provided the FASTQ data. Finally, the studies from these datasets were selected (**Figure 5-1l**). The clinical information of glioblastoma patients and their controls have been reported in the individual studies: study 1 [584], study 2 [585], study 3 [586] and study 4 [587]. From these studies, only glioblastoma and paired control samples were included in our meta-analysis.

For small RNA-seq meta-analysis, similar filtering criteria as those employed in the glioblastoma RNA-seq meta-analysis were applied, while searching for glioblastoma-related small RNA-seq datasets in the GEO database. This search was performed on 22/03/2022. The following search terms were employed in our search: (("Glioblastoma"[Mesh]) OR glioblastoma AND (mirna OR microrna)) while selecting filters for studies performed in humans and containing expression profiling by high throughput

sequencing or non-coding RNA profiling by high throughput sequencing. Then, the suitable

datasets were selected using the same criteria used for RNA-seq meta-analysis.
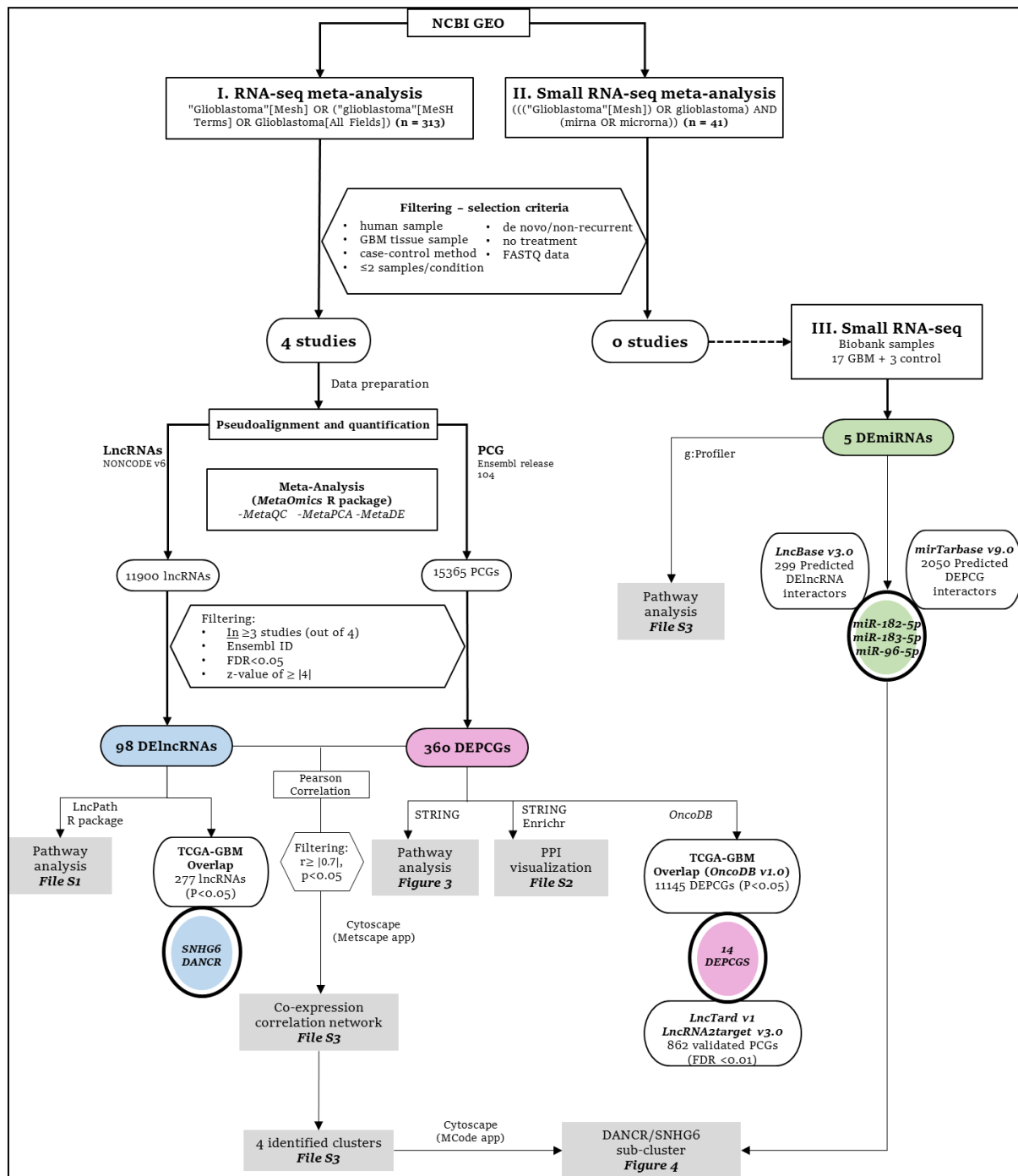
Figure 5-1 *Schematic flow chart of the methodology used in this study. The workflows for lncRNAs, PCGs and miRNAs are denoted via blue, pink and green colors, respectively. Black circles indicate intersection/overlap output with databases. **I and II**) Employed methodology for meta-analysis of glioblastoma tissue RNA-seq and small RNA-seq datasets, respectively. Four studies were selected for RNA-seq meta-analysis with identification of DElncRNAs and DEPCGs, and their overlap with experimentally verified databases and TCGA-GBM. No*

qualifying studies could be included in small RNA-seq meta-analysis and thus small RNA-seq (III) was performed on glioblastoma tissues (n=17) and normal tissue controls (n=3) for identification of DEmiRNAs and overlap with predicted miRNA targets of DElncRNAs and DEPCG. Downstream analyses performed on the filtered DElncRNAs, DEPCGs and DEmiRNAs are detailed further with corresponding figures/supplementary files including pathway analyses and co-expression correlation.

5.2.2 Quantification of long non-coding RNA (lncRNA) and protein coding gene (PCG) sequencing abundance using RNA-seq data

The sequencing data of the selected studies was downloaded by *Prefetch* and converted into FASTQ files using the *fastq-dump* tool of the SRA Toolkit software v2.11.0 [588,589]. Then, the reference sequences of lncRNA and protein coding transcripts were downloaded from the most complete annotated non-coding RNA databases, NONCODE (v6; 35), for lncRNAs and Ensembl for PCGs (release 104; 34), respectively. After merging the two FASTA format files, 199,240 transcript sequences of 173,112 human lncRNA genes were obtained from NONCODE. After removing the pseudogenes, quantification of the lncRNAs and protein coding genes was performed simultaneously by mapping the RNA-seq reads of each study to the merged reference sequence (pseudoalignment) and calculating the count values using *Kallisto* software v0.46.2 [592]. In addition to the default parameter settings, the estimated average fragment length and the standard deviation of fragment length were set to 200 and 20, respectively. Based on the annotation file *Transcript2Gene*, transcript-level count values of lncRNAs were integrated using the R package *tximport* v1.24.0 to calculate their corresponding gene-level count values.

Quality control was performed using the MetaQC module in the transcriptomic meta-analysis R package *MetaOmics* and the standardized mean difference (SMD) with its 95% confidence interval (CI) was calculated. For dimension reduction, the MetaPCA module was applied in *MetaOmics* to perform a meta-analytic approach of the principal component analysis (PCA) algorithm of the four selected studies. To identify the significantly differentially expressed lncRNAs and PCGs in glioblastoma tissues, the individual results of each study were integrated by meta-analysis using the MetaDE module of *MetaOmics* for the four selected studies. The normalization process used in this meta-analysis was performed using the random effect model (REM) for lncRNAs/PCGs with count ≥ 10

[589,593,594]. Differentially expressed lncRNAs (DElncRNA) and differentially expressed PCGs (DEPCGs) were then identified by selecting for lncRNAs/PCGs differentially expressed in at least 3 studies (out of 4), having valid Ensembl ID with FDR<0.05 and having a z-value of $\geq |4|$.

5.2.3 Identification of overlap between DElncRNAs/DEPCGs and lncRNAs/PCGs in publicly available experimentally verified databases and TCGA-GBM output

To further validate the DElncRNAs, a manual search of experimentally validated PCG targets of DElncRNAs was performed by searching in two databases using the Ensembl lncRNA ID: LncTarD v1 (53) and LncRNA2Target v3.0 (54). For RNA-seq/microarray experiments, targets were selected to have adjusted p values < 0.01. In case listed targets had an adjusted p < 0.01, all listed targets were selected. After the manual search, overlap between DEPCGs and search-identified PCGs was recorded.

Finally, we investigated the overlap of DElncRNAs and DEPCGs from our meta-analysis with those identified from the TCGA-GBM database, as supplied by LncTard v1 and OncoDB v1.0 (oncodb.org), respectively [595,597]. In LncTard, differential expression patterns of lncRNAs in the TCGA pan-cancer dataset were downloaded and only the expression patterns of the TCGA-GBM cohort were considered. Furthermore, output was filtered according to adjusted p value < 0.01. TCGA-GBM expression data were downloaded from the data download portal of OncoDB wherein $\log_2$ fold change values of tumor and matched normal (control) RNA-seq data had been calculated [597]. Gene overlap between DEPCGs and TCGA-GBM PCGs was then recorded (**Figure 5-1**).

5.2.4 Pathway analysis of DElncRNAs and DEPCGs

The LncRNAs2Pathways R package *LncPath* v1.1 was used to identify the functional pathways of supplied lncRNAs, based on identifying the pathways of associated protein coding genes (PCGs) [598]. Shortly, the Ensembl IDs of the DElncRNAs were queried using

the *LncPath* function in the KEGG and Reactome databases [599,600]. Only pathways with FDR<0.05 were considered significant.

For pathway analysis and protein-protein interactions, DEPCGs were uploaded to STRING v11.5 (Search Tool for the Retrieval of Interacting Genes/Proteins) online public database (https://string-db.org/) [370].

For visualization of the identified DEPCG enriched pathways, the STRING network produced by analysis of DEPCGs was imported into Cytoscape 3.9.0 [371]. Using the *String app* v1.7.0 in Cytoscape, we imported the PPI network of DEPCGs, performed STRING enrichment and visualized the identified KEGG and Reactome pathways using the *EnrichmentMap* v3.3.3 app with an edge cut-off of 0.4 and p<0.05. To simplify the resultant STRING network, the Molecular Complex Detection (*MCODE* v2.0.0) app was used to detect densely connected regions in networks and thus identify the biggest DEPCG clusters containing ≥10 members [601]. The cluster finding cutoff parameters were as follows: a p-value cutoff of 0.05 and an edge (the degree of gene overlap that exists between two gene sets) cutoff of 0.4.

5.2.5 Co-expression analysis of DElncRNAs and DEPCGs and identification of highly connected nodes

Using the normalized counts of DElncRNAs and DEPCGs, a lncRNA-mRNA co-expression network was built to identify the relationships between DElncRNAs and DEPCGs. We filtered DElncRNAs and DEPCGs to build the network according to the Pearson correlation coefficient (r) > |0.7| with p < 0.05. Visualization of the DElncRNAs/DEPCGs correlation was performed using the *Metscape* v.3.1.3 app from Cytoscape software v.3.9.0. Highly connected nodes that had ≥ 10 DElncRNAs/DEPCGs were identified by clustering the co-expression network using *MCODE*.

5.2.6 Small RNA-seq of glioblastoma and control tissue samples

Freshly frozen brain tissue samples from patients with glioblastoma (*n* = 17) and tumor-adjacent normal tissue controls (*n* = 3) were collected from the Biobank Antwerp

(University Hospital of Antwerp (UZA), Antwerp, Belgium; ID: BE 71030031000) [602]. These tissue samples were residual material collected within the opt-out system, as stated in the Belgian law of 19th of December 2008 whereby residual material may be used for translational research. The study was approved by the local medical ethics committee (Contract number: BB20079).

Total RNA, including microRNAs (miRNAs), was isolated from the glioblastoma tissues and normal controls using the miRNeasy Serum/Plasma kit (Qiagen, Hilden, Germany) according to the manufacturer's protocol. Total RNA was eluted in a volume of 30 µL RNase-free water. Concentration, purity and integrity of the RNA were determined by spectrophotometry (Little Lunatic, Unchained labs, CA, USA) and the Agilent 2100 Bioanalyzer/Agilent RNA 6000 Nano Kit (Agilent, CA, USA). Library preparation for small RNA-seq and sequencing on Illumina HiSeq of total RNA was performed by GENEWIZ Inc (GENEWIZ, NJ, USA).

Functional enrichment of the identified differentially expressed miRNAs (DEmiRNAs) was performed by importing the Ensembl IDs (ENSG00000283203, ENSG00000207990, ENSG00000207691, ENSG00000208003, and ENSG00000199158 for miR-1246, miR-182, miR-183, miR-549a and miR-96, respectively) into g:Profiler [465]. G: Profiler is a web server offering Gene Ontology (GO) and pathway enrichment analysis resulting from mining high-throughput genomic data [603].

5.2.7 Prediction of interacting miRNAs of DElncRNAs and DEPCGs in publicly available experimentally verified databases

DElncRNA-interacting miRNAs were investigated by supplying our DElncRNAs list into DIANA-LncBase v3.0, which provides a free repository of experimentally supported miRNA targets of lncRNAs [604]. DEPCG-interacting miRNAs were investigated by supplying our DEPCG list into mirTarBase v9.0, which provides the most current miRNA–target interactions by comparing with other similar databases, such as TarBase, miRecords and

miR2Disease [605,606]. Overlap between database-identified interacting miRNAs and differentially expressed miRNAs in glioblastoma tissue samples was identified (**Figure 5-1**).

5.3 Results

5.3.1 Four glioblastoma RNA-seq datasets were selected for meta-analysis

Using keyword search and quality filtering, we identified 4 glioblastoma tissue-related RNA-seq datasets, including: GSE59612, GSE62731, GSE86202 and GSE165595. From the two-dimensional PCA plots of the four selected studies (**Figure 5-2**), little variation was found between the glioblastoma tissue samples in each study, while showing distinct variation from controls. After examining the quality control parameters calculated by the MetaQC module, which included internal quality control (IQC), accuracy quality control of gene (AQCg), consistency quality control of gene (CQCg) and standardized mean rank (SMR), no studies were excluded from our analysis.

After analyzing the homogenized data using the bias resilient random effect model (REM), LncRNA abundance was quantified in the 84 samples from the 4 selected studies. In total, 11900 lncRNAs and 15365 PCGs were identified from REM meta-analysis. We further limited our downstream validation by selecting lncRNAs differentially expressed in at least 3 studies (out of 4), having Ensembl ID, FDR<0.05 and a z-value (weighted effect size) of $\geq$ |4|. Consequently, we identified 98 DElncRNAs (**Supplementary table 3.1 in Supplementary materials for Chapter 5**) and 360 DEPCGs fulfilling these criteria (**Supplementary table 3.3 in Supplementary materials for Chapter 5**). Details of the selected datasets can be found in **Table 5-1.**

Overlap between the list of DElncRNAs and DEPCGs with the TCGA-GBM cohort identified two DElncRNAs (DANCR and SNHG6) and 222 DEPCGs.

Of these 222 DEPCGs, 14 were identified as experimentally validated targets of DANCR during our manual search of experimental databases LncTarD and LncRNA2target (ROCK1,

ZWILCH, RPGR, GK, ZNF460, METAP2, CIP2A, ASAH1, ZNF528, C5orf15, QTRT2, STX2, MAP3K2 and CNTRL). Literature-based functionality of these 14 DEPCGs showed that several of these were previously implicated in glioblastoma pathogenesis (**Supplementary table 3.5 in Supplementary materials for Chapter 5**).
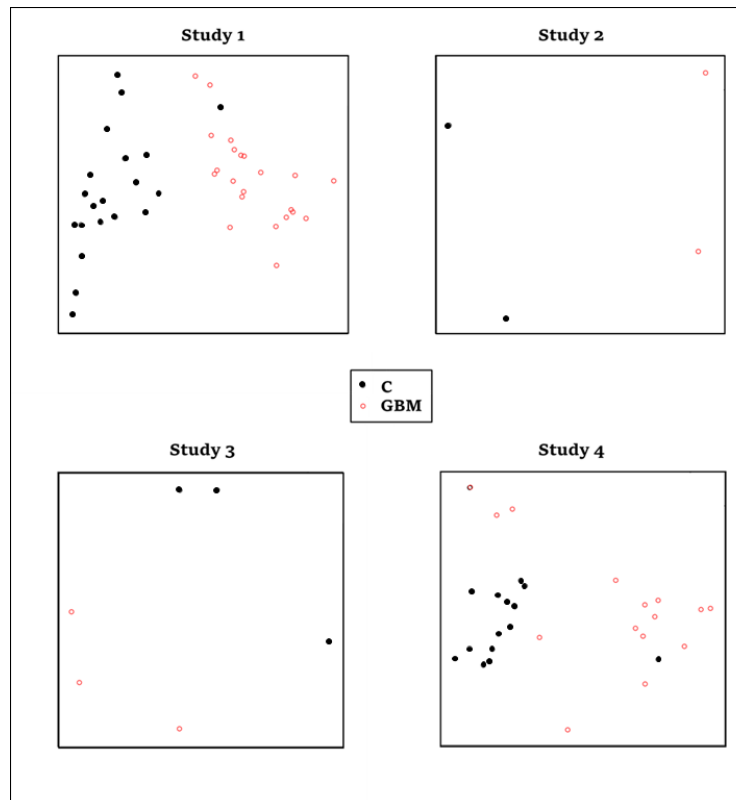

Figure 5-2 *Output from the MetaPCA analytical module of the MetaOmics package showing principal component analyses (PCA) plots for the four selected studies (C: normal tissue controls, GBM: glioblastoma).*

Table 5-1 Details of studies fulfilling the predefined criteria with quality control measurements as supplied by the MetaOmics MetaQC module. IQC, internal quality control; AQCg, accuracy quality control of gene; CQCg, consistency quality control of gene; SMR, standardized mean rank.

No	Dataset	Platform	Sample Size	IQC	AQCg	CQCg	SMR	Ref
1	GSE59612	Illumina HiSeq 2000	22 glioblastoma tumor tissue, 22 controls	5.6	61.25	145.18	1.67	[584]
2	GSE62731	Illumina HiSeq 2000	2 glioblastoma tumor tissue, 2 controls	3.3	2.49	52.78	3.33	[585]
3	GSE86202	Illumina HiSeq 2500	3 glioblastoma tumor tissue, 3 controls	1.3	2.66	17.74	3.67	[586]
4	GSE165595	Illumina HiSeq 4000	15 glioblastoma tumor tissue, 15 controls	5.6	23.08	240.99	1.33	[587]

5.3.2 Pathway analysis of DElncRNAs reveals several glioblastoma-associated pathways

Pathway analysis identified 4 KEGG and 37 Reactome significantly enriched pathways (FDR<0.05) that were associated with DElncRNAs (**Supplementary table 3.2 in Supplementary materials for Chapter 5**). The top pathways according to the normalized enrichment scores were glycoprotein related pathways (O-glycan biosynthesis, O-linked glycosylation of mucins, termination of O-glycan biosynthesis and HS-GAG degradation of glycoprotein), fanconi anemia pathway, glutamate neurotransmitter release cycle, interaction between L1 and ankyrins and SRP-dependent cotranslational protein targeting to membrane, which have been previously associated with glioblastoma [607,608]

5.3.3 DEPCGs show a highly connected PPI network with several enriched glioblastoma-linked pathways

Analysis of DEPCGs using STRING databases produced a highly connected protein-protein interaction network (PPI). Functional enrichment of the produced PPI network identified a number of significantly enriched KEGG and Reactome pathways (FDR<0.05) (**Figure 5-3**) e.g., nonsense mediated decay (NMD), L13a mediated silencing of ceruloplasmin expression, EIF2AK4 response to amino acid deprivation, regulation of expression of SLITs and ROBOs and selenocysteine synthesis.

Clustering of the PPI network into individual clusters containing ≥ 10 DEPCGs yielded only one cluster that showed nearly identical functional enrichment as the parent PPI.

Pathway enrichment overlap between DEPCGs and DElncRNAs revealed several overlapping pathways (**Table 5-2**). From these, NMD and SRP-dependent cotranslational protein targeting to membrane have been associated with glioblastoma. While others, such as influenza viral RNA transcription and replication, have not been directly associated with glioblastoma.
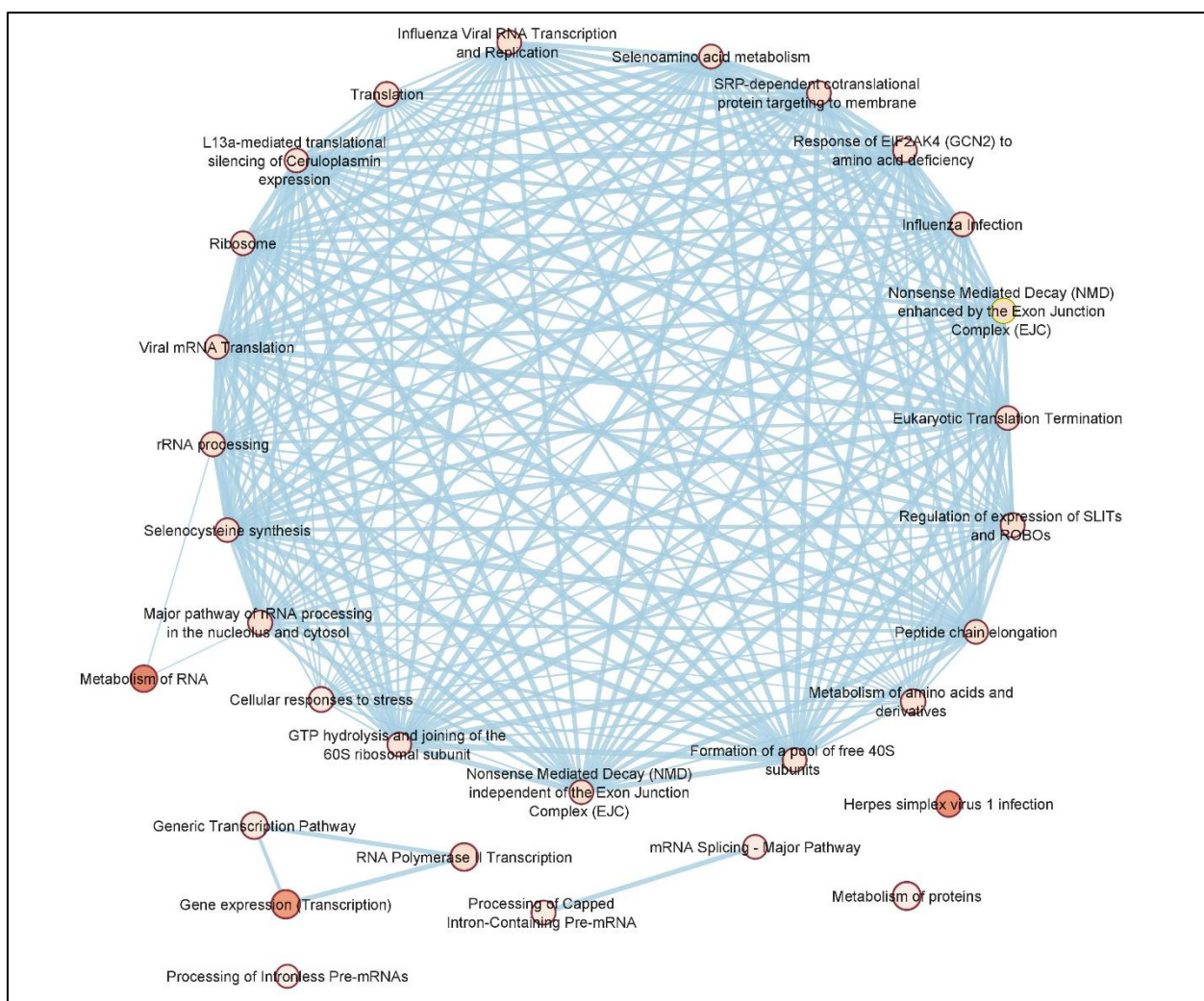

Figure 5-3 *Enrichment map of KEGG (dark pink nodes) and Reactome (light pink nodes) pathways of DEPCGs as indicated by STRING enrichment in Cytoscape. The thickness of a line indicates the strength of the interaction between the proteins it connects.*

Table 5-2: Significantly enriched pathways associated with both DElncRNAs and DEPCGs (FDR<0.0.5) as identified by LncPath R package and STRING database, respectively.

Database	Overlapping DElncRNA/DEPCGs associated pathways (FDR<0.05)
KEGG	Ribosome
Reactome	Translation
	Peptide Chain Elongation
	Influenza Viral RNA Transcription And Replication
	Nonsense Mediated Decay Enhanced By The Exon Junction Complex
	SRP-dependent co-translational protein targeting to membrane

5.3.4 Three DEmiRNAs identified by small RNA-seq of glioblastoma tissue overlap with predicted DElncRNA and DEPCGs-interacting miRNAs

The glioblastoma-related small RNA-seq dataset search yielded 41 datasets. After applying filtering criteria, none of these datasets qualified for inclusion in our analyses. Subsequently, analysis of small RNA-seq of glioblastoma tumor tissue and controls identified several differentially expressed miRNAs, of which 5 were significantly differentially expressed miRNAs (DEmiRNAs): hsa-miR-1246, hsa-miR-182-5p, hsa-miR-183 (-3p and -5p), hsa-miR-549a and hsa-miR-96-5p (p<0.05). Functional enrichment of DEmiRNAs identified an enrichment in several GO: Biological Processes, which were all associated with the traditional miRNA roles in post-transcriptional regulation as well as enrichment of the KEGG pathway "MiRNAs in cancer" (**Supplementary figure 3.1 in Supplementary materials for Chapter 5**).

From mirTarBase, 2050 unique miRNAs were identified as interacting miRNAs of DEPCGs by one of the following methods: reporter assay, western blot, qPCR, microarray, pSILAC, NGS, other validation methods or CLIP-Seq. From LncBase, 299 unique miRNAs were identified as interacting miRNAs of DElncRNAs.

Overlap between DEmiRNAs and predicted interacting miRNAs of DElncRNAs and DEPCGs identified 3 miRNAs: hsa-miR-182-5p, hsa-miR-183 (-3p and -5p) and hsa-miR-96-5p, which were previously identified as experimentally validated targets of DANCR and SNHG6.

5.3.5 Co-expression analysis identifies 4 clusters of DElncRNAs/DEPCGs

Analysis of co-expression of DElncRNA and DEPCGs revealed 15731 correlation pairs having r≥ |0.7| and p<0.05. Clustering of the network using MCODE default settings into clusters containing ≥10 members yielded four individual clusters of which the first cluster was further clustered into 3 main sub-clusters (**Supplementary figure 3.2 in Supplementary materials for Chapter 5**).

Pathway analysis of the individual clusters and sub-clusters revealed that only one sub-cluster (**Figure 5-4**) (containing DANCR and SNHG6) was responsible for the majority of the enriched pathway associations identified for DEPCGs and DElncRNAs e.g., L13a mediated silencing of ceruloplasmin expression, regulation of expression of SLITs and ROBOs and selenocysteine synthesis, EIF2AK4 response to amino acid deprivation and NMD (**Supplementary table 3.4 in Supplementary materials for Chapter 5**).
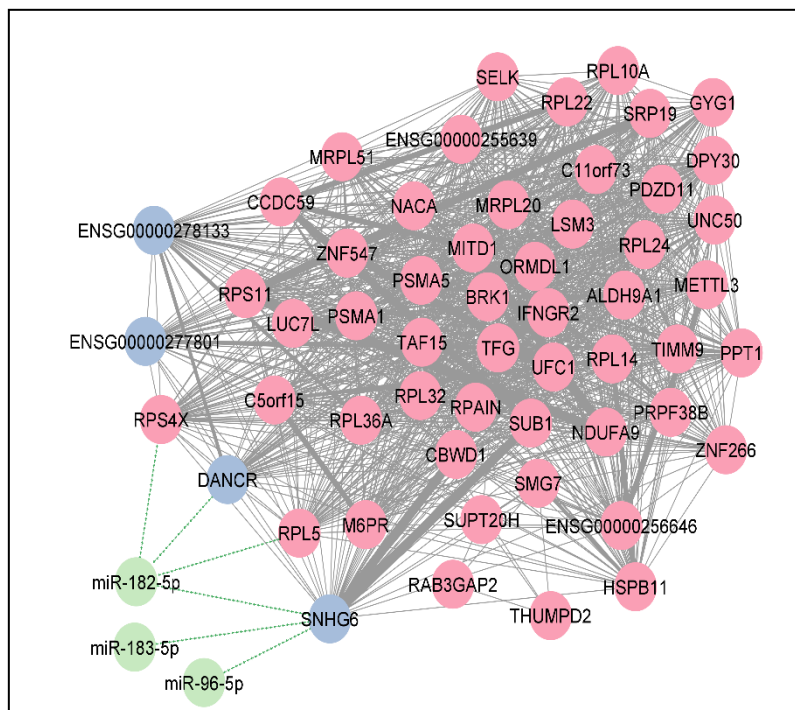

Figure 5-4 *The DANCR/SNHG6 sub-cluster of DElncRNA-DEPCG (blue and pink circles, respectively) co-expression correlation network produced was visualized using MCODE in Cytoscape, supplemented with interacting DEmiRNAs (green circles) as supplied by mirTarBase and LncBase databases. STRING enrichment*

analysis of this sub-cluster shows strong similarity with DEPCG enrichment, thereby denoting sub-cluster relevance.

5.4 Discussion

Previous meta-analyses have elucidated unexamined relevance to specific pathways as well as aided in the identification of candidate biomarkers [593,609]. Compared to single studies, meta-analyses have enhanced statistical power and provide insight in the consistency across studies [610]. Therefore, we performed a meta-analysis of publicly available RNA-seq glioblastoma datasets of non-recurrent glioblastoma and control samples from the same patient. In this manner, 98 DElncRNAs and 360 DEPCGs were identified. We also performed small RNA-seq of glioblastoma tissues and normal controls.

5.4.1 Meta-analysis of glioblastoma RNA-seq datasets

5.1.1.1 DElncRNAs

The top five identified DElncRNAs according to absolute weighted effect size included 4 DElncRNAs that had no previously characterized roles in glioblastoma; RNFT1-DT, ENSG00000233184, ENSG00000268205 and ENSG00000268362, as well as glioblastoma prognostic biomarker, MROCKI (LINC01268) [611]. Due to the high differential expression of these DElncRNAs, future studies determining their specific roles in glioblastoma could reveal novel involvements.

Functional enrichment of the full 98 DElncRNAs revealed over 30 significantly enriched pathways previously identified in glioma, including pathways associated with O-glycans (O-glycan biosynthesis, O-linked glycosylation of mucins, termination of O-glycan biosynthesis and HS-GAG degradation of glycoproteins), fanconi anemia pathway, glutamate neurotransmitter release cycle, insulin receptor recycling, interaction between L1 and ankyrins as well as transferrin endocytosis and recycling. O-glycans are found on glycoproteins, of which mucins are the main class, which regulate protein folding, stability and trafficking, and also mediate many cell-cell interactions [612,613]. Many cancers express altered mucin-type O-glycans (reviewed in [614]) including glioma where aberrant glycosylation of tumor glycan-rich extracellular matrix promotes tumor progression and

treatment resistance [607]. On the other hand, the fanconi anemia (FA) pathway relates to DNA damage repair processes of lesions in the replication fork which impede replication [615]. This pathway is reactivated in glioblastoma, mediating survival of the mutated cells and thereby accelerating carcinogenesis [608,615]. Alternately, glutamate is produced in glioma cells as a byproduct of glutathione synthesis, leading to tumor expansion and invasion [616,617]. Insulin receptor recycling frees insulin receptors to engage in downstream signaling regulating cell proliferation, which worsens glioblastoma prognosis, and mediates treatment resistance [618]. L1 cell adhesion molecule (L1cam) is a neural adhesion molecule whose levels have been shown to associate with glioblastoma, and its knockdown can suppress glioma stem cell growth [619,620]. Finally, transferrin is a glycoprotein responsible for iron ion delivery that is overexpressed in glioblastoma, leading to increased cell proliferation and worsening prognosis [621].

5.1.1.2 *DEPCGs*

Similarly, the top five DEPCGs according to weighted effect size included ATF6, AHCTF1, ZCCHC10, ZNF234 and IFNGR2. Of these, only ATF6 and IFNGR2 have been previously associated with glioblastoma viability and treatment resistance, while the remaining three have only been identified in other cancer types, which encourages further investigations [622–627]. Moreover, several significantly enriched pathways were identified by pathway enrichment analysis of the 360 DEPCGs (**Figure 5-3**), such as nonsense mediated decay (NMD), ceruloplasmin expression, selenocysteine synthesis, SLIT/ROBO signaling, as well as EIF2AK4 and Hedgehog signaling. NMD functions to eliminate truncated mRNA transcripts resulting from premature termination codons (PTCs), protecting against their dominant negative effect on the functional wild-type alleles [628]. Inhibition of NMD regulates tumorigenesis and stemness properties in glioma stem cells [629]. Ceruloplasmin is a copper-binding protein which regulates iron efflux [630]. In glioblastoma, ceruloplasmin leads to excessive extracellular iron with subsequent oxidative stress, impacting blood-brain barrier integrity [631]. Another enriched pathway was synthesis of selenocysteine which is a selenium containing amino acid incorporated in anti-oxidant selenoproteins, such as glutathione peroxidases, and has been shown to induce apoptosis of glioblastoma

cells in vitro [632,633]. On the other hand, Slits (ligands) and Robos (receptors) are glycoproteins involved in several cell signaling pathways including axon guidance, cell proliferation, cell motility and angiogenesis (reviewed in [634]). The effects of Slit/Robo signaling in glioblastoma are not clearly characterized. On the one hand, Slit2 expression is suppressed in glioma cells and intracranial mice xenografts with forced expression hampering glioma cell migration and invasion [635]. On the other hand, Slit2 knockdown in mouse glioma cells and patient-derived GBM xenografts decreased tumor growth and increased treatment resistance [636]. In either case, Slit2 levels seem to influence glioblastoma growth and treatment resistance, though, further research is needed to elucidate its exact role. Alternately, EIF2AK4, eukaryotic translation initiation factor 2 alpha kinase 4, is activated by metabolic stress signals to induce global protein translation inhibition and cell survival control [637]. Normally, as tumor growth progresses, access to nutrients such as amino acids decreases, which activates EIF2AK4 to induce downstream effects of increased tumor cell survival and treatment resistance [638,639]. This was shown in our pathway analysis by the identification of the involvement of amino acid metabolism and peptide chain elongation pathways. Finally, the Hedgehog pathway is essential during development for intercellular communication, organogenesis, regeneration and homeostasis [640]. The exact mechanisms of Hedgehog pathway tumorigenic activity are reviewed in [641,642]. In glioblastoma, Hedgehog pathway inhibitors were shown to decrease cancer stem cell growth and drug resistance [643,644].

5.4.2 Small RNA-seq of glioblastoma tissues and normal controls

In the current study, small RNA-seq identified 5 differentially expressed microRNAs (DEmiRNAs): miR-1246, miR-182-5p, miR-183 (-3p and -5p), miR-549a and miR-96-5p. Functional enrichment of these DEmiRNAs was uninformative. However, each of these 5 DEmiRNAs has been previously identified in glioblastoma. Increased exosomal miR-1246 expression was found to promote a pro-oncogenic immunosuppressive microenvironment, while it was associated with a higher glioma recurrence rate in postoperative patients [645]. Previous studies also linked miR-182-5p to glioblastoma tumorigenesis, angiogenesis

and metastasis [646,647]. Alternatively, mir-183 is a TGFβ-induced miRNA which also contributes to the immunosuppressive glioma microenvironment [648,649]. In fact, miR-183-5p has been proposed to be a prognostic biomarker of glioblastoma progression [650,651]. Similarly, mir-549a was previously shown to be of prognostic importance in tumors of glial origin [652]. Finally, miR- 96-5p was found to be upregulated in glioma cells, with effects on proliferation and metastasis [653]. Upregulation of miR-96 was also found to promote radioresistance in T98G glioblastoma cells [654]. Interestingly, miR-182, miR-183 and miR-96 are located within less than 4.5 kbp of one another and comprise the miR-183**/**96/182 cluster [655]. This miR-183/96/182 cluster was associated with the progression from low to high grade glioma (glioblastoma) while knockdown of this cluster in glioblastoma inhibited cell survival [650,655].

5.4.3 Overlap with other genetic glioblastoma databases

Overlap of our DElncRNA and DEPCGs with The Cancer Genome Atlas glioblastoma (TCGA-GBM) database yielded two lncRNAs (DANCR and SNHG6) and 222 DEPCGs. DANCR is an oncogenic lncRNA which induces several cancer promoting effects, such as promotion of angiogenesis and epigenetic silencing of tumor-suppressors as well as regulating cancer promoting signaling pathways such as the Wnt/β-catenin, JAK/STAT, Notch, PI3K/AKT pathways (reviewed in [656]). Due to its pan-oncogenic effect, DANCR has been considered to be a candidate therapeutic target [657,658]. In glioma, DANCR knockdown leads to decreased proliferation and migration [659]. The oncogenic effects of DANCR seem to be caused mainly by its role as a competing endogenous RNA (ceRNA), which binds miRNAs competitively thereby influencing miRNA capacity to inhibit mRNA translation [658]. In glioma cells, DANCR was shown to act as ceRNA to miR-634, a miRNA shown to increase glioma cell sensitivity to temozolomide [660,661]. DANCR was also shown to promote cisplatin resistance via ceRNA mediated inhibition of sponging miR-33a-5p, miR-33b-5p, miR-1-3p, miR-206, and miR-613 with resultant activation of AXL/PI3K/Akt/NF-κB signaling pathway [662].

Similarly to DANCR, SNHG6 was shown to promote glioma progression via a similar ceRNA activity by interfering with glioma-relevant miRNAs: miR-543 and miR-101-3p [663,664]. SNHG6 was also shown to promote glioma malignant progression by inducing histone modifications in tumor suppressor genes [665].

Of the 222 DEPCG overlapping with TCGA-GBM, 14 were identified to be DANCR regulated by searching of LncRNA2Target and LncTard databases. Literature-based functionality of these 14 DEPCGs showed that several of them were previously implicated in glioblastoma proliferation, invasiveness and treatment resistance (**Supplementary table 3.5 in Supplementary materials for Chapter 5**)**,** thereby explaining some of the pro-tumorigenic effects of DANCR. For the remaining 7 DEPCGs (ZWILCH, RPGR, ZNF460, ZNF528, QTRT2, C5orf15 and CNTRL), no previous functional associations were found with glioblastoma progression, despite a number of them being associated with other cancer types [666–670]. Future investigations into potential previously unaddressed roles of these genes could reveal new players in glioblastoma pathogenesis.

Due to the study selection process and applied filtering criteria, the data from the Ivy Glioblastoma Atlas (IVY GAP) [671] and Chinese Glioma Genome Atlas (CGGA) [672] were not included in our assays (both not being in case control format). However, in CGGA, the co-expression correlation between the 2 TCGA-GBM overlapping DElncRNAs (DANCR and SNHG6) and 3 DEmiRNAs (miR-96, miR-182 and miR-183) was assayed through the 'Analyze' portal on the CGGA website (http://www.cgga.org.cn/). In the CGGA RNA-seq datasets, DANCR expression showed a significant medium correlation to SNHG6 expression (R=0.446 and 0.449 for dataset mRNAseq_693 and mRNAseq_325, respectively, p<0.001 for both) (**Supplementary figure 3.3 in Supplementary materials for Chapter 5**). Using the CGGA miRNA array dataset, a significant strong correlation was identified between the 3 miRNAs (miR96/miR182: R=0.721, p<0.001, miR96/miR183: R=0.745, p<0.001 and miR182/miR183: R=0.937, p<0.001) which is unsurprising as they form the miR-183/96/182 cluster (**Supplementary figure 3.3 in Supplementary materials for Chapter 5**). This

confirms the strong interaction between DANCR and SNHG6, as well as between the DEmiRNAs in the miR-183/96/182 cluster in CGGA, as was replicated by our analyses.

5.4.4 Co-expression network construction and functional enrichment

A co-expression network was constructed to identify DElncRNA/DEPCG highly interacting pairs with possible functional associations. A strong correlation was found between DANCR and SNHG6 expression (r=0.76 and p<0.001) which confirms the similar correlation observed in CGGA datasets.

In addition, clustering of the co-expression network and pathway analysis of the clusters and sub-clusters revealed that the sub-cluster containing DANCR and SNHG6 was responsible for a majority of the pathway enrichments of the 360 DEPCGs. Interestingly, both DANCR and SNHG6 are targets of the miR-183**/**96/182 cluster in the DIANA-LncBase database, which suggests a possible DElncRNA/DEmiRNA interplay in glioblastoma. In addition, 2 novel DElncRNAs (ENSG00000278133 and ENSG00000277801) were found to belong to this cluster. The high degree of interactions between these 2 DElncRNAs with the DEPCGs sub-cluster members suggests a possible novel relevance in glioblastoma, thereby necessitating future research.

Seven DEPCGs in the DANCR/SNHG6 sub-cluster were also differentially expressed in TCGA-GBM, while being involved in ≥ 20 of the enriched pathways of the sub-cluster. These genes were ribosomal proteins RPS11, RPL5, RPL10, RPL24, RPL14, RPL36A and RPL32. Only RPS11 and RPL36A were previously found to be beneficial in glioma as prognostic predictors [673–677]. Therefore, it may be useful to examine the exact roles of the remaining unexplored DEPCGs in glioblastoma.

5.4.5 Literature-based associations of the pathways: deducible involvement of ferroptosis?

Literature-based research of the DElncRNA and DEPCG enriched pathways led to the identification of their shared association to the novel cell death pathway, ferroptosis [678].

Ferroptosis is a recently discovered intracellular iron-dependent form of cell death characterized by the overproduction of reactive oxygen species (ROS) and accumulation of lipid peroxidation, leading to cell death [679]. As glioblastoma cells have higher ROS and iron accumulation than healthy tissues, they are especially susceptible to death by ferroptosis [680,681]. As a result, ferroptosis induction inhibits glioblastoma tumor growth, improves patient survival and increases the efficacy of radio- and chemotherapy thereby providing adjuvant antitumor options [682,683].

Ferroptosis was shown to be regulated by DElncRNA enriched pathways, protein O-glycosylation as well as glutamine, glutamate and transferrin [684–687]. On the other hand, ferroptosis was previously shown to be influenced by DEPCG enriched pathways; induced by glutathione peroxidase suppression (selenocysteine containing enzyme) and SMG9 (a component of the NMD machinery) and inhibited by ceruloplasmin and Hedgehog pathway activation [688–694]. EIF2AK4 was also identified in a ferroptosis-associated gene signature in glioma [695]. While concurrent dysregulation of ferroptosis and SLIT/ROBO signaling pathway has been associated with low-Grade endometrial cancer [696]. Consequently, the DElncRNAs/DEPCGs seem to suggest an association between glioblastoma and ferroptosis in our analyzed datasets.

As the DANCR/SNHG6 sub-cluster possesses similar enrichments to the d DEPCG pathways, we investigated whether these sub-cluster members had identifiable associations with ferroptosis. Both DANCR and SNHG6 were previously associated with ferroptosis [697,698]. Some of the DEPCG members of the sub-cluster have also been shown to regulate ferroptosis (**Supplementary table 3.6 in Supplementary materials for Chapter 5**). However, the majority of the sub-cluster members had no previous connections to ferroptosis. Consequently, due to the high interaction between this sub-cluster and its enriched pathways, this sub-cluster could identify future candidates for glioblastoma biomarkers or treatment modulators.

To further confirm this connection, we also investigated whether the DEmiRNAs had previous associations with ferroptosis. All DEmiRNAs in the miR-183/96/182 had been previously associated with ferroptotic processes in the literature [699–701]. However, the exact involvement of these DEmiRNAs in ferroptosis processes in glioblastoma is currently under-researched. Therefore, future studies could reveal a role for these DEmiRNA in modulation of glioblastoma responsiveness to treatment.

5.4.6 Limitations

Our study does have some limitations. Firstly, only four glioblastoma datasets were included in our analysis, due to the study selection criteria. Quality assessment (MetaQC) of the included studies resulted in the inclusion of all 4 studies in our analyses, despite the low sample size in certain instances. However, we attempted to overcome this limitation by overlapping our findings with larger glioblastoma datasets, such as TCGA and CGGA. Secondly, glioblastoma can be sub-classified into proneural, neural, mesenchymal, and classical according to differential gene expression profiles, as well as the mutation status of certain key genes including platelet-derived growth factor receptor (PDGFRA), Neurofibromatosis Type 1 (NF1) and epidermal growth factor receptor (EGFR) [702,703]. Also, recent WHO updates to CNS tumor nomenclature have limited glioblastoma classification to IDH-wildtype adult-type diffuse gliomas [568]. Unfortunately, only 2 of our included studies contained detailed information about the subclass of the assayed glioblastoma tumors and thus these classifications could not be included in our analyses. We attempted to overcome this heterogeneity by employing a random effects model (REM), which combines the effect size of the individual studies using a simple linear model with sampling error, while assuming a possible random effect on the effect size of each study [704,705]. However, repeat analyses of previously published datasets after reclassification, according to the current guidelines, could offer novel insights and warrant further research. Thirdly, the limited residual glioblastoma tissue available impacted the number of possible wet-lab validations. Therefore, we recommend the validation of the promising DElncRNA and DEPCG candidates in independent glioblastoma sample cohorts.

Finally, our study analyzed RNA-seq of glioblastoma tissues, which involves an invasive sampling procedure that is unsuitable for regular treatment monitoring. Further studies addressing the need for circulating glioblastoma biomarkers are thus of particular interest, with a specific focus on ncRNA due to their relatively higher stability [706,707]. Consequently, further research addressing the usefulness of the DElncRNAs and DEmiRNAs as candidate biomarkers and their utilization for routine monitoring is required.

5.5 Conclusions

In this study, we have presented DElncRNAs/DEPCGs which were identified by overlap with a TCGA-GBM cohort and experimental databases, or by inclusion in the most pathway enriched sub-cluster in our co-expression network (also interacting with 3 of the DEmiRNAs). We reviewed the literature for the DElncRNAs/DEPCGs associations with glioblastoma. For some DElncRNAs/DEPCGs, no previous connections to glioblastoma were found, which could provide starting points for future studies. Using literature association of DElncRNAs/DEPCGs, we also found a reproducible involvement of ferroptosis. Several DElncRNAs, DEPCGs and DEmiRNAs were previously associated with ferroptosis, while the majority still require further investigation.

A summary of the main findings of our study is presented in **Figure 5-5.**
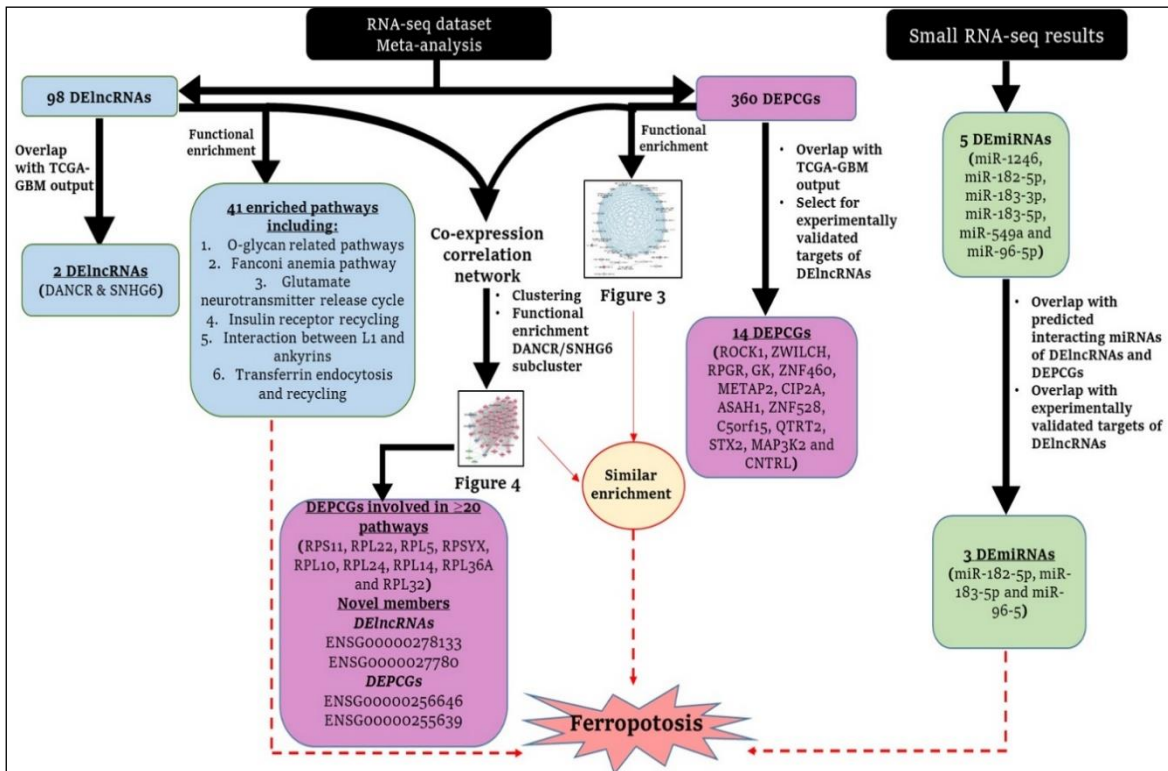
Figure 5-5 *Summary of DElncRNAs (blue), DEPCGs (pink) and DEmiRNAs (green) identified in our study and their connection to ferroptosis.*

Chapter 6 **General discussion**

Ionizing radiation (IR) is frequently used in medicine for both diagnosis and therapy. The use of IR in medicine is regulated by radiation protection measures to maintain the ALARA concept of keeping radiation exposure "*as low as reasonably achievable*" [708]. However, concerns regarding IR's long term negative effects still remain.

In the current PhD thesis, we aimed to investigate the involvement of epigenetic mechanisms in the development of two IR-induced adverse effects: cardiovascular disease (CVD) and secondary cancers. Epigenetics is a relatively new field that has already contributed to the development of clinical biomarkers for cancer diagnosis and treatment response. One example of the latter being the therascreen PITX2 RGQ PCR Kit (QIAGEN, Germany) for predicting the response to anthracycline-based chemotherapy based on PITX2 promoter methylation [360]. Using this epigenetic perspective, we aimed to find candidate biomarkers for the identification of patients at risk of developing delayed IR-induced adverse effects.

This thesis is part of Horizon 2020 project MEDIRAD (http://www.medirad-project.eu/) which attempts to improve the understanding of IR's health effects through the integration of six interdependent work packages (WPs) [13]. As such, we focused on radiation-induced CVD (RICVD) by investigating the DNA methylation profiles of whole-heart irradiated rats (**Chapter 3**) and irradiated breast cancer patients (**Chapter 4**) while validating the expression of selected differentially methylated regions (DMRs). We also investigated noncoding RNA (microRNA and long noncoding RNA) players in glioblastoma which is a common IR secondary cancer (**Chapter 5**) [328,331].

In **Chapter 3**, we investigated IR-induced DNA methylation in a rat model developed by MEDIRAD colleagues, Ribeiro et al. [364]. Rats are a frequently employed model system in cardiovascular disease research due to their reduced lifespans (1 rat month $\cong$ 2.5-3 human

years) which facilitate the assessment of long-term IR effects [709–711]. The irradiation protocol (total dose of 0.92, 6.9 or 27.6 Gy in 23 fractions (maximum dose rate of 600 MU per min)) was selected to emulate the MHD received by breast cancer patients. Current protocols for breast cancer patients involve either 50 Gy in 25 fractions or a hypofractionation of 40 Gy in 15 fractions [712]. Thus, the rat irradiation was divided over 23 days/fractions to better represent the clinical scenario. The average MHD of RT in left sided breast cancer patients reported by systemic review was 5.4 Gy, which drops to 3.6 Gy with modern radiation sparing techniques [123,713]. However, as these techniques are not enforced in all RT centers, the irradiation doses were selected according to conventional RT techniques. Consequently, 0.92 Gy was selected to represent the MHD from RT in right sided breast cancer patients while 6.9 Gy was selected for left sided patients. Finally, a 27.6 Gy group was added to serve as a positive control of cardiac toxicity. Indeed, Ribeiro et al reported a dose dependent decrease in global longitudinal strain (GLS) (>15%) and decreased microvascular density after 27.6 Gy fractionated irradiation (FI) [364]. Our results showed that local heart irradiation induces changes in rat blood DNA methylation profiles, detectable in blood until 7 months after irradiation. However, the effect of these methylation changes on expression is inconsistent with no clear trend. Nonetheless, three of the selected DMRs (SLMAP, ITPR2 and E2F6) showed dysregulated expression profiles as well as Connexin-43 (CX43) whose inhibition alleviated radiation-induced endothelial cell damage [389]. Both SLMAP and E2F6 are particularly promising as they show dysregulation in both irradiated rats and breast cancer patients of the MEDIRAD EARLY HEART cohort. SLMAP, specifically, has no previous breast cancer association in literature, suggesting that the differential expression in patients is most likely radiation-induced with possible contribution to cardiovascular consequences.

Recently, Yao et al presented the first ever investigation of DNA methylation in a RICVD rat model [396] which employed a single acute 18 Gy dose and identified DMRs in rat heart tissue 6 months after irradiation. None of our rat DMRs were identified by Yao et al. This could be partly due to our dose fractionation protocol as radiation-induced DNA methylation effects vary according to dose and radiation quality, with no clear guidelines

[162]. Fractionated irradiation (FI) is employed in radiotherapy to maximize killing of the rapidly dividing cancer cells while allowing time for the repair of normal cells [714]. Therefore, the magnitude of cardiac damage caused by our FI protocol could be less than that caused by the acute irradiation performed by Yao et al. Yao et al. also utilized heart tissue samples which is not possible in clinical patients thereby contributing to the inter-study variability. Finally, our SureSelect MethylSeq platform utilizes methylation capture sequencing (MC-seq) technology to identify DNA methylation alterations at single base resolution. On the other hand, Yao et al utilized a rat specific methylation array which could offer a more budget option for DNA methylation analysis [396]. The two techniques, SureSelect and methylation array, are composed of different probes with the methylation array probes targeting only gene promoter regions [396]. On the other hand, SureSelect probes target promoters, CpG islands, island shores, as well as other GC-rich regions, thereby offering higher coverage [368]. Due to these study differences, reaching a consensus on IR-induced DNA methylation alterations in RICVD is challenging. Furthermore, deciding on which technique to use in future research should include an assessment of desired genomic coverage, costs as well as the need for designing study-specific probes, which is only available in MC-seq technology [715].

Blood contains methylated DNA originating from whole blood cells (red blood cells, platelets and the different fractions of leucocytes) and circulating cell-free DNA (cfDNA) originating from cell necrosis, apoptosis and active release of DNA [449,716]. Endothelial cells can also enter the general circulation after endothelial injury as occurs in RICVD [717]. Normally, researchers opt to minimize the confounder of different blood cell levels by measuring DNA methylation selectively in the peripheral blood mononuclear cell (PBMC) fraction [718–721]. Unfortunately, the blood in our study was collected in the absence of cryopreserving agent and separation of PBMCs was not possible after cell lysis [722,723]. Recently, computational deconvolution algorithms have been applied to infer the cell type composition from whole blood methylation profiles [724,725]. Applying such deconvolution methods such as Houseman correction could allow the exclusion of blood

cell-specific CpG sites thereby identifying more disease-relevant DMRs not affected by blood cell composition [189].

One procedural technique to eliminate blood cell interference is extracting only cfDNA from patient blood using commercially available kits such as QIAamp circulating nucleic acid kit (QIAGEN, Germany). Such techniques have been used for prenatal screening of cfDNA methylation signatures in maternal plasma [726]. However, preliminary optimization experiments (in rat and human volunteer blood, data not shown) revealed a very low concentration of cfDNA thereby presenting whole blood methylation analysis as the better option. Therefore, optimization to extract enough cfDNA could be useful for follow-up studies. In our rat analysis, the delayed methylation alterations are most likely not the result of blood cell irradiation, due to the short lifespans of the cells, and more likely the result of a systemic influence of IR [452]. This conclusion is supported by the functional enrichment of heart specific pathways such as the dilated cardiomyopathy pathway.

A critical assessment of our rat model reveals some design flaws. DNA methylation and expression analyses were performed solely in the blood and not irradiated cardiac tissue. While blood offers a more clinically relevant biomarker source, cardiac tissues offer higher specificity. Therefore, concurrent analyses of blood and cardiac tissues could facilitate the identification of cardiac-specific DNA biomarkers in blood. Rat blood was also collected in the absence of cryopreservation which would've allowed the separation of the PBMC fraction thereby minimizing the blood cell confounder.

An interesting model system that can be used in future research to overcome some of the disadvantages of animal models is human cardiac organoids [727]. These organoids offer 3D constructs of patient-derived cardiomyocytes which conserve the genetic and epigenetic profiles of their parent tissue [727]. Thus, these organoids offer a more accurate representation of the complex pathophysiology of human disease while avoiding the species-specific differences introduced by animal models [728]. Organoids can also provide

more tissue material to work with thereby permitting more analyses to be carried out [729]. Consequently, organoids have provided useful preclinical models for epigenetic investigations of endometriosis and familial adenomatous polyposis [730,731]. Unfortunately, the lack of standardized organoid growth protocols and the yet unexamined effect of extracellular matrix composition on organoid culture growth are technical challenges still facing organoid preclinical model [732]. As such, organoids sometimes show high variability even when comparing organoid batches from the same starting material or different areas of the same organoid [733]. Despite these challenges, Lee et al. recently created cardiac organoids that are reported to be structurally and functionally similar to a human heart [734]. In addition, Richards et al. generated cardiac organoids that can model doxorubicin cardiotoxicity; another major cardiovascular complication in cancer patients [735]. Thus, cardiac organoids could offer a unique model capable of mimicking RICVD pathophysiology once experimental variability can be controlled.

In **Chapter 4**, we investigated the DNA methylation profiles of patients of the MEDIRAD EARLY HEART breast cancer cohort [365]. To our knowledge, this is the first methylation analysis to profile early (6 months) DNA methylation changes in breast cancer patient blood after RT in the context of RICVD. Methylation was assayed using Illumina EPIC array which covers over 850,000 CpG sites with high reproducibility and reliability at a moderate cost [736]. One recurrent candidate in our rat and human analyses was CACNA1C. CACNA1C was one of two top DMRs identified in 27.6 Gy irradiated rats at both 1.5 and 7 months. It was also identified as a DMR in left sided breast cancer patients after RT. Recent research also showed differential methylation of CACNA1C after chronic doxorubicin administration in a rat model of doxorubicin-induced cardiotoxicity [737]. Pathway analyses associated CACNA1C with the enriched cardiac-specific pathways in both rats e.g. dilated cardiomyopathy and left sided breast cancer patients e.g. adrenergic signaling in cardiomyocytes. Unfortunately, we were unable to quantify CACNA1C expression using qPCR due to low abundance in both the rat and human (blood) samples. A literature search of studies investigating CACNA1C expression showed only tissue-based investigations [738–742]. From The human proteome atlas, a comprehensive database of tissue/cell

protein expression [743], CACNA1C shows low expression in circulating immune cells. This decreased expression could help reduce the confounding effect of blood cells on CACNA1C differential expression. Therefore, optimization of RNA extraction techniques from blood or opting to measure CACNA1C protein expression in patient serum/plasma can help quantify CACNA1C expression [743].

One confounder complicating the interpretation of our DNA methylation analyses in breast cancer patients is that they are all, in fact, cancer patients. Breast cancer has been associated with altered DNA methylation profiles with different breast cancer subtypes presenting differences in methylation [744–746]. Most of our top DMRs (including STK38L and STAT5A) have also been shown to change in breast cancer [516,747]. In addition, investigating the expression of the top DMRs and DMPs in MEXPRESS (https://mexpress.be) -an online tool for the visualization of TCGA gene expression, DNA methylation and clinical data and the relationships between them- revealed several associations [748]. Namely, the expression of our DMRs and DMPs, except CCRL2 and ATP5G2, shows significant variability in TCGA breast cancer (TCGA-BRCA) dataset of 1063 samples [749]. As such, most of our DMRs and DMPs are influenced by tumor-associated factors such as tumor type, stage and estrogen/progesterone receptor status. Another limitation facing the interpretation of our methylation data is that the analysis of patient cardiac function is still ongoing (by MEDIRAD partners). Consequently, no correlations could be performed between the DMRs and patient cardiac function. However, integration of the patient methylation profiles (our results) with circulating classical biomarkers, miRNA profiles and cardiac function assays is a planned MEDIRAD subtask. In this subtask, network analyses and Bayesian variable selection techniques will be performed which can help clarify the contribution of the DMRs to RICVD development with the possible development of a mechanistic model.

As for our investigations on the involvement of noncoding RNA in radiation-induced secondary cancers (**Chapter 5**), the initial aim was to profile salivary noncoding RNA (ncRNA) biomarkers in patients subjected to diagnostic IR and then followed up for

secondary cancer development. The included patients belonged to the EPI-CT cohort which is a European cohort of children and young adults exposed to IR during CT examinations [750]. A significant positive association was reported in this cohort between brain cancer risk and the cumulative number of head/neck CT examinations (excess relative risk=1.27) [750]. Saliva presents an ideal source of biomarkers due to its easy non-invasive collection process and good correlation to blood constituents [751]. On the other hand, microRNA (miRNA) and long noncoding RNA (lncRNAs) biomarkers have been reported in a number of cancers including pancreatic and esophageal cancer [752–755]. Consequently, we initially planned to quantify miRNAs and lncRNAs in patient saliva with the aim of identifying saliva-based biomarkers for secondary cancer development [754]. We successfully optimized RNA extraction, reverse transcription and qPCR procedures to concomitantly quantify miRNAs and lncRNAs in volunteer saliva (data not shown). However, absence of saliva samples due to regulatory obstacles faced by our MEDIRAD colleagues, mostly during COVID time, rendered our plan unfeasible. Consequently, an alternative plan was devised to perform a meta-analysis on publicly available glioblastoma tissue RNA-seq datasets to identify differentially expressed lncRNAs. Differentially expressed miRNAs in glioblastoma tissue were identified by small RNA-seq. RNA-seq datasets were selected for meta-analysis if they were of untreated non-recurrent glioblastoma tissues in case-control format and containing ≥2 samples per condition in FASTQ format. We identified connections between our differentially expressed lncRNAs and protein coding genes (PCGs) and the novel cell death pathway, ferroptosis (reviewed here [756,757]). From co-expression analysis, we constructed a transcriptomic network composed of the lncRNAs identified as differentially expressed in both our meta-analysis and in the TCGA-GBM database (DANCR and SNHG6) and their interacting PCGs and miRNAs (miR-183/96/182 cluster members). While ferroptosis is currently investigated for the therapeutic targeting of glioblastoma and is thus not a novel player, the members of our transcriptomic network could provide new targets for investigating ferroptosis in glioblastoma.

One limitation of our meta-analysis is the rather low number of included studies, in part due to stringent selection criteria. Therefore, a broader analysis of literature using less stringent selection criteria to include all available glioblastoma RNA-seq datasets, regardless of source (cell line/ tissue) and recurrence/treatment, might be beneficial. This re-examination should also not include IDH$^+$ and pediatric tumors on account of their exclusion in the new WHO glioblastoma classification [568].

6.1 Clinical impact and future perspectives

The current thesis presents the 2nd preclinical and 1st clinical investigation focusing on DNA methylation as a possible mechanism in RICVD. Considering the scarcity of existing research, our data enriches available literature on the topic. We also recommend follow-up of MEDIRAD EARLY HEART patients for radiation-induced coronary artery disease development using stress echocardiography or coronary artery calcium (CAC-score) [758]. Reanalysis of our methylation data, while taking into account the cardiovascular status of the patients, could help identify RICVD-specific methylation profiles. Previous research using similar strategies identified diagnostic/prognostic DNA methylation profiles for prefibrotic primary myelofibrosis and prostate cancer [759,760].

Given the physical stability of methylated DNA and its quantifiable levels in blood and other fluids, DNA methylation presents an ideal marker for clinical purposes [761–763]. Several methods can be employed for validating the methylation status of identified DMRs/DMPs which are bisulfite conversion-based methods, restriction enzyme-based approaches or affinity enrichment-based assays [764,765]. Bisulfite conversion-based methods such as methylation sensitive high resolution melting (MSHRM) are the most frequently used site-specific methylation assays [764,765]. However, these are PCR-based assays that suffer from PCR bias due to differences in amplification efficiency between unmethylated and methylated strands [766]. This bias can be overcome by increasing the annealing temperature and careful primer design or by using assays that include single molecule PCR such as digital MSHRM [766]. Another disadvantage of bisulfite conversion based-methods

is their inability to differentiate between mC and 5-hydroxymC, another stable epigenetic mark [766]. For this purpose, mC and 5-hydroxymC can be quantified using technologies employing single-molecule detection such as Oxford Nanopore or single-molecule real-time sequencing (SMRT) [767]. Therefore, selection of a suitable method for validation of DMR methylation depends on the required resolution as well as the available technology and budget for the experiment.

As of yet, no DNA methylation-based markers have made it into clinical practice with the exception of some oncologic biomarkers [768]. This is partly due inter-study differences in sample processing, selected DNA methylation assay with different advantages/limitations and different correction for confounding parameters [768]. These differences therefore affect the reproducibility of DNA methylation biomarkers and thus their clinical utility. DNA methylation can also be influenced by other molecular species such as 8-OHDG produced by oxidative damage, as occurs with IR, or by SNP-based genetic variants forming DNA methylation quantitative trait loci or meQTLs [769,770]. While 8-OHDG can be enzymatically quantified [771], this dynamic profile complicates the utility of DNA methylation biomarkers. Perhaps a shift from investigating single gene DNA methylation biomarkers to polygenic DNA methylation profiles/panels of DMRs could better predict treatment response and/or adverse effects. DNA methylation signatures have previously helped elucidate pathophysiological mechanisms as well as predict disease risk and treatment responsiveness [772,773]. Another shift is to consider DNA methylation as a single layer of multiple which provides limited insight and thereby opting for an integrative multiomics-based research approach [774]. While multiomics integration still faces some methodological challenges, this multi-dimensional examination can reveal novel disease mechanisms and biomarkers [775,776]. As such, follow-up research of our rat and breast cancer patient methylomes could involve integration with other -omics profile e.g. coding (mRNAs) and noncoding (miRNA and lncRNAs) transcriptomics as well as proteomic analyses of the same samples. This integration would help to identify functional DMRs in disease pathophysiology, as was recommended by previous research [777–779].

On the other hand, dysregulation of ncRNAs such as miRNAs and lncRNAs is a common occurrence in disease pathophysiology including autoimmune diseases, schizophrenia as well as most cancers [780–782]. In the current thesis, we confirmed, by meta-analysis, the involvement of ferroptosis in glioblastoma while presenting DANCR/SNHG6 network members as candidates for future biomarker research. Within this network, we identified a number of novel lncRNAs that have not been previously characterized in glioblastoma including ENSG00000278133 and ENSG00000277801. Knockdown models using in *vitro* glioblastoma cell lines e.g. U87-luc2 and U251-RedFLuc, which recapitulate glioblastoma heterogeneity, could help determine the functional roles of these novel candidates [783]. MiRNAs as biomarkers have been suggested for early diagnosis, cancer staging/grading and therapy monitoring of a number of cancers including ovarian, hepatocellular, breast and pancreatic cancer [784–791]. Beyond diagnosis, a few clinical trials have investigated the usefulness of miRNA mimics, which substitute tumor-suppressor miRNAs, and miRNA inhibitors which target oncogenic miRNAs e.g. antisense oligonucleotides (ASOs) and miRNA sponges in cancer therapy [792,793]. Targeted delivery of miRNA-based cancer therapeutics, using cancer-specific receptors or viral carriers, has shown promise in preclinical models of pancreatic cancer as well as in the treatment resistant glioblastoma [794–797]. On the other hand, lncRNA biomarkers such as PCA3 (prostate cancer associated 3) and UCA1 (urothelial carcinoembryonic antigen 1) are currently available for the diagnosis of prostatic and bladder cancer, respectively [798,799]. We also found that both DANCR and SNHG6 [800–804] and the miR-183/96/182 cluster [805–810] have been previously associated with hypoxia, a characteristic of glioblastoma microenvironment which promotes invasiveness and treatment resistance [811,812]. Previous research measuring miRNAs in patient cerebrospinal fluid identified impairment of angiogenesis and autophagy in Parkinson's disease [813]. In a similar manner, research using knock-out/knock-in of DANCR/SNHG6 network members may help elucidate novel glioblastoma mechanisms and therapeutic targets. To that end, experimental models to be used should be capable of mimicking glioblastoma's microenvironment e.g. brain organoids genetically modified for DANCR/SNHG6 overexpression or 3D-bioprinted glioblastoma (e.g.

glioblastoma-on-a-chip) [814–816]. Considering the aggressive nature of glioblastoma, glioblastoma-specific miRNAs and lncRNAs can contribute to earlier diagnosis and improved treatment response in diagnosed patients. In addition, these miRNAs and lncRNAs biomarkers could help monitor patients receiving low dose IR for secondary glioblastoma development.

6.2 Conclusions

The epigenetic effects of IR have been reported by previous research as well as by the current thesis. However, characterization of the mechanistic involvement of DNA methylation in RICVD pathophysiology remains elusive. IR-induced DNA methylation effects seem to be influenced by several factors such as DNA methylation analysis techniques as well as radiation-specific factors. Consequently, research on IR-induced DNA methylation effects presents varying outcomes of global hypo- and hypermethylation as well as inconsistent gene-specific alterations, which complicates conclusive interpretation. In **Chapter 3 and Chapter 4**, we showed that IR-induced methylation alterations were enriched in cardiac-specific pathways in rats (as late as 7 months after IR). This enrichment, while inconclusive, suggests the involvement of DNA methylation in the observed myocardial dysfunction. In addition, the enrichment of cardiac-specific pathways in left sided patients immediately after RT suggests DNA methylation alterations as MHD-sensitive blood biomarker candidates. However, confirming the validity of these candidates necessities future integration of our data with functional cardiac assays still under analysis at MEDIRAD consortium partners. We also offer several recommendations regarding model selection, sample collection and preservation as well as the benefit of integration of methylomes with the other omics platforms.

Alternatively, in **Chapter 5**, we employed a meta-analysis of RNA-seq datasets to characterize lncRNAs in glioblastoma while investigating differentially expressed miRNAs by small RNA. This led to the confirmation of previously characterized lncRNAs as well as the identification of novel lncRNAs in glioblastoma. Co-expression analysis of differentially

expressed lncRNAs and protein coding genes led to the identification of DANCR/SNHG6 network. This network and its associated miR-183/96/182 cluster showed connections to ferroptosis, a current therapeutic target for glioblastoma treatment resistance. Further research is needed to ascertain the roles of the novel lncRNAs candidates identified and their validity as biomarkers

List of tables

List of figures

Bibliography

1. Funk RK, Stockham AL, Laack NNI. Basics of radiation therapy. In: Herrmann JBT-CC-O, editor. Clinical Cardio-Oncology. Elsevier; 2016. p. 39–60.
2. Zeman EM, Schreiber EC, Tepper JE. 27 - Basics of Radiation Therapy. In: Niederhuber JE, Armitage JO, Kastan MB, Doroshow JH, Tepper JEBT-ACO (Sixth E, editors. Abeloff's Clinical Oncology (Sixth Edition). Philadelphia: Elsevier; 2020. p. 431-460.e3.
3. Adler AM, Carlton RR. Introduction to Radiologic and Imaging Sciences and Patient Care-E-Book. Elsevier Health Sciences; 2015.
4. Giaccia AJ, Hall EJ, Amato J. Radiobiology for the radiologist. 7th ed. Lippincott Williams & Williams; 2012.
5. Clegg FM, Sears M, Friesen M, Scarato T, Metzinger R, Russell C, et al. Building science and radiofrequency radiation: What makes smart and healthy buildings. Build Environ. 2020;176:106324.
6. Henriksen T, Maillie DH. Radiation and health. CRC Press; 2002.
7. Forshier S. Essentials of radiation, Biology and Protection. Cengage Learning; 2012.
8. Voshart DC, Wiedemann J, van Luijk P, Barazzuol L. Regional Responses in Radiation-Induced Normal Tissue Damage. Vol. 13, Cancers . 2021.
9. Baskar R, Dai J, Wenlong N, Yeo R, Yeoh K-W. Biological response of cancer cells to radiation treatment. Front Mol Biosci. 2014;1:24.
10. Knapp FF, Dash A. Radiopharmaceuticals for Therapy [Internet]. New Delhi: Springer India; 2016.
11. Elgazzar AH, Kazem N. Biological Effects of Ionizing Radiation BT - The Pathophysiologic Basis of Nuclear Medicine. In: Elgazzar AH, editor. Cham: Springer International Publishing; 2015. p. 715–26.
12. Joiner MC, van der Kogel AJ. Basic clinical radiobiology. CRC press; 2018.
13. Palma A, Cisbani E, Angelis C De, Monaca S Della, Dini V, Grande S, et al. 342. "MEDIRAD – Implications of Medical Low Dose Radiation Exposure": A European-funded project aims to enhance the protection of patients and health professionals from exposure to low dose medical radiation. Phys Medica. 2018 Dec 1;56:268–9.
14. Bushong SC. Radiologic science for technologists e-book: physics, biology, and protection. Elsevier Health Sciences; 2020.
15. Desouky O, Ding N, Zhou G. Targeted and non-targeted effects of ionizing radiation. J Radiat Res Appl Sci. 2015 Apr 1;8(2):247–54.
16. WARDMAN P. The importance of radiation chemistry to radiation and free radical biology (The 2008 Silvanus Thompson Memorial Lecture). Br J Radiol. 2009 Feb 1;82(974):89–104.
17. Fardid R, Najafi M, Salajegheh A, Kazemi E, Rezaeyan A. Radiation-induced non-targeted effect in vivo: Evaluation of cyclooygenase-2 and endothelin-1 gene expression in rat heart tissues. J Cancer Res Ther. 2017 Jan 1;13(1):51–5.
18. Borrego-Soto G, Ortiz-López R, Rojas-Martínez A. Ionizing radiation-induced DNA injury and damage detection in patients with breast cancer. Genet Mol Biol. 2015;38:420–32.
19. Kavanagh JN, Redmond KM, Schettino G, Prise KM. DNA Double Strand Break Repair: A Radiation Perspective. Antioxid Redox Signal. 2013 Jan 11;18(18):2458–72.
20. Dextraze M-E, Gantchev T, Girouard S, Hunting D. DNA interstrand cross-links induced by ionizing radiation: An unsung lesion. Mutat Res Mutat Res. 2010;704(1):101–7.
21. Balaji K, Subramanian B, Yadav P, Radha CA, Ramasubramanian V. Radiation therapy for breast cancer: Literature review. Med Dosim. 2016;41:253–7.
22. Mavragani I V, Nikitaki Z, Kalospyros SA, Georgakilas AG. Ionizing Radiation and Complex DNA Damage: From Prediction to Detection Challenges and Biological Significance. Vol. 11, Cancers . 2019.
23. Formenti SC, Demaria S. Systemic effects of local radiotherapy. Lancet Oncol. 2009;10(7):718–26.
24. Lombardi MH, Sutton L, Cato III A. Radiation safety in nuclear medicine. CRC press; 2006.
25. Li L, Guan Y, Chen X, Yang J, Cheng Y. DNA Repair Pathways in Cancer Therapy and Resistance [Internet]. Vol. 11, Frontiers in Pharmacology . 2021.

26.   Srinivas US, Tan BWQ, Vellayappan BA, Jeyasekharan AD. ROS and the DNA damage response in cancer. Redox Biol. 2019;25:101084.

27.   Ford JM, Kastan MB. 11 - DNA Damage Response Pathways and Cancer. In: Niederhuber JE, Armitage JO, Kastan MB, Doroshow JH, Tepper JEBT-ACO (Sixth E, editors. Philadelphia: Elsevier; 2020. p. 154-164.e4.

28.   Arena C, De Micco V, Macaeva E, Quintens R. Space radiation effects on plant and mammalian cells. Acta Astronaut. 2014 Nov 1;104(1):419–31.

29.   Mettler FA. Medical effects and risks of exposure to ionising radiation. J Radiol Prot. 2012;32(1):N9–13.

30.   White SC, Pharoah MJ. White and Pharoah's Oral Radiology: Principles and Interpretation. Elsevier Health Sciences; 2018.

31.   Bakar NFA, Othman SA, Azman NFAN, Jasrin NS. Effect of ionizing radiation towards human health: A review. In: IOP Conference Series: Earth and Environmental Science. IOP Publishing; 2019. p. 12005.

32.   Belli M, Tabocchini MA. Ionizing Radiation-Induced Epigenetic Modifications and Their Relevance to Radiation Protection. Vol. 21, International Journal of Molecular Sciences . 2020.

33.   Goodhead DT. New radiobiological, radiation risk and radiation protection paradigms. Mutat Res Mol Mech Mutagen. 2010;687(1):13–6.

34.   Kalinich JF, Catravas GN, Snyder SL. The Effect of γ Radiation on DNA Methylation. Radiat Res. 1989 Feb 1;117(2):185–97.

35.   Carlberg C, Molnár F. Human epigenetics: How science works. Springer; 2019.

36.   Waddington CH. The epigenotype. Endeavour. 1942;1:18–20.

37.   Lu M, Liu S, Kumarsangaiah A, Zhou Y, Pan Z, Zuo Y. Nucleosome Positioning With Fractal Entropy Increment of Diversity in Telemedicine. IEEE Access. 2017 Dec 15;PP:1.

38.   Kouzarides T. Chromatin Modifications and Their Function. Cell. 2007;128(4):693–705.

39.   Lawrence M, Daujat S, Schneider R. Lateral Thinking: How Histone Modifications Regulate Gene Expression. Trends Genet. 2016;32(1):42–56.

40.   Neganova ME, Klochkov SG, Aleksandrova YR, Aliev G. Histone modifications in epigenetic regulation of cancer: Perspectives and achieved progress. Semin Cancer Biol. 2022;83:452–71.

41.   Audia JE, Campbell RM. Histone modifications and cancer. Cold Spring Harb Perspect Biol. 2016;8(4):a019521.

42.   Lu H-C, Dai W-N, He L-Y. Epigenetic Histone Modifications in the Pathogenesis of Diabetic Kidney Disease [Internet]. Vol. 14, Diabetes, metabolic syndrome and obesity : targets and therapy. Department of Nephrology, The Second Xiangya Hospital, Central South University, Hunan Key Laboratory of Kidney Disease and Blood Purification, Changsha, Hunan, People's Republic of China.; 2021. p. 329–44.

43.   Araki Y, Mimura T. The Histone Modification Code in the Pathogenesis of Autoimmune Diseases. Xu J-W, editor. Mediators Inflamm. 2017;2017:2608605.

44.   Sadri-Vakili G, Cha J-HJ. Mechanisms of Disease: histone modifications in Huntington's disease. Nat Clin Pract Neurol. 2006;2(6):330–8.

45.   Ren W, Gao L, Song J. Structural Basis of DNMT1 and DNMT3A-Mediated DNA Methylation. Genes (Basel). 2018 Dec 11;9(12).

46.   Strichman-Almashanu LZ, Lee RS, Onyango PO, Perlman E, Flam F, Frieman MB, et al. A Genome-Wide Screen for Normally Methylated Human CpG Islands That Can Identify Novel Imprinted Genes. Genome Res. 2002 Mar 20;12(4):543–54.

47.   Deaton AM, Bird A. CpG islands and the regulation of transcription. Genes Dev. 2011 May 15;25(10):1010–22.

48.   Sarda S, Das A, Vinson C, Hannenhalli S. Distal CpG islands can serve as alternative promoters to transcribe genes with silenced proximal promoters. Genome Res. 2017/02/21. 2017 Apr;27(4):553–66.

49.   Yang X, Han H, De Carvalho DD, Lay FDD, Jones PAA, Liang G, et al. Gene Body Methylation Can Alter Gene Expression and Is a Therapeutic Target in Cancer. Cancer Cell. 2014 Oct 13;26(4):577–90.

50.   Portela A, Esteller M. Epigenetic modifications and human disease. Nat Biotechnol. 2010 Oct 13;28(10):1057–68.

51.   Bird A. DNA methylation patterns and epigenetic memory. Genes Dev. 2002 Jan 1;16(1):6–21.

52.   Feng J, Fan G. Chapter - 4 The Role of DNA Methylation in the Central Nervous System and Neuropsychiatric Disorders. Nov Approaches to Stud Basal Ganglia Relat Neuropsychiatr Disord. 2009;89:67–84.

53.   Kumar S, Singh A, Mohapatra T. Epigenetics : History, present status and future perspective. Indian J Genet. 2017;77(4):445–63.

54. Moore LD, Le T, Fan G. DNA methylation and its basic function. Neuropsychopharmacology. 2013 Jan;38(1):23–38.

55. Klose RJ, Bird AP. Genomic DNA methylation: the mark and its mediators. Trends Biochem Sci. 2006 Feb 1;31(2):89–97.

56. Feng J, Zhou Y, Campbell SL, Le T, Li E, Sweatt JD, et al. Dnmt1 and Dnmt3a maintain DNA methylation and regulate synaptic function in adult forebrain neurons. Nat Neurosci. 2010 Apr;13(4):423–30.

57. Jang HS, Shin WJ, Lee JE, Do JT. CpG and Non-CpG Methylation in Epigenetic Gene Regulation and Brain Function. Genes (Basel). 2017 May 23;8(6).

58. Carlberg C, Molnár F. DNA Methylation. In: Human Epigenomics. Singapore: Springer Singapore; 2018. p. 57–73.

59. Bhutani N, Burns DM, Blau HM. DNA Demethylation Dynamics. Cell. 2011 Sep 16;146(6):866–72.

60. Rasmussen KD, Helin K. Role of TET enzymes in DNA methylation, development, and cancer. 2016;

61. Santiago M, Antunes C, Guedes M, Sousa N, Marques CJ. TET enzymes and DNA hydroxymethylation in neural development and function — How critical are they? Genomics. 2014;104(5):334–40.

62. Papait R, Serio S, Condorelli G. Role of the Epigenome in Heart Failure. Physiol Rev. 2020 Apr;100(4):1753–77.

63. Pulczinski J, Yeung BHY, Wu Q, Cheng RYS, Tang W. Chapter 2-4 - DNA Hydroxymethylation: Implications for Toxicology and Epigenetic Epidemiology. In: McCullough SD, Dolinoy DCBT-T, editors. Academic Press; 2019. p. 191–214.

64. Jiang D, Wang Y, Chang G, Duan Q, You L, Sun M, et al. DNA hydroxymethylation combined with carotid plaques as a novel biomarker for coronary atherosclerosis. Aging (Albany NY). Jan;11(10):3170–81.

65. Jiang D, Sun M, You L, Lu K, Gao L, Hu C, et al. DNA methylation and hydroxymethylation are associated with the degree of coronary atherosclerosis in elderly patients with coronary heart disease. Life Sci. 2019 May 1;224:241–8.

66. Greco CM, Kunderfranco P, Rubino M, Larcher V, Carullo P, Anselmo A, et al. DNA hydroxymethylation controls cardiomyocyte gene expression in development and hypertrophy. Nat Commun. 2016;7(1):12418.

67. Becker B V, Kaatsch L, Obermair R, Schrock G, Port M, Ullmann R. X-ray irradiation induces subtle changes in the genome-wide distribution of DNA hydroxymethylation with opposing trends in genic and intergenic regions. Epigenetics. 2019 Jan;14(1):81–93.

68. Rithidech KN, Jangiam W, Tungjai M, Gordon C, Honikel L, Whorton EB. Induction of Chronic Inflammation and Altered Levels of DNA Hydroxymethylation in Somatic and Germinal Tissues of CBA/CaJ Mice Exposed to 48Ti Ions   . Vol. 6, Frontiers in Oncology . 2016.

69. Impey S, Pelz C, Tafessu A, Marzulla T, Turker MS, Raber J. Proton irradiation induces persistent and tissue-specific DNA methylation changes in the left ventricle and hippocampus. BMC Genomics. 2016;17(1):273.

70. Wang D, Huang J-H, Zeng Q-H, Gu C, Ding S, Lu J-Y, et al. Increased 5-hydroxymethylcytosine and Ten-eleven Translocation Protein Expression in Ultraviolet B-irradiated HaCaT Cells. Chin Med J (Engl). 2017;130(5).

71. Zhang P, Wu W, Chen Q, Chen M. Non-Coding RNAs and their Integrated Networks. J Integr Bioinform. 2019;16(3).

72. Wei J-W, Huang K, Yang C, Kang C-S. Non-coding RNAs as regulators in epigenetics (Review). Oncol Rep. 2017;37(1):3–9.

73. Romano G, Veneziano D, Acunzo M, Croce CM. Small non-coding RNA and cancer. Carcinogenesis. 2017 May 1;38(5):485–91.

74. Ding S-W, Han Q, Wang J, Li W-X. Antiviral RNA interference in mammals. Curr Opin Immunol. 2018;54:109–14.

75. Svobodova E, Kubikova J, Svoboda P. Production of small RNAs by mammalian Dicer. Pflügers Arch - Eur J Physiol. 2016;468(6):1089–102.

76. Huntzinger E, Izaurralde E. Gene silencing by microRNAs: contributions of translational repression and mRNA decay. Nat Rev Genet. 2011;12(2):99–110.

77. Jonas S, Izaurralde E. Towards a molecular understanding of microRNA-mediated gene silencing. Nat Rev Genet. 2015;16(7):421–33.

78. Friedman RC, Farh KK-H, Burge CB, Bartel DP. Most mammalian mRNAs are conserved targets of microRNAs. Genome Res. 2009;19(1):92–105.

79. Wang C, Lin H. Roles of piRNAs in transposon and pseudogene regulation of germline mRNAs and lncRNAs.

Genome Biol. 2021;22(1):27.

80. Wu X, Pan Y, Fang Y, Zhang J, Xie M, Yang F, et al. The Biogenesis and Functions of piRNAs in Human Diseases. Mol Ther - Nucleic Acids. 2020;21:108–20.

81. Siomi MC, Sato K, Pezic D, Aravin AA. PIWI-interacting small RNAs: the vanguard of genome defence. Nat Rev Mol Cell Biol. 2011;12(4):246–58.

82. Bhan A, Mandal SS. Long noncoding RNAs: emerging stars in gene regulation, epigenetics and human disease. ChemMedChem. 2014;9(9):1932–56.

83. Kornienko AE, Guenzl PM, Barlow DP, Pauler FM. Gene regulation by the act of long non-coding RNA transcription. BMC Biol. 2013;11(1):59.

84. Bove F, Calabresi P. Chapter 11 - Plasticity, genetics, and epigenetics in l-dopa-induced dyskinesias. In: Quartarone A, Ghilardi MF, Boller FBT-H of CN, editors. Neuroplasticity. Elsevier; 2022. p. 167–84.

85. Bhat SA, Ahmad SM, Mumtaz PT, Malik AA, Dar MA, Urwat U, et al. Long non-coding RNAs: Mechanism of action and functional utility. Non-coding RNA Res. 2016;1(1):43–50.

86. Tsai M-C, Manor O, Wan Y, Mosammaparast N, Wang JK, Lan F, et al. Long Noncoding RNA as Modular Scaffold of Histone Modification Complexes. Science (80-). 2010 Aug 6;329(5992):689–93.

87. Sun T-T, He J, Liang Q, Ren L-L, Yan T-T, Yu T-C, et al. LncRNA GClnc1 Promotes Gastric Carcinogenesis and May Act as a Modular Scaffold of WDR5 and KAT2A Complexes to Specify the Histone Modification Pattern. Cancer Discov. 2016 Jun 30;6(7):784–801.

88. Somarowthu S, Legiewicz M, Chillón I, Marcia M, Liu F, Pyle AM. HOTAIR Forms an Intricate and Modular Secondary Structure. Mol Cell. 2015;58(2):353–61.

89. Statello L, Guo C-J, Chen L-L, Huarte M. Gene regulation by long non-coding RNAs and its biological functions. Nat Rev Mol Cell Biol. 2021;22(2):96–118.

90. Fang Y, Fullwood MJ. Roles, Functions, and Mechanisms of Long Non-coding RNAs in Cancer. Genomics Proteomics Bioinformatics. 2016;14(1):42–54.

91. Fan J, Xing Y, Wen X, Jia R, Ni H, He J, et al. Long non-coding RNA ROR decoys gene-specific histone methylation to promote tumorigenesis. Genome Biol. 2015;16(1):139.

92. Tripathi V, Ellis JD, Shen Z, Song DY, Pan Q, Watt AT, et al. The nuclear-retained noncoding RNA MALAT1 regulates alternative splicing by modulating SR splicing factor phosphorylation. Mol Cell. 2010;39(6):925–38.

93. Grelet S, Link LA, Howley B, Obellianne C, Palanisamy V, Gangaraju VK, et al. A regulated PNUTS mRNA to lncRNA splice switch mediates EMT and tumour progression. Nat Cell Biol. 2017;19(9):1105–15.

94. Thomson DW, Dinger ME. Endogenous microRNA sponges: evidence and controversy. Nat Rev Genet. 2016;17(5):272–83.

95. Keniry A, Oxley D, Monnier P, Kyba M, Dandolo L, Smits G, et al. The H19 lincRNA is a developmental reservoir of miR-675 which suppresses growth and Igf1r. Nat Cell Biol. 2012;14:659–65.

96. Cai X, Cullen BR. The imprinted H19 noncoding RNA is a primary microRNA precursor. Rna. 2007;13(3):313–6.

97. Zhang X, Wang W, Zhu W, Dong J, Cheng Y, Yin Z, et al. Mechanisms and Functions of Long Non-Coding RNAs at Multiple Regulatory Levels. Vol. 20, International Journal of Molecular Sciences . 2019.

98. Zhang L, Yang Z, Trottier J, Barbier O, Wang L. Long noncoding RNA MEG3 induces cholestatic liver injury by interaction with PTBP1 to facilitate shp mRNA decay. Hepatology. 2017;65(2):604–15.

99. Gong C, Maquat LE. lncRNAs transactivate STAU1-mediated mRNA decay by duplexing with 3' UTRs via Alu elements. Nature. 2011;470(7333):284–8.

100. Wang G, Wang Y, Xiong Y, Chen X-C, Ma M, Cai R, et al. Sirt1 AS lncRNA interacts with its mRNA to inhibit muscle formation by attenuating function of miR-34a. Sci Rep. 2016;6(1):1–13.

101. Zhao Y, Liu Y, Lin L, Huang Q, He W, Zhang S, et al. The lncRNA MACC1-AS1 promotes gastric cancer cell metabolic plasticity via AMPK/Lin28 mediated mRNA stability of MACC1. Mol Cancer. 2018;17(1):1–16.

102. Prior S, Miousse IR, Nzabarushimana E, Pathak R, Skinner C, Kutanzi KR, et al. Densely ionizing radiation affects DNA methylation of selective LINE-1 elements. Environ Res. 2016;150:470–81.

103. Koturbash I, Miousse IR, Sridharan V, Nzabarushimana E, Skinner CM, Melnyk SB, et al. Radiation-induced changes in DNA methylation of repetitive elements in the mouse heart. Mutat Res Mol Mech Mutagen. 2016 May 1;787:43–53.

104. Chaudhry MA, Omaruddin RA. Differential DNA Methylation Alterations in Radiation-Sensitive and -Resistant Cells. DNA Cell Biol. 2011 Dec 20;31(6):908–16.

105. Pogribny I, Raiche J, Slovack M, Kovalchuk O. Dose-dependence, sex- and tissue-specificity, and persistence of radiation-induced genomic DNA methylation changes. Biochem Biophys Res Commun. 2004 Aug 6;320(4):1253–61.

106. Koturbash I, Pogribny I, Kovalchuk O. Stable loss of global DNA methylation in the radiation-target tissue—A possible mechanism contributing to radiation carcinogenesis? Biochem Biophys Res Commun. 2005 Nov 18;337(2):526–33.

107. Pollack BP, Sapkota B, Boss JM. Ultraviolet Radiation-induced Transcription is Associated with Gene-specific Histone Acetylation. Photochem Photobiol. 2009 May 1;85(3):652–62.

108. Kim J-G, Yi JM, Park S-J, Kim J-S, Son TG, Yang K, et al. Histone demethylase JMJD2B-mediated cell proliferation regulated by hypoxia and radiation in gastric cancer cell. Biochim Biophys Acta - Gene Regul Mech. 2012;1819(11):1200–7.

109. Hunt CR, Ramnarain DB, Horikoshi N, Iyengar P, Pandita RK, Shay JW, et al. Histone Modifications and DNA Double-Strand Break Repair after Exposure to Ionizing Radiations. In: Radiation research. 2013.

110. Di Nisio E, Lupo G, Licursi V, Negri R. The role of histone lysine methylation in the response of mammalian cells to ionizing radiation. Front Genet. 2021;12:639602.

111. Chinnaiyan P, Vallabhaneni G, Armstrong E, Huang S-M, Harari PM. Modulation of radiation response by histone deacetylase inhibition. Int J Radiat Oncol. 2005;62(1):223–9.

112. Karagiannis TC, El-Osta A. Modulation of cellular radiation responses by histone deacetylase inhibitors. Oncogene. 2006;25(28):3885–93.

113. Yang X, Ni J, Li Y, Zou L, Guo T, Li Y, et al. LncRNA-RP11 modulates TGF-β1-activated radiation-induced lung injury through downregulating microRNA-29a. Dose-Response. 2020;18(4):1559325820949071.

114. Aryankalayil MJ, Martello S, Bylicky MA, Chopra S, May JM, Shankardass A, et al. Analysis of lncRNA-miRNA-mRNA expression pattern in heart tissue after total body radiation in a mouse model. J Transl Med. 2021;19(1):336.

115. Li Y, Zou L, Yang X, Chu L, Ni J, Chu X, et al. Identification of lncRNA, MicroRNA, and mRNA-associated CeRNA network of radiation-induced lung injury in a mice model. Dose-Response. 2019;17(4):1559325819891012.

116. Rogers CJ, Lukaszewicz AI, Yamada-Hanff J, Micewicz ED, Ratikan JA, Starbird MA, et al. Identification of miRNA signatures associated with radiation-induced late lung injury in mice. PLoS One. 2020 May 11;15(5):e0232411.

117. Simone NL, Soule BP, Ly D, Saleh AD, Savage JE, DeGraff W, et al. Ionizing Radiation-Induced Oxidative Stress Alters miRNA Expression. PLoS One. 2009 Jul 27;4(7):e6377.

118. Dickey JS, Zemp FJ, Martin OA, Kovalchuk O. The role of miRNA in the direct and indirect effects of ionizing radiation. Radiat Environ Biophys. 2011;50(4):491.

119. Taylor C, Correa C, Duane FK, Aznar MC, Anderson SJ, Bergh J, et al. Estimating the Risks of Breast Cancer Radiotherapy: Evidence From Modern Radiation Doses to the Lungs and Heart and From Previous Randomized Trials. J Clin Oncol. 2017 May 20;35(15):1641–9.

120. Dafni U, Tsourti Z, Alatsathianos I. Breast Cancer Statistics in the European Union: Incidence and Survival across European Countries. Breast Care. 2019 Dec 1;14(6):344–53.

121. Cardoso F, Kyriakides S, Ohno S, Penault-Llorca F, Poortmans P, Rubio IT, et al. Early breast cancer: ESMO Clinical Practice Guidelines for diagnosis, treatment and follow-up†. Ann Oncol. 2019 Aug 1;30(8):1194–220.

122. Kindts I, Laenen A, Depuydt T, Weltens C. Tumour bed boost radiotherapy for women after breast-conserving surgery. Cochrane database Syst Rev. 2017 Nov 6;11(11):CD011987.

123. L D, C Y, H L, L Z, M W, C M, et al. A Systematic Review of Heart Dose in Breast Radiotherapy. Clin Breast Cancer. 2018 Oct 1;18(5):e819–24.

124. Darby SC, Cutter DJ, Boerma M, Constine LS, Fajardo LF, Kodama K, et al. Radiation-related heart disease: current knowledge and future prospects. Int J Radiat Oncol Biol Phys. 2010 Mar 1;76(3):656–65.

125. Hayes AW. Principles and Methods of Toxicology, Fifth Edition. Principles and Methods of Toxicology, Fifth Edition. CRC Press; 2007.

126. Darby SC, Ewertz M, McGale P, Bennet AM, Blom-Goldman U, Brønnum D, et al. Risk of Ischemic Heart Disease in Women after Radiotherapy for Breast Cancer. N Engl J Med. 2013 Mar 14;368(11):987–98.

127. Aggarwal R, Rao S, Dhawan S, Bhalla S, Kumar A, Chopra P. Primary mediastinal lymphomas, their morphological features and comparative evaluation. Lung India. 2017;34(1):19–24.

128. Yusuf SW, Venkatesulu BP, Mahadevan LS, Krishnan S. Radiation-Induced Cardiovascular Disease: A Clinical

Perspective. Front Cardiovasc Med. 2017 Oct 26;4.

129. Bradshaw PT, Stevens J, Khankari N, Teitelbaum SL, Neugut AI, Gammon MD. Cardiovascular Disease Mortality among Breast Cancer Survivors. Epidemiology. 2016 Jan 1;27(1):6–13.

130. Lancellotti P, Nkomo VT, Badano LP, Bergler J, Bogaert J, Davin L, et al. Expert Consensus for Multi-Modality Imaging Evaluation of Cardiovascular Complications of Radiotherapy in Adults: A Report from the European Association of Cardiovascular Imaging and the American Society of Echocardiography. J Am Soc Echocardiogr. 2013;26:1013–32.

131. Bogaard VAB van den, Ta BDP, Schaaf A van der, Bouma AB, Middag AMH, Bantema-Joppe EJ, et al. Validation and Modification of a Prediction Model for Acute Cardiac Events in Patients With Breast Cancer Treated With Radiotherapy Based on Three-Dimensional Dose Distributions to Cardiac Substructures. J Clin Oncol. 2017 Apr 10;35(11):1171.

132. Ellahham S, Khalouf A, Elkhazendar M, Dababo N, Manla Y. An overview of radiation-induced heart disease. Radiat Oncol J. 2022;40(2):89.

133. Walls GM, O'Kane R, Ghita M, Kuburas R, McGarry CK, Cole AJ, et al. Murine models of radiation cardiotoxicity: A systematic review and recommendations for future studies. Radiother Oncol. 2022;173:19–31.

134. Zhang K, He X, Zhou Y, Gao L, Qi Z, Chen J, et al. Atorvastatin ameliorates radiation-induced cardiac fibrosis in rats. Radiat Res. 2015;184(6):611–20.

135. van der Veen SJ, Ghobadi G, de Boer RA, Faber H, Cannon M V, Nagle PW, et al. ACE inhibition attenuates radiation-induced cardiopulmonary damage. Radiother Oncol. 2015;114(1):96–103.

136. Viczenczova C, Kura B, Egan Benova T, Yin C, Kukreja RC, Slezak J, et al. Irradiation-induced cardiac connexin-43 and miR-21 responses are hampered by treatment with atorvastatin and aspirin. Int J Mol Sci. 2018;19(4):1128.

137. Spetz J, Moslehi J, Sarosiek K. Radiation-Induced Cardiovascular Toxicity: Mechanisms, Prevention, and Treatment. Curr Treat Options Cardio Med. 2018 Apr 20;20(4):31.

138. Cuomo JR, Sharma GK, Conger PD, Weintraub NL. Novel concepts in radiation-induced cardiovascular disease. 2016/09/26. 2016 Sep 26;8(9).

139. Taunk NK, Haffty BG, Kostis JB, Goyal S. Radiation-Induced Heart Disease: Pathologic Abnormalities and Putative Mechanisms. Front Oncol. 2015;5:39.

140. Heidenreich PA, Kapoor JR. Radiation induced heart disease. Heart. 2008 Nov 25;95(3):252–8.

141. Gujral DM, Lloyd G, Bhattacharyya S. Radiation-induced valvular heart disease. Heart. 2016 Feb 15;102(4):269–76.

142. Marks LB, Yu X, Prosnitz RG, Zhou S-M, Hardenbergh PH, Blazing M, et al. The incidence and functional consequences of RT-associated cardiac perfusion defects. Int J Radiat Oncol Biol Phys. 2005 Sep;63(1):214–23.

143. Quintero-Martinez JA, Cordova-Madera SN, Villarraga HR. Radiation-Induced Heart Disease. Vol. 11, Journal of Clinical Medicine. 2022.

144. Halle M, Hall P, Tornvall P. Cardiovascular disease associated with radiotherapy: Activation of nuclear factor kappa-B. J Intern Med. 2011 May;269(5):469–77.

145. Sylvester CB, Abe JI, Patel ZS, Grande-Allen KJ. Radiation-Induced Cardiovascular Disease: Mechanisms and Importance of Linear Energy Transfer. Front Cardiovasc Med. 2018 Jan 31;5:5.

146. Baselet B, Sonveaux P, Baatout S, Aerts A. Pathological effects of ionizing radiation: endothelial activation and dysfunction [Internet]. Vol. 76, Cellular and Molecular Life Sciences. Birkhauser Verlag AG; 2019. p. 699–728.

147. Li M, You L, Xue J, Lu Y. Ionizing Radiation-Induced Cellular Senescence in Normal, Non-transformed Cells and the Involved DNA Damage Response: A Mini Review. Front Pharmacol. 2018 May 22;9(May):522.

148. Wang H, Wei J, Zheng Q, Meng L, Xin Y, Yin X, et al. Radiation-induced heart disease: A review of classification, mechanism and prevention [Internet]. Vol. 15, International Journal of Biological Sciences. Ivyspring International Publisher; 2019. p. 2128–38.

149. Podlesnikar T, Berlot B, Dolenc J, Goričar K, Marinko T. Radiotherapy-Induced Cardiotoxicity: The Role of Multimodality Cardiovascular Imaging . Vol. 9, Frontiers in Cardiovascular Medicine . 2022.

150. Čelutkienė J, Pudil R, López-Fernández T, Grapsa J, Nihoyannopoulos P, Bergler-Klein J, et al. Role of cardiovascular imaging in cancer patients receiving cardiotoxic therapies: a position statement on behalf of

the Heart Failure Association (HFA), the European Association of Cardiovascular Imaging (EACVI) and the Cardio-Oncology Council of the Eur. Eur J Heart Fail. 2020 Sep;22(9):1504–24.

151.   Zamorano JL, Lancellotti P, Rodriguez Muñoz D, Aboyans V, Asteggiano R, Galderisi M, et al. 2016 ESC Position Paper on cancer treatments and cardiovascular toxicity developed under the auspices of the ESC Committee for Practice Guidelines: The Task Force for cancer treatments and cardiovascular toxicity of the European Society of Cardiology (ES. Eur Heart J. 2016 Sep;37(36):2768–801.

152.   Bergom C, Bradley JA, Ng AK, Samson P, Robinson C, Lopez-Mattei J, et al. Past, Present, and Future of Radiation-Induced Cardiotoxicity: Refinements in Targeting, Surveillance, and Risk Stratification. JACC CardioOncology. 2021;3(3):343–59.

153.   Trivedi SJ, Choudhary P, Lo Q, Sritharan HP, Iyer A, Batumalai V, et al. Persistent reduction in global longitudinal strain in the longer term after radiation therapy in patients with breast cancer. Radiother Oncol. 2019;132:148–54.

154.   Walker V, Lairez O, Fondard O, Pathak A, Pinel B, Chevelle C, et al. Early detection of subclinical left ventricular dysfunction after breast cancer radiation therapy using speckle-tracking echocardiography: Association between cardiac exposure and longitudinal strain reduction (BACCARAT study). Radiat Oncol. 2019 Nov 14;14(1).

155.   Greenland P, Blaha MJ, Budoff MJ, Erbel R, Watson KE. Coronary Calcium Score and Cardiovascular Risk. J Am Coll Cardiol. 2018;72(4):434–47.

156.   Roos CTG, van den Bogaard VAB, Greuter MJW, Vliegenthart R, Schuit E, Langendijk JA, et al. Is the coronary artery calcium score associated with acute coronary events in breast cancer patients treated with radiotherapy? Radiother Oncol. 2018;126(1):170–6.

157.   Miousse IR, Shao L, Chang J, Feng W, Wang Y, Allen AR, et al. Exposure to Low-Dose 56 Fe-Ion Radiation Induces Long-Term Epigenetic Alterations in Mouse Bone Marrow Hematopoietic Progenitor and Stem Cells. Radiat Res. 2014;182:92–101.

158.   Miousse IR, Chang J, Shao L, Pathak R, Nzabarushimana É, Kutanzi KR, et al. Inter-Strain Differences in LINE-1 DNA Methylation in the Mouse Hematopoietic System in Response to Exposure to Ionizing Radiation. Int J Mol Sci. 2017 Jul 4;18(7):1430.

159.   Pogribny I, Koturbash I, Tryndyak V, Hudson D, Stevenson SMLL, Sedelnikova O, et al. Fractionated Low-Dose Radiation Exposure Leads to Accumulation of DNA Damage and Profound Alterations in DNA and Histone Methylation in the Murine Thymus. Mol Cancer Res. 2005 Oct 1;3(10):553–61.

160.   Kennedy EM, Powell DR, Li Z, Bell JSK, Barwick BG, Feng H, et al. Galactic Cosmic Radiation Induces Persistent Epigenome Alterations Relevant to Human Lung Cancer. Sci Rep. 2018 Dec 1;8(1):1–14.

161.   Tawa R, Kimura Y, Komura J-II, MIYAMURA Y, KURISHITA A, SASAKI MS, et al. Effects of X-ray Irradiation on Genomic DNA Methylation Levels in Mouse Tissues. J Radiat Res. 1998 Dec;39(4):271–8.

162.   Miousse IR, Kutanzi KR, Koturbash I. Effects of ionizing radiation on DNA methylation: from experimental biology to clinical applications. Int J Radiat Biol. 2017/02/21. 2017 May;93(5):457–69.

163.   Kuhmann C, Weichenhan D, Rehli M, Plass C, Schmezer P, Popanda O. DNA methylation changes in cells regrowing after fractioned ionizing radiation. Radiother Oncol. 2011 Oct 1;101(1):116–21.

164.   Wang J, Zhang Y, Xu K, Mao X, Xue L, Liu X, et al. Genome-wide screen of DNA methylation changes induced by low dose X-ray radiation in mice. PLoS One. 2014 Mar 10;9(3):e90804.

165.   Koturbash I, Boyko A, Rodriguez-Juarez R, McDonald RJ, Tryndyak VP, Kovalchuk I, et al. Role of epigenetic effectors in maintenance of the long-term persistent bystander effect in spleen in vivo. Carcinogenesis. 2007 Aug 1;28(8):1831–8.

166.   Kumar A, Rai PS, Upadhya R, Vishwanatha, Shama Prasada K, Satish Rao BS, et al. γ-radiation induces cellular sensitivity and aberrant methylation in human tumor cell lines. Int J Radiat Biol. 2011 Nov 7;87(11):1086–96.

167.   Loree J, Koturbash I, Kutanzi K, Baker M, Pogribny I, Kovalchuk O. Radiation-induced molecular changes in rat mammary tissue: Possible implications for radiation-induced carcinogenesis. Int J Radiat Biol. 2006 Jan 3;82(11):805–15.

168.   Luzhna L, Ilnytskyy Y, Kovalchuk O. Mobilization of LINE-1 in irradiated mammary gland tissue may potentially contribute to low dose radiation-induced genomic instability. Genes&Cancer Genes & Cancer. 2015;6(2):71–81.

169.   Jangiam W, Udomtanakunchai C, Reungpatthanaphong P, Tungjai M, Honikel L, Gordon CR, et al. Late Effects of Low-Dose Radiation on the Bone Marrow, Lung, and Testis Collected From the Same Exposed BALB/cJ

Mice. Dose-Response. 2018 Oct 19;16(4):155932581881503.

170. Acharya MM, Baddour AAD, Kawashita T, Allen BD, Syage AR, Nguyen TH, et al. Epigenetic determinants of space radiation-induced cognitive dysfunction. Sci Rep. 2017 Feb 21;7(January):1–15.

171. Antwih DA, Gabbara KM, Lancaster WD, Ruden DM, Zielske SP. Radiation-induced epigenetic DNA methylation modification of radiation-response pathways. Epigenetics. 2013 Aug 27;8(8):839–48.

172. Aypar U, Morgan WF, Baulch JE. Radiation-induced epigenetic alterations after low and high LET irradiations. Mutat Res Mol Mech Mutagen. 2011 Feb 10;707(1–2):24–33.

173. Goetz W, Morgan MNMM, Baulch JE. The Effect of Radiation Quality on Genomic DNA Methylation Profiles in Irradiated Human Cell Lines. Radiat Res. 2011 May 1;175(5):575–87.

174. Zheng Y, Joyce BT, Liu L, Zhang Z, Kibbe WA, Zhang W, et al. Prediction of genome-wide DNA methylation in repetitive elements. Nucleic Acids Res. 2017 Sep 1;45(15):8697–711.

175. Kietzmann T, Petry A, Shvetsova A, Gerhold JM, Görlach A. The epigenetic landscape related to reactive oxygen species formation in the cardiovascular system. Br J Pharmacol. 2017;174(12):1533–54.

176. Yara S, Lavoie J-C, Levy E. Oxidative stress and DNA methylation regulation in the metabolic syndrome. Epigenomics. 2015 Apr;7(2):283–300.

177. Wu Q, Ni X. ROS-mediated DNA methylation pattern alterations in carcinogenesis. Curr Drug Targets. 2015;16(1):13–9.

178. Lee S-J, Dimtchev A, Lavin MF, Dritschilo A, Jung M. A novel ionizing radiation-induced signaling pathway that activates the transcription factor NF-κB. Oncogene. 1998 Oct 9;17(14):1821–6.

179. Janssens S, Tschopp J. Signals from within: the DNA-damage-induced NF-κB response. Cell Death Differ. 2006 May 13;13(5):773–84.

180. Hei TK, Zhou H, Chai Y, Ponnaiya B, Ivanov VN. Radiation induced non-targeted response: mechanism and potential clinical implications. Curr Mol Pharmacol. 2011 Jun;4(2):96–105.

181. Di Maggio F, Minafra L, Forte G, Cammarata F, Lio D, Messa C, et al. Portrait of inflammatory response to ionizing radiation treatment. J Inflamm. 2015 Feb 18;12(1):14.

182. Liu Y, Mayo MW, Nagji AS, Smith PW, Ramsey CS, Li D, et al. Phosphorylation of RelA/p65 promotes DNMT-1 recruitment to chromatin and represses transcription of the tumor metastasis suppressor gene BRMS1. Oncogene. 2012 Mar 18;31(9):1143–54.

183. Li Y, Deuring J, Peppelenbosch MP, Kuipers EJ, de Haar C, van der Woude CJ. IL-6-induced DNMT1 activity mediates SOCS3 promoter hypermethylation in ulcerative colitis-related colorectal cancer. Carcinogenesis. 2012 Oct 1;33(10):1889–96.

184. Brasier AR. The nuclear factor-B-interleukin-6 signalling pathway mediating vascular inflammation. Cardiovasc Res. 2010 May 1;86(2):211–8.

185. Metabolic E, Genitourinary Pathobiology The A. DNA Methyl Transferase 1 Reduces Expression of SRD5A2 in the Aging Adult Prostate. Am J Pathol. 2015;185(3):870–82.

186. MA S-CC, ZHANG H-PP, Kong F-QQ, Zheng H, YANG C, HE Y-YY, et al. Integration of gene expression and DNA methylation profiles provides a molecular subtype for risk assessment in atherosclerosis. Mol Med Rep. 2016 Jun 1;13(6):4791–9.

187. Peng P, Wang L, Yang X, Huang X, Ba Y, Chen X, et al. A Preliminary Study of the Relationship between Promoter Methylation of the ABCG1, GALNT2 and HMGCR Genes and Coronary Heart Disease. Coleman WB, editor. PLoS One. 2014 Aug 1;9(8):e102265.

188. Pfeiffer L, Wahl S, Pilling LC, Reischl E, Sandling JK, Kunze S, et al. DNA Methylation of Lipid-Related Genes Affects Blood Lipid Levels. Circ Cardiovasc Genet. 2015 Apr;8(2):334–42.

189. Istas G, Declerck K, Pudenz M, Szic KSV, Lendinez-Tortajada V, Leon-Latre M, et al. Identification of differentially methylated BRCA1 and CRISP2 DNA regions as blood surrogate markers for cardiovascular disease. Sci Rep. 2017 Dec 11;7(1):1–14.

190. Xu LL, Zheng D, Wang L, Jiang D, Liu H, Xu LL, et al. GCK gene-body hypomethylation is associated with the risk of coronary heart disease. Biomed Res Int. 2014 Feb 17;2014:151723.

191. Indumathi B, Katkam SK, Krishna LSR, Kutala VK. Dual Effect of IL-6 -174 G/C Polymorphism and Promoter Methylation in the Risk of Coronary Artery Disease Among South Indians. Indian J Clin Biochem. 2019 Apr 21;34(2):180–7.

192. Bakshi C, Vijayvergiya R, Dhawan V. Aberrant DNA methylation of M1-macrophage genes in coronary artery disease. Sci Rep. 2019 Dec 5;9(1):1429.

193.   Ghose S, Ghosh S, Tanwar VS, Tolani P, Kutum R, Sharma A, et al. Investigating Coronary Artery Disease methylome through targeted bisulfite sequencing. Gene. 2019 Dec 30;721:144107.

194.   Wei L, Zhao S, Wang G, Zhang S, Luo W, Qin Z, et al. SMAD7 methylation as a novel marker in atherosclerosis. Biochem Biophys Res Commun. 2018 Feb 5;496(2):700–5.

195.   Kim M, Long TI, Arakawa K, Wang R, Yu MC, Laird PW. DNA Methylation as a Biomarker for Cardiovascular Disease Risk. Bader JS, editor. PLoS One. 2010 Mar 15;5(3):e9692.

196.   Fernández-Sanlés A, Sayols-Baixeras S, Subirana I, Degano IR, Elosua R. Association between DNA methylation and coronary heart disease or other atherosclerotic events: a systematic review. Running title: DNA methylation and coronary heart disease. Atherosclerosis. 2017 Aug 1;263:325–33.

197.   Hiltunen MO, Turunen MP, Häkkinen TP, Rutanen J, Hedman M, Mäkinen K, et al. DNA hypomethylation and methyltransferase expression in atherosclerotic lesions. Vasc Med. 2002 Feb 3;7(1):5–11.

198.   Aavik E, Lumivuori H, Leppanen O, Wirth T, Hakkinen S-K, Brasen J-H, et al. Global DNA methylation analysis of human atherosclerotic plaques reveals extensive genomic hypomethylation and reactivation at imprinted locus 14q32 involving induction of a miRNA cluster. Eur Heart J. 2015 Apr 2;36(16):993–1000.

199.   Pogribny IP, Beland FA. DNA hypomethylation in the origin and pathogenesis of human diseases. Cell Mol Life Sci. 2009 Jul 27;66(14):2249–61.

200.   Zaina SA, Garay-Sevilla ME, Hernández-González MA, Solís-Martínez MO, Zaina S. Extensive demethylation of normally hypermethylated CpG islands occurs in human atherosclerotic arteries. Int J Mol Med. 2010 Sep 21;26(5):691–700.

201.   Jiang Y, Zhang H, Sun T, Wang J, Sun W, Gong H, et al. The comprehensive effects of hyperlipidemia and hyperhomocysteinemia on pathogenesis of atherosclerosis and DNA hypomethylation in ApoE-/- mice. Acta Biochim Biophys Sin (Shanghai). 2012 Oct 1;44(10):866–75.

202.   Zaina S, Heyn H, Carmona FJ, Varol N, Sayols S, Condom E, et al. DNA Methylation Map of Human Atherosclerosis. Circ Cardiovasc Genet. 2014 Oct 1;7(5):692–700.

203.   Lund G, Andersson L, Lauria M, Lindholm M, Fraga MF, Villar-Garea A, et al. DNA Methylation Polymorphisms Precede Any Histological Sign of Atherosclerosis in Mice Lacking Apolipoprotein E*. J Biol Chem. 2004 Jul 9;279(28):29147–54.

204.   Huang Y-S, Zhi Y-F, Wang S-R. Hypermethylation of estrogen receptor-α gene in atheromatosis patients and its correlation with homocysteine. Pathophysiology. 2009 Oct 1;16(4):259–65.

205.   Aavik E, Babu M, Ylä-Herttuala S. DNA methylation processes in atheosclerotic plaque. Atherosclerosis. 2019 Feb 1;281:168–79.

206.   Dunn J, Qiu H, Kim S, Jjingo D, Hoffman R, Kim CW, et al. Flow-dependent epigenetic DNA methylation regulates endothelial gene expression and atherosclerosis. 2014 Jul 1;124(7):3187–99.

207.   Cao Q, Wang X, Jia L, Mondal AK, Diallo A, Hawkins GA, et al. Inhibiting DNA Methylation by 5-Aza-2†-deoxycytidine Ameliorates Atherosclerosis Through Suppressing Macrophage Inflammation. Endocrinology. 2014 Dec 1;155(12):4925–38.

208.   Calkin AC, Tontonoz P. Liver X receptor signaling pathways and atherosclerosis. Vol. 30, Arteriosclerosis, Thrombosis, and Vascular Biology. 2010. p. 1513–8.

209.   Grbić E, Peterlin A, Kunej T, Petrovič D. PPARγ gene and atherosclerosis: Genetic polymorphisms, epigenetics and therapeutic implications. Balk J Med Genet. 2018;21(1):39–46.

210.   Yu J, Qiu Y, Yang J, Bian S, Chen G, Deng M, et al. DNMT1-PPARγ pathway in macrophages regulates chronic inflammation and atherosclerosis development in mice. Sci Rep. 2016 Aug 17;6.

211.   Chistiakov DA, Orekhov AN, Bobryshev Y V. Treatment of cardiovascular pathology with epigenetically active agents: Focus on natural and synthetic inhibitors of DNA methylation and histone deacetylation. Vol. 227, International Journal of Cardiology. Elsevier Ireland Ltd; 2017. p. 66–82.

212.   Nicorescu I, Dallinga GM, de Winther MPJ, Stroes ESG, Bahjat M. Potential epigenetic therapeutics for atherosclerosis treatment. Vol. 281, Atherosclerosis. Elsevier Ireland Ltd; 2019. p. 189–97.

213.   Schiano C, Vietri MT, Grimaldi V, Picascia A, Pascale MR De, Napoli C. Epigenetic-related therapeutic challenges in cardiovascular disease. Trends Pharmacol Sci. 2015 Apr 1;36(4):226–35.

214.   Tang C, Oram JF. The cell cholesterol exporter ABCA1 as a protector from cardiovascular disease and diabetes. Biochim Biophys Acta - Mol Cell Biol Lipids. 2009 Jul 1;1791(7):563–72.

215.   Ghaznavi H, Mahmoodi K, Soltanpour MS. A preliminary study of the association between the ABCA1 gene promoter DNA methylation and coronary artery disease risk. Mol Biol Res Commun. 2018 Jun;7(2):59–65.

216. Guay S-P, Légaré C, Houde A-A, Mathieu P, Bossé Y, Bouchard L. Acetylsalicylic acid, aging and coronary artery disease are associated with ABCA1 DNA methylation in men. Clin Epigenetics. 2014 Jul 29;6(1):14.

217. Guay S-P, Brisson D, Munger J, Lamarche B, Gaudet D, Bouchard L. *ABCA1* gene promoter DNA methylation is associated with HDL particle profile and coronary artery disease in familial hypercholesterolemia. Epigenetics. 2012 May 27;7(5):464–72.

218. Akinyemiju T, Do AN, Patki A, Aslibekyan S, Zhi D, Hidalgo B, et al. Epigenome-wide association study of metabolic syndrome in African-American adults. Clin Epigenetics. 2018 Dec 10;10(1):49.

219. Hedman ÅK, Mendelson MM, Marioni RE, Gustafsson S, Joehanes R, Irvin MR, et al. Epigenetic Patterns in Blood Associated With Lipid Traits Predict Incident Coronary Heart Disease Events and Are Enriched for Results From Genome-Wide Association Studies. Circ Cardiovasc Genet. 2017 Jan;10(1):e001487.

220. Rudel LL, Lee RG, Cockman TL. Acyl coenzyme A : cholesterol acyltransferase types 1 and 2: structure and function in atherosclerosis. Curr Opin Lipidol. 2001 Apr;12(2):121–7.

221. Chen C-H, Budas GR, Churchill EN, Disatnik M-H, Hurley TD, Mochly-Rosen D. Activation of aldehyde dehydrogenase-2 reduces ischemic damage to the heart. Science. 2008 Sep 12;321(5895):1493–5.

222. Gong D, Zhang H, Hu S. Mitochondrial aldehyde dehydrogenase 2 activation and cardioprotection. J Mol Cell Cardiol. 2013 Feb 1;55:58–63.

223. Yang M-Y, Wang Y-B, Han B, Yang B, Qiang Y-W, Zhang Y, et al. Activation of aldehyde dehydrogenase 2 slows down the progression of atherosclerosis via attenuation of ER stress and apoptosis in smooth muscle cells. Acta Pharmacol Sin. 2018 Jan;39(1):48–58.

224. Wang P, Shen C, Diao L, Yang Z, Fan F, Wang C, et al. Aberrant Hypermethylation of Aldehyde Dehydrogenase 2 Promoter Upstream Sequence in Rats with Experimental Myocardial Infarction. Biomed Res Int. 2015 Jan 5;2015:1–13.

225. Kadomatsu T, Endo M, Miyata K, Oike Y. Diverse roles of ANGPTL2 in physiology and pathophysiology. Trends Endocrinol Metab. 2014 May 1;25(5):245–54.

226. Zhou J, Chen L, Yang X, Huang X, Wang Z, Peng P, et al. Preliminary study of the relationship between promoter methylation of the ANGPTL2 gene and coronary heart disease. J Clin Lab Anal. 2018 Nov 21;e22702.

227. Nguyen A, Mamarbachi M, Turcot V, Lessard S, Yu C, Luo X, et al. Lower Methylation of the ANGPTL2 Gene in Leukocytes from Post-Acute Coronary Syndrome Patients. Gaetano C, editor. PLoS One. 2016 Apr 21;11(4):e0153920.

228. van Westerop LLMLM, Arts-de Jong M, Hoogerbrugge N, de Hullu JAA, Maas AHEMHEM. Cardiovascular risk of BRCA1/2 mutation carriers: A review. Maturitas. 2016 Sep 1;91:135–9.

229. Chen M, Ni J, Zhang Y, Muyan M, Yeh S. ERAP75 functions as a coactivator to enhance estrogen receptor α transactivation in prostate stromal cells. Prostate. 2008 Sep 1;68(12):1273–82.

230. Yamada Y, Horibe H, Oguri M, Sakuma J, Takeuchi I, Yasukochi Y, et al. Identification of novel hyper- or hypomethylated CpG sites and genes associated with atherosclerotic plaque using an epigenome-wide association study. Int J Mol Med. 2018 Feb 2;41(5):2724–32.

231. Papait R, Kunderfranco P, Stirparo GG, Latronico MVG, Condorelli G. Long Noncoding RNA: a New Player of Heart Failure? J Cardiovasc Transl Res. 2013 Dec 9;6(6):876–83.

232. Chen X, Jiang D, Xu L, Han L, Hu H, Huang Y, et al. Elevated methylation of cyclin dependent kinase inhibitor 2B contributes to the risk of coronary heart disease in women. Exp Ther Med. 2018 Nov 2;17(1):205–13.

233. Bastos P, Gomes T, Ribeiro L. Catechol-O-Methyltransferase (COMT): An Update on Its Role in Cancer, Neurological and Cardiovascular Diseases. In 2017. p. 1–39.

234. Zhong J, Chen X, Wu N, Shen C, Cui H, Du W, et al. Catechol-O-methyltransferase promoter hypomethylation is associated with the risk of coronary heart disease. Exp Ther Med. 2016 Nov 1;12(5):3445–9.

235. Akhtar S, Gremse F, Kiessling F, Weber C, Schober A. CXCL12 promotes the stabilization of atherosclerotic lesions mediated by smooth muscle progenitor cells in Apoe-deficient mice. Arterioscler Thromb Vasc Biol. 2013 Apr;33(4):679–86.

236. Farouk SS, Rader DJ, Reilly MP, Mehta NN. CXCL12: a new player in coronary disease identified through human genetics. Trends Cardiovasc Med. 2010 Aug;20(6):204–9.

237. van der Vorst EPC, Döring Y, Weber C. Chemokines and their receptors in Atherosclerosis. J Mol Med. 2015 Sep 15;93(9):963–71.

238. Miao L, Yin R-X, Zhang Q-H, Hu X-J, Huang F, Chen W-X, et al. Integrated DNA methylation and gene expression analysis in the pathogenesis of coronary artery disease. Aging (Albany NY). 2019 Mar 7;11(5):1486–500.

239. Zhang J, Liu J, Li Z, Wang L, Jiang Y, Wang S. Dysfunction of endothelial NO system originated from homocysteine-induced aberrant methylation pattern in promoter region of DDAH2 gene. Chin Med J (Engl). 2007 Dec 5;120(23):2132–7.

240. Niu P-P, Cao Y, Gong T, Guo J-H, Zhang B-K, Jia S-J. Hypermethylation of DDAH2 promoter contributes to the dysfunction of endothelial progenitor cells in coronary artery disease patients. J Transl Med. 2014 Jun 16;12(1):170.

241. Menazza S, Murphy E. The Expanding Complexity of Estrogen Receptor Signaling in the Cardiovascular System. Circ Res. 2016 Mar 18;118(6):994–1007.

242. Mahmoodzadeh S, Eder S, Nordmeyer J, Ehler E, Huber O, Martus P, et al. Estrogen receptor alpha up-regulation and redistribution in human heart failure. FASEB J. 2006 May 1;20(7):926–34.

243. Deroo BJ, Korach KS. Estrogen receptors and human disease. J Clin Invest. 2006 Mar 1;116(3):561–70.

244. Post WS, Goldschmidt-Clermont PJ, Wilhide CC, Heldman AW, Sussman MS, Ouyang P, et al. Methylation of the estrogen receptor gene is associated with aging and atherosclerosis in the cardiovascular system [Internet]. Cardiovascular Research Narnia; Sep 1, 1999 p. 985–91.

245. Min J, Weitian Z, Peng C, Yan P, Bo Z, Yan W, et al. Correlation between insulin-induced estrogen receptor methylation and atherosclerosis. Cardiovasc Diabetol. 2016 Dec 10;15(1):156.

246. Rothenbacher D, Koenig W, Brenner H. Comparison of N-Terminal Pro–B-Natriuretic Peptide, C-Reactive Protein, and Creatinine Clearance for Prognosis in Patients With Known Coronary Heart Disease. Arch Intern Med. 2006 Dec 11;166(22):2455.

247. Breitling LP, Salzmann K, Rothenbacher D, Burwinkel B, Brenner H. Smoking, F2RL3 methylation, and prognosis in stable coronary heart disease. Eur Heart J. 2012 Nov 1;33(22):2841–8.

248. Zhang Y, Yang R, Burwinkel B, Breitling LP, Brenner H. F2RL3 methylation as a biomarker of current and lifetime smoking exposures. Environ Health Perspect. 2014 Feb;122(2):131–7.

249. Waters CE, Saldivar JC, Hosseini SA, Huebner K. The FHIT gene product: tumor suppressor and genome "caretaker". Cell Mol Life Sci. 2014 Dec;71(23):4577–87.

250. Lü C-X, Xu R-D, Cao M, Wang G, Yan F-Q, Shang S-S, et al. FOXP3 demethylation as a means of identifying quantitative defects in regulatory T cells in acute coronary syndrome. Atherosclerosis. 2013 Jul 1;229(1):263–70.

251. Jia L, Zhu L, Wang JZ, Wang XJ, Chen JZ, Song L, et al. Methylation of FOXP3 in regulatory T cells is related to the severity of coronary artery disease. Atherosclerosis. 2013 Jun 1;228(2):346–52.

252. Di Paola R, Marucci A, Trischitta V. GALNT2 effect on HDL-cholesterol and triglycerides levels in humans: Evidence of pleiotropy? Nutr Metab Cardiovasc Dis. 2017 Apr 1;27(4):281–2.

253. Marucci A, Antonucci A, De Bonis C, Mangiacotti D, Scarale MG, Trischitta V, et al. GALNT2 as a novel modulator of adipogenesis and adipocyte insulin signaling. Int J Obes. 2019 Apr 30;

254. Webster RJ, Warrington NM, Weedon MN, Hattersley AT, McCaskie PA, Beilby JP, et al. The association of common genetic variants in the APOA5, LPL and GCK genes with longitudinal changes in metabolic and cardiovascular traits. Diabetologia. 2009 Jan 19;52(1):106–14.

255. Iynedjian PB. Molecular Physiology of Mammalian Glucokinase. Cell Mol Life Sci. 2009 Jan 26;66(1):27–42.

256. FAN R, WANG W-J, ZHONG Q-L, DUAN S-W, XU X-T, HAO L-M, et al. Aberrant methylation of the GCK gene body is associated with the risk of essential hypertension. Mol Med Rep. 2015 Aug 1;12(2):2390–4.

257. Tracy MR, Dormans JP, Kusumi K. Klippel-Feil Syndrome. Clin Orthop Relat Res. 2004 Jul;424:183–90.

258. YAMADA Y, NISHIDA T, HORIBE H, OGURI M, KATO K, SAWABE M. Identification of hypo- and hypermethylated genes related to atherosclerosis by a genome-wide analysis of DNA methylation. Int J Mol Med. 2014 May 1;33(5):1355–63.

259. Nova-Lampeti E, Aguilera V, Oporto K, Guzmán P, Ormazábal V, Zúñiga F, et al. Hox Genes in Adult Tissues and Their Role in Endothelial Cell Differentiation and Angiogenesis. In: Endothelial Dysfunction - Old Concepts and New Challenges. InTech; 2018.

260. Gorski DH, Patel C V., Walsh K. Homeobox transcription factor regulation in the cardiovascular system. Trends Cardiovasc Med. 1993 Sep 1;3(5):184–90.

261. Fontes JA, Rose NR, Čiháková D. The varying faces of IL-6: from cardiac protection to cardiac failure. Cytokine. 2015 Jul;74(1):62.

262. van der Heijden T, Bot I, Kuiper J. The IL-12 cytokine family in cardiovascular diseases. Cytokine. 2019 Oct 1;122:154188.

263. Umar S, van der Laarse A. Nitric oxide and nitric oxide synthase isoforms in the normal, hypertrophic, and failing heart. Mol Cell Biochem. 2010 Jan 19;333(1–2):191–201.

264. Shah A. Inducible nitric oxide synthase and cardiovascular disease. Cardiovasc Res. 2000 Jan 1;45(1):148–55.

265. Barry SP, Townsend PA, Latchman DS, Stephanou A. Role of the JAK–STAT pathway in myocardial injury. Trends Mol Med. 2007 Feb 1;13(2):82–9.

266. Davies RW, Wells GA, Stewart AFR, Erdmann J, Shah SH, Ferguson JF, et al. A genome-wide association study for coronary artery disease identifies a novel susceptibility locus in the major histocompatibility complex. Circ Cardiovasc Genet. 2012 Apr 1;5(2):217–25.

267. Missala I, Kassner U, Steinhagen-Thiessen E. A Systematic Literature Review of the Association of Lipoprotein(a) and Autoimmune Diseases and Atherosclerosis. Int J Rheumatol. 2012 Dec 5;2012:480784.

268. Clarke R, Peden JF, Hopewell JC, Kyriakou T, Goel A, Heath SC, et al. Genetic Variants Associated with Lp(a) Lipoprotein Level and Coronary Disease. N Engl J Med. 2009 Dec 24;361(26):2518–28.

269. Rozanski A, Takano APC, Kato PN, Soares AG, Lellis-Santos C, Campos JC, et al. M-protein is down-regulated in cardiac hypertrophy driven by thyroid hormone in rats. Mol Endocrinol. 2013 Dec;27(12):2055–65.

270. Sequeira V, Nijenkamp LLA. AM, Regan JA, van der Velden J. The physiological role of cardiac cytoskeleton and its alterations in heart failure. Biochim Biophys Acta (BBA)-Biomembranes. 2014 Feb 1;1838(2):700–22.

271. Liu X, Xu H, Xu H, Geng Q, Mak W-H, Ling F, et al. New genetic variants associated with major adverse cardiovascular events in patients with acute coronary syndromes and treated with clopidogrel and aspirin. bioRxiv. 2018 Sep 9;411165.

272. Forstermann U, Sessa WC. Nitric oxide synthases: regulation and function. Eur Heart J. 2012 Apr 1;33(7):829–37.

273. Yu X-H, Jiang N, Yao P-B, Zheng X-L, Cayabyab FS, Tang C-K. NPC1, intracellular cholesterol trafficking and atherosclerosis. Clin Chim Acta. 2014 Feb 15;429:69–75.

274. Afzali M, Nakhaee A, Tabatabaei SP, Tirgar-Fakheri K, Hashemi M. Aberrant promoter methylation profile of Niemann-pick type C1 gene in cardiovascular disease. Iran Biomed J. 2013;17(2):77–83.

275. Sutton BS, Crosslin DR, Shah SH, Nelson SC, Bassil A, Hale AB, et al. Comprehensive genetic analysis of the platelet activating factor acetylhydrolase (PLA2G7) gene and cardiovascular disease in case–control and family datasets. Hum Mol Genet. 2008 May 1;17(9):1318–28.

276. Karabina S, Ninio E. Plasma PAFAH/PLA2G7 Genetic Variability, Cardiovascular Disease, and Clinical Trials. In 2015. p. 145–55.

277. Jiang D, Zheng D, Wang L, Huang Y, Liu H, Xu L, et al. Elevated PLA2G7 Gene Promoter Methylation as a Gender-Specific Marker of Aging Increases the Risk of Coronary Heart Disease in Females. Oudejans C, editor. PLoS One. 2013 Mar 28;8(3):e59752.

278. Sorrentino S. The eight human "canonical" ribonucleases: Molecular diversity, catalytic properties, and special biological actions of the enzyme proteins. FEBS Lett. 2010 Jun 3;584(11):2194–200.

279. Koczera P, Martin L, Marx G, Schuerholz T. The Ribonuclease A Superfamily in Humans: Canonical RNases as the Buttress of Innate Immunity. Int J Mol Sci. 2016 Aug 5;17(8):1278.

280. Wei L, Chao N, Gao S, Yu Y, Shi L, Ma X, et al. Homocysteine induces vascular inflammatory response via SMAD7 hypermethylation in human umbilical vein smooth muscle cells. Microvasc Res. 2018 Nov 1;120:8–12.

281. Papait R, Greco C, Kunderfranco P, Latronico MVG, Condorelli G. Epigenetics: a new mechanism of regulation of heart failure? Basic Res Cardiol. 2013 Jul 6;108(4):361.

282. Guo X, Wang X, Wang Y, Zhang C, Quan X, Zhang Y, et al. Variants in the SMARCA4 gene was associated with coronary heart disease susceptibility in Chinese han population. Oncotarget. 2017 Jan 31;8(5):7350.

283. Nakatochi M, Ichihara S, Yamamoto K, Naruse K, Yokota S, Asano H, et al. Epigenome-wide association of myocardial infarction with DNA methylation sites at loci related to cardiovascular disease.

284. Chmielewski S, Piaszyk-Borychowska A, Wesoly J, Bluyssen HAR. STAT1 and IRF8 in Vascular Inflammation and Cardiovascular Disease: Diagnostic and Therapeutic Potential. Int Rev Immunol. 2016 Sep 2;35(5):434–54.

285. Hammer S, Toenjes M, Lange M, Fischer JJ, Dunkel I, Mebus S, et al. Characterization of TBX20 in human hearts and its regulation by TFAP2. J Cell Biochem. 2008 Jun 1;104(3):1022–33.

286. Shen T, Zhu Y, Patel J, Ruan Y, Chen B, Zhao G, et al. T-Box20 Suppresses Oxidized Low-Density Lipoprotein-induced Human Vascular Endothelial Cell Injury by Upregulation of PPAR-γ. Cell Physiol Biochem.

2013;32(5):1137–50.

287. Johnson JL. Metalloproteinases in atherosclerosis. Eur J Pharmacol. 2017 Dec 5;816:93–106.

288. Guay S-P, Voisin G, Brisson D, Munger J, Lamarche B, Gaudet D, et al. Epigenome-wide analysis in familial hypercholesterolemia identified new loci associated with high-density lipoprotein cholesterol concentration. Epigenomics. 2012 Dec;4(6):623–39.

289. Guay S-P, Légaré C, Brisson D, Mathieu P, Bossé Y, Gaudet D, et al. Epigenetic and genetic variations at the *TNNT1* gene locus are associated with HDL-C levels and coronary artery disease. Epigenomics. 2016 Mar 7;8(3):359–71.

290. Li C, Wang F, Yang Y, Fu F, Xu C, Shi L, et al. Significant association of SNP rs2106261 in the ZFHX3 gene with atrial fibrillation in a Chinese Han GeneID population. Hum Genet. 2011 Mar;129(3):239–46.

291. Kao Y-H, Hsu J-C, Chen Y-C, Lin Y-K, Lkhagva B, Chen S-A, et al. ZFHX3 knockdown increases arrhythmogenesis and dysregulates calcium homeostasis in HL-1 atrial myocytes. Int J Cardiol. 2016 May 1;210:85–92.

292. Xue Y, Shi N, Zhang B, Gao X, Gao Y, Zhou X, et al. Genetic variant in ZFHX3 Geneon 16q22 associated with risk of stroke in Chinese Han population. Int J Clin Exp Pathol. 2016;9:8650–6.

293. Liu C, Yao M-D, Li C-P, Shan K, Yang H, Wang J-J, et al. Silencing Of Circular RNA-ZNF609 Ameliorates Vascular Endothelial Dysfunction. Theranostics. 2017;7(11):2863–77.

294. Lin T, Zhang X, Lu Y, Gong L. Identification of Circular RNA Related to Inflammation-Induced Lymphangiogenesis by Microarray Analysis. DNA Cell Biol. 2019 Aug;38(8):887–94.

295. Thomas PD, Campbell MJ, Kejariwal A, Mi H, Karlak B, Daverman R, et al. PANTHER: A library of protein families and subfamilies indexed by function. Genome Res. 2003 Sep 1;13(9):2129–41.

296. Mi H, Muruganujan A, Huang X, Ebert D, Mills C, Guo X, et al. Protocol Update for large-scale genome and gene function analysis with the PANTHER classification system (v.14.0). Nat Protoc. 2019 Mar 1;14(3):703–21.

297. Segiet OA, Piecuch A, Mielańczyk Ł, Michalski M, Nowalany-Kozielska E. Role of interleukins in heart failure with reduced ejection fraction [Internet]. Vol. 22, Anatolian Journal of Cardiology. Turkish Society of Cardiology; 2019. p. 287–99.

298. Abbate A, Toldo S, Marchetti C, Kron J, Van Tassell BW, Dinarello CA. Interleukin-1 and the Inflammasome as Therapeutic Targets in Cardiovascular Disease. Circ Res. 2020 Apr 24;1260–80.

299. Rose NR. Critical cytokine pathways to cardiac inflammation [Internet]. Vol. 31, Journal of Interferon and Cytokine Research. Mary Ann Liebert, Inc.; 2011. p. 705–10.

300. Aoyagi T, Matsui T. Phosphoinositide-3 Kinase Signaling in Cardiac Hypertrophy and Heart Failure. Curr Pharm Des. 2011 Jul 11;17(18):1818–24.

301. Kitamura Y, Koide M, Akakabe Y, Matsuo K, Shimoda Y, Soma Y, et al. Manipulation of cardiac phosphatidylinositol 3-kinase (PI3K)/Akt signaling by apoptosis regulator through modulating IAP expression (ARIA) regulates cardiomyocyte death during doxorubicin-induced cardiomyopathy. J Biol Chem. 2014 Jan 31;289(5):2788–800.

302. Hoyer FF, Nahrendorf M. Interferon-γregulates cardiac myeloid cells in myocardial infarction [Internet]. Vol. 115, Cardiovascular Research. Oxford University Press; 2019. p. 1815–6.

303. Ferreira LRP. Interferon-γ and other inflammatory mediators in cardiomyocyte signaling during Chagas disease cardiomyopathy. World J Cardiol. 2014;6(8):782.

304. Wagner MA, Siddiqui MAQ. The JAK-STAT pathway in hypertrophic stress signaling and genomic stress response. JAK-STAT. 2012 Apr;1(2):131–41.

305. Barry SP, Townsend PA, Latchman DS, Stephanou A. Role of the JAK-STAT pathway in myocardial injury [Internet]. Vol. 13, Trends in Molecular Medicine. Elsevier; 2007. p. 82–9.

306. Goswami R. JAK-STAT Signaling in Diseases. 1st ed. JAK-STAT Signaling in Diseases. Boca Raton: CRC Press; 2020.

307. Ivashkiv LB. Crosstalk with the Jak-STAT pathway in inflammation. In: Jak-Stat Signaling: From Basics to Disease. Springer-Verlag Wien; 2012. p. 353–70.

308. Boshuizen MCS, de Winther MPJ. Interferons as Essential Modulators of Atherosclerosis. Arterioscler Thromb Vasc Biol. 2015 Jul 27;35(7):1579–88.

309. Zhang J, Alcaide P, Liu L, Sun J, He A, Luscinskas FW, et al. Regulation of endothelial cell adhesion molecule expression by mast cells, macrophages, and neutrophils. PLoS One. 2011;6(1).

310. Whitman SC, Ravisankar P, Elam H, Daugherty A. Exogenous interferon-γ enhances atherosclerosis in

apolipoprotein E-/- mice. Am J Pathol. 2000;157(6):1819–24.

311. Fougerat A, Gayral S, Malet N, Briand-Mesange F, Breton-Douillon M, Laffargue M. Phosphoinositide 3-kinases and their role in inflammation: Potential clinical targets in atherosclerosis? [Internet]. Vol. 116, Clinical Science. Portland Press; 2009. p. 791–804.

312. Ghigo A, Li M. Phosphoinositide 3-kinase: friend and foe in cardiovascular disease. Front Pharmacol. 2015 Aug 13;6(Aug):169.

313. Choi KH, Kim JE, Song NR, Son JE, Hwang MK, Byun S, et al. Phosphoinositide 3-kinase is a novel target of piceatannol for inhibiting PDGF-BB-induced proliferation and migration in human aortic smooth muscle cells. Cardiovasc Res. 2010 Mar 1;85(4):836–44.

314. Buckley ML, Williams JO, Chan Y-H, Laubertová L, Gallagher H, Moss JWE, et al. The interleukin-33-mediated inhibition of expression of two key genes implicated in atherosclerosis in human macrophages requires MAP kinase, phosphoinositide 3-kinase and nuclear factor-κB signaling pathways. Sci Rep. 2019;9(1):11317.

315. Libby P. Interleukin-1 Beta as a Target for Atherosclerosis Therapy: Biological Basis of CANTOS and Beyond. Vol. 70, Journal of the American College of Cardiology. Elsevier USA; 2017. p. 2278–89.

316. Hartman J, Frishman WH. Inflammation and atherosclerosis: A review of the role of interleukin-6 in the development of atherosclerosis and the potential for targeted drug therapy [Internet]. Vol. 22, Cardiology in Review. Lippincott Williams and Wilkins; 2014. p. 147–51.

317. Tian Y, Ling X, Chen D, Zhang X, Qiu C. Interleukin-36 receptor antagonist attenuates atherosclerosis development by inhibiting NLRP3 inflammasome. J Cell Physiol. 2020 Dec 2;235(12):9992–6.

318. Fatkhullina AR, Peshkova IO, Koltsova EK. The role of cytokines in the development of atherosclerosis [Internet]. Vol. 81, Biochemistry (Moscow). Maik Nauka Publishing / Springer SBM; 2016. p. 1358–70.

319. Von der Thüsen JH, Kuiper J, Van Berkel TJC, Biessen EAL. Interleukins in atherosclerosis: Molecular pathways and therapeutic potential [Internet]. Vol. 55, Pharmacological Reviews. Pharmacol Rev; 2003. p. 133–66.

320. Wouters K, Deleye Y, Hannou SA, Vanhoutte J, Maréchal X, Coisne A, et al. The tumour suppressor CDKN2A/p16INK4a regulates adipogenesis and bone marrow-dependent development of perivascular adipose tissue. Diabetes Vasc Dis Res. 2017 Nov 1;14(6):516–24.

321. Morton LM, Onel K, Curtis RE, Hungate EA, Armstrong GT. The Rising Incidence of Second Cancers: Patterns of Occurrence and Identification of Risk Factors for Children and Adults. Am Soc Clin Oncol Educ B. 2014 May 15;(34):e57–67.

322. Dracham CB, Shankar A, Madan R. Radiation induced secondary malignancies: a review article. Radiat Oncol J. 2018;36(2):85.

323. Cahan WG, Woodard HQ, Higinbotham NL, Stewart FW, Coley BL. Sarcoma arising in irradiated bone: report of eleven cases. Cancer Interdiscip Int J Am Cancer Soc. 1998;82(1):8–34.

324. Dincer Y, Sezgin Z. Medical Radiation Exposure and Human Carcinogenesis-Genetic and Epigenetic Mechanisms. Biomed Environ Sci. 2014;27(9):718–28.

325. Bao X, Zhang J, Huang G, Yan J, Xu C, Dou Z, et al. The crosstalk between HIFs and mitochondrial dysfunctions in cancer development. Cell Death Dis. 2021;12(2):1–13.

326. Kudryavtseva A V, Krasnov GS, Dmitriev AA, Alekseev BY, Kardymon OL, Sadritdinova AF, et al. Mitochondrial dysfunction and oxidative stress in aging and cancer. Oncotarget. 2016;7(29):44879.

327. Paulino AC, Mai WY, Chintagumpala M, Taher A, Teh BS. Radiation-Induced Malignant Gliomas: Is There a Role for Reirradiation? Int J Radiat Oncol. 2008;71(5):1381–7.

328. Prasad G, Haas-Kogan DA. Radiation-induced gliomas. Expert Rev Neurother. 2009;9(10):1511–7.

329. Hauptmann M, Byrnes G, Cardis E, Bernier M-O, Blettner M, Dabin J, et al. Brain cancer after radiation exposure from CT examinations of children and young adults: Results from the EPI-CT cohort study. Lancet Oncol. 2023;24(1):45–53.

330. Kleinschmidt-DeMasters BK, Kang JS, Lillehei KO. The Burden of Radiation-Induced Central Nervous System Tumors: A Single Institution s Experience. J Neuropathol Exp Neurol. 2006 Mar 1;65(3):204–16.

331. Donson AM, Erwin NS, Kleinschmidt-DeMasters BK, Madden JR, Addo-Yobo SO, Foreman NK. Unique Molecular Characteristics of Radiation-Induced Glioblastoma. J Neuropathol Exp Neurol. 2007 Aug 1;66(8):740–9.

332. Calin GA, Dumitru CD, Shimizu M, Bichi R, Zupo S, Noch E, et al. Frequent deletions and down-regulation of micro-RNA genes miR15 and miR16 at 13q14 in chronic lymphocytic leukemia. Proc Natl Acad Sci. 2002;99(24):15524–9.

333. Klein U, Lia M, Crespo M, Siegel R, Shen Q, Mo T, et al. The DLEU2/miR-15a/16-1 cluster controls B cell proliferation and its deletion leads to chronic lymphocytic leukemia. Cancer Cell. 2010;17(1):28–40.

334. Wang X, He Y, Mackowiak B, Gao B. MicroRNAs as regulators, biomarkers and therapeutic targets in liver diseases. Gut. 2021;70(4):784–95.

335. Loh H-Y, Norman BP, Lai K-S, Rahman NMANA, Alitheen NBM, Osman MA. The regulatory role of microRNAs in breast cancer. Int J Mol Sci. 2019;20(19):4940.

336. Gabriely G, Yi M, Narayan RS, Niers JM, Wurdinger T, Imitola J, et al. Human glioma growth is controlled by microRNA-10b. Cancer Res. 2011;71(10):3563–72.

337. Li J, Zhang M, An G, Ma Q. LncRNA TUG1 acts as a tumor suppressor in human glioma by promoting cell apoptosis. Exp Biol Med (Maywood). 2016 Mar;241(6):644–9.

338. Kim ES, Choi YE, Hwang SJ, Han Y-H, Park M-J, Bae IH. IL-4, a direct target of miR-340/429, is involved in radiation-induced aggressive tumor behavior in human carcinoma cells. Oncotarget. 2016;7(52):86836.

339. Cui J, Cheng Y, Zhang P, Sun M, Gao F, Liu C, et al. Down regulation of miR200c promotes radiation-induced thymic lymphoma by targeting BMI1. J Cell Biochem. 2014;115(6):1033–42.

340. Peng Y, Croce CM. The role of MicroRNAs in human cancer. Signal Transduct Target Ther. 2016 Jan 28;1(1):1–9.

341. O'Donnell KA, Wentzel EA, Zeller KI, Dang C V, Mendell JT. c-Myc-regulated microRNAs modulate E2F1 expression. Nature. 2005;435(7043):839–43.

342. Chen X, Zeng K, Xu M, Liu X, Hu X, Xu T, et al. P53-induced miR-1249 inhibits tumor growth, metastasis, and angiogenesis by targeting VEGFA and HMGA2. Cell Death Dis. 2019;10(2):1–15.

343. Mantho CIT, Harbuzariu A, Gonzalez-Perez RR. Histone deacetylases, microRNA and leptin crosstalk in pancreatic cancer. World J Clin Oncol. 2017;8(3):178.

344. Heller G, Altenberger C, Steiner I, Topakian T, Ziegler B, Tomasich E, et al. DNA methylation of microRNA-coding genes in non-small-cell lung cancer patients. J Pathol. 2018;245(4):387–98.

345. Hata A, Kashima R. Dysregulation of microRNA biogenesis machinery in cancer. Crit Rev Biochem Mol Biol. 2016;51(3):121–34.

346. Ghossein CA, Dogan S, Farhat N, Landa I, Xu B. Expanding the spectrum of thyroid carcinoma with somatic DICER1 mutation: a survey of 829 thyroid carcinomas using MSK-IMPACT next-generation sequencing platform. Virchows Arch. 2022;480(2):293–302.

347. Liz J, Esteller M. lncRNAs and microRNAs with a role in cancer development. Vol. 1859, Biochimica et Biophysica Acta - Gene Regulatory Mechanisms. Elsevier B.V.; 2016. p. 169–76.

348. Chiu H-S, Somvanshi S, Patel E, Chen T-W, Singh VP, Zorman B, et al. Pan-Cancer Analysis of lncRNA Regulation Supports Their Targeting of Cancer Genes in Each Tumor Context. Cell Rep. 2018;23(1):297-312.e12.

349. Huarte M. The emerging role of lncRNAs in cancer. Nat Med. 2015;21(11):1253–61.

350. Wang M, Zhao C, Shi H, Zhang B, Zhang L, Zhang X, et al. Deregulated microRNAs in gastric cancer tissue-derived mesenchymal stem cells: novel biomarkers and a mechanism for gastric cancer. Br J Cancer. 2014;110(5):1199–210.

351. Jiang YJ, Bikle DD. LncRNA profiling reveals new mechanism for VDR protection against skin cancer formation. J Steroid Biochem Mol Biol. 2014;144:87–90.

352. Badowski C, He B, Garmire LX. Blood-derived lncRNAs as biomarkers for cancer diagnosis: the Good, the Bad and the Beauty. NPJ Precis Oncol. 2022;6(1):1–18.

353. Gu Y, Chen T, Li G, Yu X, Lu Y, Wang H, et al. LncRNAs: emerging biomarkers in gastric cancer. Futur Oncol. 2015;11(17):2427–41.

354. Sallam M, Benotmane MA, Baatout S, Guns P-JJ, Aerts A. Radiation-induced cardiovascular disease: an overlooked role for DNA methylation? Epigenetics. 2022 Jan 31;17(1):59–80.

355. Jacob S, Pathak A, Franck D, Latorzeff I, Jimenez G, Fondard O, et al. Early detection and prediction of cardiotoxicity after radiation therapy for breast cancer: the BACCARAT prospective cohort study. Radiat Oncol. 2016;11(1).

356. Suelves M, Carrió E, Núñez-Álvarez Y, Peinado MA. DNA methylation dynamics in cellular commitment and differentiation. Brief Funct Genomics. 2016 Nov 1;15(6):443–53.

357. Schübeler D. Function and information content of DNA methylation. Nature. 2015 Jan 14;517(7534):321–6.

358. Wang C, Chen L, Yang Y, Zhang M, Wong G. Identification of potential blood biomarkers for Parkinson's disease by gene expression and DNA methylation data integration analysis. Clin Epigenetics 2019 111. 2019

Feb 11;11(1):1–15.

359.   Ahmed SAH, Ansari SA, Mensah-Brown EPK, Emerald BS. The role of DNA methylation in the pathogenesis of type 2 diabetes mellitus. Clin Epigenetics. 2020 Jul 11;12(1):1–23.

360.   Locke WJ, Guanzon D, Ma C, Liew YJ, Duesing KR, Fung KYCC, et al. DNA Methylation Cancer Biomarkers: Translation to the Clinic. Front Genet. 2019 Nov 14;10:1150.

361.   Fernández-Sanlés A, Sayols-Baixeras S, Curcio S, Subirana I, Marrugat J, Elosua R. DNA Methylation and Age-Independent Cardiovascular Risk, an Epigenome-Wide Approach. Arterioscler Thromb Vasc Biol. 2018 Jan 1;38(3):645–52.

362.   Navas-Acien A, Domingo-Relloso A, Subedi P, Riffo-Campos AL, Xia R, Gomez L, et al. Blood DNA Methylation and Incident Coronary Heart Disease: Evidence From the Strong Heart Study. JAMA Cardiol. 2021;

363.   International Journal A, Tabaei S, Samaneh Tabaee S, Tabaee SS. DNA methylation abnormalities in atherosclerosis. 2019 Dec 4;47(1):2031–41.

364.   Ribeiro S, Simões AR, Rocha F, Vala IS, Pinto AT, Ministro A, et al. Molecular Changes In Cardiac Tissue As A New Marker To Predict Cardiac Dysfunction Induced By Radiotherapy   [Internet]. Vol. 12, Frontiers in Oncology . 2022.

365.   Valentin, Crijns A, Langendijk J, Spoor D, Vliegenthart R, Combs SE, et al. Early detection of cardiovascular changes after radiotherapy for Breast cancer: Protocol for a European multicenter prospective cohort study (MEDIRAD EARLY HEART study). J Med Internet Res. 2018 Oct 1;20(10):e9906.

366.   Lee JR, Ryu DS, Park SJ, Choe SH, Cho HM, Lee SR, et al. Successful application of human-based methyl capture sequencing for methylome analysis in non-human primate models. BMC Genomics. 2018 Apr 18;19(1).

367.   Shu C, Zhang X, Aouizerat BE, Xu K. Comparison of methylation capture sequencing and Infinium MethylationEPIC array in peripheral blood mononuclear cells. Epigenetics and Chromatin. 2020 Dec 1;13(1):1–15.

368.   Carey JL, Cox OH, Seifuddin F, Marque L, Tamashiro KL, Zandi PP, et al. A Rat Methyl-Seq Platform to Identify Epigenetic Changes Associated with Stress Exposure. J Vis Exp. 2018;(140):58617.

369.   F S, G W, O C, M P, L M, X Y, et al. Genome-wide Methyl-Seq analysis of blood-brain targets of glucocorticoid exposure. Epigenetics. 2017 Aug 3;12(8):637–52.

370.   Szklarczyk D, Gable AL, Nastou KC, Lyon D, Kirsch R, Pyysalo S, et al. The STRING database in 2021: customizable protein–protein networks, and functional characterization of user-uploaded gene/measurement sets. Nucleic Acids Res. 2021 Jan 8;49(D1):D605–12.

371.   Shannon P, Markiel A, Ozier O, Baliga NS, Wang JT, Ramage D, et al. Cytoscape: A Software Environment for Integrated Models of Biomolecular Interaction Networks. Genome Res. 2003 Nov;13(11):2498.

372.   Reinert T, Modin C, Castano FM, Lamy P, Wojdacz TK, Hansen LL, et al. Comprehensive genome methylation analysis in bladder cancer: Identification and validation of novel methylated genes and application of these as urinary tumor markers. Clin Cancer Res. 2011 Sep 1;17(17):5582–92.

373.   Chernoff MB, Demanelis K, Gillard M, Delgado D, Griend DJ Vander, Pierce BL. Abstract 160: Identifying differential methylation patterns of benign and tumor prostate tissue in African American and European American prostate cancer patients. Cancer Res. 2020 Aug 15;80(16_Supplement):160–160.

374.   Tarr IS, McCann EP, Benyamin B, Peters TJ, Twine NA, Zhang KY, et al. Monozygotic twins and triplets discordant for amyotrophic lateral sclerosis display differential methylation and gene expression. Sci Reports 2019 91. 2019 Jun 4;9(1):1–17.

375.   Andersen CL, Jensen JL, Ørntoft TF. Normalization of real-time quantitative reverse transcription-PCR data: A model-based variance estimation approach to identify genes suited for normalization, applied to bladder and colon cancer data sets. Cancer Res. 2004 Aug 1;64(15):5245–50.

376.   Locquet M, Spoor D, Crijns A, van der Harst P, Eraso A, Guedea F, et al. Subclinical Left Ventricular Dysfunction Detected by Speckle-Tracking Echocardiography in Breast Cancer Patients Treated With Radiation Therapy: A Six-Month Follow-Up Analysis (MEDIRAD EARLY-HEART study)   [Internet]. Vol. 12, Frontiers in Oncology . 2022.

377.   Nader M, Westendorp B, Hawari O, Salih M, Stewart AFR, Leenen FHH, et al. Tail-anchored membrane protein SLMAP is a novel regulator of cardiac function at the sarcoplasmic reticulum. Am J Physiol - Hear Circ Physiol. 2012 Mar;302(5):1138–45.

378.   Nader M. The SLMAP/Striatin complex: An emerging regulator of normal and abnormal cardiac excitation-contraction coupling [Internet]. Vol. 858, European Journal of Pharmacology. Elsevier B.V.; 2019. p. 172491.

379. Franceschini N, Muallem H, Rose KM, Boerwinkle E, Maeda N. Low density lipoprotein receptor polymorphisms and the risk of coronary heart disease: The Atherosclerosis Risk in Communities Study. Vol. 7, Journal of Thrombosis and Haemostasis. NIH Public Access; 2009. p. 496–8.

380. Wilker E, Mittleman MA, Litonjua AA, Poon A, Baccarelli A, Suh H, et al. Postural Changes in Blood Pressure Associated with Interactions between Candidate Genes for Chronic Respiratory Diseases and Exposure to Particulate Matter. Environ Health Perspect. 2009 Jun;117(6):935–40.

381. Sankar N, Detombe PP, Mignery GA. Calcineurin-NFATc regulates type 2 inositol 1,4,5-trisphosphate receptor (InsP3R2) expression during cardiac remodeling. J Biol Chem. 2014 Feb 28;289(9):6188.

382. Chen CP, Chang SY, Lin CJ, Chern SR, Wu PS, Chen SW, et al. Prenatal diagnosis of a familial 5p14.3-p14.1 deletion encompassing CDH18, CDH12, PMCHL1, PRDM9 and CDH10 in a fetus with congenital heart disease on prenatal ultrasound. Taiwan J Obstet Gynecol. 2018 Oct 1;57(5):734–8.

383. Soemedi R, Wilson IJ, Bentham J, Darlay R, Töpf A, Zelenika D, et al. Contribution of global rare copy-number variants to the risk of sporadic congenital heart disease. Am J Hum Genet. 2012 Sep 7;91(3):489–501.

384. Zhang Q, Chen J, Qin Y, Wang J, Zhou L. Mutations in voltage-gated L-type calcium channel: Implications in cardiac arrhythmia. Vol. 12, Channels. Taylor and Francis Inc.; 2018. p. 201–18.

385. Wang X, Sun CL, Quiñones-Lombraña A, Singh P, Landier W, Hageman L, et al. CELF4 variant and anthracycline-related cardiomyopathy: A children's oncology group genome-wide association study. J Clin Oncol. 2016 Mar 10;34(8):863–70.

386. Movassagh M, Bicknell KA, Brooks G. Characterisation and regulation of E2F-6 and E2F-6b in the rat heart: a potential target for myocardial regeneration? J Pharm Pharmacol. 2006 Jan;58(1):73–82.

387. Westendorp B, Major JL, Nader M, Salih M, Leenen FHH, Tuana BS. The E2F6 repressor activates gene expression in myocardium resulting in dilated cardiomyopathy. FASEB J. 2012 Jun;26(6):2569–79.

388. Wang B, Gu TX, Yu FM, Zhang GW, Zhao Y. Overexpression of miR-210 promotes the potential of cardiac stem cells against hypoxia. Scand Cardiovasc J. 2018 Nov 2;52(6):367–71.

389. Ramadan R, Vromans E, Anang DC, Goetschalckx I, Hoorelbeke D, Decrock E, et al. Connexin43 Hemichannel Targeting With TAT-Gap19 Alleviates Radiation-Induced Endothelial Cell Damage. Front Pharmacol. 2020 Mar 5;11:212.

390. Piroth MD, Baumann R, Budach W, Dunst J, Feyer P, Fietkau R, et al. Heart toxicity from breast cancer radiotherapy: Current findings, assessment, and prevention. Strahlentherapie und Onkol. 2019 Jan 21;195(1).

391. Koturbash I, Jadavji NM, Kutanzi K, Rodriguez-Juarez R, Kogosov D, Metz GAS, et al. Fractionated low-dose exposure to ionizing radiation leads to DNA damage, epigenetic dysregulation, and behavioral impairment. Environ Epigenetics. 2016 Dec 1;2(4).

392. Maierhofer A, Flunkert J, Dittrich M, Müller T, Schindler D, Nanda I, et al. Analysis of global DNA methylation changes in primary human fibroblasts in the early phase following X-ray irradiation. PLoS One. 2017 May 1;12(5):e0177442.

393. Li D-X, Fei X-R, Dong Y-F, Cheng C-D, Yang Y, Deng X-F, et al. The long non-coding RNA CRNDE acts as a ceRNA and promotes glioma malignancy by preventing miR-136-5p-mediated downregulation of Bcl-2 and Wnt2 [Internet]. 2017.

394. HU C-X. Relationship between global DNA methylation and hydroxymethylation levels in peripheral blood of elderly patients with myocardial infarction and the degree of coronary atherosclerosis. J Shanghai Jiaotong Univ (Medical Sci. 2018;769–74.

395. Guarrera S, Fiorito G, Onland-Moret NC, Russo A, Agnoli C, Allione A, et al. Gene-specific DNA methylation profiles and LINE-1 hypomethylation are associated with myocardial infarction risk. Clin Epigenetics. 2015;7(1):133.

396. Yao Y, Chen L-F, Li J, Chen J, Tian X-L, Wang H, et al. Altered DNA Methylation and Gene Expression Profiles in Radiation-Induced Heart Fibrosis of Sprague-Dawley Rats. Radiat Res. 2022 Apr 27;

397. Yan X, Huang Y, Wu J. Identify cross talk between circadian rhythm and coronary heart disease by multiple correlation analysis. J Comput Biol. 2018;25(12):1312–27.

398. Gibson EM, Williams III WP, Kriegsfeld LJ. Aging in the circadian system: considerations for health, disease prevention and longevity. Exp Gerontol. 2009;44(1–2):51–6.

399. Cong X, Kong W. Endothelial tight junctions and their regulatory signaling pathways in vascular homeostasis and disease. Cell Signal. 2020;66:109485.

400. Nikolaev VO, Moshkov A, Lyon AR, Miragoli M, Novak P, Paur H, et al. β2-adrenergic receptor redistribution

in heart failure changes cAMP compartmentation. Science (80-). 2010;327(5973):1653–7.

401. Communal C, Colucci WS. The control of cardiomyocyte apoptosis via the beta-adrenergic signaling pathways. Arch Mal Coeur Vaiss. 2005;98(3):236–41.

402. Packer M. Longevity genes, cardiac ageing, and the pathogenesis of cardiomyopathy: implications for understanding the effects of current and future treatments for heart failure. Eur Heart J. 2020;41(39):3856–61.

403. Mokhles MM, Trifirò G, Dieleman JP, Haag MD, van Soest EM, Verhamme KMC, et al. The risk of new onset heart failure associated with dopamine agonist use in Parkinson's disease. Pharmacol Res. 2012;65(3):358–64.

404. Yamaguchi T, Sumida TS, Nomura S, Satoh M, Higo T, Ito M, et al. Cardiac dopamine D1 receptor triggers ventricular arrhythmia in chronic heart failure. Nat Commun. 2020;11(1):4364.

405. Azimzadeh O, Moertl S, Ramadan R, Baselet B, Laiakis EC, Sebastian S, et al. Application of radiation omics in the development of adverse outcome pathway networks: an example of radiation-induced cardiovascular disease. Int J Radiat Biol. 2022 Aug 17;1–30.

406. Juárez Olguín H, Calderón Guzmán D, Hernández García E, Barragán Mejía G. The role of dopamine and its dysfunction as a consequence of oxidative stress. Oxid Med Cell Longev. 2016;2016.

407. Corbi G, Conti V, Russomanno G, Longobardi G, Furgi G, Filippelli A, et al. Adrenergic signaling and oxidative stress: a role for sirtuins? Front Physiol. 2013;4:324.

408. Wilking M, Ndiaye M, Mukhtar H, Ahmad N. Circadian rhythm connections to oxidative stress: implications for human health. Antioxid Redox Signal. 2013;19(2):192–208.

409. Andersson L, Cinato M, Mardani I, Miljanovic A, Arif M, Koh A, et al. Glucosylceramide synthase deficiency in the heart compromises β1-adrenergic receptor trafficking. Eur Heart J. 2021 Nov 14;42(43):4481–92.

410. Ramadan R, Baatout S, Aerts A, Leybaert L. The role of connexin proteins and their channels in radiation-induced atherosclerosis. Cell Mol Life Sci. 2021 Apr 1;78(7):3087–103.

411. Gredilla R, Barja G. Minireview: The Role of Oxidative Stress in Relation to Caloric Restriction and Longevity. Endocrinology. 2005 Sep 1;146(9):3713–7.

412. Guzzo RM, Salih M, Moore ED, Tuana BS. Molecular properties of cardiac tail-anchored membrane protein SLMAP are consistent with structural role in arrangement of excitation-contraction coupling apparatus. Am J Physiol - Hear Circ Physiol. 2005 Apr;288(4 57-4):1810–9.

413. Nazarenko MS, Markov A V, Lebedev IN, Freidin MB, Sleptcov AA, Koroleva IA, et al. A Comparison of Genome-Wide DNA Methylation Patterns between Different Vascular Tissues from Patients with Coronary Heart Disease. PLoS One. 2015 Apr 9;10(4):e0122601.

414. Mia MM, Singh MK. The Hippo Signaling Pathway in Cardiac Development and Diseases. Vol. 7, Frontiers in Cell and Developmental Biology. Frontiers Media S.A.; 2019.

415. Yamamoto S, Yang G, Zablocki D, Liu J, Hong C, Kim SJ, et al. Activation of Mst1 causes dilated cardiomyopathy by stimulating apoptosis without compensatory ventricular myocyte hypertrophy. J Clin Invest. 2003;111(10):1463–74.

416. Bertini E, Oka T, Sudol M, Strano S, Blandino G. At the crossroad between transformation and tumor suppression [Internet]. Vol. 8, Cell Cycle. Taylor and Francis Inc.; 2009. p. 49–57.

417. Jones PA. Functions of DNA methylation: islands, start sites, gene bodies and beyond. Nat Rev Genet. 2012 Jul 29;13(7):484–92.

418. Jjingo D, Conley AB, Yi S V., Lunyak V V., Jordan IK, King Jordan I. On the presence and role of human gene-body DNA methylation. Oncotarget. 2012 Apr 9;3(4):462–74.

419. Spainhour JCG, Lim HS, Yi S V., Qiu P. Correlation Patterns Between DNA Methylation and Gene Expression in The Cancer Genome Atlas. Cancer Inform. 2019 Feb 1;18.

420. Beltrami CM, dos Reis MB, Barros-Filho MC, Marchi FA, Kuasne H, Pinto CAL, et al. Integrated data analysis reveals potential drivers and pathways disrupted by DNA methylation in papillary thyroid carcinomas. Clin Epigenetics. 2017 May 2;9(1):1–11.

421. Luan ZM, Zhang H, Qu XL. Prediction efficiency of PITX2 DNA methylation for prostate cancer survival. Genet Mol Res. 2016 Apr 25;15(2).

422. Li B, Feng Z-H, Sun H, Zhao Z-H, Yang S-B, Yang P. The blood genome-wide DNA methylation analysis reveals novel epigenetic changes in human heart failure. Eur Rev Med Pharmacol Sci. 2017 Apr;21(8):1828–36.

423. Varley KE, Gertz J, Bowling KM, Parker SL, Reddy TE, Pauli-Behn F, et al. Dynamic DNA methylation across

diverse human cell lines and tissues. Genome Res. 2013 Mar;23(3):555–67.

424. Kulis M, Heath S, Bibikova M, Queirós AC, Navarro A, Clot G, et al. Epigenomic analysis detects widespread gene-body DNA hypomethylation in chronic lymphocytic leukemia. Nat Genet. 2012 Nov;44(11):1236–42.

425. Maunakea AK, Nagarajan RP, Bilenky M, Ballinger TJ, Dsouza C, Fouse SD, et al. Conserved role of intragenic DNA methylation in regulating alternative promoters. Nature. 2010 Jul 8;466(7303):253–7.

426. Yang Q, Wu F, Wang F, Cai K, Zhang Y, Sun Q, et al. Impact of DNA methyltransferase inhibitor 5-azacytidine on cardiac development of zebrafish in vivo and cardiomyocyte proliferation, apoptosis, and the homeostasis of gene expression in vitro. J Cell Biochem. 2019 Oct 1;120(10):17459–71.

427. Chu Q, Li A, Chen X, Qin Y, Sun X, Li Y, et al. Overexpression of miR-135b attenuates pathological cardiac hypertrophy by targeting CACNA1C. Int J Cardiol. 2018 Oct 15;269:235–41.

428. Li Z, Wang X, Wang W, Du J, Wei J, Zhang Y, et al. Altered long non-coding RNA expression profile in rabbit atria with atrial fibrillation: TCONS_00075467 modulates atrial electrical remodeling by sponging miR-328 to regulate CACNA1C. J Mol Cell Cardiol. 2017 Jul 1;108:73–85.

429. Deplus R, Blanchon L, Rajavelu A, Boukaba A, Defrance M, Luciani J, et al. Regulation of DNA Methylation Patterns by CK2-Mediated Phosphorylation of Dnmt3a. Cell Rep. 2014;8(3):743–53.

430. Weinberg DN, Rosenbaum P, Chen X, Barrows D, Horth C, Marunde MR, et al. Two competing mechanisms of DNMT3A recruitment regulate the dynamics of de novo DNA methylation at PRC1-targeted CpG islands. Nat Genet. 2021;53(6):794–800.

431. Chatterjee A, Stockwell PA, Rodger EJ, Duncan EJ, Parry MF, Weeks RJ, et al. Genome-wide DNA methylation map of human neutrophils reveals widespread inter-individual epigenetic variation. Sci Reports 2015 51. 2015 Nov 27;5(1):1–16.

432. Davies MN, Volta M, Pidsley R, Lunnon K, Dixit A, Lovestone S, et al. Functional annotation of the human brain methylome identifies tissue-specific epigenetic variation across brain and blood. Genome Biol. 2012 Jun 15;13(6):1–14.

433. de la Rocha C, Zaina S, Lund G. Is Any Cardiovascular Disease-Specific DNA Methylation Biomarker Within Reach? Curr Atheroscler Rep. 2020 Oct 1;22(10):1–9.

434. Veenstra C, Karlsson E, Mirwani SM, Nordenskjöld B, Fornander T, Pérez-Tenorio G, et al. The effects of PTPN2 loss on cell signalling and clinical outcome in relation to breast cancer subtype. J Cancer Res Clin Oncol. 2019 Jul 1;145(7):1845–56.

435. Nader M, Alsolme E, Alotaibi S, Alsomali R, Bakheet D, Dzimiri N. SLMAP-3 is downregulated in human dilated ventricles and its overexpression promotes cardiomyocyte response to adrenergic stimuli by increasing intracellular calcium. 2019;97(7):623–30.

436. Azimzadeh O, Azizova T, Merl-Pham J, Blutke A, Moseeva M, Zubkova O, et al. Chronic occupational exposure to ionizing radiation induces alterations in the structure and metabolism of the heart: a proteomic analysis of human formalin-fixed paraffin-embedded (FFPE) cardiac tissue. Int J Mol Sci. 2020;21(18):6832.

437. Natesan S, Maxwell JT, Hale PR, Mignery GA. Abstract 298: CaMKII-Mediated Phosphorylation of InsP3R2 Activates Hypertrophic Gene Transcription. Circ Res. 2012 Aug 3;111(suppl_1).

438. Harzheim D, Talasila A, Movassagh M, Foo RS-Y, Figg N, Bootman MD, et al. Elevated InsP3R expression underlies enhanced calcium fluxes and spontaneous extra-systolic calcium release events in hypertrophic cardiac myocytes. Channels. 2010 Jan;4(1):67–71.

439. Santulli G, Chen B, Forrester F, Wu H, Reiken S, Marks AR. Abstract 16984: Role of Inositol 1,4,5-Triphosphate Receptor 2 in Post-Ischemic Heart Failure. Circulation. 2014 Nov 25;130(suppl_2).

440. MJ O, DR I, PJ F. E2F6 negatively regulates BRCA1 in human cancer cells without methylation of histone H3 on lysine 9. J Biol Chem. 2003 Oct 24;278(43):42466–76.

441. Major JL, Dewan A, Salih M, Leddy JJ, Tuana BS. E2F6 Impairs Glycolysis and Activates BDH1 Expression Prior to Dilated Cardiomyopathy. PLoS One. 2017 Jan 1;12(1):e0170066.

442. J V, L de S-G, L L, MA B, Verheyde J, de Saint-Georges L, et al. The role of Trp53 in the transcriptional response to ionizing radiation in the developing brain. DNA Res. 2006 Jan 1;13(2):65–75.

443. Sáez JC, Retamal MA, Basilio D, Bukauskas FF, Bennett MVL. Connexin-based gap junction hemichannels: Gating mechanisms. Biochim Biophys Acta. 2005 Jun 10;1711(2):215.

444. Wong CW, Burger F, Pelli G, Mach F, Kwak BR. Dual benefit of reduced Cx43 on atherosclerosis in LDL receptor-deficient mice. Cell Commun Adhes. 2003;10(4–6):395–400.

445. Kwak BR, Veillard N, Pelli G, Mulhaupt F, James RW, Chanson M, et al. Reduced connexin43 expression inhibits

atherosclerotic lesion formation in low-density lipoprotein receptor-deficient mice. Circulation. 2003 Feb 25;107(7):1033–9.

446. Ramadan R, Vromans E, Anang DC, Decrock E, Mysara M, Monsieurs P, et al. Single and fractionated ionizing radiation induce alterations in endothelial connexin expression and channel function. Sci Rep. 2019 Dec 1;9(1).

447. Sharma P, Sahni NS, Tibshirani R, Skaane P, Urdal P, Berghagen H, et al. Early detection of breast cancer based on gene-expression patterns in peripheral blood cells. Breast Cancer Res. 2005 Jun 14;7(5):1–11.

448. Wu HC, Delgado-Cruzata L, Flom JD, Kappil M, Ferris JS, Liao Y, et al. Global methylation profiles in DNA from different blood cell types. Epigenetics. 2011;6(1):76.

449. Li L, Choi JY, Lee KM, Sung H, Park SK, Oze I, et al. DNA Methylation in Peripheral Blood: A Potential Biomarker for Cancer Molecular Epidemiology. J Epidemiol. 2012;22(5):384.

450. Zemmour H, Planer D, Magenheim J, Moss J, Neiman D, Gilon D, et al. Non-invasive detection of human cardiomyocyte death using methylation patterns of circulating DNA. Nat Commun. 2018;9(1).

451. Liu Q, Ma J, Deng H, Huang SJ, Rao J, Xu W Bin, et al. Cardiac-specific methylation patterns of circulating DNA for identification of cardiomyocyte death. BMC Cardiovasc Disord. 2020 Jun 29;20(1).

452. Scheiermann C, Frenette PS, Hidalgo A. Regulation of leucocyte homeostasis in the circulation. Cardiovasc Res. 2015 Aug 1;107(3):340.

453. Agha G, Mendelson MM, Ward-Caviness CK, Joehanes R, Huan TX, Gondalia R, et al. Blood Leukocyte DNA Methylation Predicts Risk of Future Myocardial Infarction and Coronary Heart Disease. Circulation. 2019 Aug 20;140(8):645–57.

454. Huan T, Joehanes R, Song C, Peng F, Guo Y, Mendelson M, et al. Genome-wide identification of DNA methylation QTLs in whole blood highlights pathways for cardiovascular disease. Nat Commun 2019 101. 2019 Sep 19;10(1):1–14.

455. Adams MJ, Lipshultz SE, Schwartz C, Fajardo LF, Coen V, Constine LS. Radiation-associated cardiovascular disease: Manifestations and management. In: Seminars in Radiation Oncology. W.B. Saunders; 2003. p. 346–56.

456. LeBaron TW, Kura B, Kalocayova B, Tribulova N, Slezak J. A New Approach for the Prevention and Treatment of Cardiovascular Disorders. Molecular Hydrogen Significantly Reduces the Effects of Oxidative Stress. Molecules. 2019 May 31;24(11):2076.

457. Demissei BG, Freedman G, Feigenberg SJ, Plastaras JP, Maity A, Smith AM, et al. Early Changes in Cardiovascular Biomarkers with Contemporary Thoracic Radiation Therapy for Breast Cancer, Lung Cancer, and Lymphoma. Int J Radiat Oncol. 2019 Mar 15;103(4):851–60.

458. Serrano NA, Mikkelsen R, Canada J, Mezzaroma E, Weiss E, Abbate A. BIOMARKERS OF CARDIAC INJURY IN PATIENTS UNDERGOING THORACIC RADIATION THERAPY. Int J Cardiol. 2016 Nov 11;223:507.

459. Westerman KE, Ordovás JM. DNA methylation and incident cardiovascular disease. Curr Opin Clin Nutr Metab Care. 2020 Jul 1;23(4):236–40.

460. Hai Z, Zuo W. Aberrant DNA methylation in the pathogenesis of atherosclerosis. Clin Chim Acta. 2016 May 1;456:69–74.

461. Kim GH, Ryan JJ, Archer SL. The role of redox signaling in epigenetics and cardiovascular disease. Antioxid Redox Signal. 2013 May 20;18(15):1920–36.

462. Johansson Å, Enroth S, Gyllensten U. Continuous Aging of the Human DNA Methylome Throughout the Human Lifespan. PLoS One. 2013 Jun 27;8(6):e67378.

463. Aavik E, Babu M, Ylä-Herttuala S. DNA methylation processes in atherosclerotic plaque. Atherosclerosis. 2019;281:168–79.

464. Touleimat N, Tost J. Complete pipeline for Infinium(®) Human Methylation 450K BeadChip data processing using subset quantile normalization for accurate DNA methylation estimation. Epigenomics. 2012 Jun;4(3):325–41.

465. Raudvere U, Kolberg L, Kuzmin I, Arak T, Adler P, Peterson H, et al. g: Profiler: a web server for functional enrichment analysis and conversions of gene lists (2019 update). Nucleic Acids Res. 2019 Jul 2;47(W1):W191–8.

466. Irizarry RA, Ladd-Acosta C, Wen B, Wu Z, Montano C, Onyango P, et al. The human colon cancer methylome shows similar hypo- and hypermethylation at conserved tissue-specific CpG island shores. Nat Genet 2009 412. 2009 Jan 18;41(2):178–86.

467. Ullrich M, Aßmus B, Augustin AM, Häbich H, Abeßer M, Martin Machado J, et al. SPRED2 deficiency elicits cardiac arrhythmias and premature death via impaired autophagy. J Mol Cell Cardiol. 2019 Apr 1;129:13–26.

468. Zheng D, Chen X, Li N, Sun L, Zhou Q, Shi H, et al. Differentially methylated regions in patients with rheumatic heart disease and secondary pulmonary arterial hypertension. Exp Ther Med. 2017 Aug 1;14(2):1367–72.

469. Xu S, Jiang J, Zhang Y, Chen T, Zhu M, Fang C, et al. Discovery of potential plasma protein biomarkers for acute myocardial infarction via proteomics. J Thorac Dis. 2019 Sep 1;11(9):3962.

470. Zechendorf E, O'Riordan CE, Stiehler L, Wischmeyer N, Chiazza F, Collotta D, et al. Ribonuclease 1 attenuates septic cardiomyopathy and cardiac apoptosis in a murine model of polymicrobial sepsis. JCI Insight. 2020 Apr 4;5(8).

471. Loeffen J, Elpeleg O, Smeitink J, Smeets R, Stöckler-Ipsiroglu S, Mandel H, et al. Mutations in the complex I NDUFS2 gene of patients with cardiomyopathy and encephalomyopathy. Ann Neurol. 2001 Feb 1;49(2):195–201.

472. Tardif JC, Rheaúme E, Lemieux Perreault LP, Grégoire JC, Feroz Zada Y, Asselin G, et al. Pharmacogenomic determinants of the cardiovascular effects of dalcetrapib. Circ Cardiovasc Genet. 2015 Apr 4;8(2):372–82.

473. Rautureau Y, Deschambault V, Brand G, Higgins M-E, Mecteau M, Uy K, et al. Abstract 184: Adenylate Cyclase Type 9 Promotes Atherosclerosis in Mice. Arterioscler Thromb Vasc Biol. 2017 May;37(suppl_1).

474. Rautureau Y, Berlatie M, Rivas D, Uy K, Blanchette A, Miquel G, et al. Adenylate cyclase type 9 antagonizes cAMP accumulation and regulates endothelial signalling involved in atheroprotection. Cardiovasc Res. 2022 May 16;

475. Rautureau Y, Y R, V D, MÈ H, D RR, M M, et al. ADCY9 (Adenylate Cyclase Type 9) Inactivation Protects From Atherosclerosis Only in the Absence of CETP (Cholesteryl Ester Transfer Protein). Circulation. 2018 Oct 16;138(16):1677–92.

476. Marinković G, Koenis S, De Camp L, Jablonowski R, Graber N, de Waard V, et al. S100A9 Links Inflammation and Repair in Myocardial Infarction. Circ Res. 2020 Aug 14;127(5):664–76.

477. Ionita MG, Vink A, Dijke IE, Laman JD, Peeters W, Van Der Kraak PH, et al. High levels of myeloid-related protein 14 in human atherosclerotic plaques correlate with the characteristics of rupture-prone lesions. Arterioscler Thromb Vasc Biol. 2009 Aug 1;29(8):1220–7.

478. Healy AM, Pickard MD, Pradhan AD, Wang Y, Chen Z, Croce K, et al. Platelet expression profiling and clinical validation of myeloid-related protein-14 as a novel determinant of cardiovascular events. Circulation. 2006 May 16;113(19):2278–84.

479. Zhang XQ, Moorman JR, Ahlers BA, Carl LL, Lake DE, Song J, et al. Phospholemman overexpression inhibits Na+-K+-ATPase in adult rat cardiac myocytes: relevance to decreased Na+ pump activity in postinfarction myocytes. J Appl Physiol. 2006 Jan;100(1):212–20.

480. Mirza MA, Lane S, Yang Z, Karaoli T, Akosah K, Hossack J, et al. Phospholemman Deficiency in Postinfarct Hearts: Enhanced Contractility but Increased Mortality. Clin Transl Sci. 2012 Jun;5(3):235.

481. Jia LG, Donnet C, Bogaev RC, Blatt RJ, McKinney CE, Day KH, et al. Hypertrophy, increased ejection fraction, and reduced Na-K-ATPase activity in phospholemman-deficient mice. Am J Physiol Heart Circ Physiol. 2005 Apr;288(4).

482. Cuomo M, Florio E, Della Monica R, Costabile D, Buonaiuto M, Di Risi T, et al. Epigenetic remodelling of Fxyd1 promoters in developing heart and brain tissues. Sci Reports 2022 121. 2022 Apr 19;12(1):1–11.

483. Moosavi SM, Reyk D van, Bartolo B Di, Tang O, Bubb KJ, Figtree GA. Abstract 16286: Absence of Fxyd1 is Associated With a Female-specific Pro-inflammatory and Hypercholesterolemic Environment: Implications for Atherosclerosis. Circulation. 2020 Nov 17;142(Suppl_3).

484. Jevnikar Z, Obermajer N, Bogyo M, Kos J. The role of cathepsin X in the migration and invasiveness of T lymphocytes. J Cell Sci. 2008 Aug 15;121(Pt 16):2652–61.

485. Obermajer N, Repnik U, Jevnikar Z, Turk B, Kreft M, Kos J. Cysteine protease cathepsin X modulates immune response via activation of β2 integrins. Immunology. 2008 May;124(1):76.

486. Davignon D, Martz E, Reynolds T, Kürzinger K, Springer TA. Lymphocyte function-associated antigen 1 (LFA-1): A surface antigen distinct from Lyt-2,3 that participates in T lymphocyte-mediated killing. Proc Natl Acad Sci U S A. 1981;78(7 I):4535–9.

487. Cao Y, Yang F, Tang C, Hu S, Zabel BA, Zhu L. Genetic Deletion of CCRL2 Impairs Macrophage Accumulation in Arterial Intima and Attenuates Atherosclerotic Plaque Development. Blood. 2015 Dec 3;126(23).

488. Hu S, Zhu L. Abstract 249: Increased Vascular CCRL2 Expression by Disturbed Blood Flow Promotes

Atherosclerotic Plaque Formation in ApoE Deficient Mice. Arterioscler Thromb Vasc Biol. 2016 May;36(suppl_1).

489. Quttainah M, Raveendran VV, Saleh S, Parhar R, Aljoufan M, Moorjani N, et al. Transcriptomal Insights of Heart Failure from Normality to Recovery. Biomolecules. 2022 May 23;12(5):731.

490. Camargo A, Azuaje F. Identification of dilated cardiomyopathy signature genes through gene expression and network data integration. Genomics. 2008 Dec 1;92(6):404–13.

491. Han YC, Xie HZ, Lu B, Xiang RL, Zhang HP, Li JY, et al. Lipopolysaccharide Alters the m6A Epitranscriptomic Tagging of RNAs in Cardiac Tissue. Front Mol Biosci. 2021 Jul 28;8:723.

492. Torrini C, Cubero RJ, Dirkx E, Braga L, Ali H, Prosdocimo G, et al. Common Regulatory Pathways Mediate Activity of MicroRNAs Inducing Cardiomyocyte Proliferation. Cell Rep. 2019 May 28;27(9):2759-2771.e5.

493. Torres RA, Drake DA, Solodushko V, Jadhav R, Smith E, Rocic P, et al. Slingshot isoform-specific regulation of cofilin-mediated vascular smooth muscle cell migration and neointima formation. Arterioscler Thromb Vasc Biol. 2011 Nov;31(11):2424–31.

494. Martín AS, Lee MY, Williams HC, Mizuno K, Lassègue B, Griendling KK. Dual regulation of cofilin activity by LIM kinase and slingshot-1L phosphatase controls platelet-derived growth factor-induced migration of human aortic smooth muscle cells. Circ Res. 2008 Feb 29;102(4):432–8.

495. Wang J, He J, Fan Y, Xu F, Liu Q, He R, et al. Extensive mitochondrial proteome disturbance occurs during the early stages of acute myocardial ischemia. Exp Ther Med. 2022 Jan 1;23(1):1–14.

496. Gao Q, Zhao J, Fan Z, Bao J, Sun D, Li H, et al. Cardioprotective Effect of Danshensu against Ischemic/Reperfusion Injury via c-Subunit of ATP Synthase Inhibition. Evidence-based Complement Altern Med. 2017;2017.

497. Ait-Aissa K, Blaszak SC, Beutner G, Tsaih SW, Morgan G, Santos JH, et al. Mitochondrial Oxidative Phosphorylation defect in the Heart of Subjects with Coronary Artery Disease. Sci Reports 2019 91. 2019 May 20;9(1):1–15.

498. Caporizzo MA, Chen CY, Prosser BL. Cardiac microtubules in health and heart disease. Exp Biol Med. 2019 Nov 1;244(15):1255–72.

499. Warner EF, Li Y, Li X. Targeting Microtubules for the Treatment of Heart Disease. Circ Res. 2022 May 27;130(11):1723–41.

500. Hu J, Chu Z, Han J, Zhang Q, Zhang D, Dang Y, et al. Phosphorylation-dependent mitochondrial translocation of MAP4 is an early step in hypoxia-induced apoptosis in cardiomyocytes. Cell Death Dis 2014 59. 2014 Sep 18;5(9):e1424–e1424.

501. Li L, Zhang Q, Lei X, Huang Y, Hu J. MAP4 as a New Candidate in Cardiovascular Disease. Front Physiol. 2020 Aug 26;11:1044.

502. Sajjad M, Fradley M, Sun W, Kim J, Zhao X, Pal T, et al. An Exploratory Study to Determine Whether BRCA1 and BRCA2 Mutation Carriers Have Higher Risk of Cardiac Toxicity. Genes 2017, Vol 8, Page 59. 2017 Feb 2;8(2):59.

503. Miao L, Yin RX, Yang S, Huang F, Chen WX, Cao XL. Association between single nucleotide polymorphism rs9534275 and the risk of coronary artery disease and ischemic stroke. Lipids Health Dis. 2017 Oct 5;16(1):1–9.

504. Singh S, Nguyen H, Michels D, Bazinet H, Matkar PN, Liu Z, et al. BReast CAncer susceptibility gene 2 deficiency exacerbates oxidized LDL-induced DNA damage and endothelial apoptosis. Physiol Rep. 2020 Jul 1;8(13):e14481.

505. Talukdar HA, Foroughi Asl H, Jain RK, Ermel R, Ruusalepp A, Franzén O, et al. Cross-Tissue Regulatory Gene Networks in Coronary Artery Disease. Cell Syst. 2016 Mar 23;2(3):196–208.

506. Lin BC, Sullivan R, Lee Y, Moran S, Glover E, Bradfield CA. Deletion of the aryl hydrocarbon receptor-associated protein 9 leads to cardiac malformation and embryonic lethality. J Biol Chem. 2007 Dec 7;282(49):35924–32.

507. Yamaura G, Turoczi T, Yamamoto F, Siddqui MAQ, Maulik N, Das DK. STAT signaling in ischemic heart: A role of STAT5A in ischemic preconditioning. Am J Physiol - Hear Circ Physiol. 2003 Aug 1;285(2 54-2):476–82.

508. Chen H, Jing XY, Shen YJ, Wang TL, Ou C, Lu SF, et al. Stat5-dependent cardioprotection in late remote ischaemia preconditioning. Cardiovasc Res. 2018 Apr 1;114(5):679–89.

509. Westerman K, Sebastiani P, Jacques P, Liu S, DeMeo D, Ordovás JM. DNA methylation modules associate with incident cardiovascular disease and cumulative risk factor exposure. Clin Epigenetics. 2019 Nov 20;11(1):1–14.

510. Kuzmina NS, Lapteva NS, Rubanovich A V. Hypermethylation of gene promoters in peripheral blood leukocytes in humans long term after radiation exposure. Environ Res. 2016 Apr 1;146:10–7.

511. Kuzmina NS, Lapteva NS, Rusinova GG, Azizova T V., Vyazovskaya NS, Rubanovich A V. Gene hypermethylation in blood leukocytes in humans long term after radiation exposure – Validation set. Environ Pollut. 2018 Mar 1;234:935–42.

512. Kalmár A, Péterfia B, Hollósi P, Galamb O, Spisák S, Wichmann B, et al. DNA hypermethylation and decreased mRNA expression of MAL, PRIMA1, PTGDR and SFRP1 in colorectal adenoma and cancer. BMC Cancer. 2015 Oct 19;15(1):1–14.

513. Wierzbicki PM, Adrych K, Kartanowicz D, Stanislawowski M, Kowalczyk A, Godlewski J, et al. Underexpression of LATS1 TSG in colorectal cancer is associated with promoter hypermethylation. World J Gastroenterol. 2013 Jul 7;19(27):4363.

514. Yan Y, Guo Q, Wang F, Adhikari R, Zhu Z, Zhang H, et al. Cell-Free DNA: Hope and Potential Application in Cancer   [Internet]. Vol. 9, Frontiers in Cell and Developmental Biology . 2021.

515. Kageyama S, Nihei K, Karasawa K, Sawada T, Koizumi F, Yamaguchi S, et al. Radiotherapy increases plasma levels of tumoral cell-free DNA in non-small cell lung cancer patients. Oncotarget. 2018;9(27):19368.

516. Yang Y, Zhu Y, Zhou S, Tang P, Xu R, Zhang Y, et al. TRIM27 cooperates with STK38L to inhibit ULK1-mediated autophagy and promote tumorigenesis. EMBO J. 2022 Jun 7;e109777.

517. Guha M, Srinivasan S, Raman P, Jiang Y, Kaufman BA, Taylor D, et al. Aggressive triple negative breast cancers have unique molecular signature on the basis of mitochondrial genetic and functional defects. Biochim Biophys Acta - Mol Basis Dis. 2018 Apr 1;1864(4):1060–71.

518. Wang LP, Cao J, Zhang J, Wang BY, Hu XC, Shao ZM, et al. The human chemokine receptor CCRL2 suppresses chemotaxis and invasion by blocking CCL2-induced phosphorylation of p38 MAPK in human breast cancer cells. Med Oncol. 2015 Nov 1;32(11):1–9.

519. Zhuang X, Zhang H, Li X, Li X, Cong M, Peng F, et al. Differential effects on lung and bone metastasis of breast cancer by Wnt signalling inhibitor DKK1. Nat Cell Biol. 2017;19(10):1274–85.

520. Vafeiadou V, Hany D, Picard D. Hyperactivation of MAPK Induces Tamoxifen Resistance in SPRED2-Deficient ERα-Positive Breast Cancer. Cancers 2022, Vol 14, Page 954. 2022 Feb 14;14(4):954.

521. Cotarla I, Ren S, Zhang Y, Gehan E, Singh B, Furth PA. Stat5a is tyrosine phosphorylated and nuclear localized in a high proportion of human breast cancers. Int J cancer. 2004;108(5):665–71.

522. Beetch M, Harandi-Zadeh S, Yang T, Boycott C, Chen Y, Stefanska B, et al. DNA methylation landscape of triple-negative ductal carcinoma in situ (DCIS) progressing to the invasive stage in canine breast cancer. Sci Rep. 2020 Feb 12;10(1):2415.

523. Lin X, Dinglin X, Cao S, Zheng S, Wu C, Chen W, et al. Enhancer-driven lncRNA BDNF-AS induces endocrine resistance and malignant progression of breast cancer through the RNH1/TRIM21/mTOR cascade. Cell Rep. 2020;31(10):107753.

524. Li W, Xie H, Hu H, Huang J, Chen S. PEX1 is a mediator of α1-adrenergic signaling attenuating doxorubicin-induced cardiotoxicity. J Biochem Mol Toxicol. 2022 Nov 1;36(11):e23196.

525. Daydé D, Belhadef A, Bono E, Barthé M, Lefebvre F, Mika D, et al. B-adrenergic/cAMP signaling in doxorubicin-induced cardiotoxicity. Arch Cardiovasc Dis Suppl. 2022;14(2):194.

526. Saiki H, Moulay G, Guenzel AJ, Liu W, Decklever TD, Classic KL, et al. Experimental cardiac radiation exposure induces ventricular diastolic dysfunction with preserved ejection fraction. Am J Physiol Circ Physiol. 2017 May 26;313(2):H392–407.

527. Gupta MK, Kaminski R, Mullen B, Gordon J, Burdo TH, Cheung JY, et al. HIV-1 Nef-induced cardiotoxicity through dysregulation of autophagy. Sci Rep. 2017 Dec 1;7(1).

528. Wang T, Green LA, Gupta SK, Kim C, Wang L, Almodovar S, et al. Transfer of intracellular HIV Nef to endothelium causes endothelial dysfunction. PLoS One. 2014 Mar 7;9(3).

529. Zhao W, Zhang X, Rong J. SUMOylation as a Therapeutic Target for Myocardial Infarction. Front Cardiovasc Med. 2021 Jul 28;0:814.

530. Lin QQ, Zhao J, Zheng CG, Chun J. Roles of notch signaling pathway and endothelial-mesenchymal transition in vascular endothelial dysfunction and atherosclerosis. Eur Rev Med Pharmacol Sci. 2018;22(19):6485–91.

531. Wang HM, Gao JH, Lu JL. Pravastatin improves atherosclerosis in mice with hyperlipidemia by inhibiting TREM-1/DAP12. Eur Rev Med Pharmacol Sci. 2018;22(15):4995–5003.

532. Chistiakov DA, Grechko A V, Myasoedova VA, Melnichenko AA, Orekhov AN. The role of monocytosis and

neutrophilia in atherosclerosis. J Cell Mol Med. 2018;22(3):1366–82.

533. Wang T, Yi R, Green LA, Chelvanambi S, Seimetz M, Clauss M. Increased cardiovascular disease risk in the HIV-positive population on ART: potential role of HIV-Nef and Tat. Cardiovasc Pathol. 2015;24(5):279–82.

534. Reedijk M. Notch signaling and breast cancer. Notch Signal Embryol Cancer. 2012;241–57.

535. Song X, Liu Z, Yu Z. LncRNA NEF is downregulated in triple negative breast cancer and correlated with poor prognosis. Acta Biochim Biophys Sin (Shanghai). 2019;51(4):386–92.

536. Mollinedo F. Neutrophil degranulation, plasticity, and cancer metastasis. Trends Immunol. 2019;40(3):228–42.

537. Rabellino A, Khanna KK. The implication of the SUMOylation pathway in breast cancer pathogenesis and treatment. Crit Rev Biochem Mol Biol. 2020;55(1):54–70.

538. Shabo I, Olsson H, Stål O, Svanvik J. Breast cancer expression of DAP12 is associated with skeletal and liver metastases and poor survival. Clin Breast Cancer. 2013;13(5):371–7.

539. Di Iorio P, Ronci M, Giuliani P, Caciagli F, Ciccarelli R, Caruso V, et al. Pros and Cons of Pharmacological Manipulation of cGMP-PDEs in the Prevention and Treatment of Breast Cancer. Int J Mol Sci. 2021;23(1):262.

540. Xie J, Wang Y, Ai D, Yao L, Jiang H. The role of the Hippo pathway in heart disease. FEBS J. 2022 Oct 1;289(19):5819–33.

541. Ping Z, Peng Y, Lang H, Xinyong C, Zhiyi Z, Xiaocheng W, et al. Oxidative Stress in Radiation-Induced Cardiotoxicity. Ferretti G, editor. Oxid Med Cell Longev. 2020;2020:3579143.

542. Livingston K, Schlaak RA, Puckett LL, Bergom C. The role of mitochondrial dysfunction in radiation-induced heart disease: from bench to bedside. Front Cardiovasc Med. 2020;7:20.

543. Schioppa T, Sozio F, Barbazza I, Scutera S, Bosisio D, Sozzani S, et al. Molecular Basis for CCRL2 Regulation of Leukocyte Migration   [Internet]. Vol. 8, Frontiers in Cell and Developmental Biology . 2020.

544. Liu H, Xiong W, Luo Y, Chen H, He Y, Cao Y, et al. Adipokine Chemerin Stimulates Progression of Atherosclerosis in ApoE-/- Mice. Biomed Res Int. 2019;2019.

545. Caja L, Dituri F, Mancarella S, Caballero-Diaz D, Moustakas A, Giannelli G, et al. TGF-β and the Tissue Microenvironment: Relevance in Fibrosis and Cancer. Vol. 19, International Journal of Molecular Sciences. 2018.

546. Sun Z, Schriewer J, Tang M, Marlin J, Taylor F, Shohet R V, et al. The TGF-β pathway mediates doxorubicin effects on cardiac endothelial cells. J Mol Cell Cardiol. 2016;90:129–38.

547. McCubrey JA, Steelman LS, Chappell WH, Abrams SL, Wong EWT, Chang F, et al. Roles of the Raf/MEK/ERK pathway in cell growth, malignant transformation and drug resistance. Biochim Biophys Acta - Mol Cell Res. 2007 Aug 1;1773(8):1263–84.

548. Chen KC, Liao YC, Wang JY, Lin YC, Chen CH, Juo SHH. Oxidized low-density lipoprotein is a common risk factor for cardiovascular diseases and gastroenterological cancers via epigenomical regulation of microRNA-210. Oncotarget. 2015 Sep 9;6(27):24105.

549. Eken SM, Jin H, Chernogubova E, Li Y, Simon N, Sun C, et al. MicroRNA-210 enhances fibrous cap stability in advanced atherosclerotic lesions. Circ Res. 2017 Feb 17;120(4):633–44.

550. Cheung JY, Zhang XQ, Song J, Gao E, Chan TO, Rabinowitz JE, et al. Coordinated regulation of cardiac Na+/Ca2+ exchanger and Na+-K+-ATPase by phospholemman (FXYD1). Adv Exp Med Biol. 2013;961:175–90.

551. Bubb KJ, Tang O, Gentile C, Moosavi SM, Hansen T, Liu C-CC, et al. FXYD1 Is Protective Against Vascular Dysfunction. Hypertension. 2021 Jun 1;77(6):2104–16.

552. Sarangdhar MA, Allam R. Angiogenin (ANG)—Ribonuclease Inhibitor (RNH1) System in Protein Synthesis and Disease. Vol. 22, International Journal of Molecular Sciences. 2021.

553. Su E, Yu P, Zhang B, Zhang A, Xie S, Zhang C, et al. Endothelial Intracellular ANG (Angiogenin) Protects Against Atherosclerosis by Decreasing Endoplasmic Reticulum Stress. Arterioscler Thromb Vasc Biol. 2022 Mar 1;42(3):305–25.

554. Roddie H, Fragiadaki M, Evans P. BS28 Endothelial STAT5A is enriched at atheroprone regions of the aorta and drives inflammation in response to low shear stress. Heart. 2019 May 1;105(Suppl 6):A158–A158.

555. Wang X, Ding X, Yan J, Lu Z, Cao H, Ni X, et al. STAT5 inhibitor attenuates atherosclerosis via inhibition of inflammation: the role of STAT5 in atherosclerosis. Am J Transl Res. 2021;13(3):1422.

556. Azimzadeh O, Scherthan H, Sarioglu H, Barjaktarovic Z, Conrad M, Vogt A, et al. Rapid proteomic remodeling of cardiac tissue caused by total body ionizing radiation. Proteomics. 2011;11(16):3299–311.

557. Barjaktarovic Z, Merl-Pham J, Braga-Tanaka I, Tanaka S, Hauck SM, Saran A, et al. Hyperacetylation of cardiac

mitochondrial proteins is associated with metabolic impairment and sirtuin downregulation after chronic total body irradiation of ApoE-/-mice. Int J Mol Sci. 2019;20(20):5239.

558. Azimzadeh O, Subramanian V, Sievert W, Merl-Pham J, Oleksenko K, Rosemann M, et al. Activation of PPARα by Fenofibrate Attenuates the Effect of Local Heart High Dose Irradiation on the Mouse Cardiac Proteome. Biomedicines. 2021 Dec 1;9(12):1845.

559. Barjaktarovic Z, Schmaltz D, Shyla A, Azimzadeh O, Schulz S, Haagen J, et al. Radiation–induced signaling results in mitochondrial impairment in mouse heart at 4 weeks after exposure to X-rays. PLoS One. 2011;6(12):e27811.

560. Barjaktarovic Z, Shyla A, Azimzadeh O, Schulz S, Haagen J, Dörr W, et al. Ionising radiation induces persistent alterations in the cardiac mitochondrial function of C57BL/6 mice 40 weeks after local heart exposure. Radiother Oncol. 2013;106(3):404–10.

561. Azimzadeh O, Sievert W, Sarioglu H, Yentrapalli R, Barjaktarovic Z, Sriharshan A, et al. PPAR alpha: a novel radiation target in locally exposed Mus musculus heart revealed by quantitative proteomics. J Proteome Res. 2013;12(6):2700–14.

562. Bakshi M V, Barjaktarovic Z, Azimzadeh O, Kempf SJ, Merl J, Hauck SM, et al. Long-term effects of acute low-dose ionizing radiation on the neonatal mouse heart: a proteomic study. Radiat Environ Biophys. 2013;52(4):451–61.

563. Azimzadeh O, Azizova T, Merl-Pham J, Subramanian V, Bakshi M V., Moseeva M, et al. A dose-dependent perturbation in cardiac energy metabolism is linked to radiation-induced ischemic heart disease in Mayak nuclear workers. Oncotarget. 2017;8(6):9067–78.

564. Azimzadeh O, Sievert W, Sarioglu H, Merl-Pham J, Yentrapalli R, Bakshi M V., et al. Integrative proteomics and targeted transcriptomics analyses in cardiac endothelial cells unravel mechanisms of long-term radiation-induced vascular dysfunction. J Proteome Res. 2015 Feb 6;14(2):1203–19.

565. Subramanian V, Seemann I, Merl-Pham J, Hauck SM, Stewart FA, Atkinson MJ, et al. Role of TGF beta and PPAR alpha signaling pathways in radiation response of locally exposed heart: integrated global transcriptomics and proteomics analysis. J Proteome Res. 2017 Jan 6;16(1):307–18.

566. Subramanian V, Borchard S, Azimzadeh O, Sievert W, Merl-Pham J, Mancuso M, et al. PPARα is necessary for radiation-induced activation of noncanonical TGFβ signaling in the heart. J Proteome Res. 2018;17(4):1677–89.

567. Patel AP, Fisher JL, Nichols E, Abd-Allah F, Abdela J, Abdelalim A, et al. Global, regional, and national burden of brain and other CNS cancer, 1990–2016: a systematic analysis for the Global Burden of Disease Study 2016. Lancet Neurol. 2019 Apr 1;18(4):376–93.

568. Louis DN, Perry A, Wesseling P, Brat DJ, Cree IA, Figarella-Branger D, et al. The 2021 WHO classification of tumors of the central nervous system: a summary. Neuro Oncol. 2021;23(8):1231–51.

569. Tamimi AF, Juweid M. Epidemiology and Outcome of Glioblastoma. Glioblastoma. 2017 Sep 27;143–53.

570. Tan AC, Ashley DM, López GY, Malinzak M, Friedman HS, Khasraw M. Management of glioblastoma: State of the art and future directions. CA Cancer J Clin. 2020 Jul 1;70(4):299–312.

571. Hanif F, Muzaffar K, Perveen K, Malhi SM, Simjee SU. Glioblastoma Multiforme: A Review of its Epidemiology and Pathogenesis through Clinical Presentation and Treatment. Asian Pac J Cancer Prev. 2017;18(1):3.

572. Krieger TG, Tirier SM, Park J, Jechow K, Eisemann T, Peterziel H, et al. Modeling glioblastoma invasion using human brain organoids and single-cell transcriptomics. Neuro Oncol. 2020 Aug 17;22(8):1138–49.

573. Jovčevska I, Zottel A, Šamec N, Paska AV. Coding of Glioblastoma Progression and Therapy Resistance through Long Noncoding RNAs. Cancers (Basel). 2020 Jul 1;12(7):1–23.

574. Rezaei O, Honarmand K, Nateghinia S, Taheri M, Ghafouri-Fard S. miRNA signature in glioblastoma: Potential biomarkers and therapeutic targets. Exp Mol Pathol. 2020 Dec 1;117:104550.

575. Peng Z, Liu C, Wu M. New insights into long noncoding RNAs and their roles in glioma. Mol Cancer. 2018 Feb 19;17(1):1–10.

576. Rutenberg-Schoenberg M, Sexton AN, Simon MD. The Properties of Long Noncoding RNAs That Regulate Chromatin. http://dx.doi.org/101146/annurev-genom-090314-024939. 2016 Aug 31;17:69–94.

577. Balas MM, Johnson AM. Exploring the mechanisms behind long noncoding RNAs and cancer. Non-coding RNA Res. 2018 Sep 1;3(3):108–17.

578. Yao Q, Chen Y, Zhou X. The roles of microRNAs in epigenetic regulation. Curr Opin Chem Biol. 2019 Aug 1;51:11–7.

579. Yang X, Kui L, Tang M, Li D, Wei K, Chen W, et al. High-Throughput Transcriptome Profiling in Drug and Biomarker Discovery. Front Genet. 2020 Feb 5;11:19.

580. Thomas E, Thankan RS, Purushottamachar P, Huang W, Kane MA, Zhang Y, et al. Transcriptome profiling reveals that VNPP433-3β, the lead next-generation galeterone analog inhibits prostate cancer stem cells by downregulating epithelial–mesenchymal transition and stem cell markers. Mol Carcinog. 2022 Jul 1;61(7):643–54.

581. Richardson S, Tseng GC, Sun W. Statistical Methods in Integrative Genomics. Annu Rev Stat its Appl. 2016 Jun 1;3:181.

582. Ye Z, Ke H, Chen S, Cruz-Cano R, He X, Zhang J, et al. Biomarker Categorization in Transcriptomic Meta-Analysis by Concordant Patterns With Application to Pan-Cancer Studies. Front Genet. 2021 Jul 2;12.

583. Barrett T, Wilhite SE, Ledoux P, Evangelista C, Kim IF, Tomashevsky M, et al. NCBI GEO: archive for functional genomics data sets--update. Nucleic Acids Res. 2013 Jan 1;41(Database issue).

584. Gill BJ, Pisapia DJ, Malone HR, Goldstein H, Lei L, Sonabend A, et al. MRI-localized biopsies reveal subtype-specific differences in molecular and cellular composition at the margins of glioblastoma. Proc Natl Acad Sci U S A. 2014 Aug 26;111(34):12550–5.

585. Stathias V, Pastori C, Griffin TZ, Komotar R, Clarke J, Zhang M, et al. Identifying Glioblastoma Gene Networks Based on Hypergeometric Test Analysis. PLoS One. 2014 Dec 31;9(12):e115842.

586. Yuan Y, Jiaoming L, Xiang W, Yanhui L, Shu J, Maling G, et al. Analyzing the interactions of mRNAs, miRNAs, lncRNAs and circRNAs to predict competing endogenous RNA networks in glioblastoma. J Neurooncol. 2018 May 1;137(3):493–502.

587. Hwang T, Kim S, Chowdhury T, Yu HJ, Kim KM, Kang H, et al. Genome-wide perturbations of Alu expression and Alu-associated post-transcriptional regulations distinguish oligodendroglioma from other gliomas. Commun Biol 2022 51. 2022 Jan 18;5(1):1–10.

588. Leinonen R, Sugawara H, Shumway M. The sequence read archive. Nucleic Acids Res. 2011 Jan;39(Database issue).

589. Han Z, Hua J, Xue W, Zhu F. Integrating the Ribonucleic Acid Sequencing Data From Various Studies for Exploring the Multiple Sclerosis-Related Long Noncoding Ribonucleic Acids and Their Functions. Front Genet. 2019 Nov 12;10.

590. Fang S, Zhang L, Guo J, Niu Y, Wu Y, Li H, et al. NONCODEV5: a comprehensive annotation database for long non-coding RNAs. Nucleic Acids Res. 2018 Jan 1;46(D1):D308–14.

591. Aken BL, Achuthan P, Akanni W, Amode MR, Bernsdorff F, Bhai J, et al. Ensembl 2017. Nucleic Acids Res. 2017 Jan 4;45(D1):D635–42.

592. Bray NL, Pimentel H, Melsted P, Pachter L. Near-optimal probabilistic RNA-seq quantification. Nat Biotechnol 2016 345. 2016 Apr 4;34(5):525–7.

593. Kim HSH, Kim JJ-HH, Kim SY, Jo D, Park HJ, Kim JJ-HH, et al. Meta-Analysis of Large-Scale Toxicogenomic Data Finds Neuronal Regeneration Related Protein and Cathepsin D to Be Novel Biomarkers of Drug-Induced Toxicity. PLoS One. 2015 Sep 3;10(9):e0136698.

594. Szajewska H, Kołodziej M. Systematic review with meta-analysis: Saccharomyces boulardii in the prevention of antibiotic-associated diarrhoea. Aliment Pharmacol Ther. 2015 Oct 1;42(7):793–801.

595. Zhao H, Shi J, Zhang Y, Xie A, Yu L, Zhang C, et al. LncTarD: a manually-curated database of experimentally-supported functional lncRNA–target regulations in human diseases. Nucleic Acids Res. 2020 Jan 8;48(D1):D118–26.

596. Cheng L, Wang P, Tian R, Wang S, Guo Q, Luo M, et al. LncRNA2Target v2.0: a comprehensive database for target genes of lncRNAs in human and mouse. Nucleic Acids Res. 2019 Jan 8;47(D1):D140–4.

597. Tang G, Cho M, Wang X. OncoDB: an interactive online database for analysis of gene expression and viral infection in cancer. Nucleic Acids Res. 2022 Jan 7;50(D1):D1334–9.

598. Han J, Liu S, Sun Z, Zhang Y, Zhang F, Zhang C, et al. LncRNAs2Pathways: Identifying the pathways influenced by a set of lncRNAs of interest based on a global network propagation method. Sci Rep. 2017;7.

599. Kanehisa M, Furumichi M, Sato Y, Ishiguro-Watanabe M, Tanabe M. KEGG: integrating viruses and cellular organisms. Nucleic Acids Res. 2021 Jan 8;49(D1):D545–51.

600. Gillespie M, Jassal B, Stephan R, Milacic M, Rothfels K, Senff-Ribeiro A, et al. The reactome pathway knowledgebase 2022. Nucleic Acids Res. 2022 Jan 7;50(D1):D687–92.

601. Bader GD, Hogue CWV. An automated method for finding molecular complexes in large protein interaction

networks. BMC Bioinformatics. 2003 Jan 13;4(1):1–27.

602.   Biobank Antwerp [BB190007], BBMR-ERIC B [BIORESOURCE]. BE 71030031000. Biobank Antwerp [BB190007], BBMR-ERIC, Belgian [BIORESOURCE].;

603.   Reimand J, Kull M, Peterson H, Hansen J, Vilo J. g:Profiler—a web-based toolset for functional profiling of gene lists from large-scale experiments. Nucleic Acids Res. 2007 Jul 1;35(suppl_2):W193–200.

604.   Karagkouni D, Paraskevopoulou MD, Tastsoglou S, Skoufos G, Karavangeli A, Pierros V, et al. DIANA-LncBase v3: indexing experimentally supported miRNA targets on non-coding transcripts. Nucleic Acids Res. 2020 Jan 8;48(D1):D101–10.

605.   Hsu S Da, Lin FM, Wu WY, Liang C, Huang WC, Chan WL, et al. miRTarBase: a database curates experimentally validated microRNA–target interactions. Nucleic Acids Res. 2011 Jan 1;39(suppl_1):D163–9.

606.   Huang HY, Lin YCD, Cui S, Huang Y, Tang Y, Xu J, et al. miRTarBase update 2022: an informative resource for experimentally validated miRNA–target interactions. Nucleic Acids Res. 2022 Jan 7;50(D1):D222–30.

607.   Tondepu C, Karumbaiah L. Glycomaterials to Investigate the Functional Role of Aberrant Glycosylation in Glioblastoma. Adv Healthc Mater. 2022 Feb 1;11(4):2101956.

608.   Dan C, Pei H, Zhang B, Zheng X, Ran D, Du C. Fanconi anemia pathway and its relationship with cancer. Genome Instab Dis. 2021;2(3):175–83.

609.   de Souza Fonseca PA, Suárez-Vega A, Cánovas A. Unrevealing functional candidate genes for bovine fertility through RNA sequencing meta-analysis and regulatory elements networks of co-expressed genes and lncRNAs. Funct Integr Genomics. 2022;

610.   Cheung MW-L, Vijayakumar R. A Guide to Conducting a Meta-Analysis. Neuropsychol Rev. 2016;26(2):121–8.

611.   Liu D-H, Yang X, Guo J-F, Meng H, Shen S-H. Immune-related lncRNAs, LINC01268 and CTB-31O20. 2, as favorable prognostic markers for glioma inhibition. Transl Cancer Res. 2022;11(4):823–34.

612.   Brockhausen I. Pathways of O-glycan biosynthesis in cancer cells. Biochim Biophys Acta - Gen Subj. 1999;1473(1):67–95.

613.   Cervoni GE, Cheng JJ, Stackhouse KA, Heimburg-Molinaro J, Cummings RD. O-glycan recognition and function in mice and human cancers. Biochem J. 2020 Apr 29;477(8):1541–64.

614.   Kudelka MR, Ju T, Heimburg-Molinaro J, Cummings RD. Simple sugars to complex disease—mucin-type O-glycans in cancer. Adv Cancer Res. 2015;126:53–135.

615.   Rominiyi O, Myers K, Gomez-Roman N, Lad N, Dar D, Jellinek D, et al. RDNA-12. THE FANCONI ANAEMIA (FA) PATHWAY AND GLIOBLASTOMA: A NEW FOUNDATION FOR DNA DAMAGE RESPONSE TARGETED COMBINATIONS. Neuro Oncol. 2019 Nov 11;21(Supplement_6):vi209–vi209.

616.   de Groot J, Sontheimer H. Glutamate and the biology of gliomas. Glia. 2011 Aug 1;59(8):1181–9.

617.   Zhang C, Yuan X, Li H, Zhao Z, Liao Y, Wang X, et al. Anti-Cancer Effect of Metabotropic Glutamate Receptor 1 Inhibition in Human Glioma U87 Cells: Involvement of PI3K/Akt/mTOR Pathway. Cell Physiol Biochem. 2015;35(2):419–32.

618.   Tirrò E, Massimino M, Romano C, Martorana F, Pennisi MS, Stella S, et al. Prognostic and Therapeutic Roles of the Insulin Growth Factor System in Glioblastoma   [Internet]. Vol. 10, Frontiers in Oncology . 2021.

619.   Bao S, Wu Q, Li Z, Sathornsumetee S, Wang H, McLendon RE, et al. Targeting cancer stem cells through L1CAM suppresses glioma growth. Cancer Res. 2008;68(15):6043–8.

620.   Wachowiak R, Krause M, Mayer S, Peukert N, Suttkus A, Müller WC, et al. Increased L1CAM (CD171) levels are associated with glioblastoma and metastatic brain tumors. Medicine (Baltimore). 2018;97(38).

621.   Koneru T, McCord E, Pawar S, Tatiparti K, Sau S, Iyer AK. Transferrin: Biology and Use in Receptor-Targeted Nanotherapy of Gliomas. ACS Omega. 2021 Apr 6;6(13):8727–33.

622.   Hong L, Ye L. The interferon-γ receptor pathway: a new way to regulate CAR T cell-solid tumor cell adhesion. Signal Transduct Target Ther. 2022;7(1):315.

623.   Nayani R, Ashktorab H, Brim H, Laiyemo AO. Genetic Basis for Colorectal Cancer Disparities. Curr Colorectal Cancer Rep. 2015;11(6):408–13.

624.   Scholz BA, Sumida N, de Lima CDM, Chachoua I, Martino M, Tzelepis I, et al. WNT signaling and AHCTF1 promote oncogenic MYC expression through super-enhancer-mediated gene gating. Nat Genet. 2019;51(12):1723–31.

625.   Ma Z-H, Shi P-D, Wan B-S. MiR-410-3p activates the NF-κB pathway by targeting ZCCHC10 to promote migration, invasion and EMT of colorectal cancer. Cytokine. 2021;140:155433.

626.   Mehmood R, Jibiki K, Alsafwani ZJ, Naseem M, Yasuhara N. Systems genomics of nucleoporins provides

prognostic insights into breast cancer. Adv Life Sci. 2022;9(1):98.

627. Dadey DYA, Kapoor V, Khudanyan A, Urano F, Kim AH, Thotala D, et al. The ATF6 pathway of the ER stress response contributes to enhanced viability in glioblastoma. Oncotarget. 2016;7(2):2080.

628. Popp MW, Maquat LE. Nonsense-mediated mRNA decay and cancer. Curr Opin Genet Dev. 2018 Feb 1;48:44–50.

629. Gudikote JP, Cascone T, Poteete A, Sitthideatphaiboon P, Wu Q, Morikawa N, et al. Inhibition of nonsense-mediated decay rescues p53β/γ isoform expression and activates the p53 pathway in MDM2-overexpressing and select p53-mutant cancers. J Biol Chem. 2021 Nov 1;297(5):101163.

630. McCarthy RC, Kosman DJ. Glial cell ceruloplasmin and hepcidin differentially regulate iron efflux from brain microvascular endothelial cells. PLoS One. 2014 Feb 12;9(2).

631. McCarthy RC, Kosman DJ. Activation of C6 glioblastoma cell ceruloplasmin expression by neighboring human brain endothelia-derived interleukins in an in vitro blood-brain barrier model system. Cell Commun Signal. 2014 Oct 14;12(1):1–11.

632. Fan CD, Fu XY, Zhang ZY, Cao MZ, Sun JY, Yang MF, et al. Selenocysteine induces apoptosis in human glioma cells: evidence for TrxR1-targeted inhibition and signaling crosstalk. Sci Rep. 2017 Dec 1;7(1).

633. Carlisle AE, Lee N, Matthew-Onabanjo AN, Spears ME, Park SJ, Youkana D, et al. Selenium detoxification is required for cancer cellsurvival. Nat Metab. 2020 Jul 1;2(7):603.

634. Gara RK, Kumari S, Ganju A, Yallapu MM, Jaggi M, Chauhan SC. Slit/Robo pathway: a promising therapeutic target for cancer. Drug Discov Today. 2015 Jan 1;20(1):156–64.

635. Yiin J-J, Hu B, Jarzynka MJ, Feng H, Liu K-W, Wu JY, et al. Slit2 inhibits glioma cell invasion in the brain by suppression of Cdc42 activity. Neuro Oncol. 2009 Jan 1;11(6):779–89.

636. Geraldo LH, Xu Y, Jacob L, Pibouin-Fragner L, Rao R, Maissa N, et al. SLIT2/ROBO signaling in tumor-associated microglia and macrophages drives glioblastoma immunosuppression and vascular dysmorphia. J Clin Invest. 2021 Aug 16;131(16).

637. Alasiri G, Jiramongkol Y, Trakansuebkul S, Ke HL, Mahmud Z, Intuyod K, et al. Reciprocal regulation between GCN2 (eIF2AK4) and PERK (eIF2AK3) through the JNK-FOXO3 axis to modulate cancer drug resistance and clonal survival. Mol Cell Endocrinol. 2020 Sep 15;515:110932.

638. Wang Y, Ning Y, Alam GN, Jankowski BM, Dong Z, Nör JE, et al. Amino acid deprivation promotes tumor angiogenesis through the GCN2/ATF4 pathway. Neoplasia (United States). 2013;15(8):989–97.

639. Chen L, He J, Zhou J, Xiao Z, Ding N, Duan Y, et al. EIF2A promotes cell survival during paclitaxel treatment in vitro and in vivo. J Cell Mol Med. 2019;23(9):6060.

640. Carballo GB, Honorato JR, de Lopes GPF, Spohr TCL de S e. A highlight on Sonic hedgehog pathway. Cell Commun Signal. 2018;16(1):11.

641. Skoda AM, Simovic D, Karin V, Kardum V, Vranic S, Serman L. The role of the Hedgehog signaling pathway in cancer: A comprehensive review. Bosn J Basic Med Sci. 2018;18(1):8.

642. Hanna A, Shevde LA. Hedgehog signaling: modulation of cancer properies and tumor mircroenvironment. Mol Cancer 2016 151. 2016 Mar 18;15(1):1–14.

643. Hung HC, Liu CC, Chuang JY, Su CL, Gean PW. Inhibition of Sonic Hedgehog Signaling Suppresses Glioma Stem-Like Cells Likely Through Inducing Autophagic Cell Death. Front Oncol. 2020 Jul 24;10:1233.

644. Melamed JR, Morgan JT, Ioele SA, Gleghorn JP, Sims-Mourtada J, Day ES. Investigating the role of Hedgehog/GLI1 signaling in glioblastoma cell response to temozolomide. Oncotarget. 2018 Jun 1;9(43):27000.

645. Qiu W, Guo X, Li B, Wang J, Qi Y, Chen Z, et al. Exosomal miR-1246 from glioma patient body fluids drives the differentiation and activation of myeloid-derived suppressor cells. Mol Ther. 2021;29(12):3449–64.

646. Li J, Yuan H, Xu H, Zhao H, Xiong N. Hypoxic Cancer-Secreted Exosomal miR-182-5p Promotes Glioblastoma Angiogenesis by Targeting Kruppel-like Factor 2 and 4. Mol Cancer Res. 2020 Aug 1;18(8):1218–31.

647. Zhang S, Qin W, Yang S, Guan N, Sui X, Guo W. Circular RNA SFMBT2 Inhibits the Proliferation and Metastasis of Glioma Cells Through Mir-182-5p/Mtss1 Pathway. Technol Cancer Res Treat. 2020 Jan 1;19.

648. Donatelli SS, Zhou JM, Gilvary DL, Eksioglu EA, Chen X, Cress WD, et al. TGF-β-inducible microRNA-183 silences tumor-associated natural killer cells. Proc Natl Acad Sci U S A. 2014 Mar 18;111(11):4203–8.

649. Fazi B, Felsani A, Grassi L, Moles A, D'Andrea D, Toschi N, et al. The transcriptome and miRNome profiling of glioblastoma tissues and peritumoral regions highlights molecular pathways shared by tumors and surrounding areas and reveals differences between short-term and long-term survivors. Oncotarget.

2015;6(26):22526.

650. Pavlakis E, Tonchev AB, Kaprelyan A, Enchev Y, Stoykova A, Tonchev B. A, et al. Interaction between transcription factors PAX6/PAX6-5a and specific members of miR-183-96-182 cluster, may contribute to glioma progression in glioblastoma cell lines. Oncol Rep. 2017 Mar 1;37(3):1579–92.

651. Guo Q, Guo J, Liu W, Hu S, Hu X, Wang Q, et al. Circ-EGFR Functions as an Inhibitory Factor in the Malignant Progression of Glioma by Regulating the miR-183-5p/TUSC2 Axis. Cell Mol Neurobiol. 2021 May 15;1–12.

652. Drusco A, Fadda P, Nigita G, Fassan M, Bottoni A, MP G, et al. Circulating Micrornas Predict Survival of Patients with Tumors of Glial Origin. EBioMedicine. 2018 Apr 1;30:105–12.

653. Zhang S, Guo W. Long non-coding RNA MEG3 suppresses the growth of glioma cells by regulating the miR-96-5p/MTSS1 signaling pathway. Mol Med Rep. 2019 Nov 1;20(5):4215–25.

654. Guo P, Yu Y, Tian Z, Lin Y, Qiu Y, Yao W, et al. Upregulation of miR-96 promotes radioresistance in glioblastoma cells via targeting PDCD4. Int J Oncol. 2018 Oct 1;53(4):1591–600.

655. Tang H, Bian Y, Tu C, Wang Z, Yu Z, Liu Q, et al. The miR-183/96/182 cluster regulates oxidative apoptosis and sensitizes cells to chemotherapy in gliomas. Curr Cancer Drug Targets. 2013;13(2):221–31.

656. Farooqi AA, Mukhanbetzhanovna AA, Yilmaz S, Karasholakova L, Yulaevna IM. Mechanistic role of DANCR in the choreography of signaling pathways in different cancers: Spotlight on regulation of Wnt/β-catenin and JAK/STAT pathways by oncogenic long non-coding RNA. Non-coding RNA Res. 2021;6(1):29–34.

657. Jin SJ, Jin MZ, Xia BR, Jin WL. Long Non-coding RNA DANCR as an Emerging Therapeutic Target in Human Cancers. Front Oncol. 2019 Nov 15;9:1225.

658. Thin KZ, Liu X, Feng X, Raveendran S, Tu JC. LncRNA-DANCR: A valuable cancer related long non-coding RNA for human cancers. Pathol - Res Pract. 2018 Jun 1;214(6):801–5.

659. Li J, Zhou L. Overexpression of lncRNA DANCR positively affects progression of glioma via activating Wnt/β-catenin signaling. Biomed Pharmacother. 2018 Jun 1;102:602–7.

660. Tan Z, Zhao J, Jiang Y. MiR-634 sensitizes glioma cells to temozolomide by targeting CYR61 through Raf-ERK signaling pathway. Cancer Med. 2018 Mar 1;7(3):913.

661. Xu D, Yu J, Gao G, Lu G, Zhang Y, Ma P. LncRNA DANCR functions as a competing endogenous RNA to regulate RAB1A expression by sponging MIR-634 in glioma. Biosci Rep. 2018 Feb 2;38(1):20171664.

662. Ma Y, Zhou G, Li M, Hu D, Zhang L, Liu P, et al. Long noncoding RNA DANCR mediates cisplatin resistance in glioma cells via activating AXL/PI3K/Akt/NF-κB signaling pathway. Neurochem Int. 2018;118:233–41.

663. Zhang Y, An J, Pei Y. LncRNA SNHG6 promotes LMO3 expression by sponging miR-543 in glioma. Mol Cell Biochem. 2020 Sep 1;472(1–2):9–17.

664. Meng Q, Yang BY, Liu B, Yang JX, Sun Y. Long non-coding RNA SNHG6 promotes glioma tumorigenesis by sponging miR-101-3p. Int J Biol Markers. 2018 May 1;33(2):148–55.

665. Li X, Zhang F, Ma J, Ruan X, Liu X, Zheng J, et al. NCBP3/SNHG6 inhibits GBX2 transcription in a histone modification manner to facilitate the malignant biological behavior of glioma cells. RNA Biol. 2020;18(1):47–63.

666. Zhang J, Lu R, Zhang Y, Matuszek Ż, Zhang W, Xia Y, et al. tRNA Queuosine Modification Enzyme Modulates the Growth and Microbiome Recruitment to Breast Tumors. Cancers 2020, Vol 12, Page 628. 2020 Mar 9;12(3):628.

667. Zhang Y, Fang Y, Ma L, Xu J, Lv C, Deng L, et al. LINC00857 regulated by ZNF460 enhances the expression of CLDN12 by sponging miR-150-5p and recruiting SRSF1 for alternative splicing to promote epithelial-mesenchymal transformation of pancreatic adenocarcinoma cells. RNA Biol. 2022;19(1):548–59.

668. Hao T, Xu J, Fang S, Jiang J, Chen X, Wu W, et al. Overexpression of ZNF460 predicts worse survival and promotes metastasis through JAK2/STAT3 signaling pathway in patient with colon cancer. J Cancer. 2021;12(11):3198.

669. Zou C, Li X, Lv X, Wu S, Song J, Tang Z, et al. Circular RNA mitochondrial translation optimization 1 homologue (CircMTO1) induced by zinc finger protein 460 (ZNF460) promotes oral squamous cell carcinoma progression through the microRNA miR-320a / alpha thalassemia/mental retardation, X-linked (ATRX) axis. https://doi.org/101080/2165597920211997699. 2021;12(2):9585–97.

670. Wang Y, Liyanarachchi S, Miller KE, Nieminen TT, Comiskey DF, Li W, et al. Identification of Rare Variants Predisposing to Thyroid Cancer. Thyroid. 2019 Jul 7;29(7):946.

671. Puchalski RB, Shah N, Miller J, Dalley R, Nomura SR, Yoon J-G, et al. An anatomic transcriptional atlas of human glioblastoma. Science (80-). 2018;360(6389):660–3.

672. Zhao Z, Zhang K-N, Wang Q, Li G, Zeng F, Zhang Y, et al. Chinese Glioma Genome Atlas (CGGA): A Comprehensive Resource with Functional Genomic Data from Chinese Glioma Patients. Genomics Proteomics Bioinformatics. 2021;19(1):1–12.

673. Awah CU, Chen L, Bansal M, Mahajan A, Winter J, Lad M, et al. Ribosomal protein S11 influences glioma response to TOP2 poisons. Oncogene. 2020;39(27):5068–81.

674. Yong WH, Shabihkhani M, Telesca D, Yang S, Tso JL, Menjivar JC, et al. Ribosomal Proteins RPS11 and RPS20, Two Stress-Response Markers of Glioblastoma Stem Cells, Are Novel Predictors of Poor Prognosis in Glioblastoma Patients. PLoS One. 2015 Oct 27;10(10):e0141334.

675. Zhao S, Ji W, Shen Y, Fan Y, Huang J, Huang H, et al. Expression of hub genes of endothelial cells in glioblastoma-A prognostic model for GBM patients integrating single cell RNA sequencing and bulk RNA sequencing [Internet]. Research Square; 2022.

676. Li R, Jiang Q, Tang C, Chen L, Kong D, Zou C, et al. Identification of Candidate Genes Associated With Prognosis in Glioblastoma   [Internet]. Vol. 15, Frontiers in Molecular Neuroscience . 2022.

677. Li S, Shi J, Gao H, Yuan Y, Chen Q, Zhao Z, et al. Identification of a gene signature associated with radiotherapy and prognosis in gliomas. Oncotarget; Vol 8, No 51. 2017;

678. Dixon SJ, Lemberg KM, Lamprecht MR, Skouta R, Zaitsev EM, Gleason CE, et al. Ferroptosis: an iron-dependent form of nonapoptotic cell death. Cell. 2012 May 25;149(5):1060–72.

679. Qu C, Peng Y, Liu S. Ferroptosis Biology and Implication in Cancers. Front Mol Biosci. 2022 Apr 20;9:366.

680. Perillo B, Di Donato M, Pezone A, Di Zazzo E, Giovannelli P, Galasso G, et al. ROS in cancer therapy: the bright side of the moon. Exp Mol Med. 2020 Feb 1;52(2):192–203.

681. De Souza I, Carolina M, Ramalho C, Guedes CB, Yumi I, Osawa A, et al. Ferroptosis Modulation: Potential Therapeutic Target for Glioblastoma Treatment. Int J Mol Sci 2022, Vol 23, Page 6879. 2022 Jun 21;23(13):6879.

682. Yuan F, Sun Q, Zhang S, Ye L, Xu Y, Xu Z, et al. HSP27 protects against ferroptosis of glioblastoma cells. Hum Cell. 2022 Jan 1;35(1):238–49.

683. Song Q, Peng S, Sun Z, Heng X, Zhu X. Temozolomide Drives Ferroptosis via a DMT1-Dependent Pathway in Glioblastoma Cells. Yonsei Med J. 2021 Sep 9;62(9):843.

684. Yu F, Zhang Q, Liu H, Liu J, Yang S, Luo X, et al. Dynamic O-GlcNAcylation coordinates ferritinophagy and mitophagy to activate ferroptosis. Cell Discov. 2022;8(1):40.

685. Dixon SJ, Patel DN, Welsch M, Skouta R, Lee ED, Hayano M, et al. Pharmacological inhibition of cystine–glutamate exchange induces endoplasmic reticulum stress and ferroptosis. Elife. 2014;3.

686. Zhang X, Yu K, Ma L, Qian Z, Tian X, Miao Y, et al. Endogenous glutamate determines ferroptosis sensitivity via ADCY10-dependent YAP suppression in lung adenocarcinoma. Theranostics. 2021;11(12):5650.

687. Gao M, Monian P, Quadri N, Ramasamy R, Jiang X. Glutaminolysis and Transferrin Regulate Ferroptosis. Mol Cell. 2015;59(2):298–308.

688. Zhang C, Liu X, Jin S, Chen Y, Guo R. Ferroptosis in cancer therapy: a novel approach to reversing drug resistance. Mol Cancer. 2022 Dec 1;21(1):1–12.

689. Shang Y, Luo M, Yao F, Wang S, Yuan Z, Yang Y. Ceruloplasmin suppresses ferroptosis by regulating iron homeostasis in hepatocellular carcinoma cells. Cell Signal. 2020 Aug 1;72.

690. Ryan F, Zarruk JG, Lößlein L, David S. Ceruloplasmin plays a neuroprotective role in cerebral ischemia. Front Neurosci. 2019;13(JAN):988.

691. Han L, Bai L, Fang X, Liu J, Kang R, Zhou D, et al. SMG9 drives ferroptosis by directly inhibiting GPX4 degradation. Biochem Biophys Res Commun. 2021 Aug 27;567:92–8.

692. Li J, Cao F, Yin H liang, Huang Z jian, Lin Z tao, Mao N, et al. Ferroptosis: past, present and future. Cell Death Dis 2020 112. 2020 Feb 3;11(2):1–13.

693. Poltorack CD, Dixon SJ. Understanding the role of cysteine in ferroptosis: progress & paradoxes. FEBS J. 2022 Jan 1;289(2):374–85.

694. Nathaniel Roybal C, Hunsaker LA, Barbash O, Vander Jagt DL, Abcouwer SF. The Oxidative Stressor Arsenite Activates Vascular Endothelial Growth Factor mRNA Transcription by an ATF4-dependent Mechanism. J Biol Chem. 2005 May 27;280(21):20331–9.

695. Sun W, Yan J, Ma H, Wu J, Zhang Y. Autophagy-Dependent Ferroptosis-Related Signature is Closely Associated with the Prognosis and Tumor Immune Escape of Patients with Glioma. Int J Gen Med. 2022 Jan;15:253.

696. López-Janeiro Á, Ruz-Caracuel I, Ramón-Patino JL, Ríos VDL, Esparza MV, Berjón A, et al. Proteomic Analysis

of Low-Grade, Early-Stage Endometrial Carcinoma Reveals New Dysregulated Pathways Associated with Cell Death and Cell Signaling. Cancers 2021, Vol 13, Page 794. 2021 Feb 14;13(4):794.

697. Li M, Zhang Y, Fan M, Ren H, Chen M, Shi P. Identification of the ferroptosis-related long non-coding RNAs signature to improve the prognosis prediction and immunotherapy response in patients with NSCLC. BMC Med Genomics. 2021 Dec 1;14(1):1–15.

698. Zhang Y, He R, Lei X, Mao L, Yin Z, Zhong X, et al. Comprehensive Analysis of a Ferroptosis-Related lncRNA Signature for Predicting Prognosis and Immune Landscape in Osteosarcoma   [Internet]. Vol. 12, Frontiers in Oncology . 2022.

699. Ding C, Ding X, Zheng J, Wang B, Li Y, Xiang H, et al. miR-182-5p and miR-378a-3p regulate ferroptosis in I/R-induced renal injury. Cell Death Dis 2020 1110. 2020 Oct 28;11(10):1–14.

700. Wu J, Sun X. Construction of a ferroptosis-associated circRNA-miRNA-mRNA network in age-related macular degeneration. Exp Eye Res. 2022;224:109234.

701. Tang L-J, Zhou Y-J, Xiong X-M, Li N-S, Zhang J-J, Luo X-J, et al. Ubiquitin-specific protease 7 promotes ferroptosis via activation of the p53/TfR1 pathway in the rat hearts after ischemia/reperfusion. Free Radic Biol Med. 2021;162:339–52.

702. Lee E, Yong RL, Paddison P, Zhu J. Comparison of glioblastoma (GBM) molecular classification methods. Semin Cancer Biol. 2018;53:201–11.

703. Couturier CP, Ayyadhury S, Le PU, Nadaf J, Monlong J, Riva G, et al. Single-cell RNA-seq reveals that glioblastoma recapitulates a normal neurodevelopmental hierarchy. Nat Commun. 2020;11(1):3406.

704. Barili F, Parolari A, Kappetein PA, Freemantle N. Statistical Primer: heterogeneity, random- or fixed-effects model analyses?†. Interact Cardiovasc Thorac Surg. 2018 Sep 1;27(3):317–21.

705. Borenstein M, Hedges L V, Higgins JPT, Rothstein HR. A basic introduction to fixed-effect and random-effects models for meta-analysis. Res Synth Methods. 2010 Apr 1;1(2):97–111.

706. Bhan A, Soleimani M, Mandal SS. Long Noncoding RNA and Cancer: A New Paradigm. Cancer Res. 2017 Aug 1;77(15):3965–81.

707. Senhaji N, Squalli Houssaini A, Lamrabet S, Louati S, Bennis S. Molecular and Circulating Biomarkers in Patients with Glioblastoma. Int J Mol Sci. 2022;23(13):7474.

708. Sutlief SG. Protection and Measurement in Radiation Therapy. Health Phys. 2015;108(2).

709. Agoston D V. How to Translate Time? The Temporal Aspect of Human and Rodent Biology   [Internet]. Vol. 8, Frontiers in Neurology . 2017.

710. NA A, EF S, MR A, LR L, Andreollo NA, Santos EF dos, et al. Rat's age versus human's age: what is the relationship? ABCD Arq Bras Cir Dig (São Paulo). 2012 Jan 1;25(1):49–51.

711. Sengupta P. The laboratory rat: Relating its age with human's. Vol. 4, International Journal of Preventive Medicine. Wolters Kluwer -- Medknow Publications; 2013. p. 624–30.

712. Meattini I, Becherini C, Boersma L, Kaidar-Person O, Marta GN, Montero A, et al. European Society for Radiotherapy and Oncology Advisory Committee in Radiation Oncology Practice consensus recommendations on patient selection and dose and fractionation for external beam radiotherapy in early breast cancer. Lancet Oncol. 2022 Jan 1;23(1):e21–31.

713. Taylor CW, Zhe W, Macaulay E, Jagsi R, Duane F, Darby SC. Exposure of the Heart in Breast Cancer Radiation Therapy: A Systematic Review of Heart Doses Published During 2003 to 2013. Int J Radiat Oncol. 2015 Nov 15;93(4):845–53.

714. Murphy A, Chmiel E. Fractionation (radiation therapy) [Internet]. Radiopaedia.org. Radiopaedia.org; 2019.

715. Teh AL, Pan H, Lin X, Lim YI, Patro CPK, Cheong CY, et al. Comparison of methyl-capture sequencing vs. Infinium 450K methylation array for methylome analysis in clinical samples. Epigenetics. 2016;11(1):36–48.

716. Dean L. Blood and the cells it contains. In: Bethesda (MD): National Center for Biotechnology Information (US). National Center for Biotechnology Information (US); 2005.

717. Erdbruegger U, Haubitz M, Woywodt A. Circulating endothelial cells: A novel marker of endothelial damage. Clin Chim Acta. 2006;373(1):17–26.

718. Bauer MA, Todorova VK, Stone A, Carter W, Plotkin MD, Hsu P-C, et al. Genome-Wide DNA Methylation Signatures Predict the Early Asymptomatic Doxorubicin-Induced Cardiotoxicity in Breast Cancer. Vol. 13, Cancers . 2021.

719. Corbett RJ, Luttman AM, Wurtz KE, Siegford JM, Raney NE, Ford LM, et al. Weaning Induces Stress-Dependent DNA Methylation and Transcriptional Changes in Piglet PBMCs   [Internet]. Vol. 12, Frontiers in Genetics .

2021.

720.   Faraji M, Pourpak Z, Naddafi K, Nodehi RN, Nicknam MH, Shamsipour M, et al. Effects of airborne particulate matter (PM10) from dust storm and thermal inversion on global DNA methylation in human peripheral blood mononuclear cells (PBMCs) in vitro. Atmos Environ. 2018;195:170–8.

721.   M Dunn C, Nevitt MC, Lynch JA, Jeffries MA. A pilot study of peripheral blood DNA methylation models as predictors of knee osteoarthritis radiographic progression: data from the Osteoarthritis Initiative (OAI). Sci Rep. 2019;9(1):1–11.

722.   Lovelock JE. The haemolysis of human red blood-cells by freezing and thawing. Biochim Biophys Acta. 1953;10:414–26.

723.   Steponkus PL, Lynch D V. Freeze/thaw-induced destabilization of the plasma membrane and the effects of cold acclimation. J Bioenerg Biomembr. 1989;21(1):21–41.

724.   Scherer M, Schmidt F, Lazareva O, Walter J, Baumbach J, Schulz MH, et al. Machine learning for deciphering cell heterogeneity and gene regulation. Nat Comput Sci. 2021;1(3):183–91.

725.   Decamps C, Privé F, Bacher R, Jost D, Waguet A, Achard S, et al. Guidelines for cell-type heterogeneity quantification based on a comparative analysis of reference-free DNA methylation deconvolution software. BMC Bioinformatics. 2020;21(1):16.

726.   Sun K, Jiang P, Chan KCA, Wong J, Cheng YKY, Liang RHS, et al. Plasma DNA tissue mapping by genome-wide methylation sequencing for noninvasive prenatal, cancer, and transplantation assessments. Proc Natl Acad Sci. 2015 Oct 6;112(40):E5503–12.

727.   Seguret M, Vermersch E, Jouve C, Hulot J-S. Cardiac Organoids to Model and Heal Heart Failure and Cardiomyopathies. Vol. 9, Biomedicines. 2021.

728.   Zhuang RZ, Lock R, Liu B, Vunjak-Novakovic G. Opportunities and challenges in cardiac tissue engineering from an analysis of two decades of advances. Nat Biomed Eng. 2022;6(4):327–38.

729.   Kim J, Koo B-K, Knoblich JA. Human organoids: model systems for human biology and medicine. Nat Rev Mol Cell Biol. 2020;21(10):571–84.

730.   Devall MA, Eaton S, Ali MW, Dampier CH, Weisenberger D, Powell SM, et al. DNA methylation analysis of normal colon organoids from familial adenomatous polyposis patients reveals novel insight into colon cancer development. Clin Epigenetics. 2022;14(1):104.

731.   Esfandiari F, Favaedi R, Heidari-Khoei H, Chitsazian F, Yari S, Piryaei A, et al. Insight into epigenetics of human endometriosis organoids: DNA methylation analysis of HOX genes and their cofactors. Fertil Steril. 2021;115(1):125–37.

732.   Zhao D, Lei W, Hu S. Cardiac organoid — a promising perspective of preclinical model. Stem Cell Res Ther. 2021;12(1):272.

733.   de Souza N. Organoids. Nat Methods. 2018;15(1):23.

734.   Lee S-G, Kim Y-J, Son M-Y, Oh M-S, Kim J, Ryu B, et al. Generation of human iPSCs derived heart organoids structurally and functionally similar to heart. Biomaterials. 2022;290:121860.

735.   Richards DJ, Li Y, Kerr CM, Yao J, Beeson GC, Coyle RC, et al. Human cardiac organoids for the modelling of myocardial infarction and drug cardiotoxicity. Nat Biomed Eng. 2020;4(4):446–62.

736.   Pidsley R, Zotenko E, Peters TJ, Lawrence MG, Risbridger GP, Molloy P, et al. Critical evaluation of the Illumina MethylationEPIC BeadChip microarray for whole-genome DNA methylation profiling. Genome Biol. 2016 Oct 7;17(1):1–17.

737.   Nordgren KKS, Hampton M, Wallace KB. Editor's Highlight: The Altered DNA Methylome of Chronic Doxorubicin Exposure in Sprague Dawley Rats. Toxicol Sci. 2017 Oct 1;159(2):470–9.

738.   Binas S, Knyrim M, Hupfeld J, Kloeckner U, Rabe S, Mildenberger S, et al. miR-221 and -222 target CACNA1C and KCNJ5 leading to altered cardiac ion channel expression and current density. Cell Mol Life Sci. 2020;77(5):903–18.

739.   Li W, Zheng N-Z, Yuan Q, Xu K, Yang F, Gu L, et al. NFAT5-mediated CACNA1C expression is critical for cardiac electrophysiological development and maturation. J Mol Med. 2016;94(9):993–1002.

740.   Shen C, Kong B, Liu Y, Xiong L, Shuai W, Wang G, et al. YY1-induced upregulation of lncRNA KCNQ1OT1 regulates angiotensin II-induced atrial fibrillation by modulating miR-384b/CACNA1C axis. Biochem Biophys Res Commun. 2018 Oct 20;505(1):134–40.

741.   Wang D, Papp AC, Binkley PF, Johnson JA, Sadée W. Highly variable mRNA expression and splicing of L-type voltage-dependent calcium channel alpha subunit 1C in human heart tissues. Pharmacogenet Genomics.

2006;16(10):735–45.

742. Guauque-Olarte S, Messika-Zeitoun D, Droit A, Lamontagne M, Tremblay-Marchand J, Lavoie-Charland E, et al. Calcium Signaling Pathway Genes RUNX2 and CACNA1C Are Associated With Calcific Aortic Valve Disease. Circ Cardiovasc Genet. 2015 Dec 1;8(6):812–22.

743. Thul PJ, Lindskog C. The human protein atlas: A spatial map of the human proteome. Protein Sci. 2018 Jan 1;27(1):233–44.

744. Batra RN, Lifshitz A, Vidakovic AT, Chin S-F, Sati-Batra A, Sammut S-J, et al. DNA methylation landscapes of 1538 breast cancers reveal a replication-linked clock, epigenomic instability and cis-regulation. Nat Commun. 2021;12(1):5406.

745. Stefansson OA, Moran S, Gomez A, Sayols S, Arribas-Jorba C, Sandoval J, et al. A DNA methylation-based definition of biologically distinct breast cancer subtypes. Mol Oncol. 2015;9(3):555–68.

746. Holm K, Hegardt C, Staaf J, Vallon-Christersson J, Jönsson G, Olsson H, et al. Molecular subtypes of breast cancer are associated with characteristic DNA methylation patterns. Breast Cancer Res. 2010;12(3):R36.

747. Sinha S, Sharma S, Vora J, Shah H, Srivastava A, Shrivastava N. Mucuna pruriens (L.) DC chemo sensitize human breast cancer cells via downregulation of prolactin-mediated JAK2/STAT5A signaling. J Ethnopharmacol. 2018;217:23–35.

748. Koch A, Jeschke J, Van Criekinge W, van Engeland M, De Meyer T. MEXPRESS update 2019. Nucleic Acids Res. 2019 Jul;47(W1):W561–5.

749. Thennavan A, Beca F, Xia Y, Garcia-Recio S, Allison K, Collins LC, et al. Molecular analysis of TCGA breast cancer histologic types. Cell Genomics. 2021;1(3):100067.

750. Hauptmann M, Byrnes G, Cardis E, Bernier M-O, Blettner M, Dabin J, et al. Brain cancer after radiation exposure from CT examinations of children and young adults: results from the EPI-CT cohort study. Lancet Oncol. 2022;

751. Gug IT, Tertis M, Hosu O, Cristea C. Salivary biomarkers detection: Analytical and immunological methods overview. TrAC Trends Anal Chem. 2019;113:301–16.

752. Xie Z, Chen G, Zhang X, Li D, Huang J, Yang C, et al. Salivary MicroRNAs as Promising Biomarkers for Detection of Esophageal Cancer. PLoS One. 2013 Apr 1;8(4):e57502.

753. Xie Z, Chen X, Li J, Guo Y, Li H, Pan X, et al. Salivary HOTAIR and PVT1 as novel biomarkers for early pancreatic cancer. Oncotarget. 2016;7(18):25408.

754. Wong DTW. Salivary extracellular noncoding RNA: emerging biomarkers for molecular diagnostics. Clin Ther. 2015;37(3):540–51.

755. Koopaie M, Kolahdooz S, Fatahzadeh M, Aleedawi ZA. Salivary noncoding RNA in the diagnosis of pancreatic cancer: Systematic review and meta-analysis. Eur J Clin Invest. 2022 Dec 1;52(12):e13848.

756. Mitre A-O, Florian AI, Buruiana A, Boer A, Moldovan I, Soritau O, et al. Ferroptosis Involvement in Glioblastoma Treatment. Medicina (B Aires). 2022;58(2):319.

757. Zhuo S, He G, Chen T, Li X, Liang Y, Wu W, et al. Emerging role of ferroptosis in glioblastoma: Therapeutic opportunities and challenges   [Internet]. Vol. 9, Frontiers in Molecular Biosciences . 2022.

758. Puckett LL, Saba SG, Henry S, Rosen S, Rooney E, Filosa SL, et al. Cardiotoxicity screening of long-term, breast cancer survivors—The CAROLE (Cardiac-Related Oncologic Late Effects) Study. Cancer Med. 2021 Aug 1;10(15):5051–61.

759. Mehdi A, Cheishvili D, Arakelian A, Bismar TA, Szyf M, Rabbani SA. DNA methylation signatures of Prostate Cancer in peripheral T-cells. BMC Cancer. 2020;20(1):588.

760. Lehmann U, Stark H, Bartels S, Schlue J, Büsche G, Kreipe H. Genome-wide DNA methylation profiling is able to identify prefibrotic PMF cases at risk for progression to myelofibrosis. Clin Epigenetics. 2021;13(1):28.

761. Ruan W, Chen X, Huang M, Wang H, Chen J, Liang Z, et al. A urine-based DNA methylation assay to facilitate early detection and risk stratification of bladder cancer. Clin Epigenetics. 2021;13(1):91.

762. Langie SAS, Moisse M, Declerck K, Koppen G, Godderis L, Vanden Berghe W, et al. Salivary DNA methylation profiling: aspects to consider for biomarker identification. Basic Clin Pharmacol Toxicol. 2017;121:93–101.

763. Juvinao-Quintero DL, Marioni RE, Ochoa-Rosales C, Russ TC, Deary IJ, van Meurs JBJ, et al. DNA methylation of blood cells is associated with prevalent type 2 diabetes in a meta-analysis of four European cohorts. Clin Epigenetics. 2021;13(1):40.

764. Pajares MJ, Palanca-Ballester C, Urtasun R, Alemany-Cosme E, Lahoz A, Sandoval J. Methods for analysis of specific DNA methylation status. Methods. 2021;187:3–12.

765.   Hussmann D, Hansen LL. Methylation-sensitive high resolution melting (MS-HRM). DNA Methylation Protoc. 2018;551–71.

766.   Awada Z, Akika R, Zgheib NK. Chapter 3 - Methods for epigenomic analyses: DNA methylation. In: Forero DA, Patrinos GPBT-GP in H and D, editors. Translational and Applied Genomics. Academic Press; 2020. p. 27–45.

767.   Du Y, Wang Y, Hu X, Liu J, Diao J. Single-molecule quantification of 5-methylcytosine and 5-hydroxymethylcytosine in cancer genome. VIEW. 2020 Jun;1(2):e9.

768.   Wagner W. How to translate DNA methylation biomarkers into clinical practice. Front Cell Dev Biol. 2022;360.

769.   Chen B, Dai Q, Zhang Q, Yan P, Wang A, Qu L, et al. The relationship among occupational irradiation, DNA methylation status, and oxidative damage in interventional physicians. Medicine (Baltimore). 2019;98(39).

770.   Villicaña S, Bell JT. Genetic impacts on DNA methylation: research findings and future perspectives. Genome Biol. 2021;22(1):127.

771.   Dworzański W, Cholewińska E, Fotschki B, Juśkiewicz J, Listos P, Ognik K. Assessment of DNA Methylation and Oxidative Changes in the Heart and Brain of Rats Receiving a High-Fat Diet Supplemented with Various Forms of Chromium. Vol. 10, Animals. 2020.

772.   Heyn H, Esteller M. DNA methylation profiling in the clinic: applications and challenges. Nat Rev Genet. 2012;13(10):679–92.

773.   Xia Y, Brewer A, Bell JT. DNA methylation signatures of incident coronary heart disease: findings from epigenome-wide association studies. Clin Epigenetics. 2021;13(1):186.

774.   Baghel R, Maan K, Haritwal T, Rana P. Chapter 2 - Integration of epigenomics and metabolomics: From biomarkers discovery to personalized medicine. In: Agrawala PK, Rana PBT-E and M, editors. Translational Epigenetics. Academic Press; 2021. p. 31–73.

775.   Miao Z, Humphreys BD, McMahon AP, Kim J. Multi-omics integration in the age of million single-cell data. Nat Rev Nephrol. 2021;17(11):710–24.

776.   Gomez-Cabrero D, Abugessaisa I, Maier D, Teschendorff A, Merkenschlager M, Gisel A, et al. Data integration in the era of omics: current and future challenges. BMC Syst Biol. 2014;8(2):I1.

777.   Ju C, Fiori LM, Belzeaux R, Theroux J-F, Chen GG, Aouabed Z, et al. Integrated genome-wide methylation and expression analyses reveal functional predictors of response to antidepressants. Transl Psychiatry. 2019;9(1):254.

778.   Sarno F, Benincasa G, List M, Barabasi A-L, Baumbach J, Ciardiello F, et al. Clinical epigenetics settings for cancer and cardiovascular diseases: real-life applications of network medicine at the bedside. Clin Epigenetics. 2021;13(1):66.

779.   Shanthikumar S, Neeland MR, Maksimovic J, Ranganathan SC, Saffery R. DNA methylation biomarkers of future health outcomes in children. Mol Cell Pediatr. 2020;7(1):1–11.

780.   Taheri M, Eghtedarian R, Dinger ME, Ghafouri-Fard S. Dysregulation of non-coding RNAs in autoimmune thyroid disease. Exp Mol Pathol. 2020;117:104527.

781.   Liu Y, Chang X, Hahn C-G, Gur RE, Sleiman PAM, Hakonarson H. Non-coding RNA dysregulation in the amygdala region of schizophrenia patients contributes to the pathogenesis of the disease. Transl Psychiatry. 2018;8(1):44.

782.   Winkle M, El-Daly SM, Fabbri M, Calin GA. Noncoding RNA therapeutics — challenges and potential solutions. Nat Rev Drug Discov. 2021;20(8):629–51.

783.   Schulz JA, Rodgers LT, Kryscio RJ, Hartz AMS, Bauer B. Characterization and comparison of human glioblastoma models. BMC Cancer. 2022;22(1):844.

784.   Cho HJ, Eun JW, Baek GO, Seo CW, Ahn HR, Kim SS, et al. Serum Exosomal MicroRNA, miR-10b-5p, as a Potential Diagnostic Biomarker for Early-Stage Hepatocellular Carcinoma. Vol. 9, Journal of Clinical Medicine. 2020.

785.   Staicu CE, Predescu D-V, Rusu CM, Radu BM, Cretoiu D, Suciu N, et al. Role of microRNAs as Clinical Cancer Biomarkers for Ovarian Cancer: A Short Overview. Vol. 9, Cells. 2020.

786.   Condrat CE, Thompson DC, Barbu MG, Bugnar OL, Boboc A, Cretoiu D, et al. miRNAs as Biomarkers in Disease: Latest Findings Regarding Their Role in Diagnosis and Prognosis. Vol. 9, Cells. 2020.

787.   Kashyap D, Kaur H. Cell-free miRNAs as non-invasive biomarkers in breast cancer: Significance in early diagnosis and metastasis prediction. Life Sci. 2020;246:117417.

788.   Salazar C, Nagadia R, Pandit P, Cooper-White J, Banerjee N, Dimitrova N, et al. A novel saliva-based microRNA biomarker panel to detect head and neck cancers. Cell Oncol. 2014;37(5):331–8.

789. Hoshino I. The usefulness of microRNA in urine and saliva as a biomarker of gastroenterological cancer. Int J Clin Oncol. 2021;26(8):1431–40.

790. Aftab M, Poojary SS, Seshan V, Kumar S, Agarwal P, Tandon S, et al. Urine miRNA signature as a potential non-invasive diagnostic and prognostic biomarker in cervical cancer. Sci Rep. 2021;11(1):10323.

791. Usuba W, Urabe F, Yamamoto Y, Matsuzaki J, Sasaki H, Ichikawa M, et al. Circulating miRNA panels for specific and early detection in bladder cancer. Cancer Sci. 2019 Jan 1;110(1):408–19.

792. Rupaimoole R, Slack FJ. MicroRNA therapeutics: towards a new era for the management of cancer and other diseases. Nat Rev Drug Discov. 2017;16(3):203–22.

793. Anastasiadou E, Seto AG, Beatty X, Hermreck M, Gilles M-E, Stroopinsky D, et al. Cobomarsen, an Oligonucleotide Inhibitor of miR-155, Slows DLBCL Tumor Cell Growth In Vitro and In VivoCobomarsen, a miRNA-based Compound for DLBCL Treatment. Clin Cancer Res. 2021;27(4):1139–49.

794. Xie Y, Hang Y, Wang Y, Sleightholm R, Prajapati DR, Bader J, et al. Stromal Modulation and Treatment of Metastatic Pancreatic Cancer with Local Intraperitoneal Triple miRNA/siRNA Nanotherapy. ACS Nano. 2020 Jan 28;14(1):255–71.

795. Binenbaum Y, Fridman E, Yaari Z, Milman N, Schroeder A, Ben David G, et al. Transfer of miRNA in Macrophage-Derived Exosomes Induces Drug Resistance in Pancreatic Adenocarcinoma. Cancer Res. 2018 Sep 14;78(18):5287–99.

796. Wu Y, Tang Y, Xie S, Zheng X, Zhang S, Mao J, et al. Chimeric peptide supramolecular nanoparticles for plectin-1 targeted miRNA-9 delivery in pancreatic cancer. Theranostics. 2020;10(3):1151.

797. Kim G, Kim M, Lee Y, Byun JW, Hwang DW, Lee M. Systemic delivery of microRNA-21 antisense oligonucleotides to the brain using T7-peptide decorated exosomes. J Control Release. 2020;317:273–81.

798. Ding Z, Ying W, He Y, Chen X, Jiao Y, Wang J, et al. lncRNA-UCA1 in the diagnosis of bladder cancer: a meta-analysis. Medicine (Baltimore). 2021;100(11).

799. Lemos AEG, da Rocha Matos A, Ferreira LB, Gimba ERP. The long non-coding RNA PCA3: an update of its functions and clinical applications as a biomarker in prostate cancer. Oncotarget. 2019;10(61):6589.

800. Fan X, Zhao Z, Song J, Zhang D, Wu F, Tu J, et al. LncRNA-SNHG6 promotes the progression of hepatocellular carcinoma by targeting miR-6509-5p and HIF1A. Cancer Cell Int. 2021;21(1):150.

801. Du F, Guo T, Cao C. Silencing of Long Noncoding RNA SNHG6 Inhibits Esophageal Squamous Cell Carcinoma Progression via miR-186-5p/HIF1α Axis. Dig Dis Sci. 2020;65(10):2844–52.

802. Li J, Xie J, Wang Y-Z, Gan Y-R, Wei L, Ding G-W, et al. Overexpression of lncRNA Dancr inhibits apoptosis and enhances autophagy to protect cardiomyocytes from endoplasmic reticulum stress injury via sponging microRNA-6324. Mol Med Rep. 2021;23(2):116.

803. Wen X, Liu XU, Mao Y-P, Yang X-J, Wang Y-Q, Zhang P-P, et al. Long non-coding RNA DANCR stabilizes HIF-1α and promotes metastasis by interacting with NF90/NF45 complex in nasopharyngeal carcinoma. Theranostics. 2018;8(20):5676.

804. Qiu L, Zhao Q, Dai L, Zhu A, Xu X, Zhao S, et al. Long non-coding RNA DANCR alleviates hypoxia-caused H9c2 cells damage through up regulation of HIF-1α. Artif Cells, Nanomedicine, Biotechnol. 2020 Jan 1;48(1):533–41.

805. Guo Z, Wang X, Yang Y, Chen W, Zhang K, Teng B, et al. Hypoxic Tumor-Derived Exosomal Long Noncoding RNA UCA1 Promotes Angiogenesis via miR-96-5p/AMOTL2 in Pancreatic Cancer. Mol Ther - Nucleic Acids. 2020;22:179–95.

806. Ye Z, Zhang Z, Wu L, Liu C, Chen Q, Liu J, et al. Upregulation of miR-183 expression and its clinical significance in human brain glioma. Neurol Sci. 2016;37(8):1341–7.

807. Li Y, Zhang D, Wang X, Yao X, Ye C, Zhang S, et al. Hypoxia-inducible miR-182 enhances HIF1α signaling via targeting PHD2 and FIH1 in prostate cancer. Sci Rep. 2015;5(1):12495.

808. Agrawal R, Pandey P, Jha P, Dwivedi V, Sarkar C, Kulshreshtha R. Hypoxic signature of microRNAs in glioblastoma: insights from small RNA deep sequencing. BMC Genomics. 2014;15(1):686.

809. Wang M, Wang W, Wang J, Zhang J. MiR-182 promotes glucose metabolism by upregulating hypoxia-inducible factor 1α in NSCLC cells. Biochem Biophys Res Commun. 2018;504(2):400–5.

810. Ma Y, Yang H-Z, Dong B-J, Zou H-B, Zhou Y, Kong X-M, et al. Biphasic regulation of autophagy by miR-96 in prostate cancer cells under hypoxia. Oncotarget. 2014;5(19):9169.

811. Emami Nejad A, Najafgholian S, Rostami A, Sistani A, Shojaeifar S, Esparvarinha M, et al. The role of hypoxia in the tumor microenvironment and development of cancer stem cell: a novel approach to developing

treatment. Cancer Cell Int. 2021;21(1):62.

812. Chédeville AL, Madureira PA. The Role of Hypoxia in Glioblastoma Radiotherapy Resistance. Vol. 13, Cancers. 2021.

813. Fowler AJ, Ahn J, Hebron M, Chiu T, Ayoub R, Mulki S, et al. CSF MicroRNAs Reveal Impairment of Angiogenesis and Autophagy in Parkinson Disease. Neurol Genet. 2021 Dec 1;7(6):e633.

814. Gómez-Oliva R, Domínguez-García S, Carrascal L, Abalos-Martínez J, Pardillo-Díaz R, Verástegui C, et al. Evolution of Experimental Models in the Study of Glioblastoma: Toward Finding Efficient Treatments [Internet]. Vol. 10, Frontiers in Oncology . 2021.

815. Datta P, Dey M, Ataie Z, Unutmaz D, Ozbolat IT. 3D bioprinting for reconstituting the cancer microenvironment. npj Precis Oncol. 2020;4(1):18.

816. Fischer J, Heide M, Huttner WB. Genetic Modification of Brain Organoids [Internet]. Vol. 13, Frontiers in Cellular Neuroscience . 2019.

817. Mertsch S, Thanos S. Opposing signaling of ROCK1 and ROCK2 determines the switching of substrate specificity and the mode of migration of glioblastoma cells. Mol Neurobiol. 2014 Oct 30;49(2):900–15.

818. Wan X, Cheng Q, Peng R, Ma Z, Chen Z, Cao Y, et al. ROCK1, a novel target of miR-145, promotes glioma cell invasion. Mol Med Rep. 2014 May 1;9(5):1877–82.

819. Xu S, Guo X, Gao X, Xue H, Zhang J, Guo X, et al. Macrophage migration inhibitory factor enhances autophagy by regulating ROCK1 activity and contributes to the escape of dendritic cell surveillance in glioblastoma. Int J Oncol. 2016 Nov 1;49(5):2105–15.

820. Wang D, Yang T, Liu J, Liu Y, Xing N, He J, et al. Propofol Inhibits the Migration and Invasion of Glioma Cells by Blocking the PI3K/AKT Pathway Through miR-206/ROCK1 Axis. Onco Targets Ther. 2020;13:361.

821. Chen X, Li D, Chen L, Hao B, Gao Y, Li L, et al. Long noncoding RNA LINC00346 promotes glioma cell migration, invasion and proliferation by up-regulating ROCK1. J Cell Mol Med. 2020 Nov 1;24(22):13010–9.

822. Tsai HF, Chang YC, Li CH, Chan MH, Chen CL, Tsai WC, et al. Type V collagen alpha 1 chain promotes the malignancy of glioblastoma through PPRC1-ESM1 axis activation and extracellular matrix remodeling. Cell Death Discov 2021 71. 2021 Oct 26;7(1):1–12.

823. Lin M, Zhang X, Jia B, Guan S. Suppression of glioblastoma growth and angiogenesis through molecular targeting of methionine aminopeptidase-2. J Neurooncol. 2018 Jan 1;136(2):243–54.

824. Khanna A, Thoms JAI, Stringer BW, Chung SA, Ensbey KS, Jue TR, et al. Constitutive CHK1 Expression Drives a pSTAT3-CIP2A Circuit that Promotes Glioblastoma Cell Survival and Growth. Mol Cancer Res. 2020 May 1;18(5):709–22.

825. Qin S, Li J, Si Y, He Z, Zhang T, Wang D, et al. Cucurbitacin B induces inhibitory effects via CIP2A/PP2A/Akt pathway in glioblastoma multiforme. Mol Carcinog. 2018 Jun 1;57(6):687–99.

826. Gao D, Nyalali AMK, Hou Y, Xu Y, Zhou J, Zhao W, et al. 2,5-Dimethyl Celecoxib Inhibits Proliferation and Cell Cycle and Induces Apoptosis in Glioblastoma by Suppressing CIP2A/PP2A/Akt Signaling Axis. J Mol Neurosci. 2021 Aug 1;71(8):1703–13.

827. Khanna A, Stringer B, Day B, Ensbey K, Shen H, Boyd A, et al. Abstract 1600: Keeping glioblastoma (GBM)in check by targeting the CHK1-STAT3-CIP2A axis. Cancer Res. 2014 Oct 1;74(19_Supplement):1600–1600.

828. Doan NB, Alhajala H, Al-Gizawiy MM, Mueller WM, Rand SD, Connelly JM, et al. Acid ceramidase and its inhibitors: a de novo drug target and a new class of drugs for killing glioblastoma cancer stem cells with high efficiency. Oncotarget. 2017 Dec 12;8(68):112662.

829. Doan NB, Nguyen HS, Al-Gizawiy MM, Mueller WM, Sabbadini RA, Rand SD, et al. Acid ceramidase confers radioresistance to glioblastoma cells. Oncol Rep. 2017 Oct 1;38(4):1932–40.

830. Ulloa F, Gonzàlez-Juncà A, Meffre D, Barrecheguren PJ, Martínez-Mármol R, Pazos I, et al. Blockade of the SNARE Protein Syntaxin 1 Inhibits Glioblastoma Tumor Growth. PLoS One. 2015 Mar 24;10(3):e0119707.

831. Lv X, Wang M, Qiang J, Guo S. Circular RNA circ-PITX1 promotes the progression of glioblastoma by acting as a competing endogenous RNA to regulate miR-379–5p/MAP3K2 axis. Eur J Pharmacol. 2019 Nov 15;863:172643.

832. Pan Y-B, Wang S, Yang B, Jiang Z, Lenahan C, Wang J, et al. Transcriptome analyses reveal molecular mechanisms underlying phenotypic differences among transcriptional subtypes of glioblastoma. J Cell Mol Med. 2020 Apr 1;24(7):3901–16.

833. Yang J, Zhou Y, Xie S, Wang J, Li Z, Chen L, et al. Metformin induces Ferroptosis by inhibiting UFMylation of SLC7A11 in breast cancer. J Exp Clin Cancer Res. 2021;40(1):206.

834. Luo C, Nie C, Zeng Y, Qian K, Li X, Wang X. LINC01564 Promotes the TMZ Resistance of Glioma Cells by Upregulating NFE2L2 Expression to Inhibit Ferroptosis. Mol Neurobiol. 2022;59(6):3829–44.

835. Chen P, Hsu W-H, Chang A, Tan Z, Lan Z, Zhou A, et al. Circadian Regulator CLOCK Recruits Immune-Suppressive Microglia into the GBM Tumor MicroenvironmentCLOCK in Tumor Immunity. Cancer Discov. 2020;10(3):371–81.

836. Xuan W, Hsu W-H, Khan F, Dunterman M, Pang L, Wainwright DA, et al. Circadian Regulator CLOCK Drives Immunosuppression in Glioblastoma. Cancer Immunol Res. 2022 Jun 3;10(6):770–84.

837. Xiang C, Liu X, Zhou D, Zhou Y, Wang X, Chen F. Identification of a glioma functional network from gene fitness data using machine learning. J Cell Mol Med. 2022 Feb 1;26(4):1253–63.

838. Gao F, Wang Z, Gu J, Zhang X, Wang H. A Hypoxia-Associated Prognostic Gene Signature Risk Model and Prognosis Predictors in Gliomas   [Internet]. Vol. 11, Frontiers in Oncology . 2021.

839. Seo SU, Cho HK, Min K, Woo SM, Kim S, Park J-W, et al. Thioridazine enhances sensitivity to carboplatin in human head and neck cancer cells through downregulation of c-FLIP and Mcl-1 expression. Cell Death Dis. 2017;8(2):e2599–e2599.

840. Xu C-H, Xiao L-M, Zeng E-M, Chen L-K, Zheng S-Y, Li D-H, et al. MicroRNA-181 inhibits the proliferation, drug sensitivity and invasion of human glioma cells by targeting Selenoprotein K (SELK). Am J Transl Res. 2019;11(10):6632.

841. Alim I, Caulfield JT, Chen Y, Swarup V, Geschwind DH, Ivanova E, et al. Selenium Drives a Transcriptional Adaptive Program to Block Ferroptosis and Treat Stroke. Cell. 2019;177(5):1262-1279.e25.

842. Tang F, Liu Z, Chen X, Yang J, Wang Z, Li Z. Current knowledge of protein palmitoylation in gliomas. Mol Biol Rep. 2022;

843. Zhao Y, Lu J, Liu M, Guan S. Toward improved human health: Nrf2 plays a critical role in regulating ferroptosis. Food Funct. 2021;

844. Song X, Long D. Nrf2 and ferroptosis: a new research direction for neurodegenerative diseases. Front Neurosci. 2020;14:267.

845. Torrente L, DeNicola GM. Targeting NRF2 and its downstream processes: opportunities and challenges. Annu Rev Pharmacol Toxicol. 2022;62:279–300.

846. Liu Y, Zhou L, Xu Y, Li K, Zhao Y, Qiao H, et al. Heat Shock Proteins and Ferroptosis   [Internet]. Vol. 10, Frontiers in Cell and Developmental Biology . 2022.

847. Yanoma T, Ogata K, Yokobori T, Ide M, Mochiki E, Toyomasu Y, et al. Heat shock-induced HIKESHI protects cell viability via nuclear translocation of heat shock protein 70 . Oncol Rep. 2017;38(3):1500–6.

848. Ji J-W, Zhang Y-D, Lai Y-J, Huang C-G. Mettl3 regulates the proliferation, migration and invasion of glioma cells by inhibiting PI3K/Akt signaling pathway. Eur Rev Med Pharmacol Sci. 2020;24(7):3818–28.

849. Xu Y, Lv D, Yan C, Su H, Zhang X, Shi Y, et al. METTL3 promotes lung adenocarcinoma tumor growth and inhibits ferroptosis by stabilizing SLC7A11 m6A modification. Cancer Cell Int. 2022;22(1):11.

850. Li N, Yi X, He Y, Huo B, Chen Y, Zhang Z, et al. Targeting Ferroptosis as a Novel Approach to Alleviate Aortic Dissection. Int J Biol Sci. 2022;18(10):4118–34.

851. Turi Z, Hocsak E, Racz B, Szabo A, Balogh A, Sumegi B, et al. Role of mitochondrial network stabilisation by a human small heat shock protein in tumour malignancy. J Cancer. 2015;6(5):470.

852. Cheng W, Li M, Jiang Y, Zhang C, Cai J, Wang K, et al. Association between small heat shock protein B11 and the prognostic value of MGMT promoter methylation in patients with high-grade glioma. J Neurosurg. 2016;125(1):7–16.

853. Dixit D, Prager BC, Gimple RC, Miller TE, Wu Q, Yomtoubian S, et al. Glioblastoma stem cells reprogram chromatin in vivo to generate selective therapeutic dependencies on DPY30 and phosphodiesterases. Sci Transl Med. 2022 Sep 26;14(626):eabf3917.

854. Zhang Y, Li Y, Qiu Q, Chen Z, Du Y, Liu X. MITD1 Deficiency Suppresses Clear Cell Renal Cell Carcinoma Growth and Migration by Inducing Ferroptosis through the TAZ/SLC7A11 Pathway. Luo L, editor. Oxid Med Cell Longev. 2022;2022:7560569.

855. Chen D, Varanasi SK, Hara T, Traina K, McDonald B, Farsakoglu Y, et al. A microglia-CD4+ T cell partnership generates protective anti-tumor immunity to glioblastoma. bioRxiv. 2022 Jan 1;2022.08.12.502093.

856. Liu Z, Wang J, Wang J, Niu J, Wang J, Tong H. CircVCAN/SUB1 up-regulates MYC/HSP90β to enhance the proliferation and migration of glioma cells. Brain Res Bull. 2021;177:332–9.

857. Trümbach D, Pfeiffer S, Poppe M, Scherb H, Doll S, Wurst W, et al. ENCoRE: an efficient software for CRISPR

screens identifies new players in extrinsic apoptosis. BMC Genomics. 2017;18(1):905.

858.   Bender S, Gronych J, Warnatz H-J, Hutter B, Gröbner S, Ryzhova M, et al. Recurrent MET fusion genes represent a drug target in pediatric glioblastoma. Nat Med. 2016;22(11):1314–20.

859.   Tiek DM, Erdogdu B, Razaghi R, Jin L, Sadowski N, Alamillo-Ferrer C, et al. Temozolomide-induced guanine mutations create exploitable vulnerabilities of guanine-rich DNA and RNA regions in drug-resistant gliomas. Sci Adv. 2022 Sep 26;8(25):eabn3471.

860.   Xu Y, Li R, Li X, Dong N, Wu D, Hou L, et al. An Autophagy-Related Gene Signature Associated With Clinical Prognosis and Immune Microenvironment in Gliomas   [Internet]. Vol. 10, Frontiers in Oncology . 2020.

Appendix A: Additional information

6.1. Supplementary materials for Chapter 3

Supplementary figure 1.1: *Summary of relevant correlations A) Correlation between global methylation (5-mC%) and GLS in rats receiving 6.9 and 27.6Gy FI. B) Correlation between E2F6 fold change (log) and GLS in rats receiving 27.6Gy FI. C) Correlation between V1 ITPR2, E2f6 and CX43 (upper left, upper right and lower left, respectively) and V2 SLMAP (lower right) fold change (log) and whole heart dose. Pearson correlation was calculated using SPSS version 28 and R program ggscatter function.*

Supplementary figure 1.2: *Mean log fold change of SLMAP, LDLR, ITPR2, E2F6, PTPN and CX43 expression in the blood of right (n=9) and left sided ((MHD >2.5 Gy, n=4), (MHD<2.5 Gy, n=12)) breast cancer patients sampled at diagnosis (V0), immediately after radiotherapy (V1) and 6 months after radiotherapy (V2). Data is presented as mean log fold changes normalized to TBP ± standard error of mean. Continuous lines represent the mean log fold changes of patients who received <2.5 Gy mean heart dose (MHD) and dotted lines represent patients who received >= 2.5 Gy MHD..(*=p<0.05). Statistical analysis was performed using SPSS generalized estimating equations module and multiple comparison correction was performed using least significant difference (LSD).*
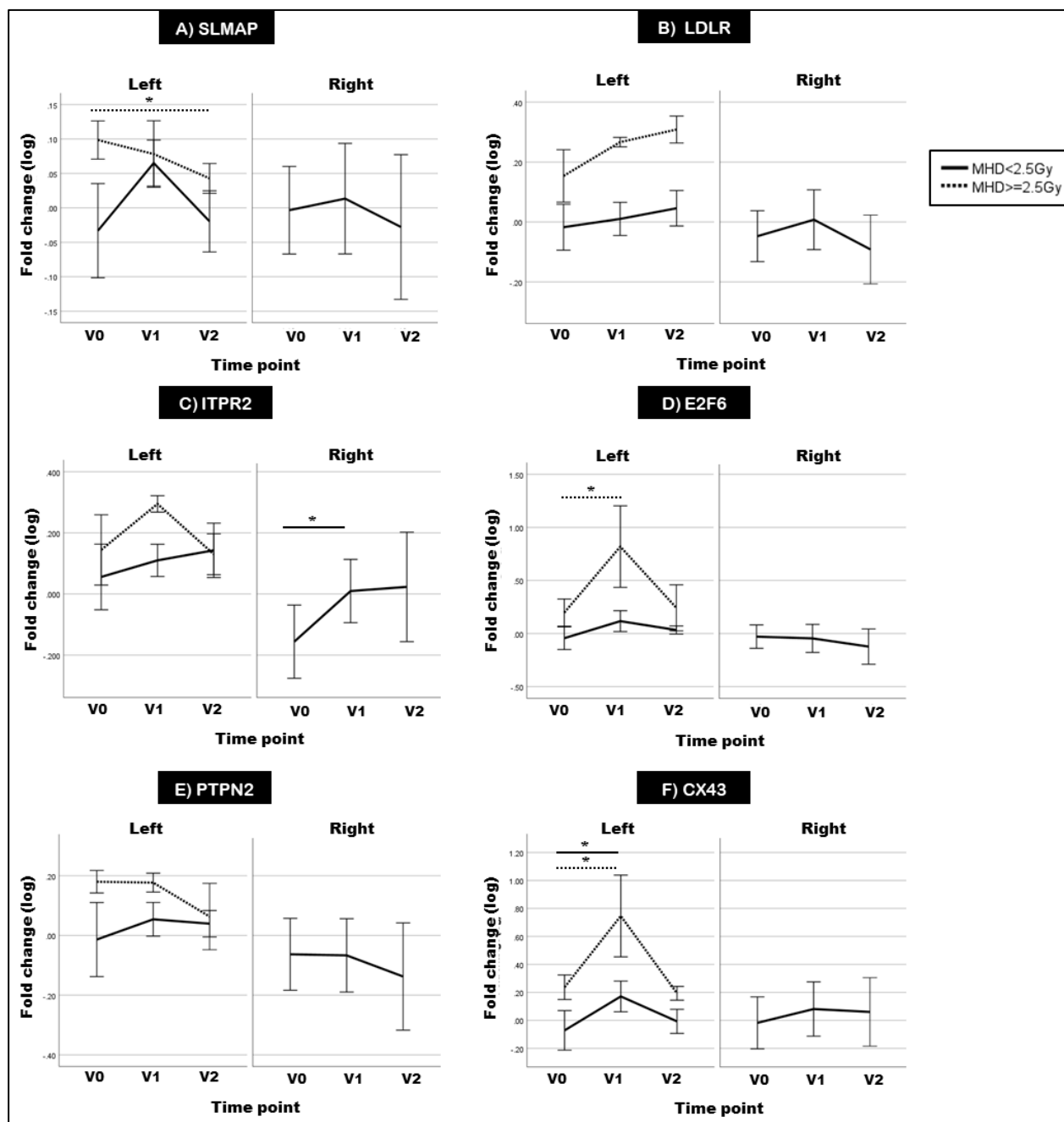
Supplementary table 1.1: *Mean heart dose (MHD) of the MEDIRAD EARLY HEART breast cancer patients included in our analyses*

Patient	Cancer side	MHD
1	Right	0.43
2	Left	2.5
3	Left	0.97
4	Right	0.61
5	Left	1.65
6	Left	1.21
7	Left	2.62
8	Right	0.28
9	Left	4.65
10	Left	1.82
11	Right	2.05
12	Left	1.72
13	Left	2.52
14	Left	1.86
15	Left	2.3
16	Right	1.01
17	Left	2.57
18	Left	2.58
19	Left	2.62
20	Left	2.11
21	Right	1.05
22	Left	2.57
23	Right	1.3
24	Right	0.94
25	Left	2.13
26	Left	1.62
27	Right	1.81
28	Right	1.31
29	Right	1.05
30	Left	1.77
31	Left	2.25
32	Left	1.49
33	Left	1.91
34	Right	1.1
35	Right	1.04
36	Left	2.45
37	Left	1.37
38	Left	1.34

39	Left	1.92
40	Right	1.48
41	Left	1.42
42	Left	0.14
43	Right	1.07

Supplementary table 1.2: *Differentially methylated regions (DMRs) showing > 25% differential methylation at 1.5 months after 27.6 Gy FI relative to sham controls*

Gene	Chromosomal location	Start	End	MeanDiff	Direction
Rassf4	Chr4	1.49E+08	1.49E+08	0.2515	hyper
Ston2	Chr6	1.15E+08	1.15E+08	0.27253	hyper
Srebf1	Chr10	46583686	46583686	0.2586	hyper
RGD1306556	Chr12	49458609	49458609	0.28004	hyper
RGD1306556	Chr12	49505705	49506258	0.26282	hyper
Zfp748	Chr1	38008484	38008484	-0.2639	hypo
Tigd3	Chr1	2.21E+08	2.21E+08	-0.3675	hypo
Mblac2	Chr2	9607537	9607537	-0.2711	hypo
Cdh18	Chr2	74241559	74241843	-0.3379	hypo
RGD1565059	Chr2	1.54E+08	1.54E+08	-0.2928	hypo
Tpk1	Chr4	72944030	72944386	-0.2872	hypo
Cacna1c	Chr4	1.51E+08	1.51E+08	-0.2856	hypo
E2f6	Chr6	42100405	42100405	-0.3561	hypo
Unc79	Chr6	1.27E+08	1.27E+08	-0.2984	hypo
Glyatl3	Chr9	23378114	23378368	-0.3033	hypo
Dnah7-2	Chr9	60143910	60143910	-0.25	hypo
Mtmr3	Chr14	84783955	84784026	-0.3978	hypo
Slmap	Chr16	2224626	2224626	-0.2624	hypo
Smim13	Chr17	21341896	21342113	-0.2851	hypo

Supplementary table 1.3: *DMRs showing > 25% differential methylation at 7 months after 27.6 Gy FI relative to sham controls*

Gene	Chromosomal location	Start	End	MeanDiff	Direction
Rassf4	Chr4	1.49E+08	1.49E+08	0.2515	hyper
Ston2	Chr6	1.15E+08	1.15E+08	0.27253	hyper
Srebf1	Chr10	46583686	46583686	0.2586	hyper
RGD1306556	Chr12	49458609	49458609	0.28004	hyper
RGD1306556	Chr12	49505705	49506258	0.26282	hyper
Zfp748	Chr1	38008484	38008484	-0.2639	hypo
Tigd3	Chr1	2.21E+08	2.21E+08	-0.3675	hypo
Mblac2	Chr2	9607537	9607537	-0.2711	hypo
Cdh18	Chr2	74241559	74241843	-0.3379	hypo
RGD1565059	Chr2	1.54E+08	1.54E+08	-0.2928	hypo
Tpk1	Chr4	72944030	72944386	-0.2872	hypo
Cacna1c	Chr4	1.51E+08	1.51E+08	-0.2856	hypo
E2f6	Chr6	42100405	42100405	-0.3561	hypo
Unc79	Chr6	1.27E+08	1.27E+08	-0.2984	hypo
Glyatl3	Chr9	23378114	23378368	-0.3033	hypo
Dnah7-2	Chr9	60143910	60143910	-0.25	hypo
Mtmr3	Chr14	84783955	84784026	-0.3978	hypo
Slmap	Chr16	2224626	2224626	-0.2624	hypo
Smim13	Chr17	21341896	21342113	-0.2851	hypo

6.2. Supplementary materials for Chapter 4

Supplementary table 2.1: *Pathway enrichment of differentially methylated positions (DMPs) immediately after RT in left sided breast cancer patients.*

Enriched pathway	DMRs associated with pathway
Chemokine signaling pathway	NFKBIA,GSK3A,CCL1,CXCL6,NFKB1,RAP1B,DOCK2,PLCB2,GNB5,PIK3R3,MAPK3,AKT3,GRK7,CXCL13,TIAM1,PIK3CB,CXCR5,CCR2,CCR5,STAT5B,CXCL16,ADCY9,MAP2K1,CXCL10,XCR1,ADCY6,ADCY4,ELMO1,ADRBK1,GNAI2,ADRBK2,ROCK2,CXCR2,GSK3B,CCR8,GNG2,PLCB1,PTK2,GPR29,CX3CR1,GNG5,SRC,CXCR3,FGR,PIK3CD,PRKCZ,GNG7,AKT2,GRK5,PRKCD,CCL26,CXCL12,CDC42,FOXO3,JAK3,PIK3R5,CXCR6,ITK,CCL24,SHC1,ARRB2,GNGT2,CXCL2,LYN,CCR3,PIK3R6,IKBKG
PI3K-Akt signaling pathway	ITGB4,IL2RB,PCK2,HGF,LAMB1,CSF3,COL1A1,VTN,NFKB1,TNN,FLT3,G6PC,CCND2,VWF,PPP2R5A,PDGFRB,GNB5,PHLPP1,PIK3R3,MAPK3,AKT3,TNC,CDK6,CDK2,FGF7,G6PC3,IFNAR1,FLT1,ITGA1,ITGB6,CSF1R,PIK3CB,FGFR4,ITGA5,NOS3,MAP2K1,IGF1,IL7R,RPTOR,RPS6KB2,VEGFB,LAMA3,GSK3B,ITGA11,LPAR5,CREB3L2,GNG2,PPP2R5E,PIK3AP1,PTK2,JAK1,PKN1,PDGFA,COL9A1,CREB5,EPHA2,COL4A2,TNR,FASLG,THBS3,IL6R,CREB3L4,CRTC2,MCL1,NGF,GNG5,YWHAB,CCND3,CSF3R,TLR4,LPAR1,ATF6B,SYK,COL4A1,PIK3CD,LPAR6,IL2RA,COL2A1,GNG7,AKT2,PPP2R2B,YWHAZ,SGK3,BCL2,CDKN1A,MAGI1,IL6,FOXO3,CREB1,JAK3,PIK3R5,LAMA2,FGFR2,PPP2R5C,BDNF,RXRA,PDGFC,GNGT2,ANGPT1,CD19,NR4A1,ITGA7,MLST8,PHLPP2,PIK3R6,CREB3L1,PRLR,IKBKG
Osteoclast differentiation	TNFRSF1A,MAPK13,NFKBIA,RELB,NFKB1,SPI1,MAPK14,PPP3R1,TYROBP,PIK3R3,MAPK3,IL1B,AKT3,FOSL2,IFNAR1,FCGR2A,CSF1R,PPARG,PIK3CB,IFNGR2,MITF,MAP2K1,JUNB,LCK,JAK1,FYN,GAB2,FCGR3A,TREM2,SYK,PIK3CD,TEC,SQSTM1,LILRB2,AKT2,NFATC2,NCF4,SIRPA,IL1R1,CREB1,CYLD,MAPK9,FCGR3B,ACP5,OSCAR,MAP3K14,IKBKG
Th1 and Th2 cell differentiation	MAPK13,IL2RB,NFKBIA,NFKB1,MAPK14,IL5,PPP3R1,NOTCH2,MAPK3,PRKCQ,ZAP70,NOTCH1,IFNGR2,MAML1,STAT5B,STAT6,CD3D,LCK,STAT5A,JAK1,RBPJ,CD3E,CD247,HLA-DMA,GATA3,IL2RA,NFATC2,RUNX3,HLA-DOB,JAK3,HLA-DPA1,MAPK9,HLA-DMB,MAML3,CD3G,MAML2,IKBKG
Th17 cell differentiation	MAPK13,IL2RB,NFKBIA,NFKB1,MAPK14,PPP3R1,RARA,RORA,MAPK3,PRKCQ,IL1B,ZAP70,IFNGR2,STAT5B,STAT6,RUNX1,CD3D,RORC,SMAD3,LCK,IL21R,STAT5A,SMAD4,JAK1,CD3E,CD247,IL6R,RXRB,HLA-DMA,GATA3,IL2RA,IRF4,IL6ST,NFATC2,IL6,IL1R1,HLA-DOB,JAK3,HLA-DPA1,MAPK9,HLA-DMB,RXRA,CD3G,IKBKG
T cell receptor signaling pathway	MAPK13,NFKBIA,NFKB1,MAPK14,IL5,NCK2,PPP3R1,PIK3R3,MAPK3,PRKCQ,AKT3,ZAP70,PIK3CB,CD3D,MAP2K1,CTLA4,RASGRP1,MALT1,GSK3B,CD28,PDCD1,LCK,GRAP2,FYN,CD3E,CD247,PIK3CD,TEC,AKT2,NFATC2,CDC42,PTPN6,MAPK9,ITK,PAK6,PTPRC,IL10,NCK1,CD3G,PAK4,MAP3K14,IKBKG
Insulin resistance	TNFRSF1A,PYGM,PCK2,NFKBIA,PYGB,NFKB1,PRKAB1,NR1H2,G6PC,PIK3R3,PRKCQ,AKT3,CPT1A,G6PC3,PRKAG2,PIK3CB,NOS3,RPS6KB2,PPARGC1B,GSK3B,CREB3L2,ACACB,PPP1CC,SREBF1,CREB5,CREB3L4,CRTC2,PPP1R3D,PTPN1,PIK3CD,TBC1D4,PRKCZ,FOXO1,AKT2,PRKCD,PPARA,IL6,CREB1,MAPK9,CD36,RPS6KA2,RPS6KA1,NR1H3,CREB3L1,SLC27A3

Yersinia infection	MAPK13,NFKBIA,MEFV,NFKB1,MAPK14,PYCARD,ACTR3C,PIK3R3,MAPK3,ACTR3,IL1B,AKT3, ZAP70,FCGR2A,IL18,PIK3CB,ELMO2,ITGA5,MAP2K1,ELMO1,BAIAP2,ROCK2,WIPF2,GSK3B,L IMK1,NLRP3,LCK,RHOG,PTK2,PKN1,MAP2K3,GIT2,SRC,TLR4,ARHGEF7,PIK3CD,AKT2,WIPF1, NFATC2,CDC42,NLRC4,IL6,MAPK9,IL10,RPS6KA2,RPS6KA1,WASF2,IKBKG
Human T-cell leukemia virus 1 infection	TNFRSF1A,IL2RB,NFKBIA,RELB,NFKB1,SPI1,LTBR,PPP3R1,MSX2,TBPL2,CANX,HLA-F,CCND2,ANAPC5,CREBBP,PIK3R3,TCF3,MAPK3,AKT3,VDAC1,CDK2,CRTC3,PIK3CB,TNFRSF1 3C,STAT5B,ADCY9,CD3D,MAP2K1,ADCY6,ADCY4,CALR,CREB3L2,IL1R2,SMAD3,LCK,STAT5A, SMAD4,JAK1,ITGAL,CREB5,CD3E,CREB3L4,CRTC2,CCND3,HLA-DMA,ATF6B,HLA-E,PIK3CD,IL2RA,AKT2,ETS1,NFATC2,ITGB2,CDKN1A,MAD1L1,IL6,IL1R1,CREB1,CHEK1,HLA-DOB,JAK3,HLA-DPA1,MAPK9,HLA-DMB,LTA,CD3G,B2M,ZFP36,CREB3L1,MAP3K14,IKBKG
Pathways in cancer	RALA,DVL2,RALBP1,GNA11,IL2RB,NFKBIA,MMP2,HGF,LAMB1,NFKB1,SPI1,IL5,MLH1,FLT3,R ARA,NOTCH2,APC,PLCB2,CCND2,TRAF5,CDH1,PDGFRB,GNB5,DAPK2,AXIN1,CREBBP,PIK3R 3,MAPK3,AKT3,CBL,MECOM,CDK6,CDK2,FGF7,IFNAR1,WNT9A,CALM2,RALB,SKP2,GNA12, NOTCH1,CSF1R,PPARG,PIK3CB,IFNGR2,FGFR4,STAT5B,ADCY9,MITF,HHIP,STAT6,RUNX1,M AP2K1,IGF1,IL7R,ARNT2,RPS6KB2,RASGRP1,PPARD,VEGFB,ADCY6,CTBP2,ADCY4,GNAI2,RO CK2,EML4,LAMA3,GSK3B,CUL1,LPAR5,PTCH1,SMAD3,GNG2,PLCB1,HEY1,PTK2,STAT5A,SM AD4,PLD1,JAK1,ESR2,CTNNB1,PDGFA,RET,PTGER3,COL4A2,FASLG,MGST3,IL6R,TPM3,SUFU ,GNG5,FRAT2,FRAT1,RALGDS,CCND3,CSF3R,TRAF1,LPAR1,RXRB,NOTCH4,ZBTB17,COL4A1, PIK3CD,LPAR6,DVL1,FOXO1,IL2RA,BRCA2,NKX3-1,IL6ST,GNG7,ALK,AKT2,ETS1,KIF7,CXCL12,MGST1,NFE2L2,WNT5B,BCL2,GSTP1,CDC42,TX NRD2,CSF2RB,CDKN1A,NCOA1,IL6,GLI2,JAK3,MAPK9,LAMA2,ESR1,FGFR2,CALML4,AGTR1, RXRA,GNGT2,CEBPA,TXNRD1,PLEKHG5,TRAF3,RASSF5,NCOA4,BIRC2,RPS6KA5,MGST2,IKB KG
TNF signaling pathway	TNFRSF1A,MAPK13,RIPK3,NFKBIA,CXCL6,NFKB1,MAPK14,IRF1,TRAF5,PIK3R3,MAPK3,IL1B, AKT3,PIK3CB,VCAM1,NOD2,MAP2K1,JUNB,CXCL10,MMP14,CREB3L2,MAP2K3,CREB5,CRE B3L4,TRAF1,ATF6B,TNFRSF1B,PIK3CD,AKT2,IL6,CREB1,MAPK9,LTA,CXCL2,TRAF3,BIRC2,RPS 6KA5,ITCH,TNFAIP3,CREB3L1,MAP3K14,IKBKG
Rap1 signaling pathway	RALA,MAPK13,SIPA1L3,HGF,MAPK14,RAP1B,PLCB2,CDH1,PDGFRB,PIK3R3,MAPK3,AKT3,F ARP2,RAPGEF2,FGF7,CALM2,RALB,FLT1,CSF1R,TIAM1,PIK3CB,FGFR4,ADCY9,MAP2K1,IGF1, VEGFB,ADCY6,ADCY4,GNAI2,LPAR5,ADORA2A,PLCB1,CTNNB1,MAP2K3,PDGFA,ITGAL,EPH A2,SIPA1L2,NGF,GRIN1,RALGDS,RAPGEF1,SRC,LPAR1,APBB1IP,PIK3CD,PRKCZ,AKT2,EVL,GR IN2A,RAPGEF4,ITGB2,CTNND1,CDC42,MAGI1,RAPGEF3,DOCK4,FGFR2,CALML4,PDGFC,AN GPT1,RAP1GAP,ITGAM,SIPA1L1,RASSF5
Adrenergic signaling in cardiomyocytes	KCNQ1,MAPK13,MAPK14,PLCB2,PPP2R5A,MAPK3,AKT3,SLC9A1,CREM,CACNA1C,CALM2,A TP1B3,FXYD2,ADCY9,ADCY6,ADCY4,GNAI2,SCN4B,CREB3L2,KCNE1,PPP2R5E,PLCB1,PPP1C C,ATP2B4,CREB5,ATP2A3,ATP2B2,RYR2,TPM3,CREB3L4,ATF6B,CACNA2D4,AKT2,PPP2R2B, RAPGEF4,BCL2,SLC8A1,CREB1,PIK3R5,RAPGEF3,SCN5A,PPP2R5C,CACNA2D2,CALML4,AGT R1,ATP2A2,ATP1A3,ATP1A1,RPS6KA5,PIK3R6,CREB3L1
Regulation of actin cytoskeleton	ITGB4,VCL,MYH9,CHRM3,RRAS2,APC,PDGFRB,PIK3R3,ARPC1A,MAPK3,ITGAE,SLC9A1,FGF7 ,IQGAP2,MYLK4,GNA12,MYL9,ITGA1,ITGB6,TIAM1,PIK3CB,FGFR4,ITGA5,ABI2,SCIN,MAP2K 1,SSH3,SSH1,BAIAP2,ROCK2,ITGA11,LPAR5,LIMK1,LIMK2,PTK2,PPP1CC,PDGFA,ITGAL,IQGA P3,SRC,GSN,LPAR1,FGD3,ARHGEF7,MYLK2,PIP4K2A,PIK3CD,CHRM5,ACTN1,CXCL12,MYH1

	1,ITGB2,DIAPH1,CDC42,DIAPH3,RDX,PAK6,FGFR2,PDGFC,ITGAM,CYFIP2,ITGA7,ITGAX,PAK4,PPP1R12B,CYFIP1,WASF2
Shigellosis	TNFRSF1A,MAPK13,VCL,NFKBIA,GSK3A,NFKB1,MAPK14,PYCARD,PLCB2,TRAF5,WIPI1,PIK3R3,ARPC1A,MAPK3,PRKCQ,IL1B,AKT3,SEPT11,FBXW11,VDAC1,MYL9,IL18,PIK3CB,ELMO2,ITGA5,CYTH3,ITPR1,RPTOR,RPS6KB2,ELMO1,UBE2N,TNIP1,ROCK2,MALT1,GSK3B,CUL1,TMEM173,NLRP3,PLCB1,PTK2,CYTH1,ARHGEF2,TIFA,SRC,UBE2D1,TLR4,PIK3CD,FOXO1,SQSTM1,AKT2,ACTN1,PRKCD,CAST,BCL2,DIAPH1,UBE2D2,CDC42,NLRC4,FOXO3,IL1R1,SEPT9,MAPK9,HK1,TECPR1,UBC,PLCD3,RPS6KA5,WASF2,IKBKG
cAMP signaling pathway	NFKBIA,NFKB1,LIPE,RAP1B,RRAS2,CREBBP,PIK3R3,MAPK3,AKT3,SLC9A1,CACNA1C,CALM2,MYL9,PDE3B,ATP1B3,TIAM1,PIK3CB,HTR6,FXYD2,ADCY9,LHCGR,HHIP,MAP2K1,ADCY6,ADCY4,GNAI2,ROCK2,CREB3L2,PTCH1,GHRL,ADORA2A,PPP1CC,PLD1,PDE4D,ACOX3,PTGER3,ATP2B4,CREB5,ATP2A3,ATP2B2,RYR2,CREB3L4,GRIN1,ABCC4,GABBR1,PIK3CD,PDE4A,AKT2,GRIN2A,RAPGEF4,CNGA1,PPARA,CREB1,HCAR1,MAPK9,RAPGEF3,BDNF,CALML4,ATP2A2,ATP1A3,ATP1A1,GIPR,FFAR2,ORAI1,FXYD1,CREB3L1
Phospholipase D signaling pathway	RALA,RRAS2,PLCB2,PDGFRB,PIK3R3,MAPK3,AKT3,DGKD,DGKG,RALB,GNA12,DGKE,PIK3CB,FCER1G,ADCY9,CYTH3,MAP2K1,ADCY6,ADCY4,AGPAT4,CXCR2,LPAR5,DGKA,PLCB1,PLD1,PDGFA,FYN,CYTH1,GAB2,PLA2G4A,FCER1A,PPAP2B,RALGDS,DNM1,LPAR1,SYK,PIK3CD,LPAR6,DNM2,AKT2,RAPGEF4,AGPAT3,DGKB,PIK3R5,RAPGEF3,SHC1,DGKZ,AGTR1,PDGFC,PIK3R6
AMPK signaling pathway	PCK2,PRKAB1,PFKFB4,LIPE,G6PC,CAB39,TBC1D1,PPP2R5A,RAB2A,PIK3R3,EEF2K,AKT3,CPT1A,G6PC3,PPARG,PRKAG2,HMGCR,PIK3CB,IGF1,RPTOR,RPS6KB2,LEP,CAMKK2,CREB3L2,PPP2R5E,ACACB,SREBF1,CREB5,CREB3L4,CRTC2,PIK3CD,FOXO1,AKT2,PPP2R2B,ELAVL1,FOXO3,CREB1,CD36,PPP2R5C,PFKFB3,CAB39L,CREB3L1,ACACA
Platelet activation	MAPK13,COL1A1,MAPK14,RAP1B,PLCB2,VWF,PIK3R3,MAPK3,AKT3,FCGR2A,MYLK4,FERMT3,PIK3CB,FCER1G,ADCY9,NOS3,GP9,FGB,ITPR1,P2RY12,RASGRP1,ADCY6,ADCY4,GNAI2,ROCK2,PLCB1,PPP1CC,FYN,PLA2G4A,SRC,PRKG1,SYK,MYLK2,APBB1IP,PIK3CD,PRKCZ,AKT2,GP1BB,PIK3R5,TBXA2R,LYN,PIK3R6,ORAI1
Hematopoietic cell lineage	CD22,CSF3,IL5,FLT3,IL1B,ITGA1,CSF1R,ITGA5,CD3D,GP9,IL7R,CD34,CD7,IL1R2,CD3E,CD1E,CD1D,IL6R,CD2,CSF3R,HLA-DMA,IL2RA,CD9,CD59,GP1BB,IL6,IL1R1,HLA-DOB,HLA-DPA1,HLA-DMB,CD36,MME,CD3G,CD19,ITGAM
PD-L1 expression and PD-1 checkpoint pathway in cancer	MAPK13,NFKBIA,NFKB1,MAPK14,PPP3R1,PIK3R3,MAPK3,PRKCQ,AKT3,ZAP70,PIK3CB,IFNGR2,CD3D,MAP2K1,RPS6KB2,RASGRP1,EML4,CD28,PDCD1,LCK,JAK1,MAP2K3,TLR9,CD3E,CD247,TLR4,PIK3CD,ALK,AKT2,NFATC2,PTPN6,TICAM2,CD3G,IKBKG
Glycerolipid metabolism	DGAT2,LPIN2,ALDH2,DGKD,DGKG,MGLL,DGKE,MBOAT2,LPL,LCLAT1,AGPAT4,MBOAT1,DGKA,PNPLA2,AGK,AKR1B10,PPAP2B,AKR1A1,DAK,AGPAT6,AGPAT3,DGKB,GLYCTK,LPIN1,DGKZ
cGMP-PKG signaling pathway	GNA11,PPP3R1,PLCB2,MAPK3,AKT3,VDAC1,CACNA1C,CALM2,KCNMB1,MYLK4,GNA12,MYL9,PDE3B,ATP1B3,KCNMA1,FXYD2,ADCY9,NOS3,MAP2K1,ITPR1,ADCY6,ADCY4,GNAI2,ROCK2,CREB3L2,GATA4,PLCB1,TRPC6,PPP1CC,ATP2B4,CREB5,ATP2A3,ATP2B2,CREB3L4,PRKG1,ATF6B,MYLK2,AKT2,NFATC2,CNGA1,SLC8A1,CREB1,BORCS8-

	MEF2B,PIK3R5,GTF2IRD1,MEF2B,CALML4,AGTR1,ATP2A2,ATP1A3,ATP1A1,PIK3R6,CREB3L1
Sphingolipid signaling pathway	TNFRSF1A,MAPK13,SPTLC2,NFKB1,MAPK14,S1PR4,CERS4,PLCB2,PPP2R5A,PIK3R3,MAPK3,AKT3,CERS2,GNA12,CERS3,PIK3CB,FCER1G,NOS3,MAP2K1,S1PR1,DEGS2,GNAI2,ROCK2,PPP2R5E,PLCB1,PLD1,FYN,SGMS1,GAB2,FCER1A,PIK3CD,PRKCZ,AKT2,PPP2R2B,SGMS2,BCL2,ABCC1,MAPK9,NSMAF,PPP2R5C,S1PR2
Focal adhesion	ITGB4,VCL,HGF,LAMB1,CAV2,COL1A1,VTN,TNN,RAP1B,CCND2,VWF,PDGFRB,PIK3R3,MAPK3,AKT3,TNC,MYLK4,MYL9,FLT1,ITGA1,ITGB6,PIK3CB,ITGA5,MAP2K1,IGF1,VEGFB,ROCK2,LAMA3,GSK3B,ITGA11,PTK2,PPP1CC,CTNNB1,PDGFA,FYN,COL9A1,COL4A2,TNR,THBS3,RAPGEF1,CCND3,SRC,COL4A1,MYLK2,PIK3CD,COL2A1,AKT2,ACTN1,BCL2,DIAPH1,CDC42,PARVG,MAPK9,LAMA2,SHC1,RASGRF1,PAK6,PDGFC,ITGA7,PAK4,PPP1R12B,BIRC2
C-type lectin receptor signaling pathway	MAPK13,NFKBIA,RELB,NFKB1,MAPK14,PPP3R1,IRF1,PYCARD,RRAS2,PIK3R3,MAPK3,IL1B,AKT3,CALM2,PIK3CB,FCER1G,CLEC4D,CLEC7A,ITPR1,MALT1,NLRP3,CARD9,SRC,SYK,PIK3CD,LSP1,AKT2,PRKCD,NFATC2,KSR1,IL6,CYLD,MAPK9,IL10,CALML4,MAP3K14,IKBKG
Viral protein interaction with cytokine and cytokine receptor	TNFRSF1A,IL2RB,CCL1,CXCL6,LTBR,TNFRSF10B,IL18,CSF1R,CXCL13,IL10RB,CXCR5,CCR2,CCR5,CXCL10,XCR1,CXCR2,CCR8,IL20RB,IL19,GPR29,TNFRSF10C,CX3CR1,IL6R,CXCR3,TNFRSF1B,IL2RA,IL6ST,CCL26,CXCL12,IL6,CCL24,LTA,IL10,CXCL2,CCR3
Hedgehog signaling pathway	CCND2,MGRN1,CUL3,FBXW11,HHIP,ADRBK1,ADRBK2,GSK3B,CUL1,PTCH1,CSNK1G3,SMURF1,SUFU,KIF7,CSNK1E,BCL2,GLI2,ARRB2,BOC,GPR161,C16orf52
Endocytosis	ARF5,PSD,SPG21,IL2RB,CAV2,ZFYVE20,HLA-F,SNX1,RAB11A,RAB11FIP3,ARPC1A,CBL,GRK7,CCR5,FGFR4,AP2M1,CYTH3,VPS37C,ADRBK1,BIN1,ADRBK2,EEA1,CXCR2,WIPF2,PSD3,RUFY1,HGS,RAB11FIP1,SMAD3,PLD1,ACAP3,GIT2,RAB11FIP2,AMPH,AP2A1,CYTH1,SMURF1,VPS45,EPS15,ARFGEF2,SMAP2,DNM1,SRC,LDLRAP1,HLA-E,VPS28,PRKCZ,SNX2,IL2RA,DNM2,WIPF1,GRK5,ARAP1,IQSEC2,AGAP3,CHMP7,CDC42,NEDD4L,KIF5C,ARRB2,CHMP3,FGFR2,SPG20,ASAP1,IST1,CLTCL1,RAB31,EHD1,IQSEC1,ITCH,VPS29,FOLR3
Viral carcinogenesis	HDAC7,NFKBIA,NFKB1,LTBR,UBE3A,TBPL2,GTF2H4,HLA-F,CCND2,TRAF5,CREBBP,PIK3R3,MAPK3,HDAC4,CDK6,CDK2,SKP2,PIK3CB,CCR5,STAT5B,SCIN,PKM,CCR8,CREB3L2,STAT5A,JAK1,USP7,RBPJ,GTF2E2,CREB5,CREB3L4,GTF2B,YWHAB,CCND3,SRC,GSN,TRAF1,ATF6B,UBR4,SYK,HLA-E,PIK3CD,IL6ST,ACTN1,YWHAZ,CDC42,CDKN1A,MAD1L1,CREB1,CHEK1,JAK3,HDAC9,LYN,CCR3,TRAF3,CREB3L1,IKBKG
Immune System	RALA,PGLYRP1,TNFRSF17,CD22,ICAM3,TNFRSF1A,CPB2,CDK13,PILRA,UNC13D,MAPK13,VCL,ARSA,MYH9,IL2RB,RIPK3,CTSG,NFKBIA,PYGB,CTSZ,OLFM4,MMP2,MEFV,CSK,PAG1,RELB,RAB3D,HGF,MPO,CSF3,COL1A1,DUSP3,VTN,NFKB1,MLEC,LTA4H,LTBR,MAPK14,TMEM30A,LNPEP,IL5,LTF,UBE3A,SLC11A1,IL1RL1,AZU1,PPP3R1,PRTN3,CD160,FLT3,TNFAIP6,PI3,CEACAM8,FBXO9,TREM1,MT2A,IRF1,NUP85,CANX,PYCARD,TUBA4A,PTPN12,PIAS1,CD68,RAP1B,PVRL2,ZFYVE20,LGALS3,NUP210,RAP1GAP2,CHI3L1,DOCK2,TCN1,FBXL8,CAB39,EDAR,BLK,IL36G,IL1RN,PSMB7,RNF144B,HLA-F,SDCBP,KIF23,ADAM10,DNAJC13,IRAK3,LYZ,CLEC2D,LMNB1,HEXB,PPP2R5A,RORA,CDH1,CYSTM1,ANAPC5,LPO,CREBBP,MGRN1,CRISPLD2,NLRC5,TYROBP,PIK3R3,TIMP2,SAMHD1,

	ARPC1A,MAPK3,PRKCQ,ACTR3,IL1B,CD81,AKT3,LNX1,TNFRSF8,CBL,CD80,IL1RL2,TXK,HERC5,CUL3,ASB1,ATP6V0A1,ZAP70,FBXW11,MAPKAP1,CD27,SLC15A4,BIN2,IRF8,GALNS,IFNAR1,ECSIT,FCN3,FCGR2A,C1orf35,ATP6V1A,SKP2,IQGAP2,KCTD7,ATP6V1B2,SERPING1,MS4A3,AIP,IL18,SEC24D,TNFSF4,LPCAT1,ATP8B4,SH3RF1,APP,CSF1R,UBE2L6,PIK3CB,FCER1G,IL10RB,IFNGR2,ELMO2,TNFRSF13C,TRIM62,CCR2,CCR5,AP2M1,STAT5B,EIF4A1,VCAM1,NCSTN,STK11IP,ABI2,IL17RC,S100P,CAMP,TREX1,FABP5,BRI3,DEFA4,NOS3,C2,RAG1,CLEC4D,STAT6,NOD2,CD3D,TUBA1C,RILP,UNKL,MAP2K1,CLEC7A,LRG1,IL16,JUNB,NKIRAS2,UBE2E1,CTLA4,ATP6V1E2,S1PR1,CXCL10,FGB,IL7R,ITPR1,ISG20,PTPN7,OLR1,CLCF1,SLCO4C1,CD34,RASGRP1,FBXW8,MUCL1,RAB6A,SPSB4,ELMO1,MID1,PRKDC,VAMP2,TOLLIP,CLU,UBE2N,BAIAP2,CPNE1,EEA1,ENPP4,CAMK2G,MALT1,CPN2,CXCR2,PKM,CALR,WIPF2,IL17RA,ASB4,FBXL13,PELI3,ACPP,CD28,EIF4A2,CUL1,RORC,P4HB,IL20RB,P2RX7,IL1R2,TMEM173,KLHL22,CD86,CFD,SYNGR1,GPR97,SMAD3,UBA7,PDCD1,EDARADD,ZNRF1,LIMK1,KLHL25,SLC44A2,NLRP3,PPP2R5E,LCK,IL21R,TUBB,GRAP2,RHOG,TSLP,PIK3AP1,MAOA,GYG1,MEF2C,COL17A1,PTK2,STAT5A,PRDX6,SLPI,IFI6,PLD1,IL19,TRIM29,JAK1,SEC24C,TNFSF13,GPR29,TRIM14,CTNNB1,NFASC,FBXL14,FBXL5,MAP2K3,IMPDH1,HMGB1,CTSB,NUP50,PGLYRP2,ANXA2,MEF2A,ATG7,FYN,KCTD6,RNF220,UBE2H,VAT1,CLEC12A,HP,RAC1,AMICA1,ORAI2,ITGAL,IL27,ARG1,TRIM38,RAET1E,DOK3,IRF5,CEACAM3,AP1B1,PTPN5,PELI1,AP2A1,PCBP2,PGLYRP4,MYO1C,TLR9,DNAJC5,CD3E,SMURF1,CD247,DCTN1,TIFA,GAB2,PJA1,TMEM63A,CR2,C4BPA,CHIT1,FASLG,POU2F1,FCGR3A,SLAMF7,FCER1A,AIM2,CD1D,IL6R,S100A7A,S100A8,S100A9,HRNR,MCL1,CD58,AHCYL1,FBXW4,UBE2U,PGM1,SH2D1A,PTPN1,CARD9,UBAC1,IFIT2,RAPGEF1,SFTPD,PLAU,YWHAB,DNM1,LCN2,CSF3R,TREM2,SRC,GSN,PTAFR,UBE2D1,TLR4,PRKG1,FGR,TXN,HLA-DMA,PSMB9,PSMB8,CDA,UBR4,CD300LD,BPIFB4,SYK,TNFRSF1B,HLA-E,TRIM39,ANXA1,FTL,PIK3CD,SLC2A5,KLHL21,TNFRSF25,CKAP4,NUP160,GATA3,YPEL5,FOXO1,NHLRC3,IL2RA,MTAP,FBXL19,COL2A1,IRF4,IL6ST,TEC,KLRD1,DEFB136,SEC13,DNM2,SIGLEC15,SQSTM1,LAIR1,LILRB2,AKT2,DYNLL1,WIPF1,PLD4,RAB37,EVL,ORMDL3,PRKCD,KIF20A,DAK,FZR1,HERC4,SEC31A,CD59,ATP6V1C1,YWHAZ,NFATC2,MGST1,RAB27A,TAX1BP1,AMPD3,RAPGEF4,NCF4,ITGB2,BCL2,LONRF1,DIAPH1,GSTP1,UBE2D2,GRB10,MYO5A,SIRPA,FKBP1A,CDC42,NEDD4L,EIF4G3,CSF2RB,IL18BP,HPSE,BCL6,FBXO11,PRR5,CDKN1A,C1S,NLRC4,SAR1B,IL6,KIF3A,FOXO3,IFITM1,IL1R1,UBE2E3,PLD3,CREB1,KIF26A,TLR6,DSN1,HLA-DOB,PTPN6,JAK3,PILRB,CYLD,EIF4E3,HLA-DPA1,SLA,MAPK9,GCA,SMARCA4,RAPGEF3,TSPAN14,PSMD13,UBE2W,ITK,HLA-DMB,CD36,PLAC8,PTPRJ,UBE2L3,HECTD2,SHC1,SIGLEC6,SERPINB2,LTA,FBXO10,RACGAP1,GPI,ANO6,CRACR2A,TMBIM1,TRIM26,LTB,PTPRC,IL10,PPP2R5C,STXBP2,TOM1,SIGLEC9,PSMA1,DCTN4,KLC1,NBEAL2,TICAM2,ICAM2,EIF4G1,NCK1,MME,TREML2,CD200,ATP11A,RNF182,MYO10,ANAPC13,DAPP1,FBXL7,KLHL5,LAMTOR3,MIB2,RNASET2,RPS6KA2,FYB,CXCL2,FBXO32,SPSB2,RNF217,LYN,RNF19A,ATOX1,CD3G,LMO7,FCGR3B,RAP1GAP,RPS6KA1,CD19,IST1,TARM1,HMHA1,UBC,ITGAM,MUC12,NUP153,CYFIP2,SOD2,MGAM,CD63,METTL7A,RPLP0,CLEC5A,ASB2,PSTPIP1,B2M,ADAM8,RNF111,TRAF3,ITGAX,MLST8,RAB31,TMC6,ELANE,FPR2,NUP62,MYO9B,ALDH3B1,HMOX2,CPNE3,BIRC2,LRRC41,STIM1,NLRP1,RAG2,TNFRSF9,OSCAR,CD177,RPS6KA5,ITCH,ORAI1,CYFIP1,RAB44,FOLR3,TNFAIP3,MAP3K14,PRLR,WASF2,IFI27,IKBKG,SERPINB6
Innate Immune System	PGLYRP1,ICAM3,CPB2,CDK13,UNC13D,MAPK13,VCL,ARSA,MYH9,RIPK3,CTSG,NFKBIA,PYGB,CTSZ,OLFM4,MEFV,RELB,RAB3D,MPO,DUSP3,VTN,NFKB1,MLEC,LTA4H,MAPK14,TMEM3

	0A,LTF,SLC11A1,AZU1,PPP3R1,PRTN3,TNFAIP6,PI3,CEACAM8,TREM1,PYCARD,CD68,RAP1B,ZFYVE20,LGALS3,CHI3L1,DOCK2,TCN1,CAB39,PSMB7,SDCBP,ADAM10,DNAJC13,IRAK3,LYZ,HEXB,CYSTM1,LPO,CREBBP,CRISPLD2,NLRC5,TYROBP,TIMP2,ARPC1A,MAPK3,PRKCQ,ACTR3,IL1B,CD81,TXK,HERC5,ATP6V0A1,FBXW11,SLC15A4,BIN2,GALNS,ECSIT,FCN3,FCGR2A,C1orf35,ATP6V1A,IQGAP2,ATP6V1B2,SERPING1,MS4A3,LPCAT1,ATP8B4,APP,UBE2L6,PIK3CB,FCER1G,ELMO2,CCR2,NCSTN,STK11IP,ABI2,S100P,CAMP,TREX1,FABP5,BRI3,DEFA4,NOS3,C2,CLEC4D,STAT6,NOD2,MAP2K1,CLEC7A,LRG1,NKIRAS2,ATP6V1E2,FGB,ITPR1,OLR1,SLCO4C1,RASGRP1,MUCL1,RAB6A,ELMO1,PRKDC,TOLLIP,CLU,UBE2N,BAIAP2,CPNE1,EEA1,ENPP4,MALT1,CPN2,CXCR2,PKM,WIPF2,PELI3,ACPP,CUL1,P2RX7,TMEM173,CFD,SYNGR1,GPR97,UBA7,LIMK1,SLC44A2,NLRP3,LCK,TUBB,GRAP2,RHOG,GYG1,MEF2C,PTK2,PRDX6,SLPI,PLD1,GPR29,CTNNB1,NFASC,MAP2K3,IMPDH1,HMGB1,CTSB,PGLYRP2,ANXA2,MEF2A,ATG7,FYN,VAT1,CLEC12A,HP,RAC1,ITGAL,ARG1,DOK3,CEACAM3,PELI1,PCBP2,PGLYRP4,MYO1C,TLR9,DNAJC5,CD247,TIFA,GAB2,TMEM63A,CR2,C4BPA,CHIT1,FCGR3A,FCER1A,AIM2,S100A7A,S100A8,S100A9,HRNR,CD58,AHCYL1,PGM1,CARD9,SFTPD,PLAU,DNM1,LCN2,TREM2,SRC,GSN,PTAFR,UBE2D1,TLR4,FGR,TXN,PSMB9,PSMB8,CDA,UBR4,BPIFB4,SYK,TNFRSF1B,HLA-E,FTL,SLC2A5,CKAP4,YPEL5,NHLRC3,TEC,KLRD1,DEFB136,DNM2,SIGLEC15,LAIR1,LILRB2,DYNLL1,WIPF1,PLD4,RAB37,ORMDL3,PRKCD,DAK,CD59,ATP6V1C1,NFATC2,MGST1,RAB27A,TAX1BP1,AMPD3,NCF4,ITGB2,BCL2,DIAPH1,GSTP1,UBE2D2,MYO5A,SIRPA,CDC42,HPSE,C1S,NLRC4,PLD3,CREB1,TLR6,DSN1,PTPN6,CYLD,MAPK9,GCA,TSPAN14,PSMD13,ITK,CD36,PLAC8,PTPRJ,SHC1,GPI,ANO6,CRACR2A,TMBIM1,PTPRC,TOM1,SIGLEC9,PSMA1,NBEAL2,TICAM2,ICAM2,NCK1,MME,ATP11A,MYO10,LAMTOR3,RNASET2,RPS6KA2,LYN,ATOX1,CD3G,FCGR3B,RPS6KA1,CD19,IST1,TARM1,HMHA1,UBC,ITGAM,MUC12,CYFIP2,MGAM,CD63,METTL7A,CLEC5A,PSTPIP1,B2M,ADAM8,TRAF3,ITGAX,RAB31,TMC6,ELANE,FPR2,MYO9B,ALDH3B1,HMOX2,CPNE3,BIRC2,NLRP1,OSCAR,CD177,RPS6KA5,ITCH,CYFIP1,RAB44,FOLR3,TNFAIP3,MAP3K14,WASF2,IKBKG,SERPINB6
Neutrophil degranulation	PGLYRP1,CDK13,UNC13D,VCL,ARSA,CTSG,PYGB,CTSZ,OLFM4,RAB3D,MPO,NFKB1,MLEC,LTA4H,MAPK14,TMEM30A,LTF,SLC11A1,AZU1,PRTN3,TNFAIP6,CEACAM8,PYCARD,CD68,RAP1B,LGALS3,CHI3L1,DOCK2,TCN1,CAB39,PSMB7,SDCBP,ADAM10,DNAJC13,LYZ,HEXB,CYSTM1,CRISPLD2,TYROBP,TIMP2,ATP6V0A1,SLC15A4,BIN2,GALNS,FCGR2A,C1orf35,IQGAP2,MS4A3,LPCAT1,ATP8B4,FCER1G,NCSTN,STK11IP,S100P,CAMP,FABP5,BRI3,DEFA4,CLEC4D,LRG1,OLR1,SLCO4C1,RAB6A,TOLLIP,CPNE1,ENPP4,CXCR2,PKM,ACPP,TMEM173,CFD,SYNGR1,GPR97,SLC44A2,TUBB,RHOG,GYG1,PRDX6,SLPI,PLD1,NFASC,IMPDH1,HMGB1,CTSB,ANXA2,ATG7,VAT1,CLEC12A,HP,RAC1,ITGAL,ARG1,DOK3,CEACAM3,DNAJC5,TMEM63A,CHIT1,S100A8,S100A9,HRNR,CD58,PGM1,PLAU,LCN2,GSN,PTAFR,FGR,CDA,UBR4,TNFRSF1B,FTL,SLC2A5,CKAP4,YPEL5,NHLRC3,LAIR1,LILRB2,DYNLL1,RAB37,ORMDL3,PRKCD,CD59,MGST1,RAB27A,AMPD3,ITGB2,DIAPH1,GSTP1,SIRPA,HPSE,DSN1,PTPN6,GCA,TSPAN14,PSMD13,CD36,PLAC8,PTPRJ,GPI,ANO6,CRACR2A,TMBIM1,PTPRC,TOM1,SIGLEC9,NBEAL2,TICAM2,MME,ATP11A,LAMTOR3,RNASET2,FCGR3B,IST1,TARM1,HMHA1,ITGAM,MGAM,CD63,METTL7A,CLEC5A,B2M,ADAM8,ITGAX,RAB31,TMC6,ELANE,FPR2,ALDH3B1,HMOX2,CPNE3,OSCAR,CD177,CYFIP1,RAB44,FOLR3,SERPINB6
Hemostasis	GNA11,CBX5,VCL,CSK,PLAT,HGF,AKAP10,COL1A1,SELPLG,MAPK14,SPARC,PLEK,PRTN3,APOA1,SRGN,CEACAM8,TREM1,IRF1,TUBA4A,RAP1B,F12,ZFYVE20,IGJ,CABLES1,DOCK2,DOCK

	10,GYPC,KIF23,VWF,PPP2R5A,SLC7A5,GNB5,PIK3R3,MAPK3,PRKCQ,APLP2,KIF1B,DGKD,DGKG,MGLL,SRI,CDK2,ITPK1,GATA6,KCNMB1,GNA12,DOK2,TNFRSF10B,SERPING1,FERMT3,SLC7A11,ITGA1,DGKE,APP,PDE11A,ATP1B3,KCNMA1,PIK3CB,FCER1G,PDE9A,ITGA5,MERTK,ANXA5,F2RL2,NOS3,TUBA1C,IGF1,GP9,FGB,ITPR1,SDC2,P2RY12,OLR1,RASGRP1,VEGFB,GNAI2,CLU,SLC7A8,SLC16A8,ZFPM1,DGKA,PRKCH,P2RX7,CFD,GNG2,GATA4,PPP2R5E,LCK,RHOG,MYB,TRPC6,PTK2,MAFK,MAFF,ANXA2,PDGFA,FYN,RAC1,AMICA1,ORAI2,ITGAL,CEACAM3,ATP2B4,MAFG,ATP2A3,SPN,ATP2B2,SCCPDH,PLA2G4A,F11R,CD244,VPS45,CD2,CD58,GNG5,PTPN1,PLAU,SRC,PRKG1,FGR,SYK,APBB1IP,DOCK9,ABCC4,PRKCZ,GATA3,LHFPL2,GNG7,CD9,MAG,ACTN1,PRKCD,KIF20A,MMRN1,YWHAZ,RAPGEF4,SLC7A7,ITGB2,SIRPA,CDC42,GP1BB,ZFPM2,SLC8A1,VPREB1,DGKB,KIF3A,KIF26A,PTPN6,PIK3R5,TBXA2R,DOCK8,RAPGEF3,PHF21A,CD36,SHC1,SERPINB2,GRB7,ARRB2,DOCK4,RACGAP1,DGKZ,PPP2R5C,STXBP2,KLC1,ITIH3,PHACTR2,RAD51B,SEPP1,GNGT2,WDR1,KIF13B,ANGPT1,LYN,FAM49B,NFE2,ATP2A2,SH2B2,ITGAM,PCDH7,CD63,ITGAX,SLC7A6,SLC16A3,STIM1,AKAP1,EHD1,CD177,PIK3R6,ORAI1,SERPINB6
Cytokine Signaling in Immune system	RALA,TNFRSF17,TNFRSF1A,IL2RB,CTSG,NFKBIA,MMP2,CSK,RELB,HGF,CSF3,DUSP3,NFKB1,LTBR,MAPK14,IL5,IL1RL1,PRTN3,FLT3,MT2A,IRF1,NUP85,CANX,PTPN12,PIAS1,RAP1B,NUP210,EDAR,IL36G,IL1RN,PSMB7,HLA-F,IRAK3,LMNB1,RORA,PIK3R3,SAMHD1,MAPK3,IL1B,AKT3,TNFRSF8,CBL,CD80,IL1RL2,HERC5,FBXW11,CD27,IRF8,IFNAR1,AIP,IL18,TNFSF4,APP,CSF1R,UBE2L6,PIK3CB,IL10RB,IFNGR2,TNFRSF13C,TRIM62,CCR2,CCR5,STAT5B,EIF4A1,VCAM1,IL17RC,RAG1,STAT6,NOD2,MAP2K1,IL16,JUNB,NKIRAS2,UBE2E1,S1PR1,CXCL10,IL7R,ISG20,PTPN7,CLCF1,MID1,VAMP2,TOLLIP,UBE2N,CAMK2G,IL17RA,PELI3,EIF4A2,CUL1,RORC,P4HB,IL20RB,IL1R2,CD86,SMAD3,UBA7,EDARADD,LCK,IL21R,GRAP2,TSLP,MAOA,MEF2C,STAT5A,IFI6,IL19,TRIM29,JAK1,TNFSF13,TRIM14,MAP2K3,HMGB1,NUP50,ANXA2,MEF2A,FYN,IL27,TRIM38,IRF5,PTPN5,PELI1,GAB2,FASLG,POU2F1,IL6R,MCL1,PTPN1,IFIT2,RAPGEF1,LCN2,CSF3R,PTAFR,PSMB9,PSMB8,SYK,TNFRSF1B,HLA-E,ANXA1,PIK3CD,TNFRSF25,NUP160,GATA3,FOXO1,IL2RA,MTAP,IRF4,IL6ST,TEC,SEC13,SQSTM1,AKT2,PRKCD,YWHAZ,ITGB2,BCL2,GRB10,CDC42,EIF4G3,CSF2RB,IL18BP,BCL6,CDKN1A,IL6,FOXO3,IFITM1,IL1R1,CREB1,PTPN6,JAK3,EIF4E3,HLA-DPA1,SLA,MAPK9,SMARCA4,PSMD13,CD36,PTPRJ,SHC1,SERPINB2,LTA,TRIM26,LTB,IL10,STXBP2,PSMA1,EIF4G1,RPS6KA2,CXCL2,LYN,RPS6KA1,UBC,ITGAM,NUP153,SOD2,RPLP0,B2M,TRAF3,ITGAX,NUP62,BIRC2,RAG2,TNFRSF9,RPS6KA5,MAP3K14,PRLR,IFI27,IKBKG
Signaling by Interleukins	RALA,TNFRSF1A,IL2RB,CTSG,NFKBIA,MMP2,HGF,CSF3,DUSP3,NFKB1,MAPK14,IL5,IL1RL1,PRTN3,CANX,PTPN12,RAP1B,IL36G,IL1RN,PSMB7,IRAK3,LMNB1,RORA,PIK3R3,MAPK3,IL1B,CBL,CD80,IL1RL2,FBXW11,AIP,IL18,APP,CSF1R,PIK3CB,IL10RB,CCR2,CCR5,STAT5B,VCAM1,IL17RC,RAG1,STAT6,NOD2,MAP2K1,IL16,JUNB,NKIRAS2,S1PR1,CXCL10,IL7R,PTPN7,CLCF1,VAMP2,TOLLIP,UBE2N,IL17RA,PELI3,CUL1,RORC,P4HB,IL20RB,IL1R2,CD86,SMAD3,LCK,IL21R,TSLP,MAOA,MEF2C,STAT5A,IL19,JAK1,MAP2K3,HMGB1,ANXA2,MEF2A,FYN,IL27,PTPN5,PELI1,GAB2,FASLG,POU2F1,IL6R,MCL1,RAPGEF1,LCN2,CSF3R,PTAFR,PSMB9,PSMB8,SYK,TNFRSF1B,ANXA1,PIK3CD,GATA3,FOXO1,IL2RA,MTAP,IRF4,IL6ST,TEC,SQSTM1,YWHAZ,ITGB2,BCL2,CDC42,CSF2RB,IL18BP,BCL6,CDKN1A,IL6,FOXO3,IL1R1,CREB1,PTPN6,JAK3,MAPK9,SMARCA4,PSMD13,CD36,SHC1,SERPINB2,IL10,STXBP2,PSMA1,RPS6KA2,CXCL2,LYN,RPS6KA1,UBC,ITGAM,SOD2,RPLP0,ITGAX,RAG2,RPS6KA5,IKBKG

194

Adaptive Immune System	CD22,ICAM3,PILRA,NFKBIA,CSK,PAG1,COL1A1,NFKB1,LNPEP,UBE3A,PPP3R1,CD160,FBXO9,TREM1,CANX,TUBA4A,RAP1B,PVRL2,RAP1GAP2,FBXL8,BLK,PSMB7,RNF144B,HLA-F,KIF23,CLEC2D,PPP2R5A,CDH1,ANAPC5,MGRN1,TYROBP,PIK3R3,PRKCQ,CD81,AKT3,LNX1,CD80,HERC5,CUL3,ASB1,ZAP70,FBXW11,MAPKAP1,SKP2,KCTD7,SEC24D,SH3RF1,UBE2L6,PIK3CB,AP2M1,VCAM1,CD3D,TUBA1C,RILP,UNKL,UBE2E1,CTLA4,ITPR1,CD34,RASGRP1,FBXW8,SPSB4,UBE2N,MALT1,CALR,ASB4,FBXL13,CD28,CUL1,KLHL22,CD86,UBA7,PDCD1,ZNRF1,KLHL25,PPP2R5E,LCK,GRAP2,PIK3AP1,COL17A1,SEC24C,FBXL14,FBXL5,CTSB,ATG7,FYN,KCTD6,RNF220,UBE2H,RAC1,AMICA1,ORAI2,ITGAL,RAET1E,AP1B1,AP2A1,CD3E,SMURF1,CD247,DCTN1,PJA1,FCGR3A,SLAMF7,CD1D,AHCYL1,FBXW4,UBE2U,SH2D1A,UBAC1,SFTPD,YWHAB,DNM1,TREM2,SRC,UBE2D1,TLR4,PRKG1,HLA-DMA,PSMB9,PSMB8,UBR4,CD300LD,SYK,HLA-E,TRIM39,PIK3CD,KLHL21,FBXL19,COL2A1,KLRD1,SEC13,DNM2,LAIR1,LILRB2,AKT2,DYNLL1,EVL,KIF20A,FZR1,HERC4,SEC31A,YWHAZ,NFATC2,RAPGEF4,NCF4,ITGB2,LONRF1,UBE2D2,FKBP1A,CDC42,NEDD4L,FBXO11,PRR5,SAR1B,KIF3A,IFITM1,UBE2E3,KIF26A,TLR6,HLA-DOB,PTPN6,PILRB,HLA-DPA1,RAPGEF3,PSMD13,UBE2W,ITK,HLA-DMB,CD36,PTPRJ,UBE2L3,HECTD2,SIGLEC6,FBXO10,RACGAP1,PTPRC,PPP2R5C,SIGLEC9,PSMA1,DCTN4,KLC1,ICAM2,NCK1,TREML2,CD200,RNF182,ANAPC13,DAPP1,FBXL7,KLHL5,MIB2,FYB,FBXO32,SPSB2,RNF217,LYN,RNF19A,CD3G,LMO7,RAP1GAP,CD19,UBC,ASB2,B2M,RNF111,MLST8,LRRC41,STIM1,OSCAR,ITCH,ORAI1,MAP3K14,IKBKG
Vesicle-mediated transport	ARF5,RALA,DVL2,RALGAPA2,MYH9,RIN3,CTSZ,BLOC1S6,CPD,COL1A1,PRKAB1,EXOC2,SPARC,LNPEP,APOA1,TUBA4A,EXOC4,IGJ,RIN2,AP3B1,SBF2,SORT1,STX6,COG3,KIF23,EXOC6,TBC1D1,SCARB1,RAB11A,TMED2,DENND3,RALGAPB,ARPC1A,SCARF1,ACTR3,PACSIN2,AKT3,KIF1B,CBL,COPS4,PIK3C2A,COPS3,GALNT1,CNIH3,VPS54,SEC24D,APP,PRKAG2,TRAPPC10,AP2M1,TBC1D24,STX5,MON1A,CYTH3,UBAP1,CD3D,TRAPPC2L,TUBA1C,VPS37C,TMED10,ANKRD27,IL7R,GCC2,RIN1,SEC22A,RAB6A,ADRBK1,STAB1,ALS2CL,VAMP2,BIN1,ADRBK2,APOL1,GCC1,MARCO,CALR,COPG1,HGS,EXOC7,GGA1,NECAP1,SEC24C,ITSN2,HP,RAC1,GJB6,AMPH,SPTBN1,AP1B1,DENND2D,AP2A1,MYO1C,COL4A2,CYTH1,DCTN1,CHML,COG2,GALNT2,ACBD3,PLA2G4A,COPA,SPTA1,RAB13,VPS45,SGIP1,EPS15,YWHAB,DNM1,GOLGA1,SRC,DENND1A,RABGAP1,MAN1C1,LDLRAP1,COL4A1,LMAN2L,FTL,VPS28,TBC1D4,SNX2,EXOC1,ITSN1,SEC13,STAB2,DNM2,TRAPPC9,ALPP,AKT2,SNX9,DYNLL1,PICALM,GAPVD1,RAB3IL1,KIF20A,SEC31A,CD59,YWHAZ,RAB27A,CHMP7,AGPAT3,HPS4,MYO5A,ANKRD28,STON1,TBC1D10A,SAR1B,KIF3A,TGOLN2,TBC1D10B,MCFD2,TBC1D14,AGFG1,KIF26A,DENND4A,DENND6B,PUM1,CD36,VPS53,ARRB2,RACGAP1,CHMP3,SYNJ1,VPS52,PPP6R1,DCTN4,KLC1,AGTR1,KIF13B,TPD52,CLINT1,CD3G,ST5,TPD52L1,CLTCL1,UBC,HPR,C2CD5,TBC1D15,STON2,SPTB,ENSP00000452252,MAN2A2,RAB31,TRAPPC5,FCHO1,TBC1D7,DENND1B,HYOU1,TBC1D2
Platelet activation, signaling and aggregation	GNA11,VCL,CSK,HGF,COL1A1,MAPK14,SPARC,PLEK,APOA1,SRGN,TUBA4A,RAP1B,VWF,GNB5,PIK3R3,MAPK3,PRKCQ,APLP2,DGKD,DGKG,MGLL,GNA12,SERPING1,FERMT3,DGKE,APP,PIK3CB,FCER1G,ANXA5,F2RL2,IGF1,GP9,FGB,ITPR1,P2RY12,RASGRP1,VEGFB,GNAI2,CLU,DGKA,PRKCH,CFD,GNG2,LCK,RHOG,TRPC6,PTK2,PDGFA,FYN,RAC1,SCCPDH,PLA2G4A,GNG5,PTPN1,SRC,SYK,APBB1IP,ABCC4,PRKCZ,LHFPL2,GNG7,CD9,ACTN1,PRKCD,MMRN1,YWHAZ,RAPGEF4,CDC42,GP1BB,DGKB,PTPN6,PIK3R5,TBXA2R,RAPGEF3,CD36,SHC1,ARRB2,DGKZ,STXBP2,ITIH3,PHACTR2,SEPP1,GNGT2,WDR1,LYN,FAM49B,PCDH7,CD63,PIK3R6

Fcgamma receptor (FCGR) dependent phagocytosis	MYH9,ARPC1A,MAPK3,ACTR3,FCGR2A,PIK3CB,ELMO2,ABI2,ITPR1,ELMO1,BAIAP2,WIPF2,LIMK1,PTK2,PLD1,FYN,RAC1,MYO1C,CD247,FCGR3A,AHCYL1,SRC,FGR,SYK,WIPF1,PLD4,PRKCD,MYO5A,CDC42,PLD3,NCK1,MYO10,LYN,CD3G,CYFIP2,MYO9B,CYFIP1,WASF2

Supplementary table 2.2: *Pathway enrichment of DMRs immediately after RT in left sided breast cancer patients.*

Enriched pathway	DMRs associated with pathway
Human T-cell leukemia virus 1 infection	TGFB1,E2F3,TCF3,CD3D,BCL2L1,CREB3L2,IL1R2,SMAD3,LCK,STAT5A,ADCY2,CD3E,CCND3,PIK3CD,ETS1,ADCY7,NFATC2,MAD1L1,IL1R1,CREB1,HLA-DMB,LTA,TLN2,CREB3L1,MAP3K14
Adherens junction	ACTN4,CDH1,PVRL1,SMAD3,TCF7,FYN,PVRL4,SRC,ACTN1,NLK,PTPRJ
Th1 and Th2 cell differentiation	NOTCH1,MAML1,CD3D,LCK,STAT5A,RBPJ,CD3E,CD247,NFATC2,RUNX3,HLA-DMB,MAML3,MAML2
T cell receptor signaling pathway	CD3D,CD8B,LCK,GRAP2,FYN,CD3E,CD247,VAV2,PIK3CD,NFATC2,ITK,PTPRC,IL10,NCK1,MAP3K14
Parathyroid hormone synthesis, secretion and action	SLC9A3R1,LRP5,ITPR1,CREB3L2,PLD1,ADCY2,RUNX2,ITPR2,ADCY7,BCL2,CREB1,ARRB2,ARRB1,RXRA,CREB3L1
Transcriptional misregulation in cancer	PLAT,MPO,FLT3,LMO2,TCF3,PPARG,RUNX1,BCL2L1,IL1R2,PDGFA,RUNX2,PLAU,ZBTB17,CDK14,ETV6,PBX1,ERG,RXRA,ELANE,BIRC2
Prostate cancer	PLAT,PDGFRB,E2F3,TGFA,CREB3L2,IL1R2,TCF7,PDGFA,PLAU,PIK3CD,BCL2,CREB1,ERG,CREB3L1
Innate Immune System	CTSG,CTSZ,RIPK2,MPO,DUSP3,TMEM30A,AZU1,PRTN3,CTSD,TNFAIP6,TREM1,DOCK2,TCN1,CAB39,SDCBP,IRAK3,HEXB,CYSTM1,LPO,NLRC5,TIMP2,ATP6V0A1,SLC15A4,FCN3,ATP6V1B2,MS4A3,LPCAT1,APP,NOD2,RNASE3,BCL2L1,ATP6V1E2,ITPR1,EEF2,ELMO1,CPN2,PKM,CUL1,AP2A2,TMEM173,SLC44A2,NLRP3,LCK,GRAP2,MEF2C,PLD1,NFASC,CTSB,ATG7,FYN,VAT1,CLEC12A,HP,RAC1,DYNC1H1,CEACAM3,PGLYRP4,CD247,TIFA,GAB2,S100A8,VAV2,PLAU,DNM1,TREM2,SRC,GSN,UBR4,TNFRSF1B,SLC2A5,KCNAB2,ITPR2,ATP8A1,SIGLEC15,LRRFIP1,RAB37,LGMN,DAK,CD59,NFATC2,RAB27A,AMPD3,TRPM2,BCL2,SIRPA,C1S,NLRC4,CREB1,GCA,TSPAN14,ITK,PLAC8,PTPRJ,SHC1,POLR2F,GPI,ANO6,PTPRC,NCK1,ATP11A,ATOX1,ATP6V0B,RPS6KA1,IST1,TARM1,TBC1D10C,CYFIP2,MGAM,PSTPIP1,RAB31,ELANE,MAP2K6,MYO9B,C5AR2,BIRC2,FOLR3,MAP3K14
Immune System	RALA,TNFRSF17,PTPN18,PILRA,CTSG,CTSZ,RIPK2,TGFB1,MPO,CSF3,DUSP3,TMEM30A,AZU1,PRTN3,CTSD,FLT3,TNFAIP6,TREM1,RAP1GAP2,DOCK2,TCN1,CAB39,IL1RN,SDCBP,IRAK3,HEXB,CDH1,CYSTM1,LPO,MGRN1,NLRC5,TIMP2,TNFRSF8,CUL3,ATP6V0A1,SLC15A4,FCN3,SKP2,ATP6V1B2,MS4A3,LPCAT1,APP,RAG1,NOD2,CD3D,RNASE3,BCL2L1,ATP6V1E2,S1PR1,ITPR1,MRC2,EEF2,PTPN7,CD34,ELMO1,CAMK2G,CPN2,DYNC1I1,PKM,CUL1,AP2A2,IL1R2,CD8B,TMEM173,SMAD3,ZNRF1,SLC44A2,NLRP3,LCK,IL21R,GRAP2,PIK3AP1,MEF2C,STAT5A,PLD1,NFASC,CTSB,ATG7,FYN,RNF220,VAT1,CLEC12A,HP,RAC1,DYNC1H1,IL27,TRIM38,IRF5,CEACAM3,PGLYRP4,CD3E,SMURF1,CD247,TIFA,GAB2,PARK2,SLAMF7,S100A8,VAV2,PLAU,DNM1,CSF3R,TREM2,SRC,GSN,UBR4,TNFRSF1B,PIK3CD,SLC2A5,KLHL21,KCNAB2,MTAP,ITPR2,ATP8A1,SIGLEC15,LRRFIP1,RAB37,EVL,LGMN,RNF14,DAK,CD59,YWHAZ,NFATC2,RAB27A,AMPD3,TRPM2,BCL2,GRB10,SIRPA,CSF2RB,C1S,NLRC4,HERC3,IL1R1,CREB1,GCA,SMARCA4,TSPAN14,ITK,HLA-

	DMB,PLAC8,PTPRJ,SHC1,LTA,POLR2F,INPP5D,GPI,ANO6,PTPRC,IL10,PPP2R5C,NCK1,ATP11A,FYB,ATOX1,ATP6V0B,RPS6KA1,IST1,TARM1,TBC1D10C,CYFIP2,MGAM,ASB2,PSTPIP1,RAB31,ELANE,MAP2K6,MYO9B,C5AR2,BIRC2,LRRC41,FOLR3,MAP3K14,PRLR
Neutrophil degranulation	CTSG,CTSZ,MPO,TMEM30A,AZU1,PRTN3,CTSD,TNFAIP6,DOCK2,TCN1,CAB39,SDCBP,HEXB,CYSTM1,TIMP2,ATP6V0A1,SLC15A4,MS4A3,LPCAT1,RNASE3,EEF2,PKM,AP2A2,TMEM173,SLC44A2,PLD1,NFASC,CTSB,ATG7,VAT1,CLEC12A,HP,RAC1,DYNC1H1,CEACAM3,S100A8,PLAU,GSN,UBR4,TNFRSF1B,SLC2A5,KCNAB2,ATP8A1,RAB37,CD59,RAB27A,AMPD3,TRPM2,SIRPA,GCA,TSPAN14,PLAC8,PTPRJ,GPI,ANO6,PTPRC,ATP11A,IST1,TARM1,TBC1D10C,MGAM,RAB31,ELANE,FOLR3
Diseases of signal transduction by growth factor receptors and second messengers	HDAC7,TGFB1,CLCN6,FLT3,PDGFRB,HDAC4,NOTCH1,MAML1,LRP5,TGFA,BCL2L1,MAP3K11,TNKS,CAMK2G,CUL1,NCBP2,KREMEN1,SMAD3,FIP1L1,LCK,PIK3AP1,STAT5A,RBPJ,ATG7,PDGFA,FYN,RAC1,SPRED2,CUX1,GAB2,SRC,PIK3CD,LRRFIP1,ETV6,KSR1,NCOR2,CREB1,SHC1,ARRB2,POLR2F,ARRB1,PPP2R5C,MAML3,MAML2,KANK1
Signal Transduction	RALA,HDAC7,KDM4B,PTPN18,RIPK2,PLAT,TGFB1,DUSP3,SPARC,CTSD,FLT3,CCR7,ALDH1A2,NR1H2,PDE6A,PHC2,DTX1,CAB39,CDH1,PDGFRB,TMED2,PHLPP1,E2F3,ARHGAP31,CUL3,HDAC4,ATP6V0A1,PXN,SH3GL1,DGKQ,ATP6V1B2,NOTCH1,APP,PPARG,PRKAG2,MAML1,CXCL16,LRP5,CDC42EP3,TGFA,PRKCI,DAGLB,ARHGEF40,RAG1,RUNX1,CXXC5,BCL2L1,ABR,ATP6V1E2,S1PR1,ITPR1,RPTOR,PTPN7,MAP3K11,PDE7B,TNKS,TNS3,ELMO1,CAMKK2,PLXND1,CAMK2G,DYNC1I1,TACC3,CUL1,NCBP2,AP2A2,TGIF1,KREMEN1,SMAD3,GNAL,OR10T2,RASA3,LCK,RTN4,HTR7,GRAP2,TRIO,PIK3AP1,LIMK2,MYB,ARHGEF10,TCF7,MEF2C,ASH2L,STAT5A,ADCY2,RBPJ,PDGFA,FYN,RAC1,SPRED2,DYNC1H1,ATN1,GATAD2A,SMURF1,GAB2,NR5A2,RASAL2,SGK1,ACKR1,S100A8,SUFU,NTSR1,VAV2,PREX1,DNM1,CCND3,SRC,ECE1,TFDP1,ARHGEF7,TRIM27,PIK3CD,SKI,PRKCZ,XK,CHD3,ITSN1,ITPR2,RHOH,GNG7,CCDC88C,EVL,ADCY7,YWHAZ,NDE1,HRH1,WNT5B,GRK4,BCL2,GRB10,KSR1,RUNX3,NCOR2,CSF2RB,NLK,MAD1L1,CREB1,TCF12,DHRS9,GPSM1,FGD4,SMARCA4,CXCR6,PTPRJ,SHC1,BMPR1B,TNRC6B,ARRB2,POLR2F,PBX1,RASGRF1,IFT140,ARRB1,NSMAF,PPP2R5C,PLTP,NCK1,RXRA,PHC3,DP2,MAML3,ANGPT1,CKAP5,MAML2,ATP6V0B,RPS6KA1,SH2B2,ACVR1B,ADAP1,ZNRF3,CYFIP2,WWOX,MYO9B,C5AR2,BIRC2,NR1H3,KANK1,LRRC41,CLIP1,CAB39L,PIK3R6,QRFP
Nef and signal transduction	DOCK2,ELMO1,LCK,FYN,RAC1,CD247
Vesicle-mediated transport	RALA,RIN3,CTSZ,SPARC,RIN2,COG3,SCARB1,TMED2,DENND3,SCARB2,SH3GL1,CNIH3,VPS54,VPS51,APP,PRKAG2,TRAPPC10,TBC1D24,STX5,TGFA,CD3D,STX18,TBC1D16,STAB1,GAK,BIN1,MARCO,DYNC1I1,TRAPPC12,AP2A2,HP,RAC1,DYNC1H1,GALNT2,ACBD3,DNM1,SRC,MAN1C1,ITSN1,VTI1A,CD59,YWHAZ,RAB27A,TBC1D10A,AAK1,PUM1,VPS53,COPG2,ARRB2,ARRB1,KIF21B,CLINT1,ST5,TPD52L1,TBC1D10C,MAN2A2,RAB31,TBC1D2
Signaling by Receptor Tyrosine Kinases	RALA,PTPN18,PLAT,DUSP3,SPARC,FLT3,PDGFRB,ATP6V0A1,PXN,SH3GL1,ATP6V1B2,TGFA,ATP6V1E2,ITPR1,TNS3,ELMO1,NCBP2,AP2A2,LCK,GRAP2,MEF2C,STAT5A,PDGFA,FYN,RAC1,SPRED2,GAB2,SGK1,VAV2,DNM1,SRC,ARHGEF7,PRKCZ,ITPR2,GRB10,CREB1,TCF12,PTPRJ,SHC1,POLR2F,NCK1,ATP6V0B,RPS6KA1,SH2B2,ADAP1,CYFIP2,WWOX

Generation of second messenger molecules	CD3D,LCK,GRAP2,CD3E,CD247,EVL,ITK,NCK1,FYB
Signaling by NOTCH	HDAC7,DTX1,TMED2,E2F3,HDAC4,NOTCH1,MAML1,PRKCI,RUNX1,PLXND1,TACC3,CUL1,SMAD3,RBPJ,TFDP1,YWHAZ,NCOR2,CREB1,TNRC6B,ARRB2,PBX1,ARRB1,DP2,MAML3,MAML2
Membrane Trafficking	RALA,RIN3,CTSZ,RIN2,COG3,TMED2,DENND3,SCARB2,SH3GL1,CNIH3,VPS54,VPS51,APP,PRKAG2,TRAPPC10,TBC1D24,STX5,TGFA,CD3D,STX18,TBC1D16,GAK,BIN1,DYNC1I1,TRAPPC12,AP2A2,RAC1,DYNC1H1,GALNT2,ACBD3,DNM1,SRC,MAN1C1,ITSN1,VTI1A,CD59,YWHAZ,RAB27A,TBC1D10A,AAK1,PUM1,VPS53,COPG2,ARRB2,ARRB1,KIF21B,CLINT1,ST5,TPD52L1,TBC1D10C,MAN2A2,RAB31,TBC1D2
Signaling by Interleukins	RALA,PTPN18,CTSG,RIPK2,TGFB1,CSF3,DUSP3,PRTN3,IL1RN,IRAK3,APP,RAG1,NOD2,BCL2L1,S1PR1,PTPN7,CUL1,IL1R2,SMAD3,LCK,IL21R,MEF2C,STAT5A,FYN,IL27,GAB2,CSF3R,TNFRSF1B,PIK3CD,MTAP,YWHAZ,BCL2,CSF2RB,IL1R1,CREB1,SMARCA4,SHC1,INPP5D,IL10,RPS6KA1,MAP2K6
Disease	HDAC7,ST6GAL1,CTSG,TGFB1,CLCN6,FLT3,G6PC,CHSY1,DOCK2,ADAMTS8,HEXB,CDH1,PDGFRB,ELL,E2F3,BRD4,HDAC4,SLC2A9,MGAT4A,SH3GL1,SKP2,NOTCH1,APP,ADAMTS1,FXYD2,MAML1,LRP5,TGFA,BCL2L1,S1PR1,ITPR1,EEF2,MAP3K11,TNKS,ELMO1,CAMK2G,DYNC1I1,RHBDF2,CUL1,NCBP2,AP2A2,CD8B,KREMEN1,SMAD3,FIP1L1,NLRP3,LCK,HTR7,PIK3AP1,SLC20A2,STAT5A,ADCY2,MCCC2,RBPJ,ATG7,PDGFA,FYN,RAC1,SPRED2,DYNC1H1,CUX1,GATAD2A,CD247,GAB2,ENTPD1,VAV2,CCND3,SRC,TFDP1,TRIM27,PIK3CD,CHD3,ITPR2,GNG7,LRRFIP1,PC,ADCY7,EXT2,ETV6,RPS8,SLC7A7,KSR1,NCOR2,CSF2RB,MGAT5,IL1R1,CREB1,SHC1,ARRB2,POLR2F,ARRB1,IL10,PPP2R5C,CDKN1C,NCK1,DP2,MAML3,SLC24A4,TXNRD1,MAML2,CYFIP2,ATP1A1,PSTPIP1,MAP2K6,MYO9B,KANK1,CTDP1
The role of Nef in HIV-1 replication and disease pathogenesis	DOCK2,ELMO1,AP2A2,CD8B,LCK,FYN,RAC1,CD247
DAP12 interactions	TREM1,LCK,GRAP2,FYN,RAC1,VAV2,TREM2,SIGLEC15,SHC1
Notch-HLH transcription pathway	HDAC7,HDAC4,NOTCH1,MAML1,RBPJ,NCOR2,MAML3,MAML2
SUMOylation of intracellular receptors	NR1H2,HDAC4,THRA,PPARG,NR1I2,NR5A2,RXRA,NR1H3
RUNX3 regulates NOTCH signaling	NOTCH1,MAML1,RBPJ,RUNX3,MAML3,MAML2
Intracellular signaling by second messengers	HDAC7,FLT3,PHC2,PDGFRB,PHLPP1,PPARG,TGFA,ITPR1,RPTOR,TNKS,CAMKK2,CAMK2G,LCK,PIK3AP1,ADCY2,PDGFA,FYN,RAC1,ATN1,GATAD2A,GAB2,SRC,TRIM27,PIK3CD,CHD3,ITPR2,ADCY7,CREB1,TNRC6B,PPP2R5C,PHC3
FCGR3A-mediated IL10 synthesis	ITPR1,ADCY2,FYN,CD247,SRC,ITPR2,ADCY7,CREB1,IL10

Hemostasis	CBX5,PLAT,TGFB1,SPARC,PRTN3,TREM1,ACTN4,DOCK2,DGKQ,APP,PDE9A,DAGLB,ITPR1,SLC7A8,SERPINF2,LCK,MYB,PDGFA,FYN,RAC1,CEACAM3,MAFG,CD2,VAV2,PLAU,SRC,PRKCZ,ITPR2,GNG7,ACTN1,YWHAZ,SLC7A7,SIRPA,SLC8A1,DOCK8,SHC1,ARRB2,INPP5D,ARRB1,KIF21B,MRVI1,PPP2R5C,WDR1,ANGPT1,SH2B2,SLC7A6,SLC16A3,EHD1,PIK3R6
Cytokine Signaling in Immune system	RALA,TNFRSF17,PTPN18,CTSG,RIPK2,TGFB1,CSF3,DUSP3,PRTN3,FLT3,IL1RN,IRAK3,TNFRSF8,APP,RAG1,NOD2,BCL2L1,S1PR1,PTPN7,CAMK2G,CUL1,IL1R2,SMAD3,LCK,IL21R,GRAP2,MEF2C,STAT5A,FYN,IL27,TRIM38,IRF5,GAB2,CSF3R,TNFRSF1B,PIK3CD,MTAP,YWHAZ,BCL2,GRB10,CSF2RB,IL1R1,CREB1,SMARCA4,PTPRJ,SHC1,LTA,INPP5D,IL10,RPS6KA1,MAP2K6,BIRC2,MAP3K14,PRLR
Signaling by SCF-KIT	LCK,GRAP2,STAT5A,FYN,RAC1,GAB2,SRC,GRB10,SH2B2
Pre-NOTCH Transcription and Translation	E2F3,NOTCH1,MAML1,PRKCI,RUNX1,RBPJ,TFDP1,TNRC6B,DP2,MAML3,MAML2
Signaling by NOTCH1	HDAC7,DTX1,HDAC4,NOTCH1,MAML1,CUL1,RBPJ,NCOR2,ARRB2,ARRB1,MAML3,MAML2
Phosphorylation of CD3 and TCR zeta chains	CD3D,LCK,CD3E,CD247,PTPRJ,PTPRC
NOTCH3 Intracellular Domain Regulates Transcription	NOTCH1,MAML1,PLXND1,RBPJ,PBX1,MAML3,MAML2

6.3. Supplementary materials for Chapter 5

Supplementary figure 3.1: Functional enrichment of DEmiRNAs performed using g:Profiler

Supplementary figure 3.2: Visualization of the top four clusters (A,B,C and D, respectively) containing ≥10 members, obtained by analyzing co- expression correlation between DElncRNAs and DEPCGs using MCODE in Cytoscape. The first cluster was further analyzed using MCODE to produce sub-clusters of which the 3 top sub-clusters were visualized (A.1, A.2 and A.3 respectively). Blue triangles and circles indicate DElncRNAs and pink circles indicate DEPCGs. The thickness of a line indicates the strength of the interaction between the proteins it connects.

A) Cluster 1 reclustered using *MCODE*
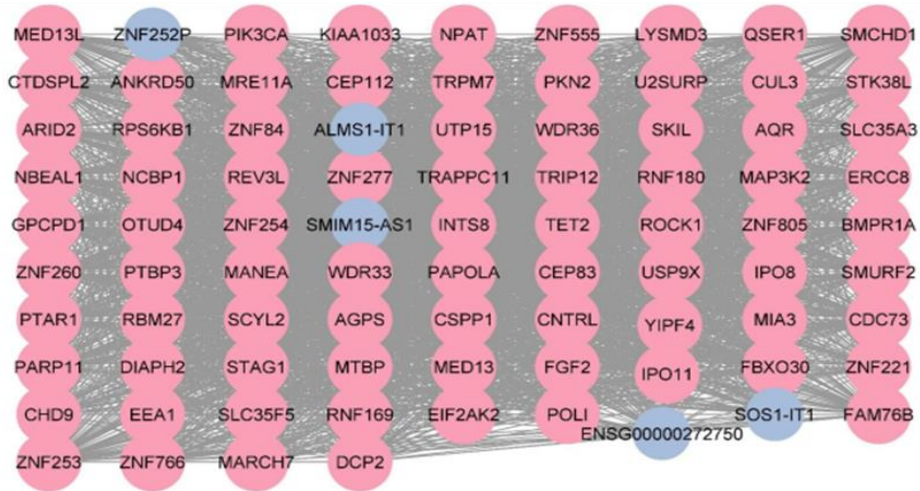
Cluster A.1

Figure 4A in manuscript
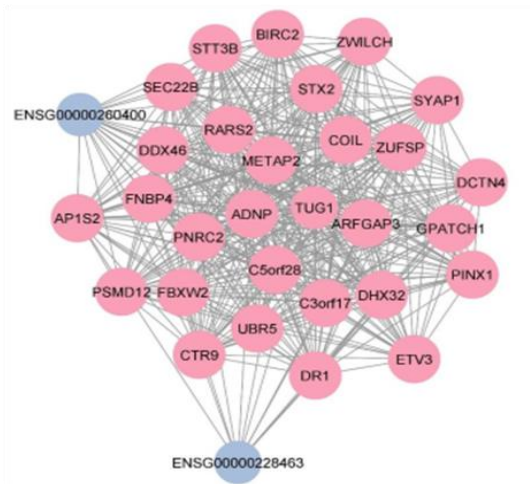
Cluster A.2
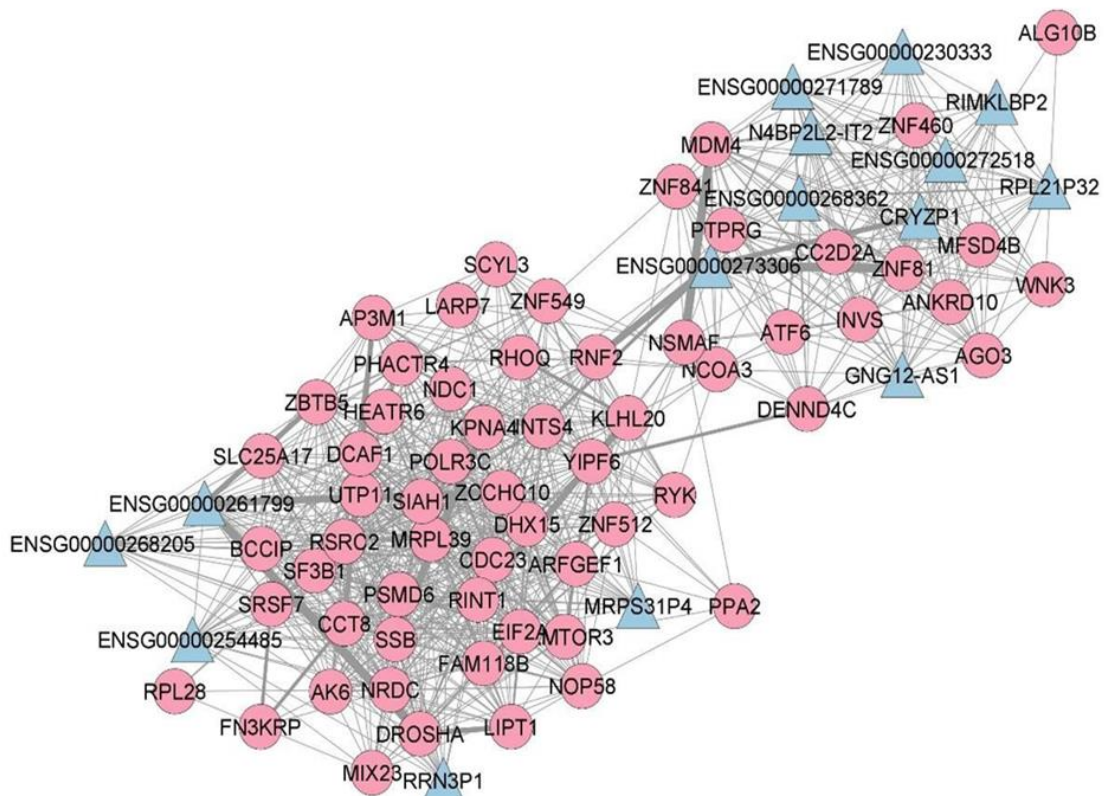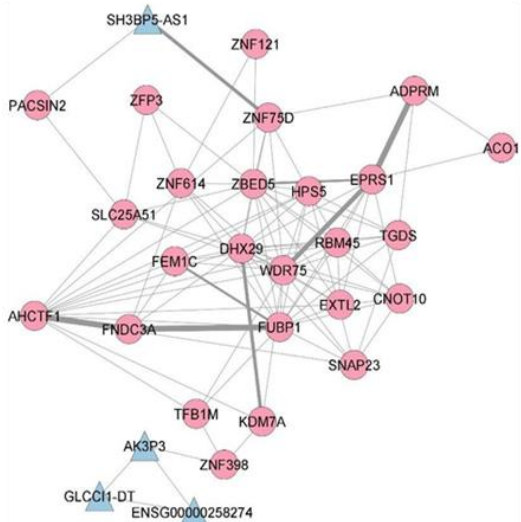
Cluster A.3
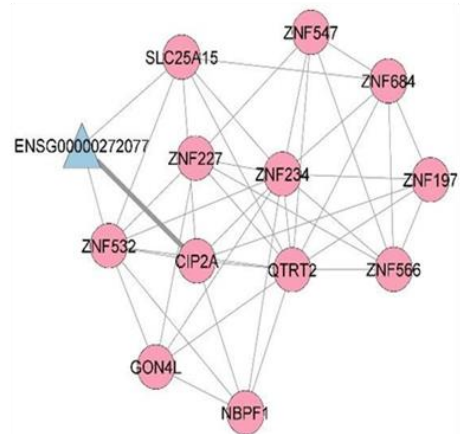
Supplementary figure 3.3: *Chinese Glioma Genome Atlas (CCGA) Pearson correlation analysis performed using the 'Analyze' tab in CCGA portal (http://www.cgga.org.cn/) between DANCR/SNHG6 in mRNAseq 693 (A) and mRNAseq 325 (B) and between miR96/miR182 (C), miR96/miR183 (D) and miR182-miR183 (E) in microRNA_array_198 of CCGA.*
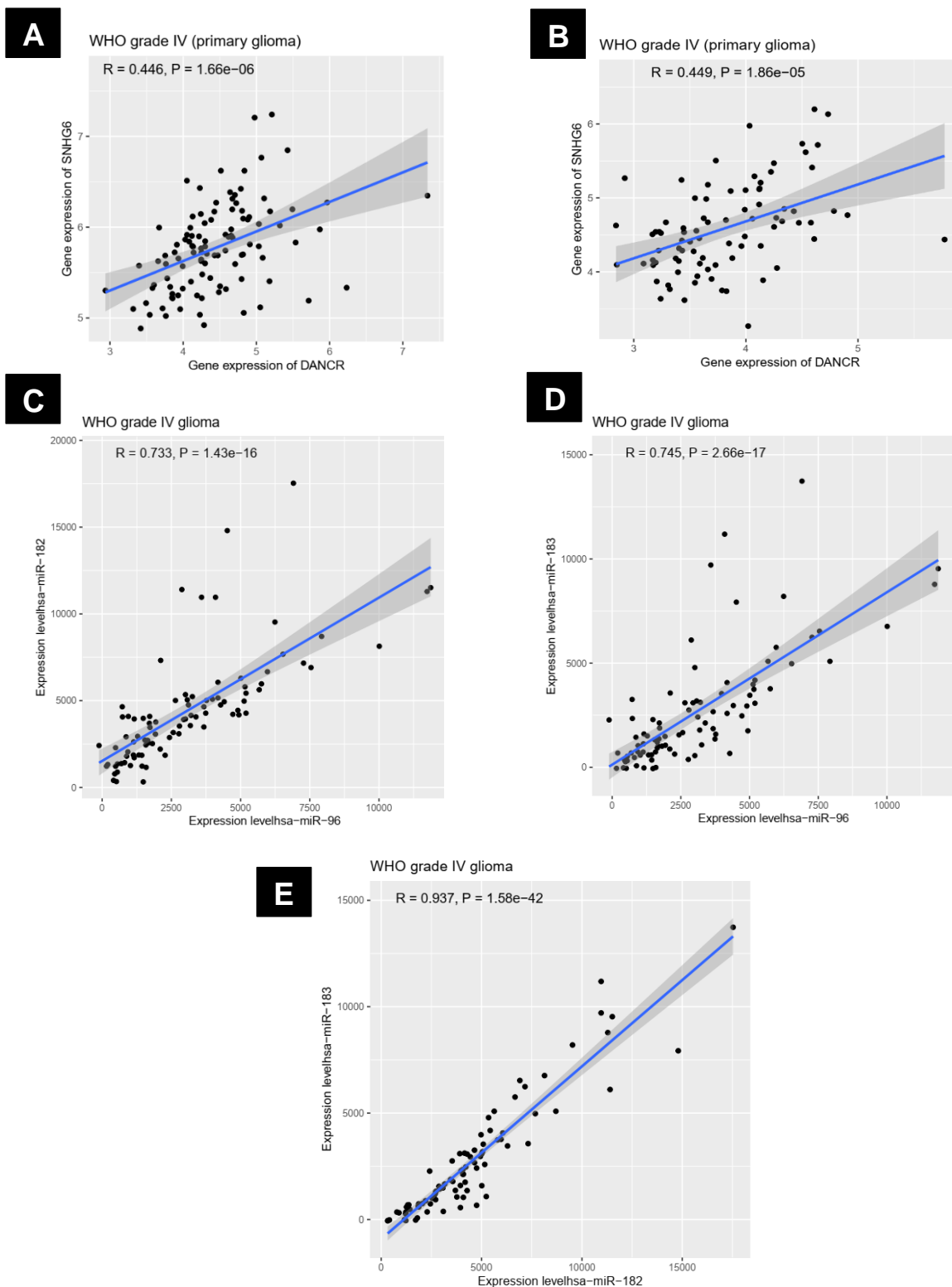
Supplementary table 3.1: *DElncRNA list showing differentially expressed lncRNAs showing differential expression in at least 3 studies, having Ensembl ID, a false discovery rate (FDR)<0.05 and a z-value of ≥|4|*

ENSEMBL ID	NONCODE ID	Gene name	zval	FDR
ENSG00000233184	NONHSAG002228	#N/A	7.29622	1.76E-09
ENSG00000227502	NONHSAG044656	MROCKI	5.978273	2.98E-06
ENSG00000268205	NONHSAG026661	#N/A	5.737542	8.79E-06
ENSG00000267302	NONHSAG022372	RNFT1-DT	5.61331	1.39E-05
ENSG00000268362	NONHSAG025369	#N/A	5.636479	1.39E-05
ENSG00000245910	NONHSAG050423	SNHG6	5.519917	2.10E-05
ENSG00000272518	NONHSAG050586	#N/A	5.504044	2.10E-05
ENSG00000261799	NONHSAG010134	#N/A	5.492392	2.13E-05
ENSG00000269893	NONHSAG038728	SNHG8	5.415747	2.79E-05
ENSG00000263424	NONHSAG024081	#N/A	5.310918	3.71E-05
ENSG00000259562	NONHSAG017558	#N/A	5.299182	3.85E-05
ENSG00000270108	NONHSAG016024	#N/A	5.283681	4.07E-05
ENSG00000196922	NONHSAG051586	ZNF252P	5.187091	5.91E-05
ENSG00000248124	NONHSAG018850	RRN3P1	5.12368	7.12E-05
ENSG00000259248	NONHSAG017136	USP3-AS1	5.101093	7.73E-05
ENSG00000270890	NONHSAG045052	#N/A	5.07968	8.18E-05
ENSG00000225733	NONHSAG034508	FGD5-AS1	5.070709	8.42E-05
ENSG00000257815	NONHSAG011658	PRANCR	5.032572	9.60E-05
ENSG00000228748	NONHSAG006297	#N/A	4.932482	0.000137
ENSG00000229692	NONHSAG027535	SOS1-IT1	4.908845	0.000143
ENSG00000251279	NONHSAG040483	SMIM15-AS1	4.906689	0.000143
ENSG00000226604	NONHSAG053298	PAPPA-AS2	4.869637	0.00016
ENSG00000233025	NONHSAG048441	CRYZP1	4.837265	0.000172
ENSG00000240399	NONHSAG011036	#N/A	4.800518	0.000192
ENSG00000272077	NONHSAG034919	#N/A	4.793857	0.000195
ENSG00000254485	NONHSAG085327	#N/A	4.780897	0.000198
ENSG00000276445	NONHSAG076511	#N/A	4.773513	0.000201
ENSG00000254559	NONHSAG007287	#N/A	4.763724	0.000206
ENSG00000230002	NONHSAG028178	ALMS1-IT1	4.759744	0.000206
ENSG00000251131	NONHSAG040298	#N/A	4.759449	0.000206
ENSG00000228242	NONHSAG034492	XPC-AS1	4.751652	0.000212
ENSG00000232284	NONHSAG001765	GNG12-AS1	4.739598	0.000218
ENSG00000261824	NONHSAG025379	LINC00662	4.740254	0.000218
ENSG00000277801	NONHSAG068938	#N/A	4.724519	0.000229
ENSG00000257176	NONHSAG010777	#N/A	4.718444	0.000234

ENSG00000258667	NONHSAG015182	HIF1A-AS3	4.671511	0.000282
ENSG00000250299	NONHSAG013582	MRPS31P4	4.665318	0.000286
ENSG00000255491	NONHSAG051204	#N/A	4.644129	0.000313
ENSG00000230825	NONHSAG046903	#N/A	4.632319	0.000322
ENSG00000244701	NONHSAG048975	#N/A	4.605429	0.000343
ENSG00000271270	NONHSAG036068	TMCC1-DT	4.598484	0.000347
ENSG00000224019	NONHSAG079293	RPL21P32	4.601331	0.000347
ENSG00000241990	NONHSAG034157	PRR34-AS1	4.581727	0.000368
ENSG00000223745	NONHSAG002086	CCDC18-AS1	4.55682	0.000412
ENSG00000240024	NONHSAG036820	LINC00888	4.532912	0.000453
ENSG00000213963	NONHSAG079272	#N/A	4.506658	0.000484
ENSG00000227076	NONHSAG060947	#N/A	4.493473	0.000496
ENSG00000255966	NONHSAG010310	#N/A	4.489133	0.000504
ENSG00000215483	NONHSAG067469	LINC00598	4.486083	0.000508
ENSG00000228463	NONHSAG000016	#N/A	4.459232	0.000567
ENSG00000224660	NONHSAG034519	SH3BP5-AS1	4.45503	0.000568
ENSG00000277027	NONHSAG052119	RMRP	4.448536	0.000578
ENSG00000270157	NONHSAG048976	#N/A	4.415562	0.000634
ENSG00000245685	NONHSAG039597	FRG1-DT	4.414261	0.000635
ENSG00000229656	NONHSAG005579	ITGB1-DT	4.409888	0.00064
ENSG00000228817	NONHSAG032626	BACH1-IT2	4.4098	0.00064
ENSG00000273568	NONHSAG065226	#N/A	4.371255	0.000735
ENSG00000261159	NONHSAG036029	#N/A	4.348144	0.000786
ENSG00000250155	NONHSAG040193	#N/A	4.34773	0.000786
ENSG00000258274	NONHSAG011931	#N/A	4.338365	0.000797
ENSG00000272240	NONHSAG099253	#N/A	4.337762	0.000797
ENSG00000265778	NONHSAG024200	ZNF516-AS1	4.334535	0.000801
ENSG00000225920	NONHSAG004316	RIMKLBP2	4.323442	0.000827
ENSG00000268583	NONHSAG026157	#N/A	4.315659	0.000834
ENSG00000281501	NONHSAG037643	SEPSECS-AS1	4.311284	0.000847
ENSG00000274859	NONHSAG065075	#N/A	4.295613	0.000897
ENSG00000226950	NONHSAG037936	DANCR	4.279801	0.000935
ENSG00000230982	NONHSAG033137	DSTNP1	4.268564	0.000971
ENSG00000230333	NONHSAG046946	#N/A	4.264081	0.000979
ENSG00000281026	NONHSAG013185	N4BP2L2-IT2	4.256536	0.000996
ENSG00000203865	NONHSAG002530	ATP1A1-AS1	4.247978	0.001027
ENSG00000246859	NONHSAG041236	STARD4-AS1	4.235058	0.001079
ENSG00000230042	NONHSAG047105	AK3P3	4.222951	0.001114
ENSG00000246308	NONHSAG007652	#N/A	4.201797	0.001194
ENSG00000267274	NONHSAG024863	#N/A	4.193626	0.001229

ENSG00000273306	NONHSAG077567	#N/A	4.193409	0.001229
ENSG00000238741	NONHSAG036534	SCARNA7	4.192141	0.001232
ENSG00000233108	NONHSAG046917	GLCCI1-DT	4.189519	0.001237
ENSG00000276166	NONHSAG071730	#N/A	4.153201	0.001403
ENSG00000260400	NONHSAG006087	#N/A	4.146941	0.001427
ENSG00000273284	NONHSAG074578	#N/A	4.134303	0.001487
ENSG00000259408	NONHSAG016475	#N/A	4.123678	0.00153
ENSG00000261716	NONHSAG002827	H2BC20P	4.121677	0.001533
ENSG00000270792	NONHSAG081356	#N/A	4.106724	0.001609
ENSG00000227518	NONHSAG051595	MIR1302-9HG	4.090474	0.00168
ENSG00000258368	NONHSAG010879	ZNF970P	4.088166	0.001691
ENSG00000229743	NONHSAG028810	LINC01159	4.06047	0.001854
ENSG00000230658	NONHSAG047103	KLHL7-DT	4.061374	0.001854
ENSG00000239218	NONHSAG050013	RPS20P22	4.055761	0.001876
ENSG00000271789	NONHSAG093512	#N/A	4.054182	0.001879
ENSG00000223476	NONHSAG047797	VN1R42P	4.048263	0.001913
ENSG00000272750	NONHSAG058499	#N/A	4.042177	0.001948
ENSG00000248265	NONHSAG011271	FLJ12825	4.023799	0.002052
ENSG00000278133	NONHSAG071611	#N/A	4.024432	0.002052
ENSG00000233527	NONHSAG076117	ZNF529-AS1	4.024575	0.002052
ENSG00000264577	NONHSAG021329	#N/A	4.022027	0.002055
ENSG00000235436	NONHSAG048161	DPY19L2P4	4.018311	0.002064
ENSG00000264235	NONHSAG023224	MYL12-AS1	4.013883	0.00209

Supplementary table 3.2: *Pathway analysis of DElncRNAs as identified by LncPath R package*

Pathway DB	Gene	Gene Set Size	Enrichment scores	Normalized Enrichment Scores
KEGG	O-GLYCAN BIOSYNTHESIS	27	0.65277	2.926012
KEGG	RIBOSOME	87	0.41381	1.854885
KEGG	PARKINSONS DISEASE	110	0.35326	1.583472
KEGG	NEUROACTIVE LIGAND RECEPTOR INTERACTION	263	0.30992	1.389202
Reactome	O-LINKED GLYCOSYLATION OF MUCINS	51	0.61035	2.394076
Reactome	TERMINATION OF O GLYCAN BIOSYNTHESIS	20	0.5844	2.292288
Reactome	FANCONI ANEMIA PATHWAY	19	0.56627	2.221174
Reactome	GLUTAMATE NEUROTRANSMITTER RELEASE CYCLE	15	0.55979	2.195756
Reactome	RESPIRATORY ELECTRON TRANSPORT	63	0.54288	2.129427
Reactome	INTERACTION BETWEEN L1 AND ANKYRINS	21	0.49604	1.945699
Reactome	INSULIN RECEPTOR RECYCLING	23	0.4939	1.937305
Reactome	HS GAG DEGRADATION	20	0.49196	1.929695
Reactome	MICRORNA MIRNA BIOGENESIS	18	0.48823	1.915065
Reactome	TRANSFERRIN ENDOCYTOSIS AND RECYCLING	25	0.485	1.902395
Reactome	INCRETIN SYNTHESIS SECRETION AND INACTIVATION	19	0.48382	1.897767
Reactome	AMINE LIGAND BINDING RECEPTORS	33	0.47904	1.879017
Reactome	MRNA CAPPING	28	0.47402	1.859326
Reactome	RESPIRATORY ELECTRON TRANSPORT ATP SYNTHESIS BY CHEMIOSMOTIC COUPLING AND HEAT PRODUCTION BY UNCOUPLING PROTEINS	79	0.46229	1.813316
Reactome	PEPTIDE CHAIN ELONGATION	85	0.42493	1.666773
Reactome	VOLTAGE GATED POTASSIUM CHANNELS	42	0.42031	1.648651
Reactome	NEUROTRANSMITTER RELEASE CYCLE	34	0.41848	1.641473

Reactome	G ALPHA S SIGNALLING EVENTS	116	0.4119	1.615663
Reactome	INFLUENZA VIRAL RNA TRANSCRIPTION AND REPLICATION	101	0.41172	1.614957
Reactome	3 UTR MEDIATED TRANSLATIONAL REGULATION	105	0.40624	1.593462
Reactome	SRP DEPENDENT COTRANSLATIONAL PROTEIN TARGETING TO MEMBRANE	108	0.39682	1.556512
Reactome	MEIOTIC RECOMBINATION	81	0.39134	1.535017
Reactome	G ALPHA Q SIGNALLING EVENTS	177	0.37707	1.479043
Reactome	NONSENSE MEDIATED DECAY ENHANCED BY THE EXON JUNCTION COMPLEX	106	0.37401	1.467041
Reactome	TRANSLATION	145	0.36333	1.425149
Reactome	CLASS A1 RHODOPSIN LIKE RECEPTORS	281	0.35867	1.40687
Reactome	GASTRIN CREB SIGNALLING PATHWAY VIA PKC AND MAPK	198	0.35586	1.395848
Reactome	MEIOSIS	109	0.35287	1.38412
Reactome	RNA POL I PROMOTER OPENING	58	0.35241	1.382316
Reactome	DNA REPAIR	102	0.35117	1.377452
Reactome	SIGNALING BY RHO GTPASES	111	0.33609	1.318301
Reactome	RNA POL I TRANSCRIPTION	82	0.33602	1.318026
Reactome	TCA CYCLE AND RESPIRATORY ELECTRON TRANSPORT	115	0.33327	1.30724
Reactome	GPCR LIGAND BINDING	378	0.32238	1.264524
Reactome	RNA POL I RNA POL III AND MITOCHONDRIAL TRANSCRIPTION	114	0.31066	1.218553
Reactome	PEPTIDE LIGAND BINDING RECEPTORS	174	0.30944	1.213767
Reactome	POST TRANSLATIONAL PROTEIN MODIFICATION	177	0.28885	1.133004

Supplementary table 3.3: DEPCG list showing protein coding genes with differential expression in at least 3 studies, having Ensembl ID, a false discovery rate (FDR)<0.05 and a z-value of ≥|4|

ENSEMBL ID	Gene name	zval	pval	FDR
ENSG00000196663	TECPR2	-5.13896	1.00E-20	1.24E-18
ENSG00000149809	TM7SF2	-5.06287	1.00E-20	1.24E-18
ENSG00000163888	CAMK2N2	-4.79406	6.51E-07	7.41E-05
ENSG00000136280	CCM2	-4.65061	1.95E-06	0.000153
ENSG00000116819	TFAP2E	-4.62602	1.95E-06	0.000153
ENSG00000132321	IQCA1	-4.5903	1.95E-06	0.000153
ENSG00000130244	FAM98C	-4.57746	1.95E-06	0.000153
ENSG00000141560	FN3KRP	-4.54631	1.95E-06	0.000153
ENSG00000123453	SARDH	-4.34822	5.86E-06	0.000367
ENSG00000108946	PRKAR1A	-4.29718	7.81E-06	0.000469
ENSG00000129968	ABHD17A	-4.24387	1.11E-05	0.000612
ENSG00000175182	FAM131A	-4.219	1.11E-05	0.000612
ENSG00000130005	GAMT	-4.06299	1.95E-05	0.000893
ENSG00000168159	RNF187	-4.01008	2.67E-05	0.001145
ENSG00000285426	RNF187	-4.01008	2.67E-05	0.001145
ENSG00000156500	PABIR3	4.000117	2.86E-05	0.001222
ENSG00000139180	NDUFA9	4.002954	2.73E-05	0.00117
ENSG00000180479	ZNF571	4.006681	2.67E-05	0.001145
ENSG00000100575	TIMM9	4.007772	2.60E-05	0.001127
ENSG00000000457	SCYL3	4.010275	2.60E-05	0.001127
ENSG00000091009	RBM27	4.011549	2.60E-05	0.001127
ENSG00000170222	ADPRM	4.012181	2.60E-05	0.001127
ENSG00000113387	SUB1	4.012423	2.60E-05	0.001127
ENSG00000123338	NCKAP1L	4.016818	2.54E-05	0.001114
ENSG00000151576	QTRT2	4.018261	2.54E-05	0.001114
ENSG00000159388	BTG2	4.021286	2.54E-05	0.001114
ENSG00000156103	MMP16	4.022545	2.47E-05	0.001095
ENSG00000158006	PAFAH2	4.026398	2.47E-05	0.001095
ENSG00000118873	RAB3GAP2	4.028381	2.41E-05	0.001072
ENSG00000149308	NPAT	4.030035	2.34E-05	0.001047
ENSG00000265808	SEC22B	4.034286	2.28E-05	0.00102
ENSG00000164164	OTUD4	4.044052	2.28E-05	0.00102
ENSG00000047315	POLR2B	4.047195	2.28E-05	0.00102
ENSG00000176018	LYSMD3	4.053669	2.02E-05	0.000912
ENSG00000101596	SMCHD1	4.054614	2.02E-05	0.000912
ENSG00000146729	NIPSNAP2	4.059368	2.02E-05	0.000912
ENSG00000018510	AGPS	4.060009	2.02E-05	0.000912

ENSG00000157259	GATAD1	4.062443	1.95E-05	0.000893
ENSG00000149262	INTS4	4.062714	1.95E-05	0.000893
ENSG00000242485	MRPL20	4.067109	1.89E-05	0.000871
ENSG00000107949	BCCIP	4.067795	1.89E-05	0.000871
ENSG00000131115	ZNF227	4.07223	1.89E-05	0.000871
ENSG00000122877	EGR2	4.07483	1.89E-05	0.000871
ENSG00000133704	IPO8	4.080973	1.82E-05	0.000851
ENSG00000197779	ZNF81	4.083694	1.76E-05	0.000823
ENSG00000136628	EPRS1	4.085947	1.76E-05	0.000823
ENSG00000092439	TRPM7	4.086155	1.76E-05	0.000823
ENSG00000204138	PHACTR4	4.092591	1.69E-05	0.0008
ENSG00000162694	EXTL2	4.093738	1.69E-05	0.0008
ENSG00000119820	YIPF4	4.09515	1.63E-05	0.000774
ENSG00000134061	CD180	4.098158	1.63E-05	0.000774
ENSG00000092531	SNAP23	4.099303	1.63E-05	0.000774
ENSG00000076650	GPATCH1	4.10267	1.63E-05	0.000774
ENSG00000137770	CTDSPL2	4.103022	1.63E-05	0.000774
ENSG00000167555	ZNF528	4.104459	1.63E-05	0.000774
ENSG00000241343	RPL36A	4.107409	1.63E-05	0.000774
ENSG00000104218	CSPP1	4.110372	1.63E-05	0.000774
ENSG00000168538	TRAPPC11	4.116828	1.63E-05	0.000774
ENSG00000176102	CSTF3	4.119302	1.63E-05	0.000774
ENSG00000163608	NEPRO	4.120336	1.63E-05	0.000774
ENSG00000198034	RPS4X	4.125753	1.63E-05	0.000774
ENSG00000021776	AQR	4.12622	1.63E-05	0.000774
ENSG00000117010	ZNF684	4.1278	1.63E-05	0.000774
ENSG00000100266	PACSIN2	4.129119	1.56E-05	0.000774
ENSG00000144724	PTPRG	4.129293	1.56E-05	0.000774
ENSG00000165819	METTL3	4.131161	1.56E-05	0.000774
ENSG00000243943	ZNF512	4.132739	1.56E-05	0.000774
ENSG00000185220	PGBD2	4.138483	1.50E-05	0.000754
ENSG00000109270	LAMTOR3	4.139306	1.50E-05	0.000754
ENSG00000068097	HEATR6	4.141545	1.50E-05	0.000754
ENSG00000111837	MAK	4.141735	1.50E-05	0.000754
ENSG00000121058	COIL	4.142278	1.50E-05	0.000754
ENSG00000254999	BRK1	4.142338	1.50E-05	0.000754
ENSG00000164035	EMCN	4.152435	1.50E-05	0.000754
ENSG00000154719	MRPL39	4.154614	1.50E-05	0.000754
ENSG00000088451	TGDS	4.160133	1.50E-05	0.000754
ENSG00000170006	TMEM154	4.162669	1.43E-05	0.000743
ENSG00000119509	INVS	4.167198	1.43E-05	0.000743

ENSG00000133773	CCDC59	4.16769	1.43E-05	0.000743
ENSG00000169403	PTAFR	4.169281	1.43E-05	0.000743
ENSG00000174442	ZWILCH	4.174696	1.37E-05	0.000719
ENSG00000198839	ZNF277	4.176899	1.37E-05	0.000719
ENSG00000135249	RINT1	4.17731	1.37E-05	0.000719
ENSG00000197170	PSMD12	4.178358	1.37E-05	0.000719
ENSG00000276833	TAF15	4.182408	1.37E-05	0.000719
ENSG00000131238	PPT1	4.182984	1.37E-05	0.000719
ENSG00000186432	KPNA4	4.189457	1.30E-05	0.000699
ENSG00000166532	RIMKLB	4.190665	1.30E-05	0.000699
ENSG00000003056	M6PR	4.194457	1.24E-05	0.000669
ENSG00000162961	DPY30	4.19592	1.24E-05	0.000669
ENSG00000086200	IPO11	4.196878	1.24E-05	0.000669
ENSG00000111639	MRPL51	4.198674	1.24E-05	0.000669
ENSG00000188846	RPL14	4.200442	1.24E-05	0.000669
ENSG00000175548	ALG10B	4.202417	1.17E-05	0.000645
ENSG00000115084	SLC35F5	4.208504	1.11E-05	0.000612
ENSG00000180787	ZFP3	4.208965	1.11E-05	0.000612
ENSG00000143149	ALDH9A1	4.210483	1.11E-05	0.000612
ENSG00000136709	WDR33	4.212053	1.11E-05	0.000612
ENSG00000149196	HIKESHI	4.218596	1.11E-05	0.000612
ENSG00000065243	PKN2	4.223273	1.11E-05	0.000612
ENSG00000117036	ETV3	4.225283	1.11E-05	0.000612
ENSG00000181704	YIPF6	4.226529	1.11E-05	0.000612
ENSG00000102221	JADE3	4.230947	1.11E-05	0.000612
ENSG00000172795	DCP2	4.239823	1.11E-05	0.000612
ENSG00000153975	ZUP1	4.24517	1.11E-05	0.000612
ENSG00000154305	MIA3	4.257138	9.76E-06	0.000566
ENSG00000186017	ZNF566	4.257747	9.11E-06	0.00053
ENSG00000083828	ZNF586	4.258603	9.11E-06	0.00053
ENSG00000029639	TFB1M	4.261446	9.11E-06	0.00053
ENSG00000104517	UBR5	4.267127	8.46E-06	0.000498
ENSG00000198093	ZNF649	4.26978	8.46E-06	0.000498
ENSG00000186141	POLR3C	4.284586	8.46E-06	0.000498
ENSG00000068654	POLR1A	4.284862	8.46E-06	0.000498
ENSG00000104763	ASAH1	4.285721	8.46E-06	0.000498
ENSG00000134987	WDR36	4.290605	7.81E-06	0.000469
ENSG00000256646		4.292923	7.81E-06	0.000469
ENSG00000172878	METAP1D	4.294077	7.81E-06	0.000469
ENSG00000020922	MRE11	4.296243	7.81E-06	0.000469
ENSG00000167766	ZNF83	4.29642	7.81E-06	0.000469

ENSG00000153037	SRP19	4.303485	7.16E-06	0.000444
ENSG00000138777	PPA2	4.322977	7.16E-06	0.000444
ENSG00000186448	ZNF197	4.328633	7.81E-06	0.000469
ENSG00000281709	ZNF197	4.328633	7.81E-06	0.000469
ENSG00000163714	U2SURP	4.336371	6.51E-06	0.000407
ENSG00000132570	PCBD2	4.340625	5.86E-06	0.000367
ENSG00000117479	SLC19A2	4.341771	5.86E-06	0.000367
ENSG00000114391	RPL24	4.34306	5.86E-06	0.000367
ENSG00000126790	L3HYPDH	4.368843	5.21E-06	0.000338
ENSG00000275111	ZNF2	4.379894	5.21E-06	0.000338
ENSG00000087884	AAMDC	4.383624	5.21E-06	0.000338
ENSG00000143222	UFC1	4.385458	5.21E-06	0.000338
ENSG00000198730	CTR9	4.389005	5.21E-06	0.000338
ENSG00000138685	FGF2	4.393184	5.21E-06	0.000338
ENSG00000122696	SLC25A51	4.396271	5.21E-06	0.000338
ENSG00000082074	FYB1	4.39652	5.21E-06	0.000338
ENSG00000198814	GK	4.397338	5.21E-06	0.000338
ENSG00000117620	SLC35A3	4.407515	4.56E-06	0.000307
ENSG00000090060	PAPOLA	4.412386	4.56E-06	0.000307
ENSG00000129084	PSMA1	4.414463	4.56E-06	0.000307
ENSG00000102189	EEA1	4.415376	4.56E-06	0.000307
ENSG00000163754	GYG1	4.41822	4.56E-06	0.000307
ENSG00000144426	NBEAL1	4.419317	4.56E-06	0.000307
ENSG00000163527	STT3B	4.422006	4.56E-06	0.000307
ENSG00000177200	CHD9	4.428031	4.56E-06	0.000307
ENSG00000182973	CNOT10	4.428117	4.56E-06	0.000307
ENSG00000197024	ZNF398	4.438295	3.90E-06	0.000274
ENSG00000159905	ZNF221	4.440691	3.90E-06	0.000274
ENSG00000256771	ZNF253	4.445606	3.90E-06	0.000274
ENSG00000067177	PHKA1	4.447544	3.90E-06	0.000274
ENSG00000004866	ST7	4.448373	3.90E-06	0.000274
ENSG00000111450	STX2	4.448792	3.90E-06	0.000274
ENSG00000132912	DCTN4	4.451247	3.90E-06	0.000274
ENSG00000134371	CDC73	4.452807	3.90E-06	0.000274
ENSG00000120280	TASL	4.457191	3.90E-06	0.000274
ENSG00000113360	DROSHA	4.460788	3.90E-06	0.000274
ENSG00000172469	MANEA	4.46277	3.90E-06	0.000274
ENSG00000156261	CCT8	4.467673	3.90E-06	0.000274
ENSG00000119314	PTBP3	4.472066	3.90E-06	0.000274
ENSG00000172850	LSM2	4.482472	5.86E-06	0.000367
ENSG00000224979	LSM2	4.482472	5.86E-06	0.000367

ENSG00000225998	LSM2	4.482472	5.86E-06	0.000367
ENSG00000231502	LSM2	4.482472	5.86E-06	0.000367
ENSG00000111846	GCNT2	4.482596	3.90E-06	0.000274
ENSG00000102710	SUPT20H	4.483507	3.90E-06	0.000274
ENSG00000110756	HPS5	4.491436	3.90E-06	0.000274
ENSG00000288445	HPS5	4.491436	3.90E-06	0.000274
ENSG00000109911	ELP4	4.500791	2.60E-06	0.000198
ENSG00000078618	NRDC	4.504017	2.60E-06	0.000198
ENSG00000254093	PINX1	4.504569	2.60E-06	0.000198
ENSG00000196531	NACA	4.508674	2.60E-06	0.000198
ENSG00000072274	TFRC	4.51087	2.60E-06	0.000198
ENSG00000121406	ZNF549	4.519071	2.60E-06	0.000198
ENSG00000144713	RPL32	4.529373	1.95E-06	0.000153
ENSG00000100055	CYTH4	4.529663	1.95E-06	0.000153
ENSG00000081870	HSPB11	4.539017	1.95E-06	0.000153
ENSG00000169359	SLC33A1	4.540784	1.95E-06	0.000153
ENSG00000118496	FBXO30	4.541748	1.95E-06	0.000153
ENSG00000155629	PIK3AP1	4.542463	1.95E-06	0.000153
ENSG00000074657	ZNF532	4.542977	1.95E-06	0.000153
ENSG00000117143	UAP1	4.547101	1.95E-06	0.000153
ENSG00000124486	USP9X	4.547731	1.95E-06	0.000153
ENSG00000129197	RPAIN	4.550673	1.95E-06	0.000153
ENSG00000116251	RPL22	4.563459	1.95E-06	0.000153
ENSG00000256060	TRAPPC2B	4.576683	1.95E-06	0.000153
ENSG00000172594	SMPDL3A	4.582917	1.95E-06	0.000153
ENSG00000255639	0	4.583189	1.95E-06	0.000153
ENSG00000059377	TBXAS1	4.586749	1.95E-06	0.000153
ENSG00000204524	ZNF805	4.586796	1.95E-06	0.000153
ENSG00000144895	EIF2A	4.58942	1.95E-06	0.000153
ENSG00000166439	RNF169	4.593879	1.95E-06	0.000153
ENSG00000186376	ZNF75D	4.59591	1.95E-06	0.000153
ENSG00000121879	PIK3CA	4.59726	1.95E-06	0.000153
ENSG00000173214	MFSD4B	4.603771	1.95E-06	0.000153
ENSG00000108443	RPS6KB1	4.607876	1.95E-06	0.000153
ENSG00000113811	SELENOK	4.612871	1.95E-06	0.000153
ENSG00000253352	TUG1	4.615618	1.95E-06	0.000153
ENSG00000122729	ACO1	4.618973	1.95E-06	0.000153
ENSG00000187068	C3orf70	4.621849	1.95E-06	0.000153
ENSG00000075884	ARHGAP15	4.624949	1.95E-06	0.000153
ENSG00000123066	MED13L	4.625026	1.95E-06	0.000153

ENSG00000154240	CEP112	4.625749	1.95E-06	0.000153
ENSG00000219481	NBPF1	4.625847	1.95E-06	0.000153
ENSG00000142556	ZNF614	4.629313	1.95E-06	0.000153
ENSG00000067900	ROCK1	4.6402	1.95E-06	0.000153
ENSG00000279247	AK6	4.640763	1.95E-06	0.000153
ENSG00000168795	ZBTB5	4.644812	1.95E-06	0.000153
ENSG00000102743	SLC25A15	4.653699	1.95E-06	0.000153
ENSG00000077458	FAM76B	4.653824	1.95E-06	0.000153
ENSG00000048342	CC2D2A	4.658431	1.95E-06	0.000153
ENSG00000138756	BMP2K	4.660359	1.95E-06	0.000153
ENSG00000152457	DCLRE1C	4.664693	1.95E-06	0.000153
ENSG00000215114	UBXN2B	4.671336	1.95E-06	0.000153
ENSG00000197608	ZNF841	4.676423	1.95E-06	0.000153
ENSG00000197714	ZNF460	4.681579	1.95E-06	0.000153
ENSG00000108107	RPL28	4.682127	1.95E-06	0.000153
ENSG00000101751	POLI	4.687498	1.95E-06	0.000153
ENSG00000198755	RPL10A	4.688806	1.95E-06	0.000153
ENSG00000163507	CIP2A	4.690536	1.95E-06	0.000153
ENSG00000036257	CUL3	4.693787	1.95E-06	0.000153
ENSG00000119402	FBXW2	4.696536	1.95E-06	0.000153
ENSG00000144182	LIPT1	4.69918	1.95E-06	0.000153
ENSG00000153827	TRIP12	4.700775	1.95E-06	0.000153
ENSG00000168038	ULK4	4.705162	1.95E-06	0.000153
ENSG00000236287	ZBED5	4.706796	1.30E-06	0.000143
ENSG00000113583	C5orf15	4.713622	1.30E-06	0.000143
ENSG00000126070	AGO3	4.735003	1.30E-06	0.000143
ENSG00000145833	DDX46	4.737296	1.30E-06	0.000143
ENSG00000241399	CD302	4.742266	1.30E-06	0.000143
ENSG00000151881	TMEM267	4.751574	6.51E-07	7.41E-05
ENSG00000138050	THUMPD2	4.752613	6.51E-07	7.41E-05
ENSG00000182287	AP1S2	4.765349	6.51E-07	7.41E-05
ENSG00000158411	MITD1	4.766564	6.51E-07	7.41E-05
ENSG00000006459	KDM7A	4.768307	6.51E-07	7.41E-05
ENSG00000066777	ARFGEF1	4.777718	6.51E-07	7.41E-05
ENSG00000184293	CLECL1	4.7791	6.51E-07	7.41E-05
ENSG00000156313	RPGR	4.780583	6.51E-07	7.41E-05
ENSG00000198625	MDM4	4.810577	1.00E-20	1.24E-18
ENSG00000142166	IFNAR1	4.817958	1.00E-20	1.24E-18
ENSG00000163785	RYK	4.818626	1.00E-20	1.24E-18
ENSG00000101126	ADNP	4.827325	1.00E-20	1.24E-18
ENSG00000186300	ZNF555	4.830261	1.00E-20	1.24E-18

ENSG00000116580	GON4L	4.832558	1.00E-20	1.24E-18
ENSG00000007392	LUC7L	4.83536	1.00E-20	1.24E-18
ENSG00000117505	DR1	4.836544	1.00E-20	1.24E-18
ENSG00000111142	METAP2	4.848148	1.00E-20	1.24E-18
ENSG00000172785	CBWD1	4.849642	1.00E-20	1.24E-18
ENSG00000145041	DCAF1	4.852261	1.00E-20	1.24E-18
ENSG00000164941	INTS8	4.852835	1.00E-20	1.24E-18
ENSG00000089876	DHX32	4.853237	1.00E-20	1.24E-18
ENSG00000100372	SLC25A17	4.866289	1.00E-20	1.24E-18
ENSG00000170860	LSM3	4.867178	1.00E-20	1.24E-18
ENSG00000169967	MAP3K2	4.870009	1.00E-20	1.24E-18
ENSG00000183520	UTP11	4.879117	1.00E-20	1.24E-18
ENSG00000169895	SYAP1	4.886433	1.00E-20	1.24E-18
ENSG00000177025	C19orf18	4.893713	1.00E-20	1.24E-18
ENSG00000145982	FARS2	4.894546	1.00E-20	1.24E-18
ENSG00000173588	CEP83	4.895797	1.00E-20	1.24E-18
ENSG00000119397	CNTRL	4.902685	1.00E-20	1.24E-18
ENSG00000076321	KLHL20	4.904982	1.00E-20	1.24E-18
ENSG00000115875	SRSF7	4.906291	1.00E-20	1.24E-18
ENSG00000128699	ORMDL1	4.910077	1.00E-20	1.24E-18
ENSG00000067248	DHX29	4.911971	1.00E-20	1.24E-18
ENSG00000136536	MARCHF7	4.914925	1.00E-20	1.24E-18
ENSG00000174652	ZNF266	4.917	1.00E-20	1.24E-18
ENSG00000170677	SOCS6	4.917529	1.00E-20	1.24E-18
ENSG00000155636	RBM45	4.926901	1.00E-20	1.24E-18
ENSG00000275600	PIGW	4.941176	1.00E-20	1.24E-18
ENSG00000009413	REV3L	4.944528	1.00E-20	1.24E-18
ENSG00000198040	ZNF84	4.946085	1.00E-20	1.24E-18
ENSG00000189266	PNRC2	4.950578	1.00E-20	1.24E-18
ENSG00000213809	KLRK1	4.960424	1.00E-20	1.24E-18
ENSG00000127328	RAB3IP	4.96356	1.00E-20	1.24E-18
ENSG00000136051	WASHC4	4.96799	1.00E-20	1.24E-18
ENSG00000116698	SMG7	4.968646	1.00E-20	1.24E-18
ENSG00000137942	FNBP1L	4.970914	1.00E-20	1.24E-18
ENSG00000115368	WDR75	4.978038	1.00E-20	1.24E-18
ENSG00000115524	SF3B1	4.98057	1.00E-20	1.24E-18
ENSG00000136021	SCYL2	4.982744	1.00E-20	1.24E-18
ENSG00000102531	FNDC3A	4.986048	1.00E-20	1.24E-18
ENSG00000146282	RARS2	4.99477	1.00E-20	1.24E-18
ENSG00000122406	RPL5	5.009283	1.00E-20	1.24E-18
ENSG00000111011	RSRC2	5.017333	1.00E-20	1.24E-18

ENSG00000285901	0	5.024554	1.00E-20	1.24E-18
ENSG00000254004	ZNF260	5.025238	1.00E-20	1.24E-18
ENSG00000005175	RPAP3	5.030592	1.00E-20	1.24E-18
ENSG00000055332	EIF2AK2	5.039656	1.00E-20	1.24E-18
ENSG00000147202	DIAPH2	5.050425	1.00E-20	1.24E-18
ENSG00000174125	TLR1	5.052871	1.00E-20	1.24E-18
ENSG00000134186	PRPF38B	5.060196	1.00E-20	1.24E-18
ENSG00000168916	ZNF608	5.073178	1.00E-20	1.24E-18
ENSG00000151458	ANKRD50	5.078823	1.00E-20	1.24E-18
ENSG00000121481	RNF2	5.08547	1.00E-20	1.24E-18
ENSG00000094880	CDC23	5.09454	1.00E-20	1.24E-18
ENSG00000105750	ZNF85	5.112806	1.00E-20	1.24E-18
ENSG00000164197	RNF180	5.115658	1.00E-20	1.24E-18
ENSG00000155307	SAMSN1	5.12339	1.00E-20	1.24E-18
ENSG00000049167	ERCC8	5.146013	1.00E-20	1.24E-18
ENSG00000115446	UNC50	5.154424	1.00E-20	1.24E-18
ENSG00000163636	PSMD6	5.166107	1.00E-20	1.24E-18
ENSG00000168961	LGALS9	5.175534	1.00E-20	1.24E-18
ENSG00000156171	DRAM2	5.177309	1.00E-20	1.24E-18
ENSG00000197798	FAM118B	5.190534	1.00E-20	1.24E-18
ENSG00000185009	AP3M1	5.195736	1.00E-20	1.24E-18
ENSG00000082212	ME2	5.216069	1.00E-20	1.24E-18
ENSG00000182774	RPS17	5.229447	1.00E-20	1.24E-18
ENSG00000055044	NOP58	5.233695	1.00E-20	1.24E-18
ENSG00000120509	PDZD11	5.244839	1.00E-20	1.24E-18
ENSG00000197782	ZNF780A	5.250654	1.00E-20	1.24E-18
ENSG00000186026	ZNF284	5.255581	1.00E-20	1.24E-18
ENSG00000196632	WNK3	5.27413	1.00E-20	1.24E-18
ENSG00000110330	BIRC2	5.278451	1.00E-20	1.24E-18
ENSG00000060749	QSER1	5.285188	1.00E-20	1.24E-18
ENSG00000162613	FUBP1	5.312691	1.00E-20	1.24E-18
ENSG00000114354	TFG	5.331727	1.00E-20	1.24E-18
ENSG00000211455	STK38L	5.350372	1.00E-20	1.24E-18
ENSG00000197961	ZNF121	5.387317	1.00E-20	1.24E-18
ENSG00000035681	NSMAF	5.387652	1.00E-20	1.24E-18
ENSG00000172167	MTBP	5.42527	1.00E-20	1.24E-18
ENSG00000196470	SIAH1	5.449329	1.00E-20	1.24E-18
ENSG00000152433	ZNF547	5.456359	1.00E-20	1.24E-18
ENSG00000143493	INTS7	5.466494	1.00E-20	1.24E-18
ENSG00000145780	FEM1C	5.501341	1.00E-20	1.24E-18
ENSG00000109920	FNBP4	5.503827	6.51E-07	7.41E-05

ENSG00000285182	FNBP4	5.503827	6.51E-07	7.41E-05
ENSG00000280568	ZNF780A	5.510635	1.00E-20	1.24E-18
ENSG00000136603	SKIL	5.52906	1.00E-20	1.24E-18
ENSG00000143106	PSMA5	5.532601	1.00E-20	1.24E-18
ENSG00000138385	SSB	5.541434	1.00E-20	1.24E-18
ENSG00000107779	BMPR1A	5.553395	1.00E-20	1.24E-18
ENSG00000125772	GPCPD1	5.554662	1.00E-20	1.24E-18
ENSG00000142534	RPS11	5.570929	1.00E-20	1.24E-18
ENSG00000108510	MED13	5.573116	1.00E-20	1.24E-18
ENSG00000164338	UTP15	5.622842	1.00E-20	1.24E-18
ENSG00000160124	MIX23	5.631446	1.00E-20	1.24E-18
ENSG00000188647	PTAR1	5.640086	1.00E-20	1.24E-18
ENSG00000213096	ZNF254	5.655889	1.00E-20	1.24E-18
ENSG00000174720	LARP7	5.674445	1.00E-20	1.24E-18
ENSG00000088448	ANKRD10	5.680425	1.00E-20	1.24E-18
ENSG00000118855	MFSD1	5.681572	1.00E-20	1.24E-18
ENSG00000137145	DENND4C	5.696087	1.00E-20	1.24E-18
ENSG00000058804	NDC1	5.701652	1.00E-20	1.24E-18
ENSG00000242247	ARFGAP3	5.710312	1.00E-20	1.24E-18
ENSG00000118007	STAG1	5.743575	1.00E-20	1.24E-18
ENSG00000111224	PARP11	5.749825	1.00E-20	1.24E-18
ENSG00000136937	NCBP1	5.754858	1.00E-20	1.24E-18
ENSG00000213625	LEPROT	5.779798	1.00E-20	1.24E-18
ENSG00000119729	RHOQ	5.844391	1.00E-20	1.24E-18
ENSG00000196214	ZNF766	5.852422	1.00E-20	1.24E-18
ENSG00000175895	PLEKHF2	5.936077	1.00E-20	1.24E-18
ENSG00000124151	NCOA3	5.956854	1.00E-20	1.24E-18
ENSG00000189079	ARID2	5.982309	1.00E-20	1.24E-18
ENSG00000147251	DOCK11	6.048905	1.00E-20	1.24E-18
ENSG00000108854	SMURF2	6.116276	1.00E-20	1.24E-18
ENSG00000168769	TET2	6.13178	1.00E-20	1.24E-18
ENSG00000109606	DHX15	6.148613	1.00E-20	1.24E-18
ENSG00000118217	ATF6	6.374994	1.00E-20	1.24E-18
ENSG00000153207	AHCTF1	6.392375	1.00E-20	1.24E-18
ENSG00000155329	ZCCHC10	6.460166	1.00E-20	1.24E-18
ENSG00000263002	ZNF234	6.538277	1.00E-20	1.24E-18
ENSG00000262795	IFNGR2	7.747547	1.00E-20	1.24E-18

Supplementary table 3.4: *Pathway analysis of cluster A2 DEPCG members*

Pathway DB	Enriched pathway	DEPCG belonging to pathway
KEGG	Ribosome	RPS11,MRPL20,RPL22,RPL5,RPS4X,RPL10A,RPL24,RPL14,RPL36A,RPL32
REACTOME	Peptide chain elongation	RPS11,RPL22,RPL5,RPS4X,RPL10A,RPL24,RPL14,RPL36A,RPL32
REACTOME	Viral mRNA Translation	RPS11,RPL22,RPL5,RPS4X,RPL10A,RPL24,RPL14,RPL36A,RPL32
REACTOME	Selenocysteine synthesis	RPS11,RPL22,RPL5,RPS4X,RPL10A,RPL24,RPL14,RPL36A,RPL32
REACTOME	Eukaryotic Translation Termination	RPS11,RPL22,RPL5,RPS4X,RPL10A,RPL24,RPL14,RPL36A,RPL32
REACTOME	Nonsense Mediated Decay (NMD) independent of the Exon Junction Complex (EJC)	RPS11,RPL22,RPL5,RPS4X,RPL10A,RPL24,RPL14,RPL36A,RPL32
REACTOME	Formation of a pool of free 40S subunits	RPS11,RPL22,RPL5,RPS4X,RPL10A,RPL24,RPL14,RPL36A,RPL32
REACTOME	Response of EIF2AK4 (GCN2) to amino acid deficiency	RPS11,RPL22,RPL5,RPS4X,RPL10A,RPL24,RPL14,RPL36A,RPL32
REACTOME	SRP-dependent cotranslational protein targeting to membrane	RPS11,RPL22,RPL5,RPS4X,RPL10A,RPL24,RPL14,RPL36A,RPL32,SRP19
REACTOME	Nonsense Mediated Decay (NMD) enhanced by the Exon Junction Complex (EJC)	RPS11,RPL22,RPL5,RPS4X,RPL10A,RPL24,RPL14,RPL36A,RPL32,SMG7
REACTOME	GTP hydrolysis and joining of the 60S ribosomal subunit	RPS11,RPL22,RPL5,RPS4X,RPL10A,RPL24,RPL14,RPL36A,RPL32
REACTOME	L13a-mediated translational silencing of Ceruloplasmin expression	RPS11,RPL22,RPL5,RPS4X,RPL10A,RPL24,RPL14,RPL36A,RPL32
REACTOME	Regulation of expression of SLITs and ROBOs	RPS11,PSMA5,RPL22,RPL5,RPS4X,RPL10A,RPL24,RPL14,RPL36A,PSMA1,RPL32
REACTOME	Major pathway of rRNA processing in the nucleolus and cytosol	RPS11,RPL22,RPL5,RPS4X,RPL10A,RPL24,RPL14,RPL36A,RPL32
REACTOME	Translation	MRPL51,RPS11,MRPL20,RPL22,RPL5,RPS4X,RPL10A,RPL24,RPL14,RPL36A,RPL32,SRP19
REACTOME	Metabolism of amino acids and derivatives	RPS11,PSMA5,RPL22,ALDH9A1,RPL5,RPS4X,RPL10A,RPL24,RPL14,RPL36A,PSMA1,RPL32
REACTOME	Cellular responses to stress	RPS11,PSMA5,C11orf73,RPL22,RPL5,RPS4X,RPL10A,RPL24,RPL14,RPL36A,PSMA1,RPL32
REACTOME	Metabolism of RNA	RPS11,PSMA5,METTL3,LSM3,RPL22,RPL5,RPS4X,RPL10A,RPL24,RPL14,RPL36A,PSMA1,RPL32,SMG7
REACTOME	Infectious disease	RPS11,PSMA5,IFNGR2,RPL22,RPL5,RPS4X,RPL10A,RPL24,RPL14,RPL36A,PSMA1,RPL32,BRK1,TAF15
REACTOME	Disease	RPS11,PSMA5,IFNGR2,GYG1,RPL22,RPL5,RPS4X,RPL10A,RPL24,RPL14,RPL36A,PSMA1,RPL32,BRK1,TAF15
REACTOME	Metabolism of proteins	MRPL51,TFG,CCDC59,RPS11,PSMA5,MRPL20,RPL22,RPL5,RPS4X,RPL10A,RPL24,RPL14,RPL36A,PSMA1,RPL32,SRP19

REACTOME	Metabolism	PDZD11,NDUFA9,RPS11,PSMA5,ORMDL1,GYG1,RPL22,ALDH9A1,RPL5,RPS4X,RPL10A,RPL24,RPL14,PPT1,RPL36A,PSMA1,RPL32

Supplementary table 3.5: *Available literature-based evidence of glioblastoma functional associations of the DANCR-targeted DEPCG overlapping with TCGA-GBM*

DEPCG	Association with GBM	Refs
ROCK1 Rho-associated kinase 1	Knockdown induced antidromic cell migration and reduced proliferation Inhibition by miR-145 decreased cell invasiveness Inhibition blocked macrophage migration inhibitory factor (MIF)- mediated increase in migration and colony formation Inhibition by miR-206 overexpression led to inhibition of migration, invasion, and PI3K/AKT pathway activation Promotion of migration, invasion and proliferation	[817] [818] [819] [820] [821]
GK Glycerol kinase	Predicted to act as downstream transcription factor in COL5A1 regulation of cell mobility, metastasis and actin polimerization status	[822]
METAP2 Methionine aminopeptidase 2	Knockdown decreased proliferation, tumorigeneicity, decreased VEGF expression and dependent angiogenesis	[823]
CIP2A Cancerous inhibitor of protein phosphatase 2A	Inhibition induced cell senescence and retarded tumor growth Silencing enhanced Cucurbitacin B-induced invasion inhibition and apoptosis Overexpression reversed cell cycle and apoptotic protein expression led by anti-tumor 2,5-Dimethyl Celecoxib Promotion of viability, clonogenicity and anchorage-independent growth	[824] [825] [826] [827]
ASAH1 Acid ceramidase	Expression associated with poor survival and inhibition increases cellular ceramide level and induces apoptosis Upregulation conferred cellular radioresistance	[828] [829]
STX2 Syntaxin 2	Inhibition reduced growth of tumor xenografts in vivo	[830]
MAP3K2 Mitogen-activated protein kinase 2	Restoration of proliferation occurring due to circ-PITX1 silencing	[831]

Supplementary table 3.6: *Available literature-based evidence of glioblastoma/ferroptosis functional associations of DEPCGs in the DANCR/SNHG6 sub-cluster of co-expression correlation network*

DEPCG	Characterized role in glioma/glioblastoma	Previously associated with ferroptosis?
LUC7L	Yes [832]	No
PDZD11	No	No
BRK1	No	No
UFC1	No	Part of UFMylation pathway which regulates ferroptosis in breast cancer [833]
ENSG00000256646	No	No
TAF15	Predicted target of LINC01564 which promotes glioma cell treatment resistance [834]	Predicted target of LINC01564 which inhibits ferroptosis [834]
ALDH9A1	Activated by CLOCK which drives immunosuppression in glioblastoma [835,836]	No
TIMM9	By machine learning from high throughput CRISPR-Cas9 [837]	No
MRPL20	No	No
RPS4X	Part of in-silico glioblastoma prognostic model [675]	No
RPL36A	Part of prognostic model for GBM (Preprint [675], [676]	No
PRPF38B	No	No
ZNF266	No	No
MRPL51	No	No
RPL5	No	No
PSMA5	Independent prognostic marker for glioma and combined treatment with carboplatin and thioridazine was shown to induce apoptosis by upregulation of Nrf2-dependent PSMA5 expression [838,839].	No
SELK	Regulates proliferation, drug sensitivity and invasion of glioma cells [840].	Induced by Selenium which drives ferroptosis inhibition [841]
ORMDL1	No	No
RPL24	No	No
RPL32	No	No
PPT1	elevated expression of PPT1 correlates with poor survival in TCGA patients with gliomas [842]	No
ENSG00000255639	No	No

RPL14	No	No
PSMA1	Identified during a screen for genes contributing to radiation and temozolamide sensitivity as well as tumoricidal activity	Induced by NRF2 which regulates ferroptosis [337,843–845]
C11orf73	No	Mediates nuclear translocation of heat shock protein 70 (HSP70) which regulates ferroptosis [846,847]
METTL3	Regulates the proliferation, migration and invasion of glioma cells [848]	Regulates ferroptosis [849,850]
ZNF547	No	No
HSPB11	inhibits cell death by HSP90 mediated mechanism [851]prognostic marker of high grade glioma [852]	No
DPY30	Drives glioblastoma growth in vivo [853]	No
SRP19	No	No
RPAIN	No	No
MITD1	No	Deficiency induces renal carcinoma growth and migration by ferroptosis induction [854]
UNC50	No	No
IFNGR2	Identified in glioblastoma by genome-wide CRISPR screen [622] and may serve as a biomarker to stratify glioblastoma patients responsiveness to immune checkpoint blockade based therapies [855]	No
NACA	No	No
RPL22	No	No
NDUFA9	No	No
M6PR	No	No
CBWD1 or ZNG1A	No	No
SUB1	Enhances proliferation and migration of glioma cells [856]	No
LSM3	No	No
RPL10A	No	No
SMG7	No	Smg7 $^{-/-}$ cells showed increased protection against cell death by ferroptosis-inducer Erastin [857]
C5orf15	No	No

TFG	Fusion with MET with overexpression of TFG-MET induces aggressive glial brain tumors in Cdkn2a- or Trp53-deficient mice [858].	No
RPS11	influences glioma response to TOP2 poisons [673] predictor of poor prognosis in glioma [674]	No
GYG1	No	No
RAB3GAP2	No	No
THUMPD2	Isoform changes regulate glioma cell line sensitivity to temozolomide [859]	No
SUPT20H	Part of prognostic risk score model for TCGA and CGGA gliomas [860]	No
CCDC59 or TAP26	No	No